

Mathieu Daëron

Rôle, cinématique et comportement sismique à long terme de la faille de Yammoûneh

INSTITUT DE PHYSIQUE DU GLOBE DE PARIS
Département de Tectonique

Thèse de Doctorat
Géophysique Interne

**Rôle, cinématique et comportement sismique à long terme
de la faille de Yammoûneh, principale branche décrochante
du coude transpressif libanais (faille du Levant)**

soutenue le 18 avril 2005 par

Mathieu Daëron



devant le jury composé de :

J.-P. Valet	Président du Jury
T. Rockwell	Rapporteur
M. Sébrier	Rapporteur
M. Campillo	Examinateur
E. Guidoboni	Examinateuse
P. Tapponnier	Directeur de thèse

Remerciements

Je veux ici remercier chaleureusement le bouillonnant, stimulant, insupportable et passionnant Paul Tapponnier, mon directeur de thèse, qui a joué de nombreux autres rôles au cours de ces quelques années, du garde-chiourme au garde-malade. J'ai eu la grande chance de le croiser par hasard en arrivant à l'IPGP et d'être emporté par son enthousiasme pour ce projet libanais. Depuis, je n'ai pas une fois eu l'occasion de le regretter.

Au Liban, rien n'aurait été possible sans le soutien permanent, l'implication et l'expérience d'Alexandre Sursock, directeur du Centre de Recherches Géophysiques de Bhannes. Un grand شكرًا à lui et à tous les membres du Centre : Tony Charbel, Rachid Jomaa, Walid Nohra, Marlène Brax, et Maya Hariri. Plus largement, depuis 1999, nous avons constamment été soutenus, financièrement et humainement, par le Conseil National de la Recherche Scientifique du Liban, sous l'impulsion de son président, Georges Thomé, et de son secrétaire général, Mouîn Hamzé, ainsi que par l'ambassade de France au Liban, qui a financé une part non négligeable des diverses missions. Le soutien de ces organismes, du CNRS français et de l'INSU a joué un rôle essentiel. Je veux également remercier ici l'École Polytechnique, qui m'a soutenu financièrement à diverses occasions.

Quotidiennement sur le terrain ou au labo, j'ai eu grand plaisir à travailler avec les autres chercheurs impliqués dans ce projet. Que soient ici remerciés Ata Elias, un peu pour m'avoir fait découvrir Hallab, pour ses leçons d'Arabe et beaucoup pour sa gentillesse ; Yann Klinger, la preuve vivante qu'on peut faire fuir son cerveau à Caltech sans que le prix à payer soit trop lourd ; Eric Jacques, qui a accompagné mes (nombreux, très nombreux) premiers pas sur le cône de Yammoûneh, et sans qui je n'aurais jamais acheté la boussole qui fait l'envie de mes petits camarades ; Geoff King, avec qui j'ai eu des discussions passionnantes, y compris, Allah merci, sur des sujets sans aucun rapport avec le Liban ou la tectonique ; Lucilla Benedetti, qui m'a fait forer la roche, casser des cailloux et jongler avec les bouteilles d'acide. Dans le désordre, merci aussi à Jean-Pierre Valet, Laure Meynadier, Faten Khatib, Albane Saintenoy, Anne-Lise Salomé, Rachel Jorand, Faten Khatib, Tony Nemer, Nazem Shreif (Abou Ali) et sa famille.

Differentes équipes m'ont accueilli à des étapes diverse de ma thèse. Merci en particulier à Françoise Gasse et aux autres chercheurs et techniciens du CEREGE, qui m'ont vu débarquer avec mon sac à dos sur le plateau de l'Arbois ; à ceux du laboratoire de Livermore, qui m'ont fait (re)découvrir les joies de la datation radiocarbone, du wok et qui m'ont také out to the ball game ; à Roger Bilham et Rebecca Bendick, de l'université de Boulder, qui ont tenté (sans grand succès, mais j'en suis le seul responsable) de faire de moi un expert GPS en dix jours ; enfin à l'IFREMER et aux membres de la mission SHALIMAR, qui, en un mois, m'a fait parcourir autant de kilomètres au large du Liban que j'en ai effectué à terre en cinq ans de missions.

Certains de mes amis ont poussé le dévouement jusqu'à sacrifier une partie de leurs vacances au Liban pour m'aider à finir l'échantillonnage d'une tranchée. Merci donc à Céline, Jules, Laetitia et Antoinette de leur efficacité enthousiasme.

Merci à Michel Sébrier et Tom Rockwell, qui ont bien voulu être les rapporteurs de cette thèse, et à Emanuela Guidoboni, Michel Campillo et Jean-Pierre Valet, qui ont accepté de faire partie du jury.

Malgré l'amianté, les déménagements, la surpopulation et les imprimantes, j'ai eu beaucoup de plaisir à travailler au laboratoire de tectonique de l'IPGP. Merci à tous ceux que j'y ai croisés, y compris ceux qui en sont partis depuis. Merci aussi à Gauthier Hulot, sans qui je n'aurais probablement jamais quitté les photons et l'ADN pour venir taquiner la faille. Si c'est Paul qui m'a ferré, c'est Gauthier qui avait appâté l'hameçon. Un merci tout particulier aux collègues et aux amis qui m'ont envoyé un petit mot au Mans. Pendant que j'y suis, le docteur Serra-Maudet n'est pas pour rien dans l'achèvement de cette thèse. Qu'elle en soit remerciée mille fois.

A ma famille entière, je veux exprimer ma profonde affection, après cette année 2004 qui nous aura tous un peu secoués. Merci à Marc et Lili, à ma (grande, maintenant) sœur Clémence, et à Antoinette : ce que j'aime bien chez moi vient beaucoup d'eux.

Un petit clin d'oeil et un grand merci à Germain, qui a encouragé mes tout premiers pas dans la recherche.

Je ne sais pas si ça se fait, mais je voudrais dédier ce manuscrit à tous mes grands-parents.

Résumé

La faille transformante sénestre qui longe la côte levantine (“faille du Levant”) s’inflechit en suivant un coude transpressif de 160 km de long à la latitude du Liban. La faille décrochante de Yammoûneh, dont la trace traverse le territoire libanais de part en part, est généralement considérée comme la branche la plus active de ce coude transpressif, bien que certains auteurs aient récemment mis en doute son degré actuel d’activité tectonique.

En combinant observations géologiques, géomorphologie quantitative et datation de surfaces et de dépôts par mesure d’isotope cosmogéniques *in situ*, nous démontrons que cette faille est bien active, et qu’elle a systématiquement décalé des objets géomorphologiques divers, façonnés par différents agents climatiques, de quantités allant de quelques mètres à quelques kilomètres, accumulées par le jeu de séismes successifs. La vitesse moyenne de glissement sur cette faille, depuis environ 25 000 ans, est comprise entre 3,8 et 6,4 mm/an d’après l’âge d’exposition de cônes alluviaux décalés par la faille.

L’examen structural et géomorphologique de la côte libanaise et du flanc occidental du Mont Liban révèle l’existence de failles inverses et d’anticlinaux actifs croissant sur des rampes de chevauchement qui pilotent le raccourcissement et le plissement dans le piémont de la montagne libanaise. Ces rampes accommodent sans doute l’essentiel du raccourcissement dû à l’infexion de la faille du Levant dans cette région. Ces chevauchements actifs continuent en mer au large du Mont Liban, de Tripoli au nord jusqu’à Beyrouth, voire Saïda, au sud. Dans ce modèle, la faille de Roûm peut être interprétée comme une simple rampe latérale reliant la faille du Jourdain, au sud, à ce système de failles inverses. Le Mont Liban correspond donc à un petit prisme crustal entièrement bordé de failles actives, entre la plaque Arabe et le bassin levantin.

Ce nouveau modèle des principales failles actives du coude transpressif libanais permet de ré-interpréter les sources des grands séismes historiques de la région. Nous proposons que ce soit le système de chevauchement sous-marin du Mont Liban, plutôt que la faille de Yammoûneh, qui soit responsable du séisme ($M>7$) et du tsunami qui ont ravagé Beyrouth en 551 après J.C. Par ailleurs, grâce au ré-examen critique des sources historiques, à des observations géomorphologiques qualitatives et à des données paléosismologiques, nous démontrons que le dernier événement sur la faille de Yammoûneh est le grand séisme de 1202 ($M\sim7.5$), et que les séismes ultérieurs de 1759 ($M\sim6.6$ et 7.4) se sont produits sur le système de Râchaïya-Serghaya.

Enfin, les résultats de tranchées paléo-sismologiques dans les dépôts du paléo-lac de Yammoûneh ont permis de mieux contraindre la récurrence des séismes sur la faille du même nom, depuis environ 15 000 ans, soit ~14 séismes. Pour ce site, le temps de retour moyen des séismes est d’environ 1 000 ans.

A partir des résultats de cette thèse, en particulier de la ré-interprétation de l’histoire sismique libanaise, du temps de retour moyen des séismes sur la faille de Yammoûneh, et de sa vitesse de glissement de l’ordre de 5 mm/an, nous concluons que le prochain séisme sur cette grande faille active risque de se produire dans un futur plus proche qu’estimé jusqu’ici. Dans cette région en croissance démographique, il est donc urgent de réévaluer l’aléa sismique à la lumière de ces nouvelles données.

Abstract

The left-lateral Levant transform system (“Levant fault”) displays a conspicuous, 160-km-long restraining bend whose location coincides with modern-day Lebanon. The Yammoûneh strike-slip fault, whose surface trace bisects Lebanon, has usually been considered the main active strand of the Lebanese restraining bend, although several authors have recently voiced doubt on its present-day activity.

By combining geological observations, quantitative geomorphology and in situ cosmogenic surface exposure dating, we are able to lift this doubt and demonstrate that the Yammoûneh fault is quite active, that it consistently offsets geomorphic markers of climatic origin, from the scale of meters to kilometers, due to the cumulative effect of recurrent, if infrequent, large earthquakes. Its Late Pleistocene to Holocene slip rate, constrained by surface exposure ages of offset limestone-clast fans, is 3.8 to 6.4 mm/yr.

Structural and geomorphic observations from the Lebanese coast and the foreland of Mount Lebanon provide evidence of active thrust faulting and folding, implying that SE-dipping thrust ramps govern the growth of anticlines in the foreland of Mount Lebanon, accounting for most the transpression related to the bend of the Levant fault. These active thrusts appear to continue offshore, as far south as Beirut and probably Saida. In this new model, the Roûm fault is simply interpreted as one of the lateral ramps transferring slip from the Jordan Valley fault to these thrusts, and Mount Lebanon is a thrust wedge completely surrounded by active faults.

This new model of the main active faults of the Lebanese restraining bend calls for a critical re-assessment of historical earthquakes. We propose that the source of the M>7 earthquake and tsunami that destroyed Beirut in A.D. 551 was the offshore Mount Lebanon thrust rather than the Yammoûneh fault. Furthermore, we demonstrate, by combining historical sources, qualitative geomorphic evidence and paleoseismology, that the latest event along the Yammoûneh fault was the great (M~7.5) A.D. 1202 earthquake, and that the two A.D. 1759 events (M~6.6 and 7.4) were generated by the Râchaiya-Serghaya fault system.

Paleoseismic trenching of a paleo-lake in the Yammoûneh basin yield further information on the earthquake record of this fault over about 15 kyr (~14 events). The average recurrence time of earthquakes at this site is ~1000 yr.

Based on the re-assessment of the three largest historical earthquakes of the restraining bend, on the long-term mean return time of events along the Yammoûneh fault, and on its 5mm/yr slip rate, we conclude that the next large earthquake on this fault is probably due earlier than previously thought. Seismic hazard in this densely populated region should be re-assessed accordingly.

Sommaire

Résumé	3
Abstract	4
Introduction	8
The Levant fault system	8
The Lebanese Restraining Bend	8
Goals of this work	10
1 Structure et failles actives du coude transpressif libanais	12
1.1 Large-scale geomorphology and geological history	12
1.1.1 Relief	12
Mount Lebanon	12
Anti-Lebanon	15
Beqaa plain	15
1.1.2 Stratigraphic and geologic setting	16
Jurassic and Cretaceous extension	16
Cenomanian to Eocene platform subsidence, and Miocene folding	18
Plio-Quaternary shortening and uplift, and probable Quaternary glaciation	18
Summary: geologic history of the LRB	19
1.2 Active faulting and tectonic evolution	19
1.2.1 The Yammoûneh fault	22
Overall geometry, geology and morphology	22
Left-lateral offsets	25
1.2.2 Mount Lebanon: a ramp mega-anticline bounded by active thrusts	32
Mount Lebanon flexure and Qalat-Tourbol anticlines	32
Tripoli, Halba and Qoubayat thrusts	33
Roûm lateral ramp	38

Nîha thrust	40
Active bookshelf faulting within Mount Lebanon	41
1.2.3 The Râchaïya-Serghaya system and the Hermon push-up	45
1.2.4 Summary: 3D active faulting in the Lebanese restraining bend	46
2 Cinématique du coude transpressif libanais	49
2.1 Existing kinematic constraints	49
2.1.1 Geological offsets	49
2.1.2 Plate motion models based on seafloor magnetic anomalies	49
2.1.3 Geomorphic, paleoseismic and archeoseismic offsets	50
2.1.4 GPS measurements	51
2.1.5 Summary of existing kinematic constraints on the LFS	51
2.2 Constraints on the post ~25-ka slip rate of the Yammoûneh fault (Lebanon) using in situ cosmogenic ^{36}Cl dating of offset limestone-clast fans	53
Abstract	53
2.2.1 Introduction	53
2.2.2 Geomorphic offsets along the Yammoûneh fault	55
Active faulting in the Lebanese restraining bend	55
Site 1: Offset fans in the Yammoûneh Basin	57
Site 2: Offset of the Zalqa fan	57
2.2.3 Cosmogenic dating of offset alluvial fans	61
Chlorine-36 surface exposure dating of limestone cobbles	61
Results	63
Slip rate	66
2.2.4 Summary and discussion	67
2.3 Jbab el-Homr	68
2.3.1 The Jbab el-Homr basin	68
2.3.2 Cumulative offsets	68
2.3.3 Time constraints	77
2.4 Aarîd Mtaïyouhâne	78
2.5 Discussion: kinematics of the LRB	83
2.5.1 Mid-Pleistocene to Holocene kinematics of the Yammoûneh fault	83
Summary of offsets along the Yammoûneh fault	83
Climatic origin of the offsets	84

Comparison with the regional climate record	85
2.5.2 Plio-Quaternary kinematics of the Yammoûneh and Roûm faults	91
Plio-Quaternary slip rate along the Yammoûneh fault	91
Inferred Plio-Quaternary slip rate along the Roûm fault	93
2.5.3 Consequences on the Plio-Quaternary kinematics of the Levant fault system across the Lebanese restraining bend	94
Shortening across the Mount Lebanon Thrust	94
Kinematic compatibility with the Ghab and Jordan valley faults	96
Extrapolation to the Roûm fault	97
3 Sismicité long terme du coude transpressif libanais	98
3.1 Historical earthquakes of the LRB area	98
3.1.1 Catalog of historical events in the LRB area	100
3.2 Sources of the large AD 1202 and 1759 Near East earthquakes	117
Abstract	117
3.2.1 Introduction	117
3.2.2 Macroseismic constraints on the 1202 and 1759 events	119
3.2.3 Surface faulting	119
3.2.4 Paleoseismic evidence	120
3.2.5 Summary and discussion	124
3.3 Paleoseismic trenching in the Yammoûneh basin	126
3.3.1 Setting of the Yammoûneh basin	126
3.3.2 The Kazzâb trench	132
Trench location	132
Exposed stratigraphy	133
Coseismic deformations	137
Dating	156
Discussion	159
Conclusion	165
Références	170

Introduction

The Levant fault system

The northward motion of Arabia away from Africa, and the corresponding opening of the Red Sea and Gulf of Aden, started in the Early Miocene (25–20 Ma) [Courtillot et al., 1987; Manighetti et al., 1997, 1998, e.g.]. All along the Levantine coast of the Eastern Mediterranean, this motion is taken up on a 1000-km-long transform fault, the Levant Fault System (LFS), which connects the NW tip of the Red Sea to the SW end of the East Anatolian Fault System (figure 1).

Historically, Lartet [1869] was the first to interpret the Dead Sea “rift” as resulting from left-lateral shear rather than continental rifting. Dubertret [1932] proposed the first estimate (~ 160 km) of the total horizontal motion on the LFS. This hypothesis, however, then lay dormant for about twenty years, until Quennell [1958, 1959] revived it. Based on the restoration of offset Precambrian to Cretaceous geological features, he argued for a total left-lateral slip of 107 km, and suggested that a younger movement of 45 km explains several prominent geomorphic features such as the shape of the deeper, northern basin of the Dead Sea. Freund et al. [1965; 1968; 1970] refined this estimate by demonstrating that all the igneous and sedimentary rocks of Precambrian to Late Cretaceous age on both sides of the LFS are offset left-laterally by 105 km. They also argued [1968] for a post-Miocene offset of 40–45 km, based on the amount of back-slip necessary to close transtensional basins all along the Dead Sea fault.

Today, this strike-slip model and cumulative offsets are generally accepted. Specific issues that remain unresolved include the identification and mapping of the active northward continuation (i.e. north of Lake Tiberias) of the Dead Sea fault, precise measurement of the slip rates and slip partitioning on the main segments of the LFS, as well as the modern and long-term seismogenic potential of the fault system.

The Lebanese Restraining Bend

The LFS has been studied in greater detail between the Gulf of Aqaba and Lake Tiberias than to the north. Both south and north of Lebanon, the fault’s surface trace is composed of en-echelon strike-slip segments, separated by large pull-aparts or small push-ups. All prominent basins along the LFS (Dead Sea, Lake Tiberias, Hula basin, cf figure 1) are associated with left steps/jogs of the fault.

This is sharp contrast with the Lebanese area (figures 1 and 2), where the Levant fault’s trace veers to the right, forming a 160-km-long restraining bend. The resulting strike-perpendicular strain has long been held responsible [e.g. Quennell, 1959; Freund et al., 1970] for crustal shortening and mountain

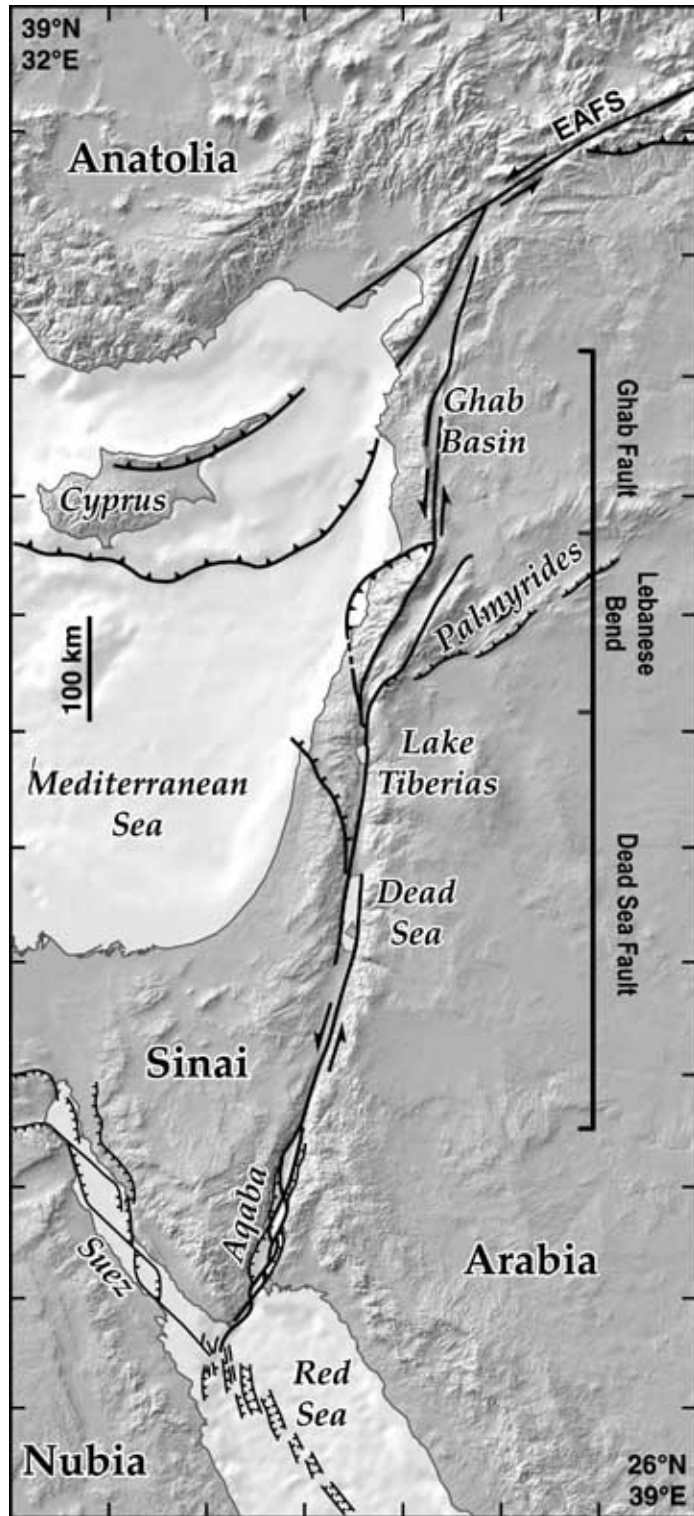


Figure 1: Map of the Levant Fault System

The trace and geometry of the faults within the Lebanese restraining bend are discussed in chapter 1.



Figure 2: Oblique, NE-looking satellite image of the Lebanese restraining bend
 Note the (dark blue) Lake Tiberias, the (white) snow-covered Mount Lebanon, and the Palmyrides folds to the east of Mount Lebanon.

building in the Lebanon and Anti-Lebanon ranges, although how exactly the crust shortens and thickens is not well understood.

Goals of this work

Most observations and theories pertaining to the Lebanese restraining bend's geology predate the advent of modern plate tectonics, due to the troubled political situation in Lebanon from 1975 to 1992. As a result, several first-order questions remain open to this day. The aim of this work is to address some of these issues:

- While the Lebanon and Anti-Lebanon mountain ranges (3100 m and 2700 m a.s.l.) likely result from transpression across the restraining bend, the active structures responsible for mountain growth within bend, as well as the precise coupling between NNE-SSW strike-slip and transpression, are poorly constrained. Chapter 1 presents a detailed account of the active faults of the Lebanese restraining bend, based on geological and geomorphic data.
- Various estimates of the slip rate along the LFS range from 2 to 10 mm/yr (cf section 2). Most of these estimates concern sections of the fault system located well south of the restraining bend. Little

is known of the slip rates along the main Lebanese faults. Chapter 2 presents new constraints on the kinematics of the region. In particular, the first direct measurement of the modern slip rate along the Yammoûneh fault, the main on-land continuation of the LFS in Lebanon, are presented and discussed. A first-order estimate of the rates on other faults of the restraining bend is then proposed, and compared with known data or models from elsewhere on the LFS.

- Near East historical accounts describe large earthquakes during the pre-instrumental period, far stronger than the events instrumentally recorded during the 20th century except for the recent 1995, $M_w \sim 7.3$ Aqaba earthquake. Sources for these historical events are generally assigned to latitudinal sections of the LFS. Such inferences are ambiguous in the Lebanon area, again because the hierarchy of active faults within the restraining bend, and their segmentation, are little known. Chapter 3 addresses some of these issues. It is based on, and presents in detail the results of the first paleoseismological investigation on the Yammoûneh fault, and discusses its implications for earthquake recurrence along this portion of the LFS. Our re-interpretation of the largest historical earthquakes in Lebanon (AD 551, 1202 and 1759) has critical consequences on modern-day earthquake hazard assessment in the region.

This work would have been impossible without the constant support of the Lebanese Center for Geophysical Research. Eight field trips related to this project were conducted in Lebanon during this PhD. At the present time, two articles discussing our results are published or in press [Daëron et al., 2004a, 2005], and are included in this thesis report (sections 2.2 and 3.2). Due to the presence of non-French-speakers in the jury of this PhD, the present report is written entirely in English.

- Chapitre I -

Structure et failles actives du coude transpressif libanais

1.1 Large-scale geomorphology and geological history

1.1.1 Relief

The first order traits of the geology and physical geography of Lebanon are fairly well known [e.g. Blanche, 1847; Zumoffen, 1926; de Vaumas, 1948, 1954; Dubertret, 1975b; Beydoun, 1977; Sanlaville, 1977; Walley, 1998]. The topography is organized into two main, roughly parallel mountain ranges rising above 2400 m (Mount Lebanon, Anti-Lebanon) separated by the Beqaa plain (figures 3 and 4). The two ranges follow the two main branches of the Levant Fault System (LFS) north of the Hula basin, the Yammoûneh and Râchaïya-Serghaya faults, respectively (figure 6).

Mount Lebanon

Mt Lebanon, the highest of these ranges, culminates at 3088 m a.s.l. (Qornet es-Saouda, cf fig. 3). It follows the NNE-trending jog of the Eastern Mediterranean coastline between Israel and Syria, forming a massive, 160-km-long barrier, above 2000 m on average, with few passes, all of them more than 1500 m a.s.l. Its crest is a radical water divide. Only the Nahr el-Kebir and Litâni rivers swing around the northern and southern extremities of the range, respectively (fig. 3). Both extremities of Mt Lebanon, north of Qoubayat and south of Marjavoûn, are abrupt relief terminations, coinciding with the two opposite, 25° swings in strike of the Yammoûneh fault (figures 3, 4 and 6).

The mountain is broadest and highest in the north, with three main massifs (Qornet es-Saouda, Jabal Mnaïtra and Jabal Sannîne) separated by broad erosional cirques (fig. 3 and 4). The massifs are capped by flat, barren, gently west-sloping surfaces (2000–2500 m a.s.l.) poked with karstic dolines. Farther west, the relief falls more rapidly toward the sea, with the steepest slopes (apart from cirque cliffs and river gorges) roughly along the Lebanese “flexure” (figure 6). This fall is particularly spectacular near Joûmieh where the mountain front towers 500–800 m a.s.l., only 1400 m east of the sea shore (figure 20, p.33). The crest of the range is generally less than 30 km away from the sea, but only 2-3 km west

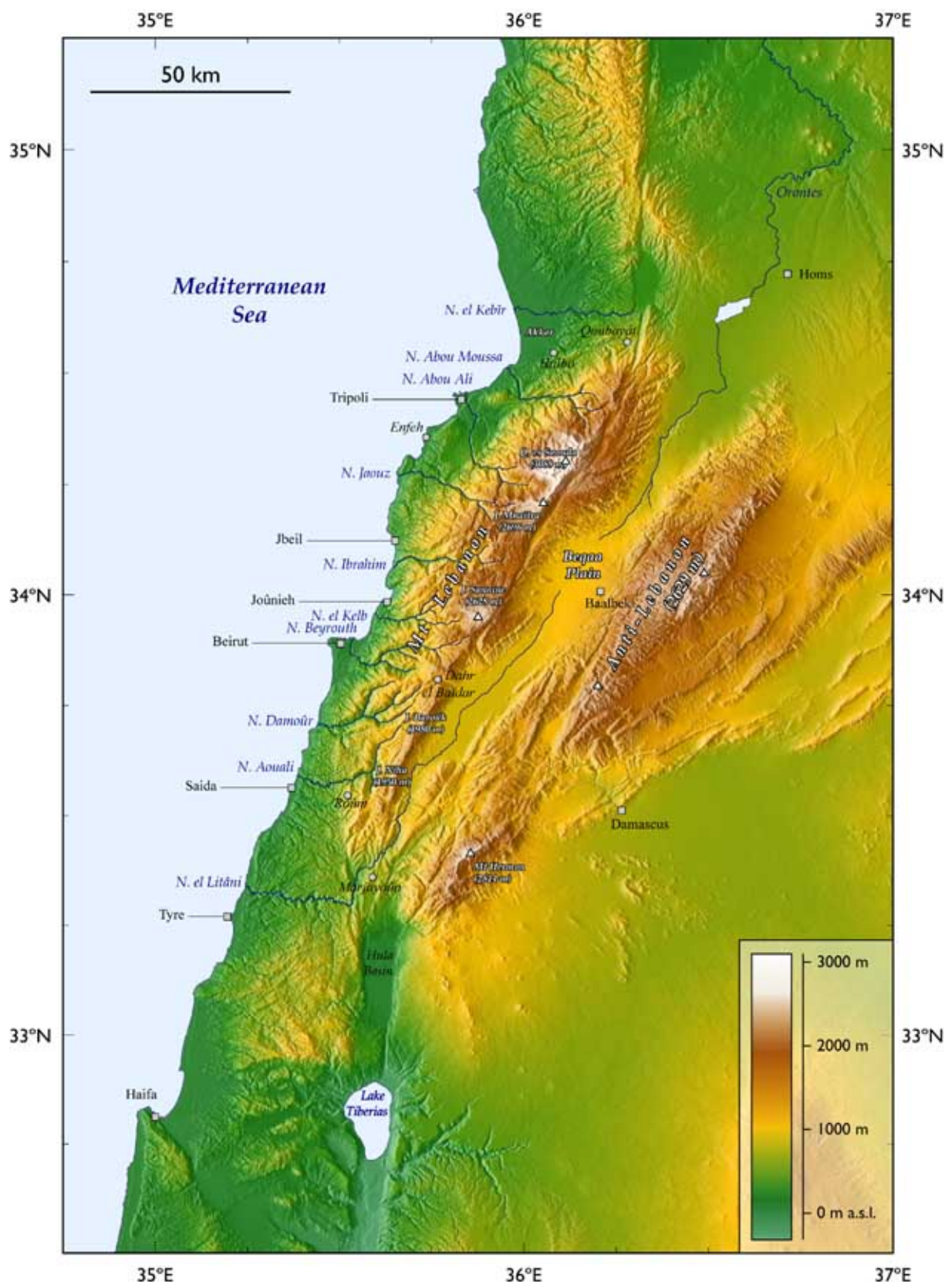


Figure 3: Topography of the Lebanese region
Squares and circles show the main cities and locations mentioned in the text.



Figure 4: Satellite image of the Lebanese region



Figure 5: Flight of abandoned marine terraces near Chekka

of the trace of the Yammoûneh fault, which it closely follows. East of the steep, east-facing wall along the fault, lower (~1800 m) and narrower (~10 km) plateaus form an east-sloping bench between the mountain backbone and the Beqaa plain (figure 11). While much broader, the western flank of the range is profoundly incised by the deep canyons of eight large rivers (“*Nahr*”) that dissect it into narrow, perched interfluves (“*Dahr*”). The headwaters of some of these rivers (Nahr Abou Moussa, N. Abou Ali, N. Jaouz, N. Ibrahim, N. el Kelb and N. Beyrouth) reach into the cliff-bounded cirques that divide the range into separate massifs.

South of the Dahr el-Baïdar pass (1500 m), where the Beirut-Damascus road crosses the mountain, the relief is less massive and the average elevation lower than in the north. Between Roûm and Marjavoûn, the Lebanese flexure rapidly converges toward the Yammoûneh fault, as it does also between Halba and Qoubayat in the north (fig. 3 and 6). The highest part of the southern stretch of Mt Lebanon is a narrow (5-km-wide) spine, the Jabal Baroûk, that culminates at 1980 m a.s.l., hugging the Yammoûneh fault’s trace west of the Beqaa.

Between the Nabatiyeh plateau south of Saïda and the Akkar alluvial plain north of Tripoli, the Mediterranean coastline is generally convex westwards, with only two peninsulas jutting out to sea (Ras Beyrouth and Tripoli/el-Mina) and two narrow embayments at Joûnieh and Enfeh. The broad structural re-entrant between Jbeil and Beirut brings the sharp Lebanese flexure closest to the sea. Nowhere, except at Ras el Kelb and Ras Chekka, is the coastline marked by steep, abrupt cliffs. Between Tripoli and Saïda, the coastal zone is characterized by flights of marine terraces and abandoned shorelines that rise up to about 500 m a.s.l. (figure 5) [Sanlaville, 1977].

Anti-Lebanon

The topography of the Anti-Lebanon mountains, which are connected eastwards with the Palmyrides, is more complex, in part because the corresponding branches of the Levant fault system are less continuous than the Yammoûneh fault. The two main faults (Râchaïya and Serghaya) do not define the western limit of Anti Lebanon (figure 6). They are offset by a prominent, ~15 km right step. Mount Hermon, the highest summit in the area (~2800 m a.s.l.) rises obliquely within this step. To the north, the Anti-Lebanon range culminates at 2629 m a.s.l. (Talât Moussa, cf fig. 3).

Beqaa plain

Between the Lebanon and Anti-Lebanon ranges, the Beqaa plain is a flat, 7–18 km-wide trough, ~1000 m a.s.l. Around 34°N, a gentle water divide separates the Orontes and Litâni catchments. The

Orontes flows north into the Homs plain, with which the northern Beqaa connects smoothly. The course of the Litâni river toward the south crosses a series of narrow ridges, including the southern tip of the Barouk spine. Other small mountain ridges separate the southern Beqaa from the Hula basin.

1.1.2 Stratigraphic and geologic setting

The geology of Lebanon is dominated by marine shelf carbonates of Lower Jurassic (Liassic dolomites, ~200 Ma, Chouane formation) to Pliocene age (Piacenzian marls, ~2–3 Ma). “Basement” rocks underneath this 4–7-km-thick sedimentary sequence do not crop out in Lebanon, but probably resemble those found to the south and under the Palmyrides. They include Permian continental clastics, and Triassic shallow marine clastics, carbonates and evaporites deposited in an extensional environment [Garfunkel, 1998]. The Lebanese carbonate succession comprises two powerful, well-bedded, massive, cherty shallow-water limestone sequences (Middle to Upper Jurassic, Toarcian to Tithonian, 175–140 Ma, up to 1750 m thick; and Middle to Upper Cretaceous, Aptian to Santonian, 110–70 Ma, up to 3 km thick). Both sequences are typical of a platform environment, with subsidence controlled by thermal cooling following a rifting event [e.g. McKenzie, 1978].

Jurassic and Cretaceous extension

While Triassic rifting is well documented in SW Israel and in the Palmyrides [e.g. Garfunkel, 1998, and references therein], only one prominent episode of rifting is visible in Lebanon. It coincides with a major stratigraphic discontinuity in the Upper Jurassic and Lower Cretaceous. Between ~145 and ~105 Ma, the calcareous sedimentation was interrupted by deposition of the fluvial and estuarine Choûf sandstone formation [Dubertret, 1975b; Beydoun, 1977; Walley, 1998], indicating local, relative uplift and withdrawal of the sea, and by the emplacement of prominent levels of basaltic dolerite and shallow sub-aqueous, explosive tuffs. The basaltic volcanism (Bhannes-Tayasir basalts), which is also known in Syria and Israel, ranges in age from Oxfordian to Albian (150–100 Ma) and has a petrology (alkali-basalts, basanites and tholeites) and chemistry (OIB, REE) typical of rifting [Laws and Wilson, 1997]. The corresponding block faulting is very clear in the central part of Mt Lebanon, with many faults exhibiting a clear normal component. Most of these faults, which strike ENE-WSW on average, terminate upward within the Cenomanian (96–92 Ma).

This second rifting episode is probably linked with the formation of the Levant basin’s oceanic floor and the actual birth of a passive continental margin in the region [cf also ricou: Ricou, 1995]. This interpretation is corroborated by the striking change in the Albian-Turonian depositional environment along a hinge line following approximately the Lebanese flexure between Joûnieh and Batroun [Walley, 1998]. From SE to NW, the limestone facies shift from shallow marine/peritidal to deep water/pelagic as coeval deposit thicknesses increase threefold. All four famous Lebanese fossil fish outcrops, whose preservation is likely due to anoxic conditions, lie NW of this hinge line [Walley, 1998]. In spite of possible horizontal block rotation in the Tertiary, the ENE-WSW strike of the Upper Jurassic – Lower Cretaceous faults implies that the passive Levant margin formed at a similar orientation, perpendicular to NNW-directed seafloor spreading, rather than parallel to the present-day Levant coast.

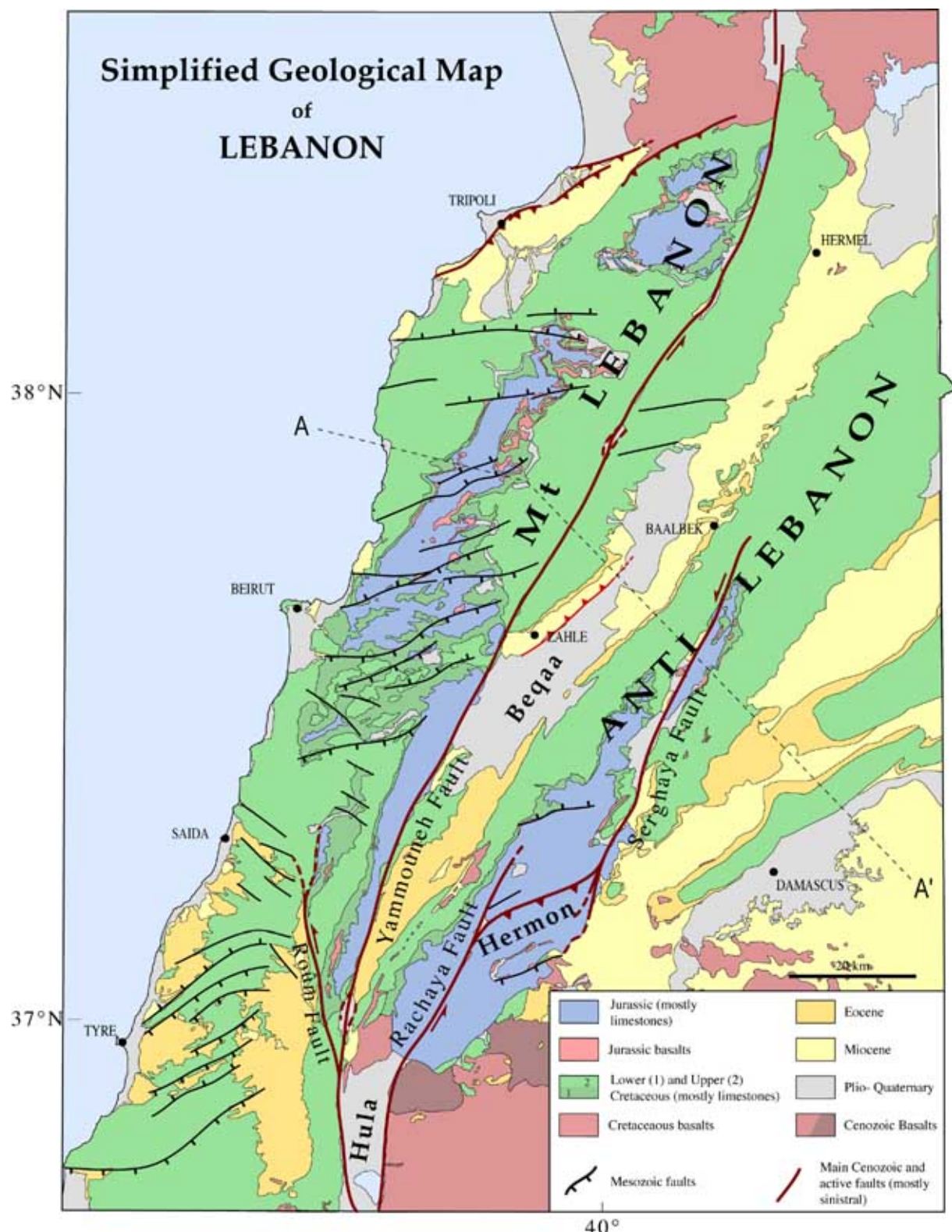


Figure 6: Geological map of Lebanon, modified from Dubertret [1955a]
 Active faults (in red) are discussed further in this chapter (section 1.2). Dashed line (AA') shows the location and orientation of the cross-section of figure 21.

Cenomanian to Eocene platform subsidence, and Miocene folding

On both sides of Mount Lebanon, in the Beqaa and Chekka-Tripoli region, the uniform, subsident sequence of Cretaceous shelf carbonates continued from the Cenomano-Turonian into the uppermost Cretaceous and Eocene, with no sizable angular unconformity, despite lateral facies (and thickness) changes. The Coniacian to Eocene part of this sequence is now missing on top of Mount Lebanon and of the Anti-Lebanon. Although this has been attributed to lack of deposition due to emersion and tectonic shortening at that time, correlated with an initial uplift of the Lebanese mountains, the conformable geometry on the flanks of the ranges suggest erosion, after the Eocene, of a sequence initially rather continuous and uniform from the Levant margin to the Syrian platform, across both Mount Lebanon and the Anti-Lebanon. The Oligocene, on the other hand, is unknown in Lebanon, which suggests regional regression of the sea, probably in response to both the opening of the Red Sea and collision along the northern edge of Arabia. Whether north of Beyrouth, near the mouth of Nahr el-Kelb and in the Batroun to Tripoli region, or near Zahle along the west side of the Beqaa, Miocene calcareous marls (Vindobonian, 16–7 Ma) lie unconformably on top of the Eocene or Senonian. In contrast with the Lebanese coast marine deposits, the marl sequence is lacustrine in the Beqaa. Except at the mouth of Nahr el-Kelb, the beds above and below the unconformity dip similarly steeply (figure 26, p.41), which indicates that much of the folding post-dates deposition of the Miocene.

Plio-Quaternary shortening and uplift, and probable Quaternary glaciation

The most recent sedimentary deposits in Lebanon are fluvial conglomerates of Pontian to Quaternary age (~5 Ma to present) in the Beqaa and in the Tripoli foreland, and marine Piacenzian marls and nodular limestone (~2–3 Ma) and Quaternary calcareous sandstones in the southern part of the Akkar plain. The Miocene lake in the Beqaa lasted into the Pontian [Dubertret, 1975b], with perhaps recurrence of lacustrine episodes in the Quaternary. Plio-Quaternary basalts drape the northernmost part of Lebanon, between the Akkar plain and the Yammoûneh fault. South of the Beqaa and at the northern tip of the Hula, basalts of a similar age have flooded valley floors and depressions. North of Beirut, Plio-Quaternary rocks, whether marine or continental, are folded on both sides of Mount Lebanon (see below), which implies that shortening continues at present along the edges of the range.

There are significant patches of Quaternary deposits within Mount Lebanon, mostly at elevations above 1200 m. These deposits are generally chaotic, coarse and poorly sorted (figure 7). They are mostly derived from the ~600-m-thick limestone units of Cenomanian and Turonian age that cap the mountain, and tend to rest on the lower Cretaceous sandstone bench underneath. They have generally been interpreted as a result of rock sliding and cliff collapse [Dubertret, 1975b; Besançon et al., 1973]. In Bcharre and Al-Arz (“Cedars”), however, we interpret the ridges parallel to the upper Qadisha valley as lateral moraines (figure 7) likely emplaced by a valley glacier during cold episodes of the Quaternary (LGM, Late Stage 6?...).

The presence of ice on top of Mount Lebanon during past glacial maxima has generally been discounted [Besançon et al., 1973], given its rather low altitude (max. 3080 m) and latitude (~34°N), particularly at a time (prior to 1975) when the systematic imprint of global climatic change had not been fully recognized. The issue remains controversial today, but the present permanent snow-line is only ~50 m above the summit of Mount Lebanon, and snow firns near Qornet es-Saouda are known to survive certain summers. As a coastal mountain barrier blocking the moisture-bearing westerlies blowing from the Mediterranean, the sea-facing summit of Mount Lebanon receives 1200–1600 mm of rainfall each

winter [Atlas climatique du Liban (Service météorologique du Liban), 1971], with local snow thicknesses of up to at least 10 m (figure 8). It thus seems likely that during the coldest epochs of the Quaternary, when the snowline was, in many places, hundreds of meters below its present level, the top of Mount Lebanon was ice-capped.

This would explain the flat summite surface on the Sannine, Mnaïtra and Qornet es-Saouda plateaus, the presence of particularly deep karstic dolines pitting that surface (subglacial karst?), and the spectacular horseshoe-shaped cirques (figures 7 and 9.a) that separate these plateaus. We thus suspect that a significant proportion of the chaotic “landslide” deposits may in fact be of glacial origin. An ice-cap atop Mount Lebanon during at least the last Quaternary glacial maxima would help explain not only the cirques, but also the size and shape of the huge valleys that are carved into the sea-facing flank of the range (figure 9.b). Although these valleys have been deeply re-incised by recent fluvial erosion, their original sections appear to have been U-shaped, and the manner in which their width tapers rapidly downstream (figure 9) suggest that they were once carved by glacier tongues spilling down from the ice-filled cirques at the edge of the ice-capped plateaus. Short and steep, hanging glacier tongues may also have existed on the eastern (leeward) side of Mount Lebanon, where the largest firns subsist today (figure 8).

Summary: geologic history of the LRB

In conclusion, based on stratigraphic evidence, the first-order geologic history of Lebanon may be divided into three distinct episodes, which are easily related to the plate-scale tectonic evolution of the Arabia-Africa Neotethys realm [cf also [Walley, 1988](#); [Butler et al., 1998](#)]. (1) NW-SE extension in the Triassic led to rifting and regional thinning of the crust, followed by subsidence and platform sedimentation throughout the Jurassic. (2) Renewed extension at the end of the Jurassic and the beginning of the Cretaceous successfully led to seafloor spreading, establishing the final geometry of the passive margin of the Levant basin. From the Middle Cretaceous to the Eocene, thermal subsidence continued unabated, in an otherwise peaceful tectonic environment. (3) A drastic change from extension to shortening occurred after the Oligocene, in relation with the opening of the Red Sea, the propagation of the Levant fault, and collision along the Zagros. Much of the shortening and topographic uplift in Lebanon took place at the end of and after the Miocene. Crustal shortening and mountain building continue today. The limestone sequence was perhaps eroded by 3–6 km (figure 21) on top of Mounts Lebanon and Hermon. As much as 1000 m of erosion might have occurred in the Plio-Quaternary, particularly during Mid- to Upper-Pleistocene glacial cycles.

1.2 Active faulting and tectonic evolution

A exhaustive study of geomorphic features resulting from tectonic action allows us to propose a new synoptic view of active faulting in Lebanon and of its relationship with the regional geological framework. There are three main fault systems at work in Lebanon: the Yammoûneh fault and related features, the Mount Lebanon coastal and offshore thrust system, and the Râchaïya-Serghaya fault system.

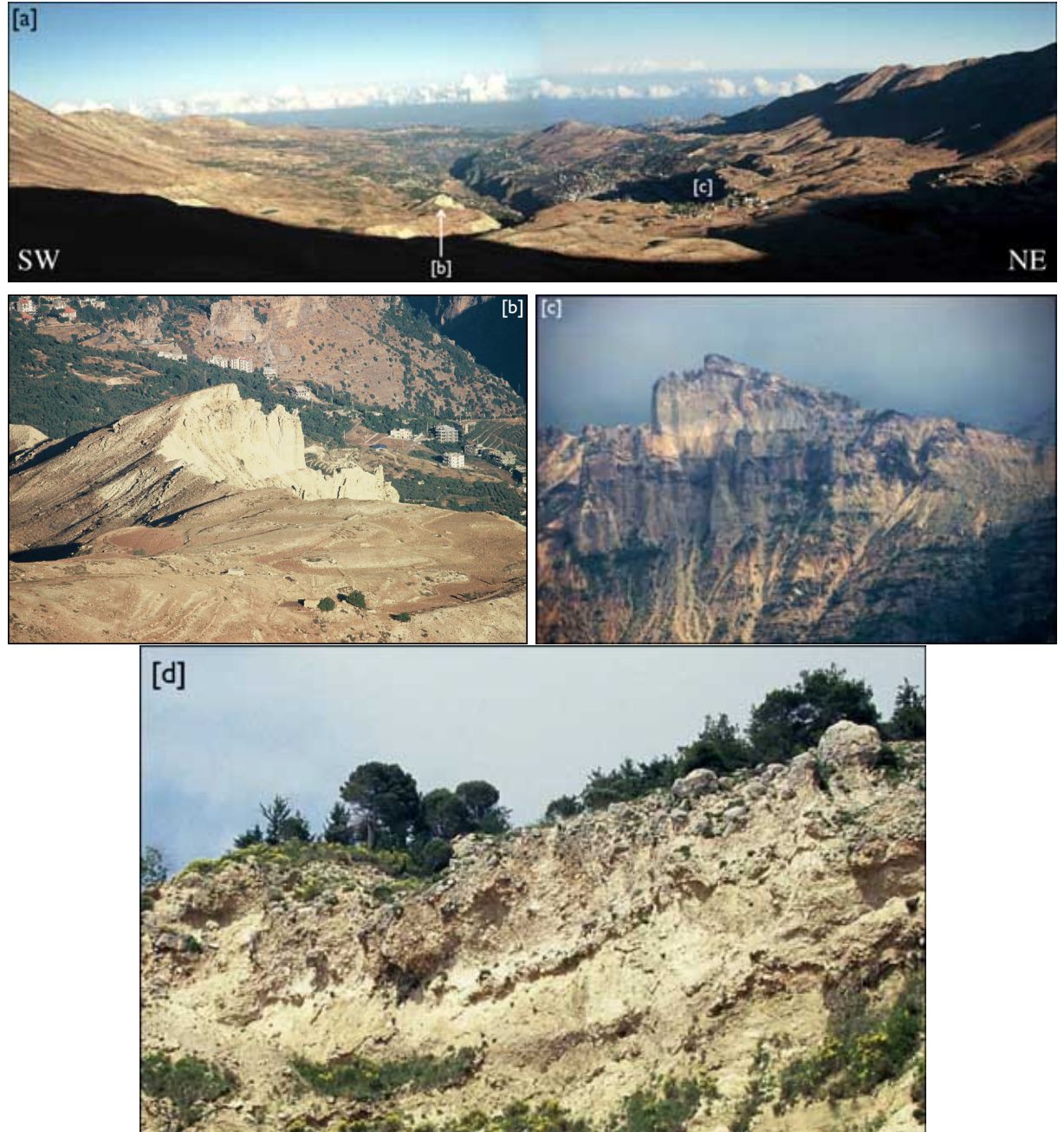


Figure 7: [a] NW-looking view of the Cedars cirque. [b] Southern lateral moraine. [c] Northern lateral moraine. [d] Close-up view of the northern lateral moraine.



Figure 8: Abundant snowfall atop Mount Lebanon

[a] S-looking view of a firn on the eastern flank of Mount Lebanon. This photograph and the next one were taken on July 1st, 2003. [b] Close-up of the same firn.

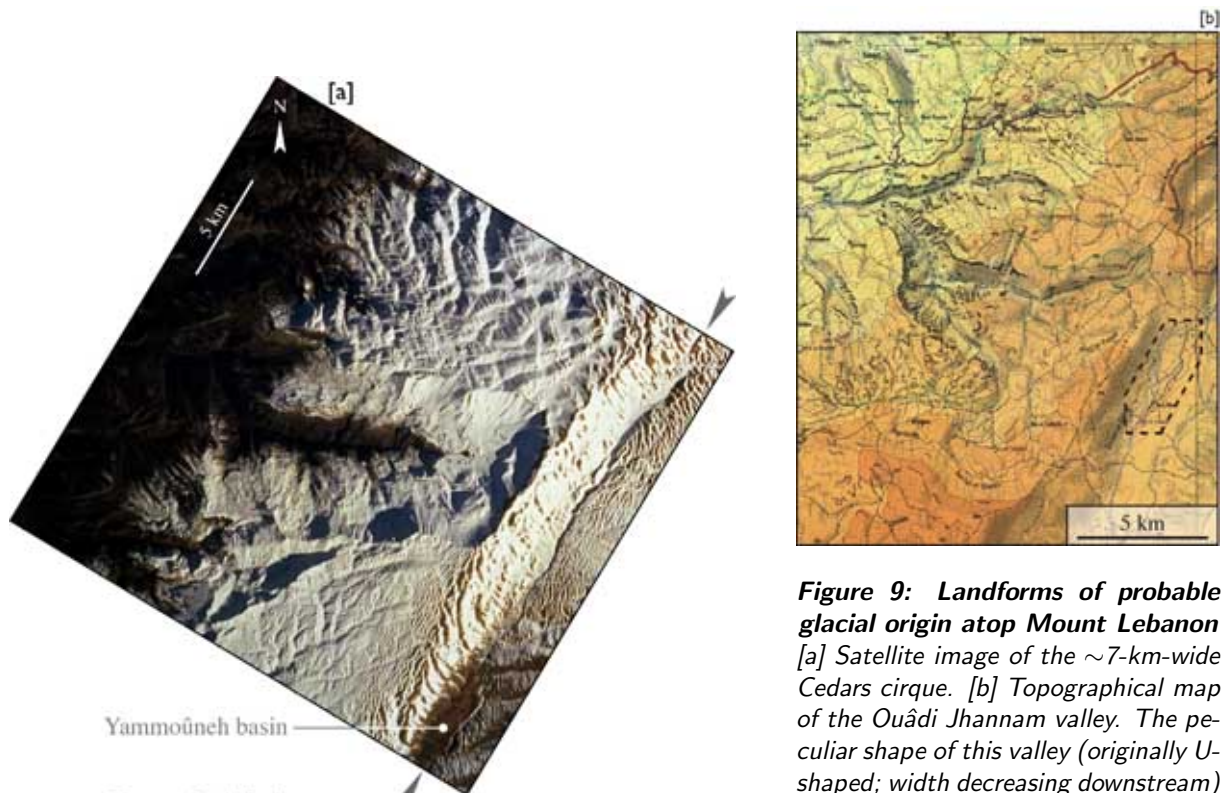


Figure 9: Landforms of probable glacial origin atop Mount Lebanon
 [a] Satellite image of the ~7-km-wide Cedars cirque. [b] Topographical map of the Ouâdi Jhannam valley. The peculiar shape of this valley (originally U-shaped; width decreasing downstream) may result from erosion by a glacier tongue fed by ice from the cirques or the summital plateaus.

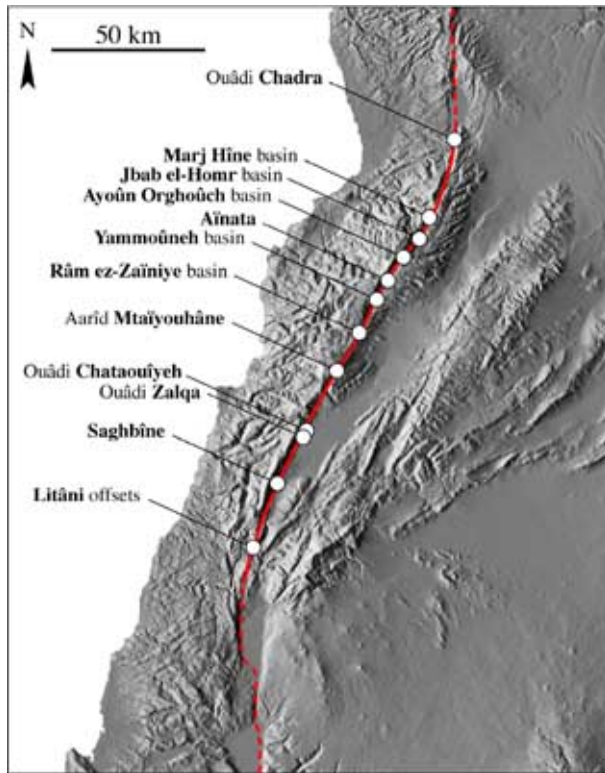


Figure 10: Sites along the Yammoûneh fault

The full red line shows the active trace of the Yammoûneh fault; the dashed red line represents sections of the LFS continuous with the Yammoûneh fault; white dots mark the location of sites mentioned in the text.

1.2.1 The Yammoûneh fault

Overall geometry, geology and morphology

Between the Litâni and Nahr el-Kebir, the trace of the Yammoûneh fault is broadly S-shaped over a length of ~ 160 km (figure 10). From its relationship to the present-day topography, it is clear that this swing of the Levant fault has controlled much of the growth of Mount Lebanon. The mountain range terminates abruptly where the fault resumes a N-S strike, at Qoubayat and Marjavoûn. Everywhere between these two bends, the fault steeply truncates the eastern flank of the range (figure 11).

In the south, between Marjavoûn and Chtaura, the fault juxtaposes the folded Jurassic beds of Jabal Baroûk and Jabal Niha (W) with mostly Eocene limestones, and with the Plio-Quaternary deposits of the Beqaa plain (E). In the north, the fault runs mostly across Cenomanian limestones. The compartment east of the fault stands about 500–1000 m above the Beqaa. The fault itself marks a sharp topographic step, up to 1000 m high. The structural relief across it, as estimated by Dubertret [1955b], is of the same order.

The fault is remarkably continuous, whether geologically or geomorphically. The active geomorphic fault trace is narrow and sharp everywhere at the surface. In most places it follows a broader cataclastic shear zone along which the limestones have been intensely brecciated and are currently exploited in numerous quarries.



Figure 11: Field view of the steep E flank of Mt Lebanon
looking north, from the SE tip of the Yammouné basin

Distinction between the active fault and the geological fault

In several areas, the actual trace of the active fault (figure 10) differs from the geologic fault mapped by Dubertret [1955a] and others. Between Saghbîne and Chtaura, for instance, the active fault trace lies west of the geologic fault, which was placed by Dubertret at the very edge of the Beqaa, between Jurassic and younger rocks.

Similarly, north of the Yammouné basin (figure 10), the active fault trace does not follow the Aïnata river but lies hundreds of meters to the west. It is marked by a distinct slope break on the steep eastern flank of Mount Lebanon. Near Aïnata, the fault follows the west side of shutter ridges (figure 12) that deviate tributaries of the Aïnata river. Two of these ridges are bounded by steep, fresh, upslope-facing cumulative scarps, whose apparent vertical offset is due to left-lateral motion (figure 12).

Finally, along the Ouâdi Chadra valley, the active fault trace lies west, not east, of the river. This is the locality where Butler et al. inferred the steeply W-dipping contact between carbonate gouge and brecciated pillows, west of Ouâdi Chadra, to be “a fault scarp unconformity” [Butler et al., 1997, 1998], demonstrating that the Yammouné fault had not been active since ~ 5 Ma. As we shall see later based on unambiguous geomorphic and paleoseismic evidence, this conclusion, derived strictly from the presence of undeformed pillows next to the carbonate gouge, is not tenable. Such discrepancies illustrate the fact that the techniques used for mapping geological and active faults are not the same. For the latter, geomorphic evidence is essential.

Dip of the Yammouné fault

There are few places where the dip of the Yammouné fault is exposed in section. Apart from the trenches that we excavated (cf section 3.3), and the outcrop near Ouâdi Chadra described by Butler et al. [1998], the fault zone is well exposed in a trench engineered to pump water a few hundred meters north of the road leading from Aïnata to the Cedars’ pass. There, recent faulting is visible between well-



Figure 12: Aïnata ridge

[a] S-looking view of the limestone ridge (foreground) that follows the active Yammoûneh fault, and of the village of Aïnata behind it. [b,c] Close-ups of the cumulative limestone escarpments. Vertical offset is apparent. Note the relatively “fresh” scarplet along the bedrock/colluvium contact.

bedded, undeformed, gently E-dipping Quaternary conglomerates and strongly faulted limestone breccia (figure 13). The uppermost part of the trench faces are unfortunately covered with rubble, hiding the possible extension of the fault to the surface, but mapping on a high-resolution (60 cm) satellite image demonstrates that the fault seen in section coincides with the active fault in map view. The dip of the active fault exposed in this trench is about 60°W, similar to that of most of the other faults in the gouge. This observation suggest that at least part or the topographic and geological throw on the east side of Mount Lebanon results from a component of high-angle reverse faulting. This is at odds with sections proposed by previous authors [e.g. Dubertret, 1975b; Walley, 1998], which sometimes show the Yammoûneh fault dipping steeply towards the east, implying that it had a normal component of throw.

Local complexities along the Yammoûneh fault

Although the active fault trace is sharp and continuous overall, it shows a few small-scale steps and bends. North of Zahle and as far north as Marj Hîne, a number of small basins are aligned along the fault.

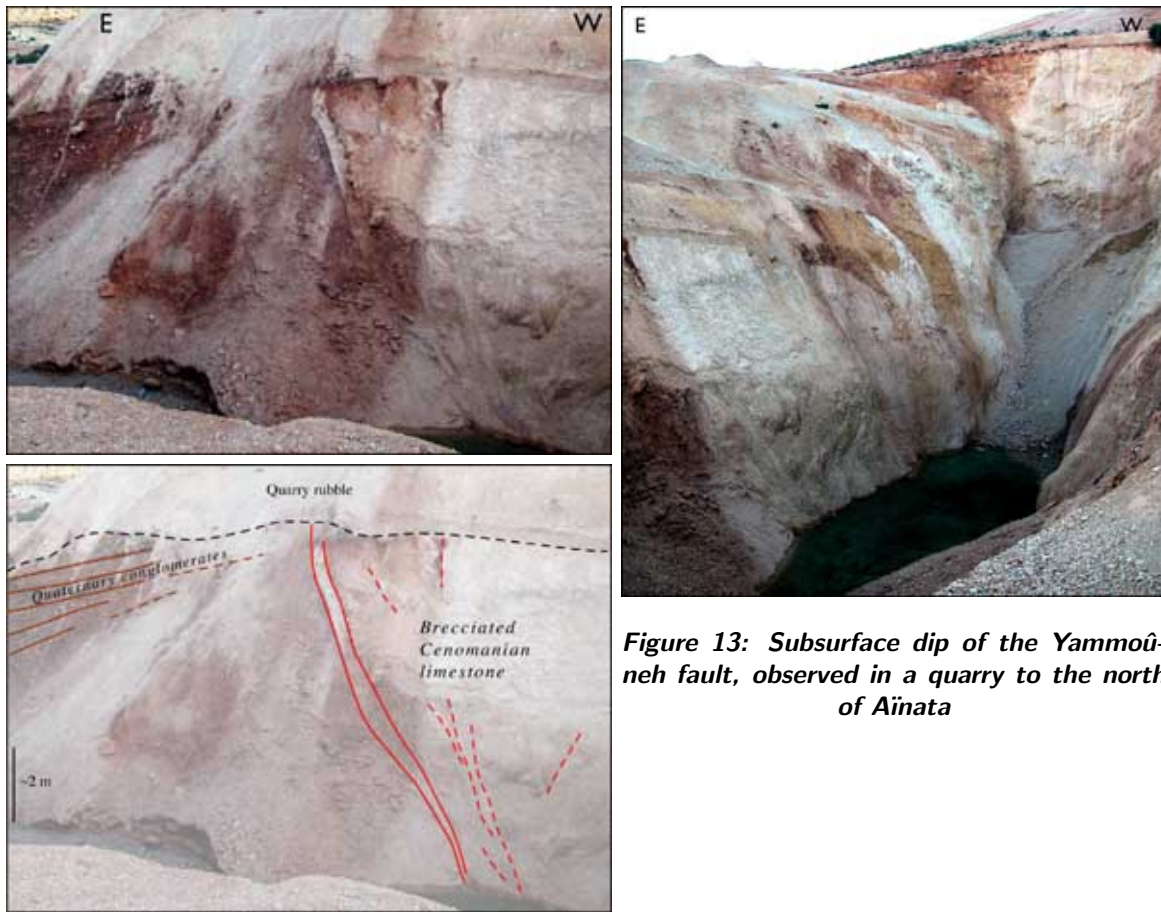


Figure 13: Subsurface dip of the Yammoûneh fault, observed in a quarry to the north of Aïnata

Some of these basins are clearly related to left-stepping of the fault trace, indicating that they formed as pull-aparts. This is the case of the Râm ez-Zâniye basin and of the larger Yammoûneh basin (figure 14). The latter was once flooded by a seasonal lake (cf section 3.3), and the former still is.

The three mountain-locked basins (Ayoûn Orghoûch, Jbab el-Homr and Marj Hîne) located north of Aïnata, on the other hand, do not exhibit clear pull-apart geometries. All of them are floored by flat, clay-rich deposits due to seasonal flooding, and are cross-cut by the active fault trace. Faulting in this northern area is more complex: north of the small Ayoûn Orghoûch basin, the fault exhibits two nearly parallel strands. In the Jbab el-Homr basin, the fault trace bends by $\sim 15^\circ$. This bend coincides with a ~ 3 -km-long push-up ridge (Jabal el-Gharbi) bounded by a minor strand west of the main fault trace. Midway into Marj Hîne (figure 15), the main fault trace, which follows the east side of the basin, steps 130 m to the right forming a large (10 m high, 400 m long) pressure ridge, “et Tall”. The geometry of faulting and its relationship with Quaternary and ongoing deposition in both the Yammoûneh and Jbab el-Homr basins will be described further in sections 3.3 and 2.3.

Left-lateral offsets

Numerous outstanding offsets of Quaternary landforms, some of which noted by previous authors [Khair, 2001; Butler et al., 1998] unambiguously demonstrate that the fault is active and left-lateral. The most common geomorphic features that display clear offsets are entrenched stream channels, alluvial fans or catchments including both. Such offsets exist at various scales, from kilometers to meters. Here, we review a few of the offsets that we find most convincing. Several of these offsets have been targeted for



Figure 14: Field views of the two most prominent pull-apart basins along the Yammoûneh fault
[a] N-looking view of the Râm ez-Zaiîniye basin. The fault trace south of this site (i.e. in the front of the photograph) is aligned with the eastern (i.e. right-side) edge of the basin, while the trace to the north is aligned with the western (left-side) edge. [b] S-looking view of the Yammoûneh basin. The fault trace enters the basin at its SE corner (center of the image). Cf section 3.3 for a detailed description of this basin.



Figure 15: Marj Hîne basin

The active trace of the Yammoûneh fault is mapped in red, over a composite image created by blending an aerial photograph and a 1:20,000 topographic map. The Marj Hîne basin's geometry suggests that it is not a simple pull-apart basin. It is cross-cut by the active fault, which created a push-up ridge (*Et Tall*) in the center of the basin.

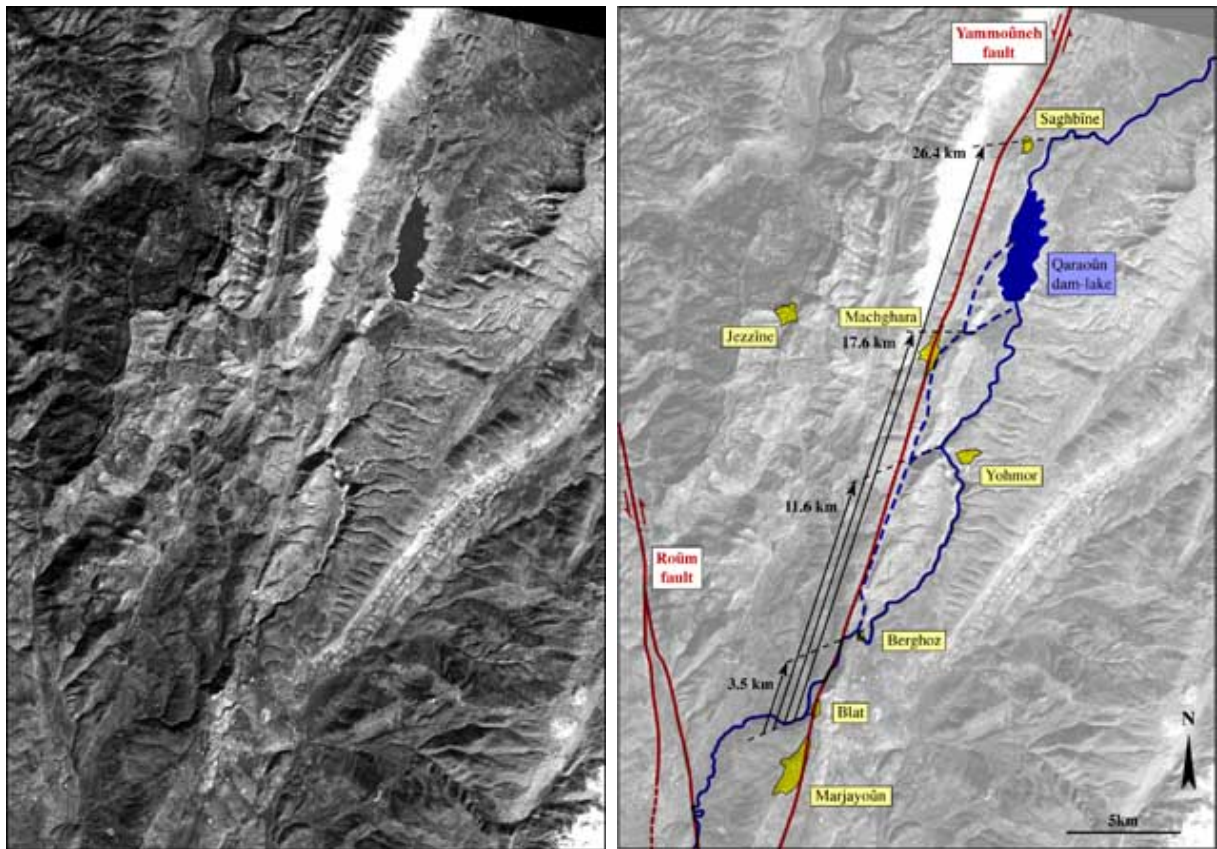


Figure 16: SPOT image and map of the Litâni river where it crosses the Yammoûneh fault

detailed topographic measurements in the field, and a few of the offset fans have been sampled for dating (cf chapter 2).

Litâni river offsets

The largest demonstrable offsets are those of the Litâni river, between Marjavoûn and Machghara (figures 10 and 16). The minimum offset is 3.5 km, along the N-S gorge that the river has incised along the fault from Blat to Berghoz. Because a prominent trough follows the fault north of this gorge all the way to Machghara and possibly Saghbîne, and because the present-day Litâni channel reaches the fault near Saghbîne, it is possible to argue that the trough is the trace of a former course of the Litâni incised along the fault, for as much as 17.6 or 26.4 km. Such values provide upper bounds of the maximum possible left-lateral offsets of the Litâni, which is the largest river to cross the Yammoûneh fault. Large offsets are expected for the longest, hence oldest, rivers crossing strike-slip faults [Gaudemer et al., 1989; Replumaz et al., 2001]. Between these extremes, another likely offset value is that from Blat to the abandoned wind-gap west of Yohmor (11.6 km). It is likely that these different offsets record different episodes of the interaction between climatic change and tectonic motion, which governed the entrenchment of the Litâni in the area where it crosses the Yammoûneh fault.

Jbab el-Homr offsets

Catchments flowing into the Jbab el-Homr basin from Qornet es-Saouda show a number of clear left-lateral offsets (figure 45, p.70), related to deposits and landforms of different ages. These are discussed in detail in section 2.3.1, and range between a few tens of meters and several kilometers (~ 3.15 km, ~ 1.2 km, ~ 490 m and 34 ± 11 m).

Northernmost section of the Yammoûneh fault

Two rivers north of the Marj Hîne basin (figure 10) show kilometric cumulative left-lateral offsets. Because smaller tributaries of these two rivers, west of the fault, show little to no offset where they meet with the main, more deeply incised channels of the rivers, Butler et al. [1998] failed to identify recent motion deflecting modern drainage systems along this stretch of the Yammoûneh fault.

We interpret the dogleg offsets of the main river channels to reflect cumulative slip along the fault, whose activity we demonstrate beyond doubt in this and following sections. We measure both offsets by back-slipping the image obtained by combining a Landsat scene (28.5 m pixel) with the 1:100000 topographic map and by direct measurements on the 1:50000 geological map (figure 17). The values obtained are 1885 ± 60 m for the Ouâdi Damdoûm, and 1640 ± 50 m for the Ouâdi Serkhâne. The uncertainties on these estimates are derived from the minimum and maximum values of displacements that do not produce an unacceptable misfit in the retro-deformation.

Beqaa plain

Between Chtaura and Saghbîne, the Yammoûneh fault follows the range front of the Jabal Baroûk. In most places, however, the fault trace does not coincide with the edge of the Beqaa. Shutter ridges of Jurassic or Cretaceous limestone separate the fault from the plain. Numerous rivers are deviated where they cross the fault, and some fans are offset from their feeder channels. Few such offsets, however, are clear enough to be quantified. Between Jdîta and Qabb Elias, for instance, it is difficult to find unambiguous matches of the upper and lower parts of the streams. Nevertheless, there are three examples of clear offset of catchments between Qabb Elias and Saghbîne.

The largest one is that of Ouâdi Chataouîyeh, whose channel is deeply incised in Jurassic limestone (figure 18). The dogleg offset of this channel is 590 ± 40 m. Downstream from the fault, the river has deposited a 1-km-wide fan on abraded Jurassic limestone which it now incises. The Chataouîyeh fanglomerates are fairly indurated and cemented, and are qualitatively similar to some found in the Jbab el-Homr basin (cf section 2.3.1)

The small stream immediately west of Saghbîne (figure 19) exhibits a clear-cut dogleg offset of about 540 m, incised entirely in Jurassic limestones. This offset is the only unambiguous one in a series of other, similar stream deflections to the north and south.

Another, smaller offset (~ 80 m) is that of the apex of the Zalqa fan. It is discussed in detail in section 2.2 (see also Daëron et al. [2004a]), together with the even smaller offset (~ 40 m) of another fan in the Yammoûneh basin, both of which were dated using cosmogenic ^{36}Cl .

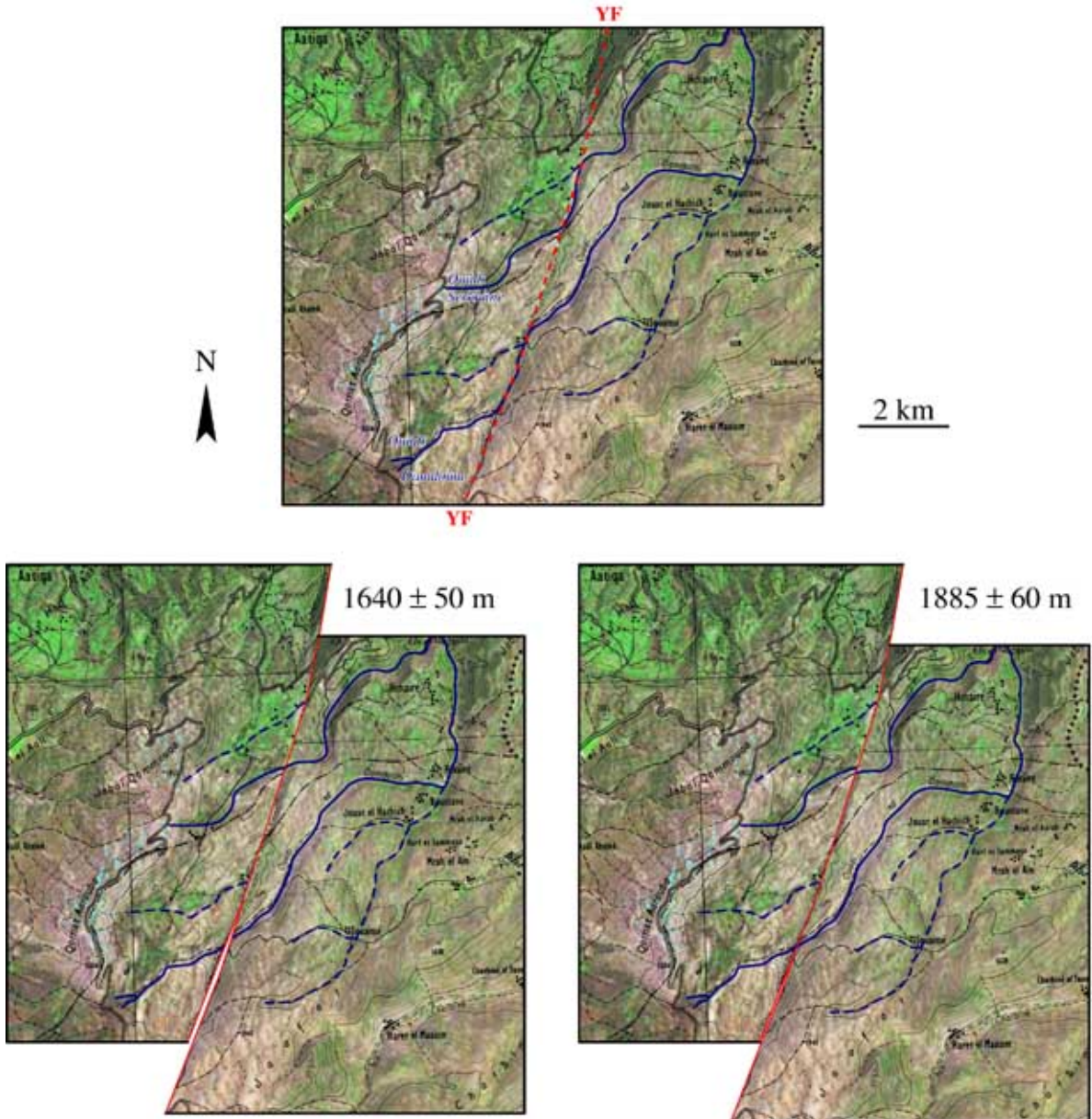


Figure 17: Cumulative offsets of Ouâdi Serkhâne and Ouâdi Damdoûm
(10 km NNE of the Marj Hîne basin)

Aarîd Mtaïyouhâne

At the foot of the Sannîne plateau (~2700 m), on the flank of Aarîd Mtaïyouhâne, the Yammoûneh fault offsets numerous channels incised in Cenomanian limestone. These offsets, which are described in detail in section 2.4, range from 4 to 200 m.

From the evidence summarized above, it is clear that the Yammoûneh fault is a major, active, left-lateral fault, with at places a second-order thrust component. The present-day kinematics and seismic behavior of the fault will be further discussed and quantified in chapters 2 and 3.

The topography, morphology and geology suggest that the development of the fault must have been intimately related to the formation of Mount Lebanon. Although the existence of relief adjacent to the restraining bend in the LFS has been attributed to strike-perpendicular shortening along the bent

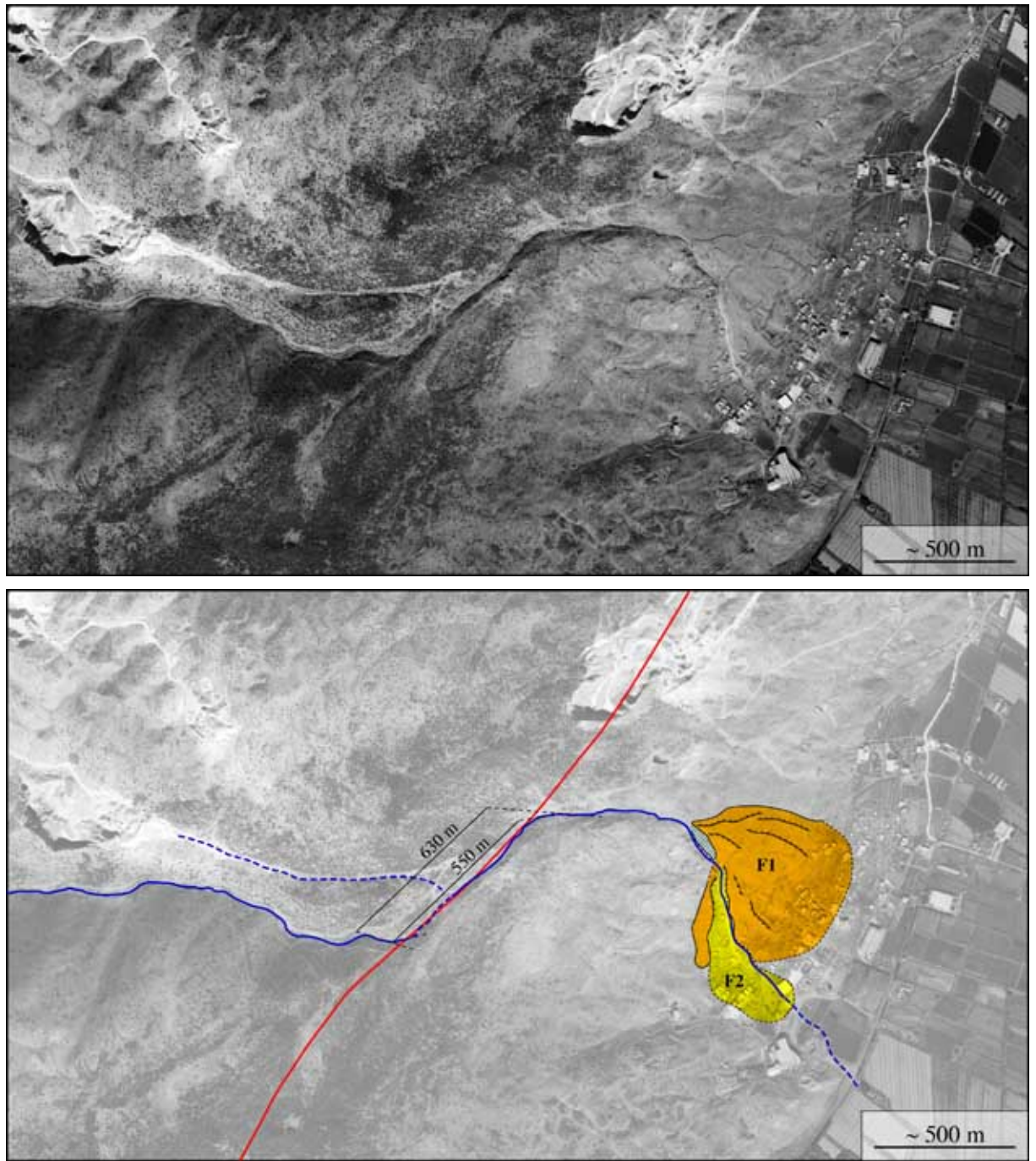


Figure 18: Cumulative offset of Ouâdi Chataouîyeh

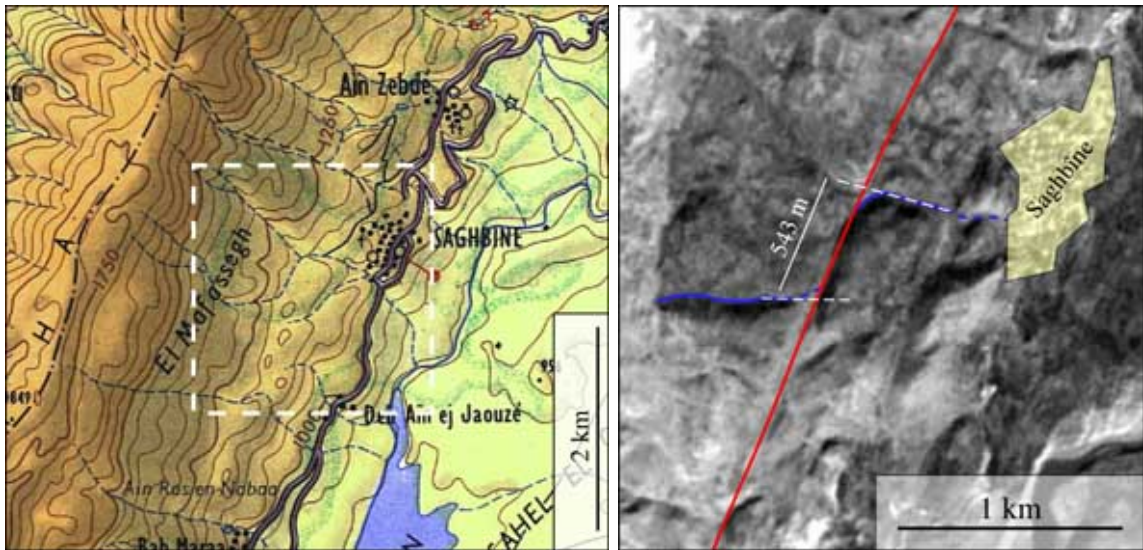


Figure 19: Offset river above Saghbîne

section of the fault, previous interpretations have emphasized diffuse folding, but have addressed neither the specific mechanisms of shortening, nor the relationships between folding and faulting. Below, we show that the Neogene, Quaternary and active faults surrounding Mount Lebanon are linked to the Yammoûneh fault. It is their combined action that has led to folding in and around Mount Lebanon, and to the uplift of a sliver of crust bounded by these faults.

1.2.2 Mount Lebanon: a ramp mega-anticline bounded by active thrusts

Mount Lebanon flexure and Qalat-Tourbol anticlines

The overall structure of Mount Lebanon is that of a broad asymmetric anticline [Dubertret, 1975b]. The most remarkable feature attesting to this anticlinal structure is the great, W-dipping “Lebanese flexure” that extends continuously from Qoubayat to Damoûr (figure 6). The dips of the flexed Cretaceous beds vary along strike, reaching 60° to 70° at places (figure 20). Rocks younger than Cenomanian crop out only west of the flexure. To the east, the core of Mount Lebanon exposes Lower Cretaceous and Jurassic rocks that reach almost into the Liassic in the narrow gorge of Nahr Ibrahim. Farther east, the mountain range is capped by subtabular Cenomanian limestones. Thus, in spite of complexities between the flexure and the summits plateaus (e.g. the Qartaba horst and thrust, Mesozoic normal faults), the overall architecture of the range in section is a 30-km-wide half anticline whose west limb plunges under the Mediterranean Sea between Beirut and Batroun, and whose east side is truncated by the Yammoûneh fault.

Between Batroun and Halba, the flexure, which here trends NE, veers far enough from the sea that foreland features are exposed in the Tripoli-Halba area. In this region, very young rocks (Vindobonian, Pontian and Piacenzian, from 16 to 2 Ma) are folded (figure 22.a), with fold axes trending either NE, roughly parallel to the flexure, or ENE. The most prominent folds are the Jabal Tourbol (680 m a.s.l., figure 22.b), Qalhât (430 m, figure 22.c) and Halba (370 m) anticlines. The marine calcareous sandstones that cap the Piacenzian marls south of Aabde, are tilted landwards (SE-dipping), and the Zgharta Quaternary fanglomerates (figure 22.d), which fill the synclinal trough between the Kousba flexure (figure 22.e)



Figure 20: N-looking view of the Lebanese flexure above Joūniché
Note the steeply W-dipping Aptian, Albian and Cenomanian limestones.

and the Qalhât-Tourbol anticlinal ridge, are involved in the folding. Dips in the Pontian conglomerates on both sides of the Tourbol anticline reach 30° (figure 22.f). Overall, the dips and stratigraphic ages of the folded sediments imply that much of the deformation postdates the Pliocene, and continues today. This deformation is typical of that found in active foreland fold-and-thrust belts, with younger, still growing folds affecting sediments deposited in front of the range [e.g. Avouac et al., 1993; Meyer et al., 1998; Van der Woerd et al., 2001].

Tripoli, Halba and Qoubayat thrusts

The three young anticlines in the Tripoli foreland all display an asymmetric structure, like Mount Lebanon, with steeper NW than SE limbs. Surprisingly, although asymmetric anticlines affecting young sediments in mountain piedmonts are nearly always associated with underlying thrust ramps [e.g. Philip and Meghraoui, 1983], there are very few descriptions of thrust faults in Lebanon [e.g. Dubertret, 1975b; Walley, 1998].

Our own investigation of the Tripoli piedmont confirm that thrust faults do indeed cut the west limbs of the Halba and Tourbol-Qalhât anticlines, and the Lebanese flexure itself. East of Tripoli, at the contact between the Pontian and the Cretaceous, the flexure is marked by overturned beds which are truncated by a SE-dipping thrust. A similar geometry is visible within the Cretaceous farther north [Dubertret, 1975a, Sir ed Danié sheet] and also between the Miocene and Cretaceous (figure 6). Both geometries are typical of fault-propagation folds. The asymmetry of the folding of the Piacenzian marls and the tilt of the Quaternary sandstones along the Halba anticline require the presence of a SE-dipping thrust ramp under this anticline. Between the Tourbol and Qalhât anticlines, the flat surface abraded in the Pontian by the Nahr Abou Ali and floored by the Zgharta fluvial conglomerates now hangs at least 60 m directly above the coastal plain, and is cut by a NE-striking escarpment (Babsâs cliff) that crosses

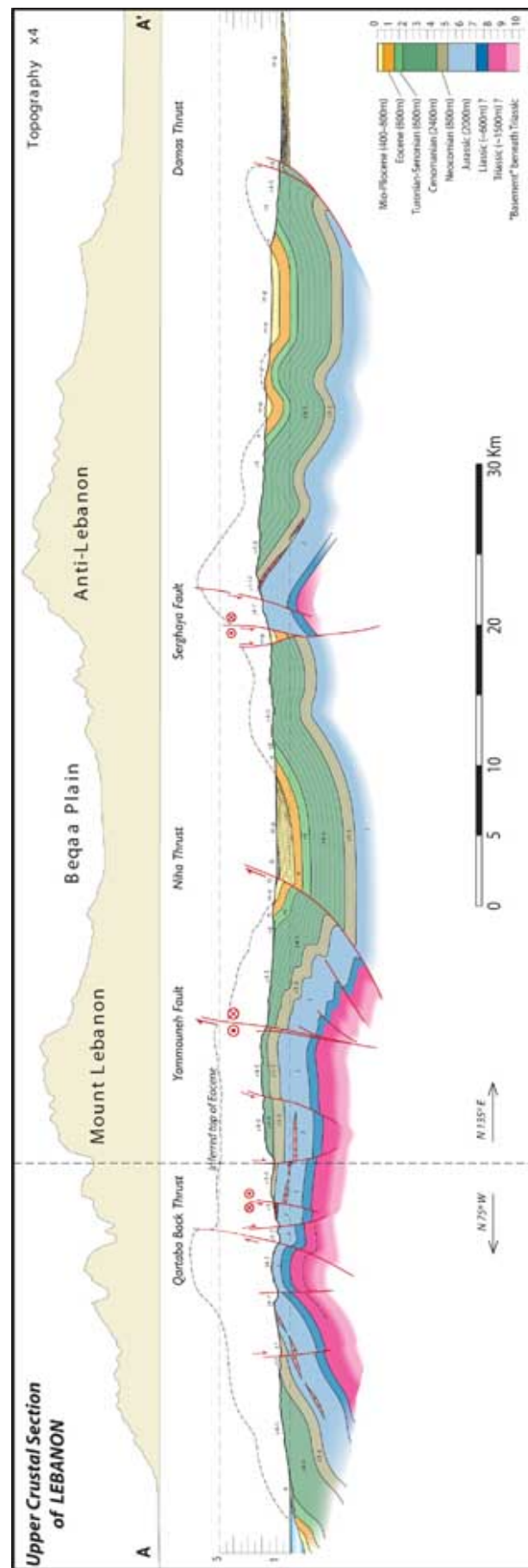


Figure 21: Geological cross-section of Mount Lebanon and the Anti-Lebanon
based on the maps and descriptions of Dubertret [1975a,b] and our own fieldwork.

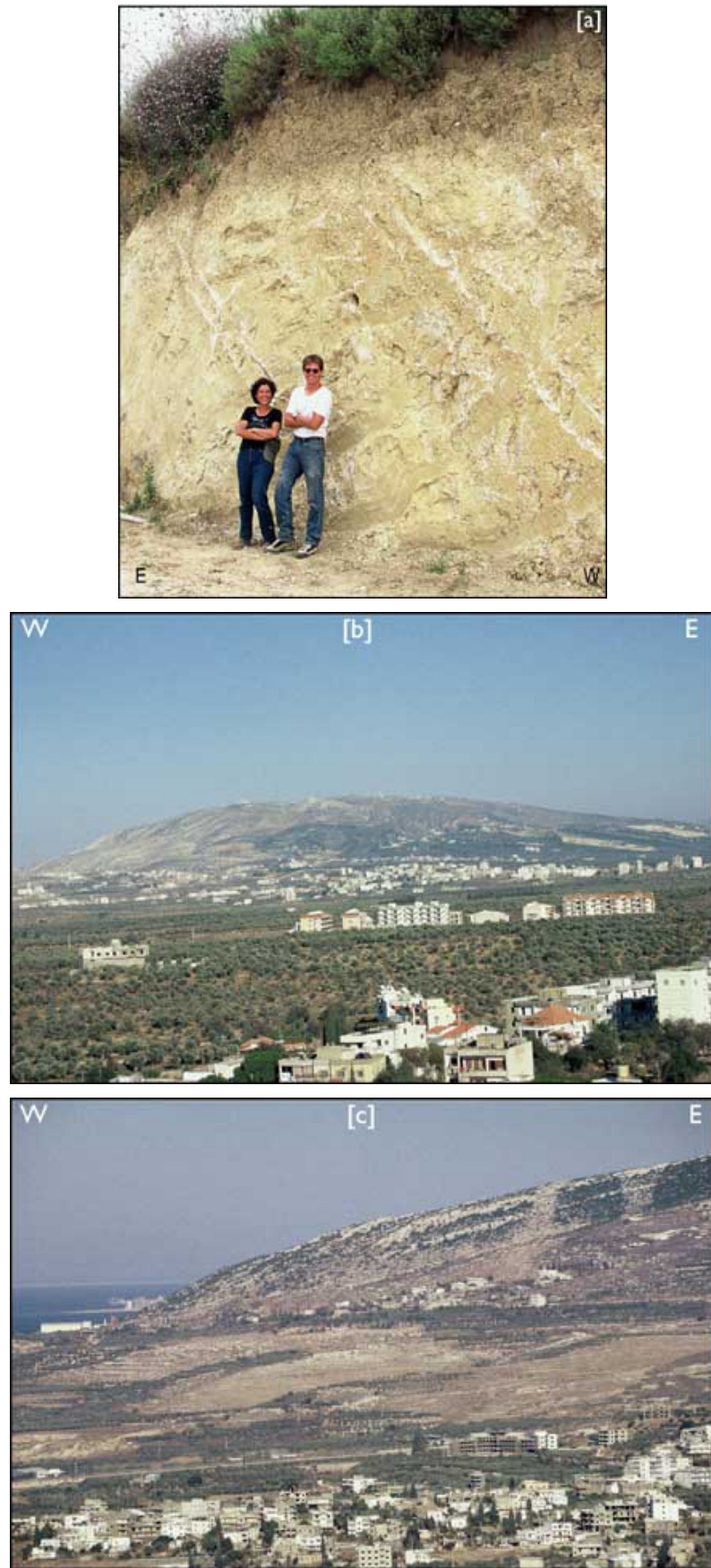


Figure 22: Young folding in the area of Tripoli
(continued next page) [a] Dip of Piacenzian marls west of Aabde. [b] Jabal Tourbol anticline. [c] Qalhât anticline.

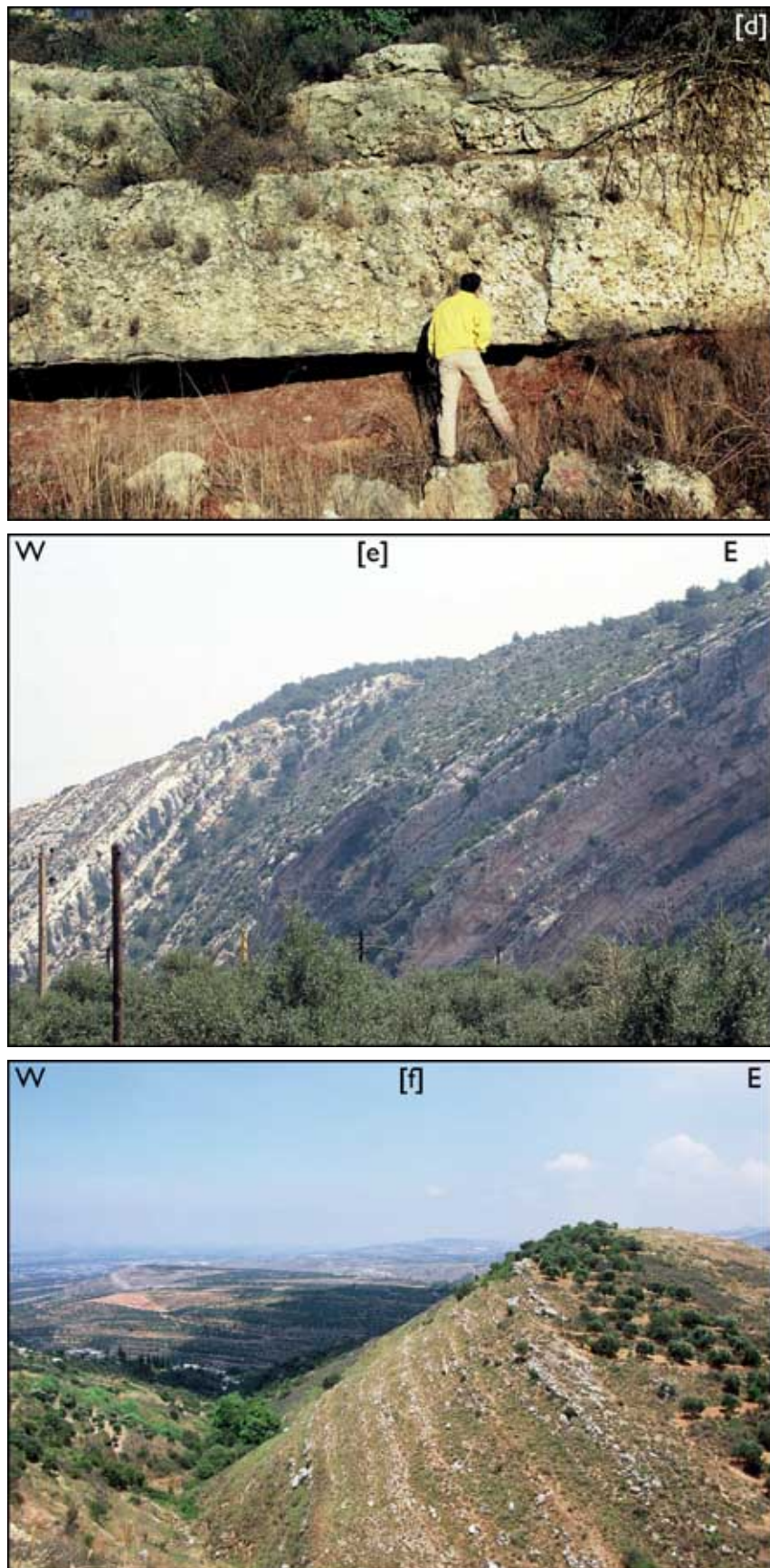


Figure 22: Young folding in the area of Tripoli
(continued from next page) [d] Slightly warped Zgharta Quaternary fanglomerates. [e] Cretaceous beds of the Kousba flexure. [f] S-dipping Pontian conglomerates on the E side of the Tourbol anticline.



Figure 23: NE-looking view of the Bahsâs cliff

This $\geq 60\text{-m-high}$ escarpment cuts through the modern city of Tripoli. It is the surface expression of the Tripoli thrust.

the modern city of Tripoli (figure 23). Although this escarpment has traditionally been interpreted as an abandoned sea cliff [Sanlaville, 1977], the fact that the fluvial conglomerates, with imbricated pebbles indicative of a NW-directed paleo-current, can be followed all the way to the top of the cliff requires vertical throw on a fault. The simplest interpretation is that this fault (the Tripoli thrust) is the SE-dipping thrust ramp that underlies the Tourbol and Qalhât anticlines. As commonly observed along foreland ramp anticlines, for instance in the ranges of Central Asia, it is across strath terraces abraded on top of the folded substratum in fluvial valleys crossing such growing anticlines that the underlying thrust ramps are most easily observed [Avouac et al., 1993; Meyer et al., 1998; Benedetti et al., 2000]. It is likely that both the Halba-Aabde and Tripoli thrusts continue at sea to the SW. In support of this inference is the fact that the islands offshore the Al-Mina peninsula of Tripoli show tilted marine-cut terraces and emerged vermetid benches. The presence of such benches, only a few tens of centimeters above the present-day sea level (figure 24.a), of abandoned sea cliffs and perched marine-cut terraces (figure 24.b), characterizes the entire coastline between Aabde and Saida, in contrast with the shoreline of the Akkar plain, north of Aabde, and of the Nabatîyeh plateau south of Saida.

Therefore, we hypothesize that a belt of active, submarine folds and thrusts (“Mount Lebanon Thrust”, or “MLT”) extends offshore the coast as least as far south as Saida, surrounding the western limb of Mount Lebanon [Tapponnier et al., 2001; Daëron et al., 2004a, 2005]. As in the Tripoli region, such thrusts would have migrated NW into the foreland of the range, reaching the seafloor of the Levant basin. Figure 31 presents a schematic map of this interpretation, which is in the process of being confirmed by the results of the October 2003 SHALIMAR cruise [Elias et al., 2004; Briais et al., 2004; Carton et al., 2004; Tapponnier et al., 2004; Daëron et al., 2004b, presented at the AGU Fall 2004 meeting].

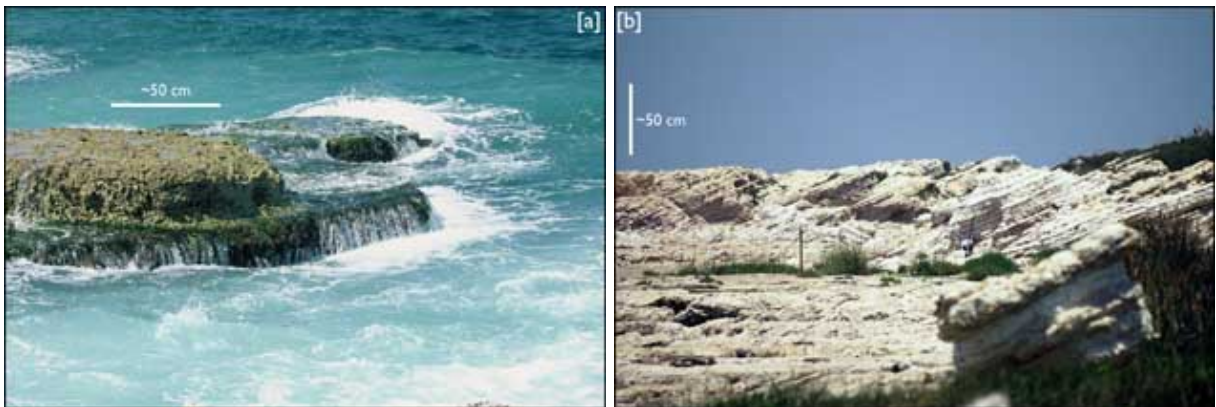


Figure 24: Vermetid benches and uplifted marine-cut terrace at Tabarja (immediately north of the bay of Joûnieh)

[a] Vermetid benches are horizontal bio-constructions that formed just at the mean sea level. Coseismic uplift of the coast has raised these benches above the water surface, killing the vermetids and thus ending lateral growth of the bench. Here, the lower, greener platform is the active bench while the higher, brownish surface is the top of the uplifted bench. [b] Wave-cut marine terrace in WNW-dipping Turonian limestone that was abraded by the sea, then raised above sea level by cumulative uplift.

Roûm lateral ramp

The western flank of the southernmost part of Mount Lebanon contrasts sharply with the Qoubayat-Tripoli range front, where structural dips and topographic gradients are similarly oriented, roughly perpendicular to the front. South of Jezzine, the series of narrow, NNE-trending anticlines and synclines that parallel the southern section of the Yammoûneh fault (figure 6, p.17) are truncated by a NNW-trending fault that bounds the high topography: the Roûm fault [Dubertret, 1975b] (figure 31). That this fault has a left-lateral component of motion has long been known [e.g. Garfunkel et al., 1981; Walley, 1988; Girdler, 1990], although the amount and age of sinistral offset have been the subject of controversy [Butler et al., 1997; Griffiths et al., 2000; Khair, 2001]. With the exception of Butler et al., who expanded on Girdler's hypothesis that the Roûm fault is the main branch of the Levant fault system in Lebanon by suggesting that it took up as much as 30 km of displacement since ~ 5.5 Ma (Messinian), most of the above authors agree with values of offsets comprised between 1.5 and 10 km. Most of them also agree that it is difficult to find evidence for left-lateral slip north of the Aouali river, which suggests that cumulative slip on the fault decreases northwards.

Our own assessment of the most prominent geomorphic offsets along the Roûm fault, using 1:20000 topographic maps and SPOT satellite images, is broadly consistent with the latter conclusions. It is possible to argue that the Litâni river has been offset by as much as 9.8 km (figure 25), with a localized dogleg along the fault yielding a smaller displacement value of ~ 1.7 km. Taking into account uncertainties in the piercing points, we estimate the larger offset to be on the order of 9.5 ± 0.4 km, and the smaller offset on order of 1.9 ± 0.3 km. For the Zahrani river farther north, there are also two possible values of the offset. The most localized, smallest offset along the fault is 2.4 ± 0.2 km. The larger offset is unlikely to exceed 4 ± 0.3 km. The Aouali offset is on the order of 1 km, as noted by Khair [2001], even though river offsets between the Aouali and Zahrani are unclear.

Unlike Griffiths et al. [2000] and Khair [2001], however, we do not attribute the larger offsets to distributed shear away from the fault. Rather, we interpret them to reflect cumulative displacements for longer periods of time, preserved away from the fault but masked near it by erosion-driven smoothing

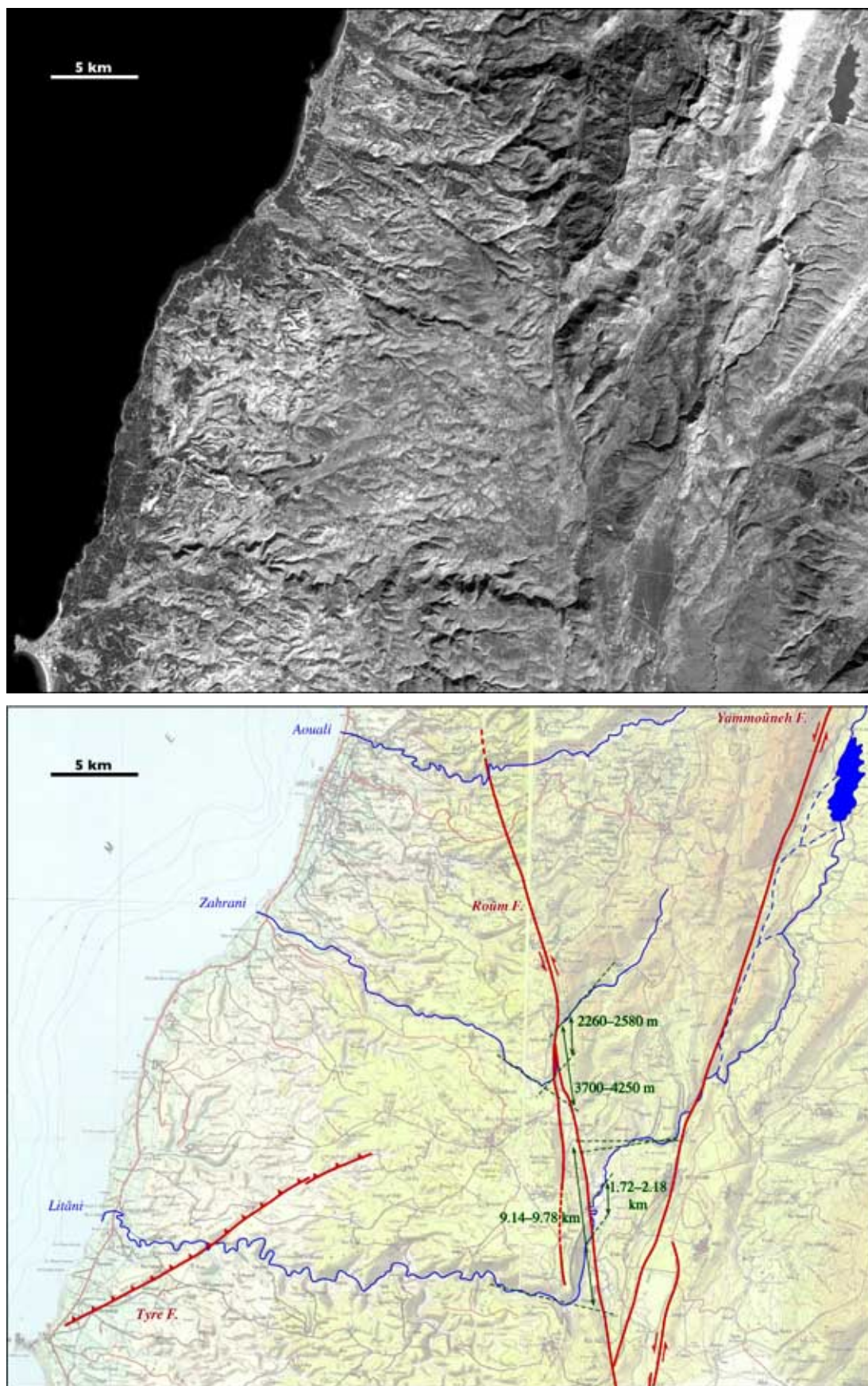


Figure 25: SPOT satellite image and map of the Tyre and Roûm faults

out of the sharp doglegs of the river trace where it crosses the fault. The existence of two offsets of the same river is thus related to geomorphic evolution, punctuated by climate-driven, rapid incision events (cf section 2.5.1), and not to fault-perpendicular deformation gradients. Similarly, although it seems likely that the cumulative displacement along the Roûm fault decreases northwards, one cannot exclude that this decrease reflects, at least in part, a northward decrease in the age of the topography, hence of the rivers. Unraveling such problems is beyond the scope of this work, but from the study of similar settings elsewhere, the interpretation we favor is that the Roûm fault propagated northwards, probably with a N-decreasing slip rate.

In any event, both the geology and geomorphology indicate that the Roûm fault is an oblique left-lateral thrust ramp (dubbed “lateral domain-bounding fault” by Griffiths et al. [2000]), which separates the relatively undeformed Tyre-Nabatîyeh platform to the SW from the thickening Mount Lebanon crust to the NE. On the scale of only a few tens of kilometers, the deformation geometry is similar to that documented by Meyer et al. [1998] along the NE end of the Altyn Tagh fault, with folds and thrusts merging at a high angle with a bounding, lateral fault. We infer that the NNW continuation of the Roûm fault, or a similar en-echelon ramp stepping out at sea between Saïda and Beirut, similarly connects offshore with the Mount Lebanon Thrust system.

Nîha thrust

East of the Yammoûneh fault and north of Chtaura, the 1500–2300-m-high hills and plateau that stand between the crest of Mount Lebanon and the Beqaa plain can be considered a small-scale eastern limb of the Mount Lebanon mega-anticline. Over a distance much shorter than west of the fault, Cretaceous layers are folded with a SE to SSE vergence. The folding is strongly asymmetric, forming a “cascading”, SE-dipping monocline (“Nîha monocline”, cf figures 6, 27 and 21). The marine Eocene and lacustrine Mio-Pliocene are involved in this folding. There is no discernable unconformity between the Cretaceous and Eocene. The unconformity between the Eocene and Miocene [Dubertret, 1975b] is, in our view, very slight. We interpret the different dips (30–35°SE in the Miocene versus 65–70° in the Lutetian) documented by Dubertret between Nîha and Zahle to result mostly from the cascading structure of the SE-facing folds (figure 21). While much of the deformation of the Nîha monocline likely postdates the Vindobonian (17 Ma), it does not seem to continue today, because the erosion surface in the Nîha hills truncates the cascading folds. Also, over most of the length of the northern Beqaa, the Pontian and Quaternary deposits of the plain are in sedimentary contact with the Cretaceous: north of Baalbek, ENE-trending, ~1-km-wide, anticlines in Cretaceous limestone, likely related to transpression along the Yammoûneh fault, show no evidence of post-Pontian growth, as they protrude out of the undeformed, tabular Beqaa in-fill. It is likely that such anticlines started to form early on while the Yammoûneh fault was in its initial propagation stage.

Between Zahle and Chmistar, however, the front of the Nîha monocline (figure 26) shows evidence of recent faulting. The fault is a NE-striking, NW-dipping active thrust about 20 km long (“Nîha thrust”). This is the only place in the Beqaa where Pontian conglomerates show SE dips superior to ~20°. Ongoing motion along the Nîha thrust is manifest across young Quaternary fans deposited at the foot of the monocline (figure 27). The most obvious evidence for such faulting is the existence of a cumulative scarp, which is particularly clear across the 3-km-wide Nîha fan. Figure 28 shows topographic profiles measured at the surface of this fan, perpendicular to the trace of the thrust. The vertical cumulative throw between the proximal and distal slopes of the fan is 8.7–11.6 m, measured where the degraded scarp-slope is steepest. In spite of surface degradation due to cultivation, the Nîha fan deposits appear to be loose,



Figure 26: *Vindobonian (~15 Ma) lacustrine marls, dipping 45° to the SE
(Niha monocline)*

well-rounded pebbles and cobbles, somewhat reminiscent of the Aajâqa or Zalqa fans (cf section 2.2).

The Niha thrust is the only clear feature absorbing current shortening east of Mount Lebanon along the west side of the Beqaa. It appears to correspond to the SW part of a “mid-Beqaa fault” whose existence was inferred by Khair [2001] on the basis of geophysical evidence. If this fault continues as far as Hermel, there seems to be little surface evidence that it is active north of Chmistar.

Active bookshelf faulting within Mount Lebanon

Although Mount Lebanon as a whole appears to be rising today (figures 5 and 24), there is little evidence for small-scale, active folding within the mountain. The relief falls rapidly towards the sea west of the summite plateaus (figure 21), but the average topographic slope is less steep than the structural dip of the Mesozoic sequence. The Qartaba back-thrust (figures 6 and 21) is the only Tertiary fault that trends parallel to the range, but there is little evidence of current motion on it.

On the other hand, a few of the ENE-striking Mesozoic normal faults (figure 6) display clear signs of reactivation. Three of them (the Nahr el-Kelb, Ghazir-Afqa and Batroun faults) appear to slip in a right-lateral sense, with subordinate vertical movement. North of Beirut, near the mouth of the Nahr el-Kelb, Miocene limestones are faulted vertically against Quaternary colluvial deposits (figure 29). The steep fault plane shows clear horizontal slickensides, with adjacent fracture orientations compatible with right-lateral motion. This sense of motion is consistent with the right-lateral offset of the Lebanese flexure in the same area. This offset, which postdates folding, amounts to about 3 km [Dubertret, 1975a,

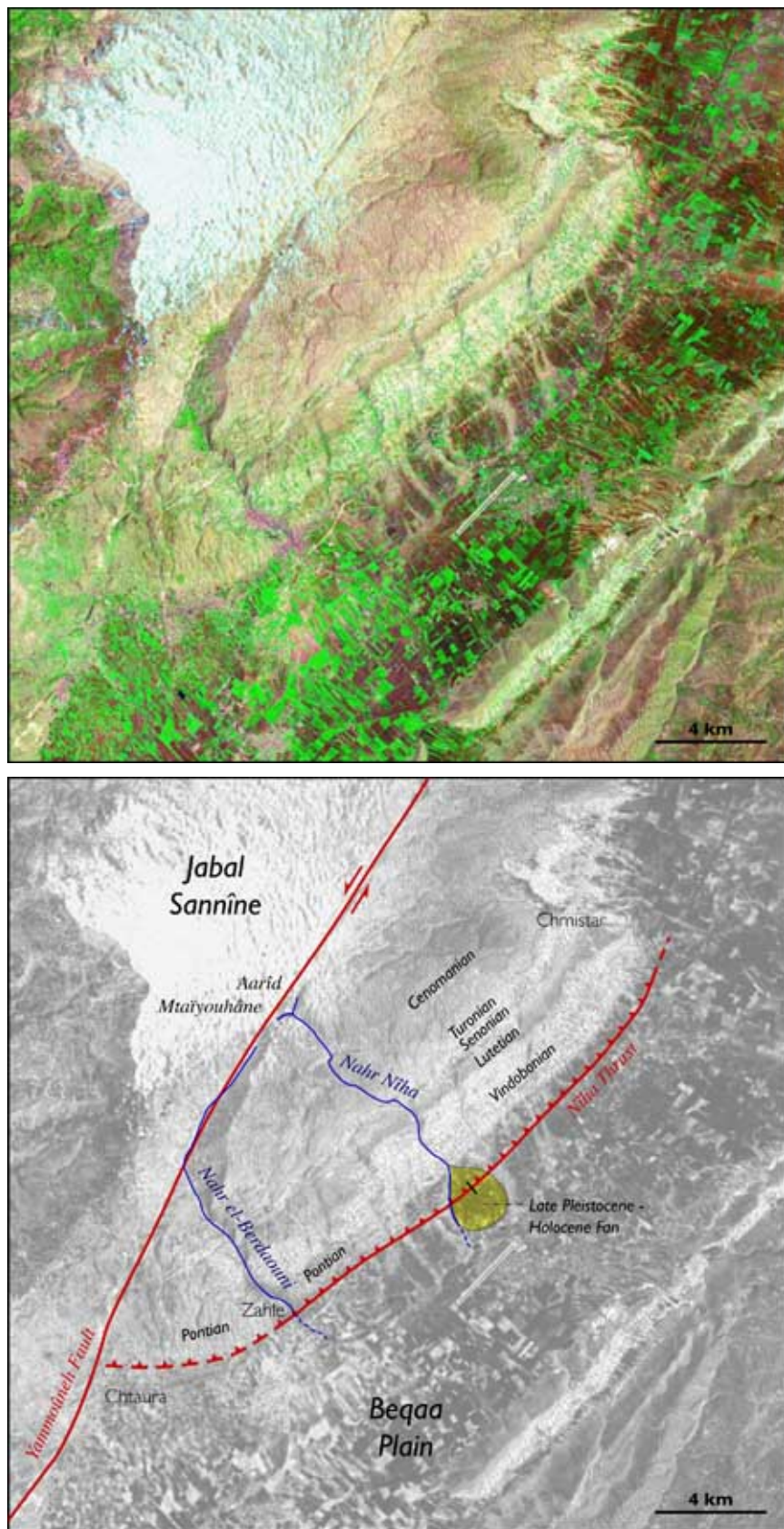


Figure 27: Landsat satellite image and map of the Nîha monocline

The black bar in the yellow Nîha fan shows the location of the topographic profile plotted in figure 28

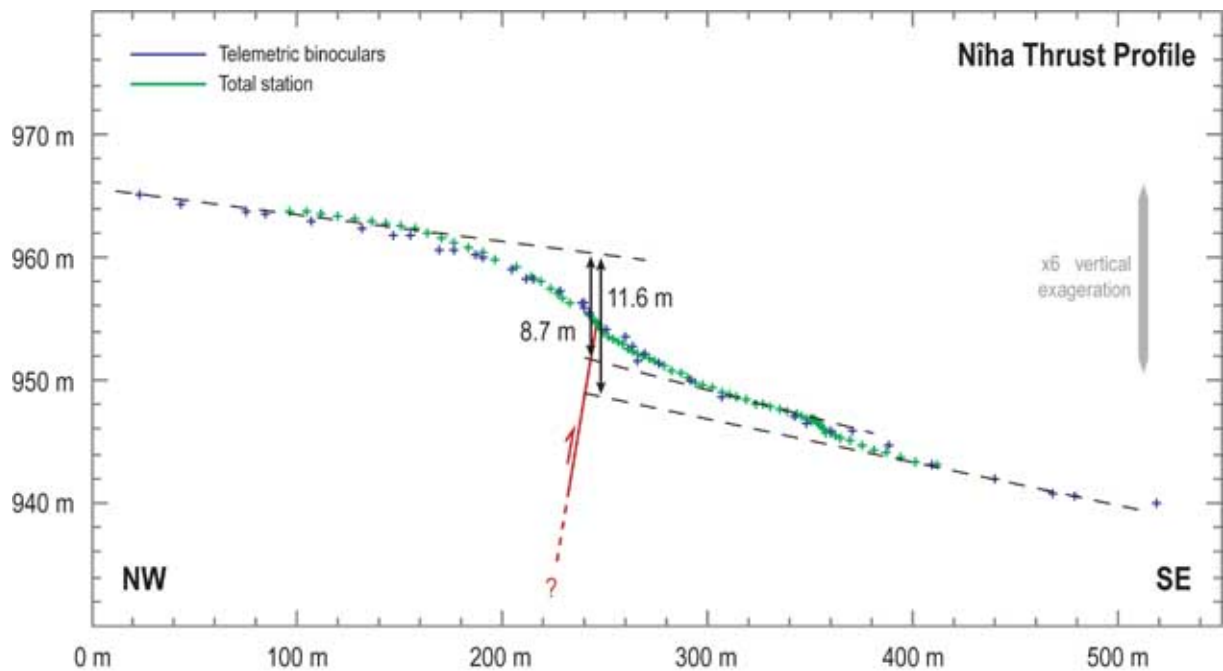


Figure 28: Topographic profile across the Nîha thrust

The cumulative vertical offset since deposition of the Nîha fan's surface is $\sim 10 \pm 1.5$ m. Telemetric binoculars provided a longer reach than the total station, but their precision is not as good. The position of the Nîha thrust (inferred 45° dip) is shown in red.



Figure 29: Outcrop of the Nahr el-Kelb fault, near the coast south of Joûnieh

Slickensides and cracks imply right-lateral motion on this fault, which juxtaposes Miocene limestones (to the north) and Quaternary colluvium (to the south). [b] is a close-up view of the central area of [a].

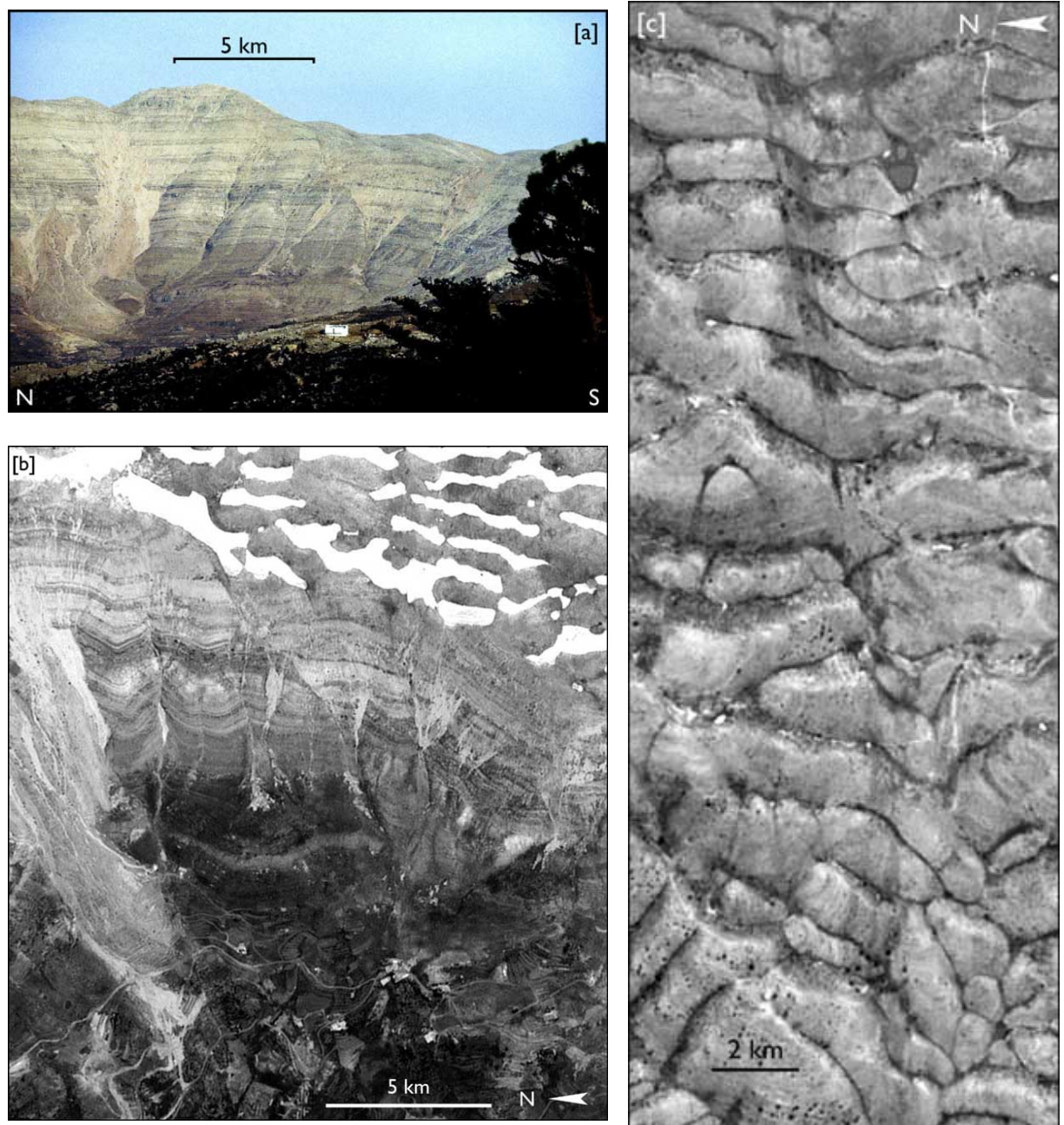


Figure 30: Bla

[a,b] Field view and corresponding SPOT-5 image of the Nahr el-Kelb fault where it crosses the cliff west of Harf Sannîne. Down-to-the-south offset of tabular Aptian to Cenomanian limestone sequence is clear. [c] SPOT-5 image of the Afqa fault trace on the Jabal Mnaïtra plateau. Note the particularly sharp expression of the fault across karstic rills, which are generally deflected right-laterally along the fault.

Beyrouth sheet]. The fault continues eastwards all the way to the Yammoûneh fault, marking the base of the 150-m-high, south-facing Harf Sannîne escarpment (figure 30.a). Along strike, the Quaternary vertical component of slip, whether geological or geomorphic, is thus down to the south. Such motion is also visible west of the Sannîne, where the fault offsets the Aptian-Albian levels.

Similar evidence of dextral slip and young geomorphic offsets are found along the Ghazîr-Afqa fault, which can be traced from the north side of the bay of Joûnieh to the sources of the Nahr Ibrahim at Afqa, and farther across the summital plateau of Jabal Mnaïtra where it displaces young karstic rills all the way to the Yammoûneh fault (figure 30.b). The Tannourîne fault is another candidate for such type of motion, although the evidence for active motion along it is less convincing. Finally, the Batroun fault also offsets the Lebanese flexure, although its vertical component of motion is down to the north. It does not appear to continue as far east as either of the previous faults.

We interpret right-lateral motion along these three or four nearly parallel faults to reflect active bookshelf faulting, in large part posterior to folding of the Lebanese flexure. Regionally, this mechanism is appropriate to accomodate counter-clockwise rotation due to left-lateral shear not taken up by the Yammoûneh fault. Although bookshelf faulting has long been advocated farther south, in Galilee, Mount Hermon and in southern Mount Lebanon to explain counter-clockwise rotations as large as 50–70° [Gregor et al., 1974; Ron and Eyal, 1985; Ron et al., 1990], evidenced by paleomagnetic declinations, such large rotations affected basalts of Cretaceous age and it unclear whether the mechanism still operates today. To our knowledge, the Mount Lebanon bookshelf faulting we document here is the only active example of this mechanism along the Levant fault system. The amounts of Cenozoic dextral shear and CCW rotation related to this process in Lebanon are much smaller: given the average width of the rotating blocks (12–20 km), their length (30–40 km), and the cumulative dextral slip on the right-lateral faults (2–3 km), the total rotation would be 6–14° and the corresponding off-fault shear 3–10 km.

1.2.3 The Râchaïya-Serghaya system and the Hermon push-up

It has long been recognized that the Levant fault system splays into several strands (Yammoûneh, Hasbaïya, Râchaïya and Serghaya faults) north of the Hula basin [e.g. Freund et al., 1970; Garfunkel et al., 1981; Walley, 1988]. Our geomorphic assessment of Quaternary motion on these faults using Landsat and SPOT images, aerial photographs and 1/20,000 topographic maps reveals no evidence of active slip on the Hasbaïya fault. Traces of very recent earthquakes, on the other hand, as well as cumulative geomorphic displacements, are very clear on both the Râchaïya and Serghaya faults. For the latter fault, our observations in Lebanon (section 3.2, figure 75) essentially confirm the conclusions reached by Gomez et al. [2001, 2003], who studied extensively the central stretch of the Serghaya fault in Syria. For the Râchaïya fault, whose northernmost stretch lies in Lebanon, the evidence we discuss (below and in section 3.2) is new.

The geomorphically active trace of the Râchaïya fault, which is spectacular all the way from the Hula to the town of Râchaïya, appears to die out less than 10 km north of Râchaïya. The trace of the Serghaya fault, on the other hand, can be followed southwards from 15 km NE of Baalbek, across the Zebadani basin [Gomez et al., 2001, 2003], to the NE termination of Mount Hermon. Although geologic faults were mapped farther south by Dubertret [1955a], there is little evidence of Quaternary strike-slip along these faults. The Râchaïya and Serghaya faults thus appear to form a ~15 km right step which coincides with the high, NE-striking ridge of Mount Hermon (2814 m a.s.l., figures 3, 4 and 31), while there is no comparable relief to the east or west. Moreover, the faults roughly follow the western and

eastern margins of a structural high exposing only Jurassic rocks (figure 6). It is thus clear, both from a structural and geomorphic point of view, that the Mount Hermon uplift is a push-up ridge that links the Râchaïya and Serghaya faults. Due to very difficult access given the current political situation involving Lebanon, Syria and Israel, our fieldwork in this area has been limited. However, a prominent slope break at the base of the northern flank of the mountain, visible both on satellite images and topographic maps, suggests the existence of an active, S-dipping thrust fault linking the most active segments of the Râchaïya and Serghaya faults. At any rate, the great height and extreme localization of Mount Hermon, as well as the attested recent slip of the Serghaya and Râchaïya faults, argues strongly for ongoing uplift. Taking the 1.4 mm/yr left-lateral slip rate measured by Gomez et al. [2003] at Zebadani would yield a current shortening rate of about 1 mm/yr, perpendicularly to Mount Hermon's NNW flank.

1.2.4 Summary: 3D active faulting in the Lebanese restraining bend

Figures 31 and 32 summarize the architecture of active folding in the Lebanese restraining bend, in map view and in section. Of all the geological faults in Lebanon, only a few can be demonstrated to be active using geomorphic criteria, both on a large scale (satellite imagery, aerial photographs...) and at the scale of the outcrop in the field. On a longer time scale, motion on these faults is consistent with all the geological data available. It is also consistent with the regional topographic relief and its evolution. The faults are organized into a coherent system, with kinematically compatible motions everywhere.

The main difference between our interpretation and previous ones [e.g. Walley, 1988; Butler et al., 1997, 1998] is the existence of active thrust faults that control the growth of anticlinal folds and the uplift of relief. It is these faults that absorb most of the strike-perpendicular shortening in the restraining bend, rather than diffuse / distributed regional deformation [Griffiths et al., 2000]. Overall, the active tectonics of the Lebanese bend offer a striking similarity with other restraining bends of comparable sizes, along other major strike-slip faults, such as the San Andreas or Haiyuan faults [e.g. Weldon et al., 1993; Allen, 1981; Gaudemer et al., 1995; Bowman et al., 2003].

Faults that connect in map view (figure 31) are inferred to merge at depth (figure 32), even though quantitative depth evidence is too limited to provide more than a sketch. Figure 32 illustrates the difference between the transtensive nature of the Levant fault in the Hula basin and farther south, and the more complex transpressive organization of the more numerous faults in Lebanon. We infer that oblique motion on a master fault or shear zone at depth is partitioned near the surface into two strike-slip-and-thrust systems. The main difference between the principal, Mount Lebanon partitioned system and the secondary, Anti-Lebanon / Palmyrides system is that the former merges back to the north, resuming a simpler geometry as the principal strand of the northern LFS (Ghab fault), while the other terminates north-eastwards. This hierarchy in the systems appears to be reflected not only by the geomorphic expression of the faults, but also by their slip rates, as discussed in chapter 2, and possibly by their long-term seismic behavior (chapter 3).

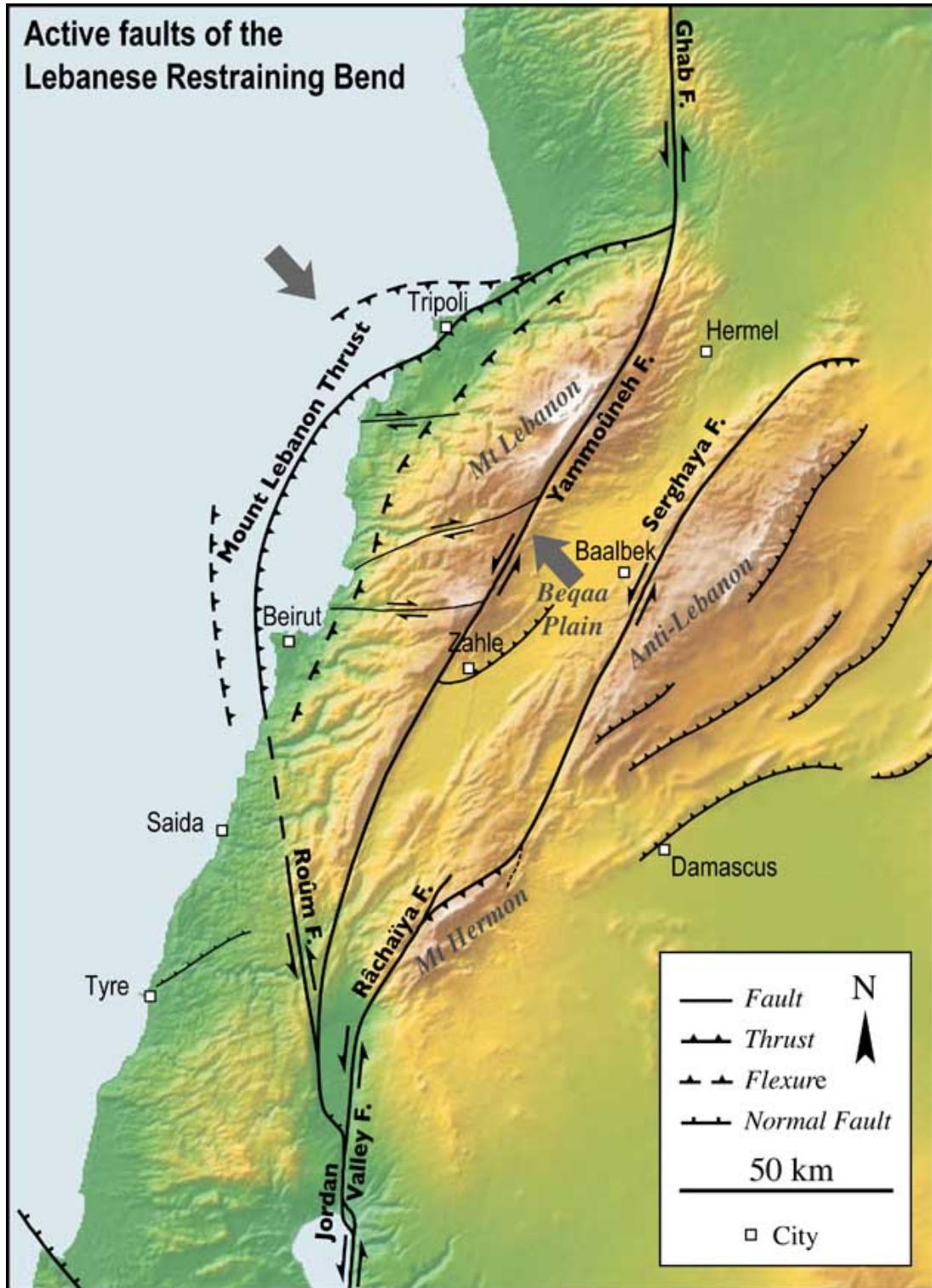


Figure 31: Map of the active faults in the Lebanese Restraining Bend

Thick grey arrows show the direction of shortening across northern Mount Lebanon (discussed in section 2.5.3, p.94).

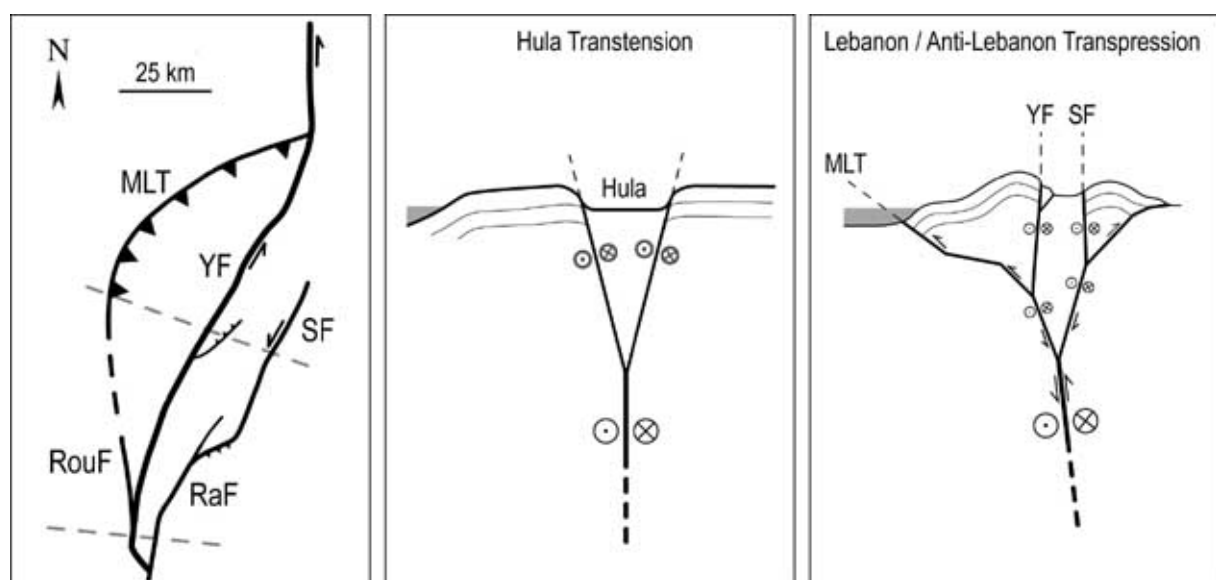


Figure 32: Inferred geometry of the Lebanese restraining bend at depth

– Chapitre II –

Cinématique du coude transpressif libanais

2.1 Existing kinematic constraints

2.1.1 Geological offsets

Quennell [1958, 1959] first demonstrated that ~ 105 km of horizontal slip along the southern Levant fault system (LFS) are necessary to re-align offset geological features of Precambrian to Cretaceous ages, and suggested that a younger movement of 45 km explains several prominent geomorphic features such as the shape of the deeper, northern basin of the Dead Sea. The ~ 105 km total offset was estimated to be 15–18 Myr old [e.g. Garfunkel, 1981; Garfunkel and Ben-Avraham, 1996]. However, it appears that slip over this period was not uniform, because numerous Late Miocene to Early Pliocene geological markers [Freund et al., 1968, 1970] are offset by as much as 40–45 km. Garfunkel [1981] also demonstrated that 35–40 km of left-lateral slip were likely responsible to the opening of most “rhomb-grabens” along the southern LFS, especially in the Gulf of Aqaba and in the Dead Sea. Roughly dating this younger phase of movement to 5 Ma yields an average Plio-Quaternary slip rate of ~ 8 mm/yr.

These long-term constraints apply only to the Dead Sea fault, the section of the LFS south of Lebanon. On the northern LFS, along the Syrian coast, the total amount of slip remains controversial, with possibly up to 80 km of motion recorded by the southern boundary of Late Cretaceous ophiolite outcrops [Freund et al., 1970].

2.1.2 Plate motion models based on seafloor magnetic anomalies

Global plate motion models using seafloor magnetic anomalies, like the NUVEL-1A model [DeMets et al., 1994], determine the Euler pole and angular velocity of Arabia relative to Africa since 3 Ma (0.4 ± 0.1 deg/Myr about a pole at 24.1°N , 24.0°E). The predicted motion along the Levant fault, in the area of Lebanon, is ~ 11 mm/yr striking $N40^\circ\text{W}$. Since the average strike of the LFS to the north and south of Lebanon is $N5^\circ\text{E}$, this motion corresponds to 7.8 mm/yr of ($N5^\circ\text{E}$) left-lateral slip and 7.8 mm/yr of $N85^\circ\text{W}$ shortening. The African-Arabian motion predicted by this model is essentially constrained by

Methods	Time span	Slip rates [mm/yr]				References
		LF	DSF	SF	GF	
Geology and geomorphology	~5 Myr	-	~8	-	-	Freund et al. [1968, 1970]; Garfunkel [1981]
Red Sea magnetic anomalies	3.1 Myr	≤ 8.5	-	-	-	Chu and Gordon [1998]
Geomorphology	≥ 25 kyr	-	4 ± 2	-	-	Klinger et al. [2000]
Paleoseismology	6 kyr	-	-	1.4 ± 0.2	-	Gomez et al. [2003]
Archeoseismology	2 kyr	-	-	-	6.9 ± 0.1	Meghraoui et al. [2003]
GPS AR/NU motions	10 yr	$\leq 6.1 \pm 1$	-	-	-	McClusky et al. [2003]
Across-fault GPS profile	3–7 yr	-	3.3 ± 0.4	-	-	Wdowinski et al. [2004]

Table 1: Summary of existing kinematic constraints on the Levant fault system
(LF: Levant fault; DSF: Dead Sea fault; SF: Serghaya fault; GF: Ghab fault)

spreading centers in the Indian ocean, because data from the Red Sea was too scarce and/or unreliable at the time.

A more reliable approach, in our view, is that of Chu and Gordon [1998], who reviewed and compiled the data from 64 Red Sea spreading centers, yielding a new model of the motion between the Arabia and Nubia. The angular velocity they determine is $0.403^\circ/\text{Myr}$ about a pole at $31.5^\circ\text{N}, 23.0^\circ\text{E}$. Projected in Lebanon along a $\text{N}5^\circ\text{E}$ -trending transform, this yields 8.5 mm/yr of left-lateral motion and 2.1 mm/yr of convergence (i.e. 8.7 mm/yr in a $\text{N}9^\circ\text{W}$ direction).

Both of these models concern the motion between the Nubian (“Africa”) and the Arabian plates. Using them at face value to deduce the slip on the LFS is equivalent to assuming that motion of the Sinai/Levantine “micro-plate” relative to Nubia is negligible. Since this is clearly not the case [e.g. Salamon et al., 2003; Courtillot et al., 1987], and since the Sinai block is moving away from Nubia across the Gulf of Suez, the left-lateral rate (~ 8.5 mm/yr) predicted by Chu and Gordon [1998] ought to be an upper bound to the slip rate along the LFS since 3 Ma.

2.1.3 Geomorphic, paleoseismic and archeoseismic offsets

Just south of the Dead Sea, Klinger et al. [2000] measured the cumulative offsets of a reportedly pre-Lisan (pre-70 ka) alluvial fan and of Holocene terraces. The age of the fan is broadly constrained using U/Th and cosmogenic ^{10}Be dating. The ages of the Holocene terraces are estimated by correlating regional aggradation episodes [Klinger et al., 2003]. Based on this data, the authors propose an average slip rate since ~ 140 ka of 2–6 mm/yr, with a preferred value of 4 mm/yr. A more detailed study of the same Holocene terraces by Niemi et al. [2001] confirms with ^{14}C and OSL dating the ages of the inset terraces, and thus this rate.

On the Ghab fault, about 50 km north of the Syro-Lebanese border, Meghraoui et al. [2003] documented the cumulative offset of a Roman aqueduct by three earthquakes, the last of which occurred more than 8 centuries ago, in AD 1170. Whether such a short time span, that encompasses only two inter-seismic periods, provides a good assessment of the geologic slip rate, is debatable. In any case, estimating the average slip rate of the Ghab fault from this short period depends on the exact time bounds and offsets chosen, thus on the earthquake recurrence model considered. Meghraoui et al. [2003] use a time-predictable model, assuming that the next earthquake is imminent (cf their figure 7). While it would seem that this yields a rate of 7.2 mm/yr (13.6 m of offset since AD 115), they conclude that the rate is 6.9 ± 0.1 mm/yr. Using a slip-predictable model would result in an even faster rate of 8.8 mm/yr

(9.3 m between AD 115 and AD 1170).

Finally, Gomez et al. [2003], based on the geometry and age of paleo-channels across the Serghaya fault, demonstrate that ~ 8 m of cumulative slip has occurred on this fault in ~ 6.1 kyr, yielding 1.4 ± 0.2 mm/yr.

2.1.4 GPS measurements

Global and regional GPS models that constrain the modern motion of Arabia relative to Nubia provide upper bounds for the slip rate along the DSF, again because motion of the Sinai block is poorly known. For instance, Sella et al. [2002], modelling global plate motions based on GPS data over 7 years (REVEL model), predict an Arabia/Nubia Euler pole at 31.26°N , 29.55°E and an angular velocity of $0.4^\circ/\text{Myr}$, which corresponds to 4.1 mm/yr of LFS-parallel motion in Lebanon, along with 2.4 mm/yr of LFS-perpendicular convergence. This value is much smaller than the 3-Myr-averaged prediction (8.5 mm/yr) of Chu and Gordon [1998]. Recall, however, that in the REVEL model, the motion of Arabia is constrained by only 3 stations. Moreover, while two of them are located east of 45°E , the third one (KATZ, 33°N , 35.69°E) is less than 6 km east of the Jordan Valley fault, just SE from the Hula basin (cf figure 2 in Wdowinski et al. [2004]). The fact that elastic strain cannot be discarded at this station, raises doubts on the reliability of the Arabia/Nubia motion predicted by REVEL.

A more “regional” GPS model, covering only Nubia, Arabia and Eurasia, is discussed by McClusky et al. [2003]. They use 4 stations to constrain the motion of Arabia, all of them at least 90 km away from the inferred plate boundaries. They do not rule out boundary effects on their three northernmost stations, located SE of the Eastern Anatolian fault system, in an area of complex faulting. Their model predicts 6.1 ± 1 mm/yr of LFS-parallel motion in Lebanon, with a Euler pole at 30.5°N , 25.7°E and an angular velocity of $0.37^\circ/\text{Myr}$.

Finally, Wdowinski et al. [2004] model elastic strain loading across the Dead Sea fault, using data from 11 stations in Israel and one in Syria, over a 3–7 yr time span. The left-lateral slip rate that fits best their data is only 3.3 ± 0.4 mm/yr, but the scarcity of stations east of the fault makes this measurement strongly dependent on the unique far-field station available (UDMC), located in Damascus. While distant from the Dead Sea fault when projected southwards, this station is only ~ 15 km SE from the southern Palmyride frontal thrust, and ~ 25 km east of the Râchaïya-Serghaya fault system. Including or excluding problematic stations east of the Dead Sea fault yields different estimates of the left-lateral slip rate, ranging from 2.9 ± 1.1 to 4.2 ± 1.1 mm/yr.

2.1.5 Summary of existing kinematic constraints on the LFS

From the above discussion, the most reliable constraints on the relative motions of Nubia and Arabia are provided, in our view, by the Red Sea spreading model of Chu and Gordon [1998] and by the Nubia/Aabia/Eurasia GPS model of McClusky et al. [2003]. Despite vastly different time scales (3 Myr versus 10 yr), the motions predicted by these models in the area of Lebanon are in fair agreement, although the GPS motion is slower by $\sim 25\%$. This might possibly be due to plate boundary effects on the three stations (out of four) used by McClusky et al. to constrain the motion of Arabia. In any case, both models only provide upper bounds to the slip rate on the LFS, due to the motion of the Sinai-Levant micro-plate relative to Nubia, which is not well known.

Data concerning the LFS itself is contradictory. The average Plio-Quaternary rate of ~ 8 mm/yr, while usually accepted, is difficult to reconcile with the Late Pleistocene rates proposed by Klinger et al. [2000] and Niemi et al. [2001], that are only about 4 mm/yr. The constraints provided by Meghraoui et al. [2003] and Gomez et al. [2003] support the hypothesis of a “fast” Levant fault. The 6.9 mm/yr slip rate proposed by Meghraoui et al. on the northern Levant fault is close to the upper bounds imposed by the GPS and magnetic anomalies plate motion models. Finally, while the 1.4 mm/yr rate on the Serghaya fault documented by Gomez et al. is much slower than other rates measured elsewhere on the Levant fault, one must take into account that, in Lebanon, the fault system splays into three strands, all of which display evidence of some amount of left-lateral faulting. Moreover, comparison of the geomorphic signatures of the two main strike-slip strands of the Lebanese restraining bend, the Yammouneh and Serghaya faults, implies that the former is more active than the latter. The 1.4 mm/yr on the Serghaya fault thus likely represents only a fraction of the overall left-lateral motion partitioned between the three strands of the LRB.

Quantitative kinematic constraints on the Yammouneh fault and the Mount Lebanon thrust are thus needed to assess the overall left-lateral slip rate across the LRB. The results we discuss in this chapter address this issue, by measuring surface exposure ages of alluvial fans offset by the Yammouneh fault, and by attempting to shed light on the relationship between past climatic events and the record of geomorphic offsets along the Lebanese faults.

2.2 Constraints on the post ~25-ka slip rate of the Yammoûneh fault (Lebanon) using *in situ* cosmogenic ^{36}Cl dating of offset limestone-clast fans

The contents of this section have been published in *Earth and Planetary Science Letters* [Daëron et al., 2004a]. This work was principally supported by a CEDRE grant from the French Ministère des Affaires Etrangères, and dating was performed under the auspices of the U.S. Department of Energy by the University of California, Lawrence Livermore National Laboratory under Contract No. W-7405-Eng-48. The authors wish to thank Antoine Charbel, Rachid Jomaa, Marlène Brax, Maya Hariri and Walid Nohra for their help in the field. Ata Elias, Yann Klinger and Eric Jacques participated in sampling and mapping. This article benefited from thoughtful discussions with Yann Klinger and constructive reviews by A. Matmon and J. Van Der Woerd. This is IPGP contribution No 2001.

Abstract

The most active seismogenic structure along the eastern shore of the Mediterranean is the N-S-trending left-lateral Levant Fault System (LFS), the plate boundary between Arabia and Africa. In Lebanon, it forms a 160-km-long restraining bend responsible for the uplift of Mount Lebanon. The resulting transpression is partitioned between the offshore Tripoli-Roûm thrust and the Yammoûneh strike-slip fault. There are few quantitative constraints on the Quaternary slip rate along the LFS. Here we present a direct estimate of the ~25 ka mean slip rate on the Yammoûneh fault. Mapped offsets of alluvial fans at two sites ~50 km apart on the eastern flank of Mount Lebanon range between 24 ± 2 and 80 ± 8 m. About thirty limestone cobbles sampled on these fans yield *in situ* cosmogenic ^{36}Cl exposure ages mostly between 6 and 27 ka. A statistical assessment of offsets versus ages provides bounds on the Late Pleistocene-Holocene slip rate on the fault: 3.8–6.4 mm/yr. These results are consistent with long-term geological inferences, confirming that the Yammoûneh fault is the main strike-slip branch of the LFS in Lebanon. They illustrate both the potential and the difficulties of using *in situ* cosmogenic ^{36}Cl dating of limestone-clast fan deposits for deciphering tectonic and geomorphic processes in the Mediterranean.

2.2.1 Introduction

Stretching from the Gulf of Aqaba to the Eastern Anatolian Fault System, the Levant Fault System (LFS) connects the Red Sea spreading center to the collisional belt of southeastern Turkey (fig. 33A). This ~1,000-km-long left-lateral transform fault accommodates the relative motion between the Arabian and Nubian plates [Freund, 1965; Freund et al., 1968; Garfunkel, 1981]. That simple picture is complicated by the presence of the Sinai micro-plate [Courtillot et al., 1987; Salamon et al., 1996; Mascle et al., 2000; McClusky et al., 2003], comprising the Sinai peninsula and the Levantine margin, and by internal deformation of the Arabian plate, most notably within the Palmyrides fold belt.

Direct knowledge of the slip rate along the LFS is thus essential to a quantitative understanding of the plate kinematics of Arabia, Nubia and the Sinai block. This slip rate is currently uncertain by more than a factor of two over time periods from 18 Myr to 10 yr (table 2). In addition, the geometry and kinematics of the LFS are better understood south of Lake Tiberias (Gulf of Aqaba and Dead Sea fault) than to the north.

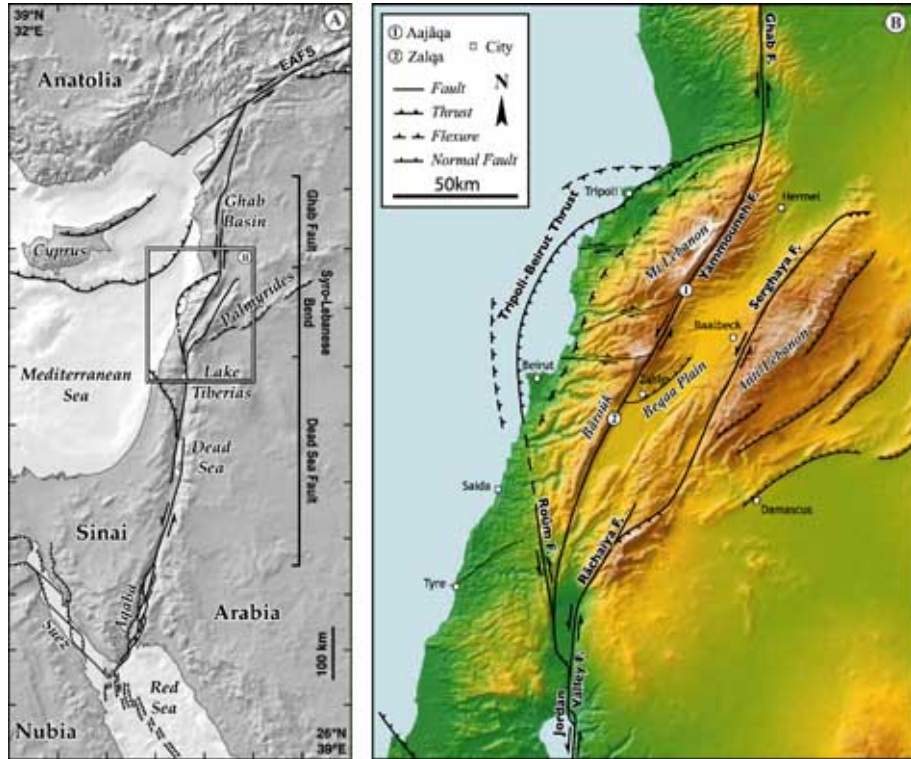


Figure 33: (A) Map of Levant Fault System. Box shows limits of panel B. Faulting in Red Sea (including gulfs of Aqaba and Suez) is from Courtillot et al. [1987]; “EAFS” = “East Anatolian Fault System”. **(B) Active faults of Lebanese restraining bend.** Circled numbers mark locations of studied sites: Aajâqa (1) and Zalqa (2).

Slip rate (along-strike, mm/yr)	Time span	Method	References
>5.8	<18 Myr	Geological offsets	Freund et al. [1968]; Garfunkel [1981]
8.5±0.5	~5 Myr	Geological offsets	Freund et al. [1968]; Garfunkel [1981]
8.4±2.8	3.2 Myr	Red Sea seafloor spreading	Chu and Gordon [1998]
4.0±2.0	>25 kyr	Geomorphology (Arabia valley)	Klinger et al. [2000]
6.9±0.1	~2 kyr	Paleoseismology (Missyaf, Syria)	Meghraoui et al. [2003]
6.0±2.0	10 yr	GPS	McClusky et al. [2003]

Table 2: Various estimations of slip rate along the LFS. Only strike-slip component predicted in Lebanon (34°N , 36°E) on LFS is shown. Both seafloor spreading and GPS models assume no significant motion between Sinai and Nubia, and predict transpressive slip north of Lake Tiberias, all the way to triple junction with EAFS.

Plate motion reconstructions for Arabia and Nubia based on the analysis of seafloor spreading recorded by magnetic anomalies in the Red Sea [Chu and Gordon, 1998] predict 5.6–11 mm/yr of left-lateral motion in the 4°E direction in Lebanon, but also about 2.4–3.7 mm/yr of E-W shortening (table 2). GPS measurements over the past 10 years are compatible with these results in terms of Euler poles and rotation rates [McClusky et al., 2003]: the GPS-predicted N-S strike-slip rate in Lebanon is \sim 4.0–8.1 mm/yr, with \sim 2.8–3.7 mm/yr of strike-perpendicular (E-W) shortening (table 2). Rates calculated from both the seafloor spreading and GPS models assume no significant movement between Nubia and the Sinai block. It is generally acknowledged, however, that such motion does exist [Courtillot et al., 1987; Chu and Gordon, 1998; McClusky et al., 2003], although it remains poorly constrained. Reliable estimates of the slip rate along the LFS therefore require geological and geomorphic field studies, or local GPS profiles. It has long been recognized that the total left-lateral slip on the southern LFS is \sim 105 km and postdates 18 Ma [Quennell, 1959; Freund et al., 1968; Garfunkel, 1981; Courtillot et al., 1987], which

yields a minimum long-term slip rate of ~ 5.8 mm/yr (table 2). Cumulative slip over the last 5 Myr, as recorded by offset Late Miocene to Early Pliocene geological markers between Zahle and the Dead Sea [Freund et al., 1968; Garfunkel, 1981], is about 40–45 km, which implies a faster slip rate of 8–9 mm/yr over this period (table 2).

Over a shorter time span, cumulative offsets of U/Th, ^{10}Be and ^{14}C -dated Mid-Pleistocene to Holocene alluvial surfaces and fans in the Araba valley, between Aqaba and the Dead Sea, record an average slip rate of 2–6 mm/yr over the past 140 ± 31 ka along the main branch of the Dead Sea fault [Klinger et al., 2000], similar to that previously inferred by Ginat et al. [1998] (3–7.5 mm/yr). In Syria, Meghraoui et al. [2003] used paleoseismologic and archeologic evidence to propose an average slip rate of 6.9 ± 0.1 mm/yr along the Missyaf segment of the Ghab fault over the past $\sim 2,000$ years. This result is, however, based on cumulative slip due to only three earthquakes. Using such a small number of seismic cycles to extrapolate to geological time scales may give rates that differ significantly from the actual mean Holocene or Pleistocene slip rate.

The aim of this study is to provide more quantitative constraints for Late Pleistocene-Holocene slip rates. We targeted the Yammoûneh fault, the main strike-slip branch of the LFS in the Lebanese restraining bend. Based on cosmogenic ^{36}Cl surface exposure dating of limestones cobbles in young alluvial fans, we have determined the age of cumulative offsets at two sites along the fault about 50 km apart (fig. 33B). The morphology of each area was accurately mapped by combining field observations with evidence from stereoscopic air photographs, topographic maps and satellite imagery in order to measure horizontal offsets. We describe below the sampling strategy and the method for exposure age calculation, and how we derive a mean slip-rate on the fault over ~ 25 ka.

2.2.2 Geomorphic offsets along the Yammoûneh fault

Active faulting in the Lebanese restraining bend

Along most of its length, the LFS is transtensional, with large-scale pull-apart structures such as the Gulf of Aqaba, Dead Sea, Lake Tiberias and Ghab basins (fig. 33A). By contrast, between 33°N and 34.5°N , about halfway along its length, the Levant fault's trace veers by $\sim 25^\circ$ along a 160-km-long right-stepping restraining bend, long held responsible for crustal shortening and mountain building in Lebanon. In this region (fig. 33B), the Levant fault splits into three branches, with clear evidence for slip partitioning: the two easternmost strands (Yammoûneh and Râchaïya-Serghaya) are left-lateral strike-slip faults, while the WNW-ESE shortening associated with the restraining bend is taken up on a previously unrecognized offshore fault, the Tripoli-Roûm Thrust, which dips ESE under Mount Lebanon [Tapponnier et al., 2001].

Geologically and geomorphically, the Yammoûneh fault appears to be the main on-land branch of the LFS. It marks the boundary between Mount Lebanon, 3,090 m a.s.l., and the Beqaa plain, 1,000 m a.s.l. (fig. 33B). Its 160 km-long surface trace is sharp and clear in the topography. We mapped it in the field, using aerial and satellite imagery. North of Zahle, it cuts across Cretaceous limestones, whereas to the south it marks the contact between Jurassic limestones (the Bâroûk ridge) to the west and younger Cretaceous, Tertiary or Quaternary rocks. The $\sim 30^\circ\text{E}$ fault strike does not vary much, except in the vicinity of small (≤ 6 -km-long) basins or ridges, which form small-scale pull-aparts or push-ups. Though the fault's seismogenic potential is still a matter of debate, it lies fully within the isoseismals of the M>7 earthquake of 1202 AD [Ambraseys and Melville, 1988; Ellenblum et al., 1998].

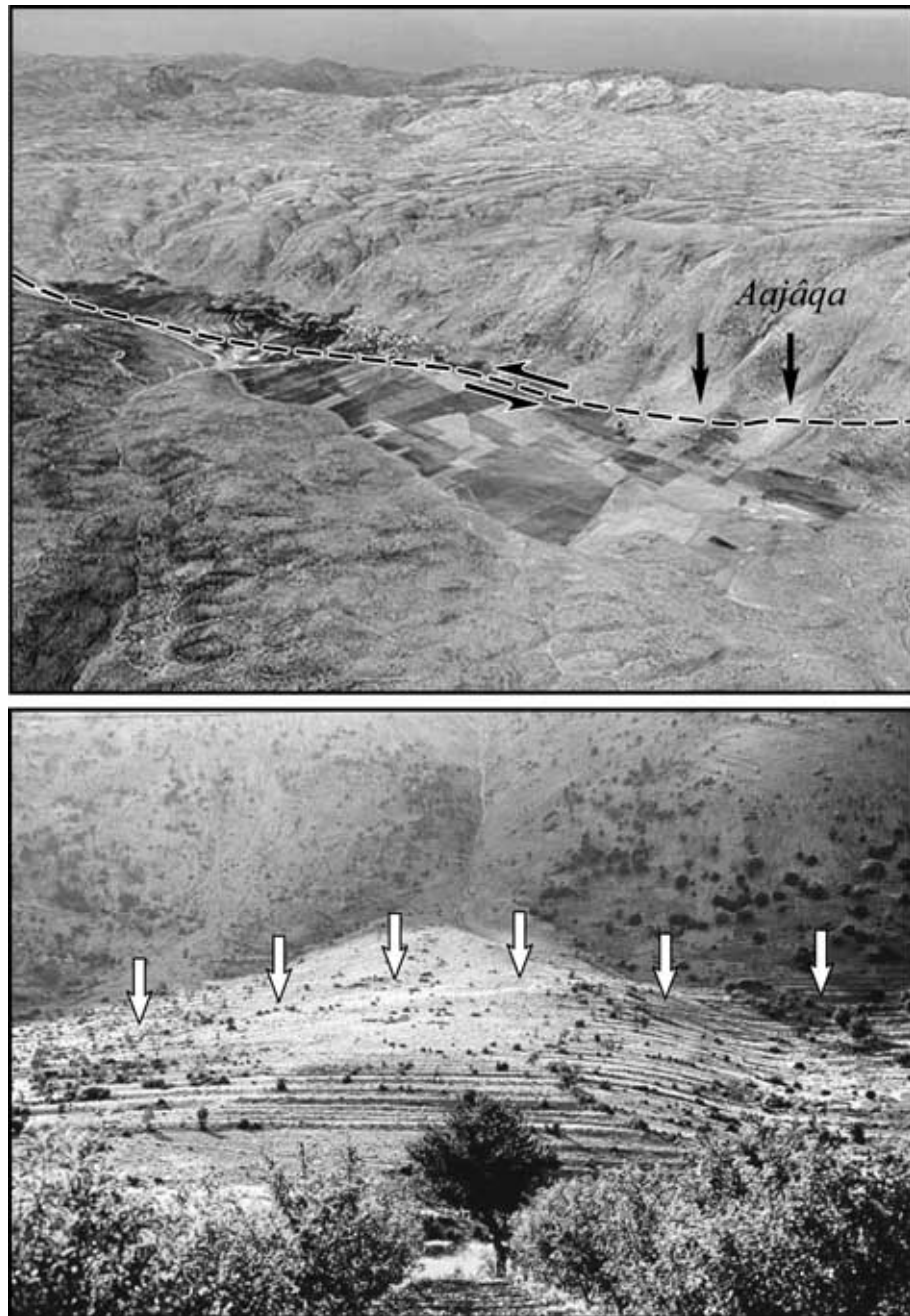


Figure 34: Aerial view of Yammoûneh basin (upper panel). Basin originally formed as active pull-apart, but there is no visible strike-slip faulting on either side. Instead, as inferred from resistivity measurements [Besançon, 1968] and confirmed by recent paleoseismologic studies [Daëron et al., 2001], active fault now shortcuts pull-apart. We studied offsets of two fans (black arrows) in northernmost part of basin. **Field view of Aajâqa fan in Yammoûneh basin (lower panel).** Distal (sunlit) part of fan is offset left-laterally by Yammoûneh fault (white vertical arrows) with respect to fan apex.

All along its trace, the fault commonly offsets Quaternary landforms such as river channels, small gullies and fans. We describe below the morphology and Quaternary geology of two such sites, 50 km apart (fig. 33B), where offset alluvial fans offer clear evidence of cumulative slip.

Site 1: Offset fans in the Yammoûneh Basin

The Yammoûneh basin lies 1,400 m a.s.l., on the eastern flank of Mount Lebanon, between thick subtabular sequences of karstified Cenomanian limestone. This 6-km-long, 2-km-wide depression is the largest pull-apart basin along the fault, to which it gives its name. The modern, active surface trace of the fault cuts across the basin. At the north end of the pull-apart, as it veers away from the basin's western rim, the active fault cuts and offsets two alluvial fans built by short, steep catchments that erode the limestone range front (fig. 34).

Figure 35 shows our map of the fans' surface geology and morphology, and of the trace of the fault, based on field observations, stereoscopic air photographs at a scale of 1/25,000, topographic maps (1/20,000) and QuickBird satellite images (60 cm resolution). In each fan, several distinctive surfaces stand out. Although it is clear that, overall, the fans are offset left-laterally by the fault, the original topography, particularly of the lowest, most gently sloping parts of each fan, has been modified by agricultural terracing. The resulting blur of most limits precludes measuring cumulative offsets, except for the northern fan (Aajâqa fan), whose NE edge is well-defined, providing a piercing line.

To assess the cumulative offsets and corresponding uncertainties, both the geomorphic map of figure 35 and the satellite image were retro-fitted (fig. 36). Back-slipping along the fault restores the continuity and linearity of different types of geomorphic markers at this site, providing different values of cumulative offset. 24 ± 2 m of back-slip are necessary to restore a shallow gully incised into the surface of the Aajâqa fan. Pairing this offset with the age of the incised surface would only yield a strict lower bound on the slip rate. With ~ 35 m of back-slip, the alignment between the fan's feeder channel west of the fault and the NW-SE-trending fan axis (*A*) is restored. Because of high-energy deposition at the base of a steep, 45° slope, this axis is uniquely defined as the only rectilinear streamline of the topographic gradient; as expected, it strikes parallel (134°E) to the fan's feeder channel, all the way down to the basin floor. Finally, 40 ± 5 m of back-slip are needed to restore the NE edge of the fan, which is unquestionably the best-defined of the three offset markers. We conclude that the cumulative offset of the fan surface is most likely between 35 and 45 m. Although all the deposits on that surface may not have been emplaced at the same time, dating the main episode(s) of aggradation should yield bounds on the slip rate.

Site 2: Offset of the Zalqa fan

Figure 37 shows a west looking view of the Zalqa fan, 50 km south of the Yammoûneh basin. It lies ~ 900 m a.s.l. on the west side of the Beqaa plain (cf fig. 33B) at the base of the steep east-facing flank of the southern tip of Mount Lebanon (Bâroûk anticline). It is a well-developed, 1-km-wide alluvial fan composed of limestone pebbles, cobbles and boulders. The fan's conic envelope is truncated near its apex and offset left-laterally with respect to its feeder channel. The main difference between this site and the Yammoûneh site is that here the fault cuts mostly across the limestone bedrock at the fan apex rather than across the fan.

Figure 38 shows our map of the Zalqa site. Upstream from the fault, three channels (C1, C2, C3) have fed the fan. C1 and C2 merge near the top of the fan apex. C1 (Ouâdi Zalqa) has the broadest catchment and has incised deepest. Its channel is filled with weakly weathered limestone debris, distinctive on the air photos and Spot 5 image from their light color. These observations strongly suggest that C1 is the main feeder channel of the Zalqa fan. The third channel C3 (Ouâdi Aaouaj), is located south of the two others and presently crosses the fault with no visible offset. We interpret this to indicate

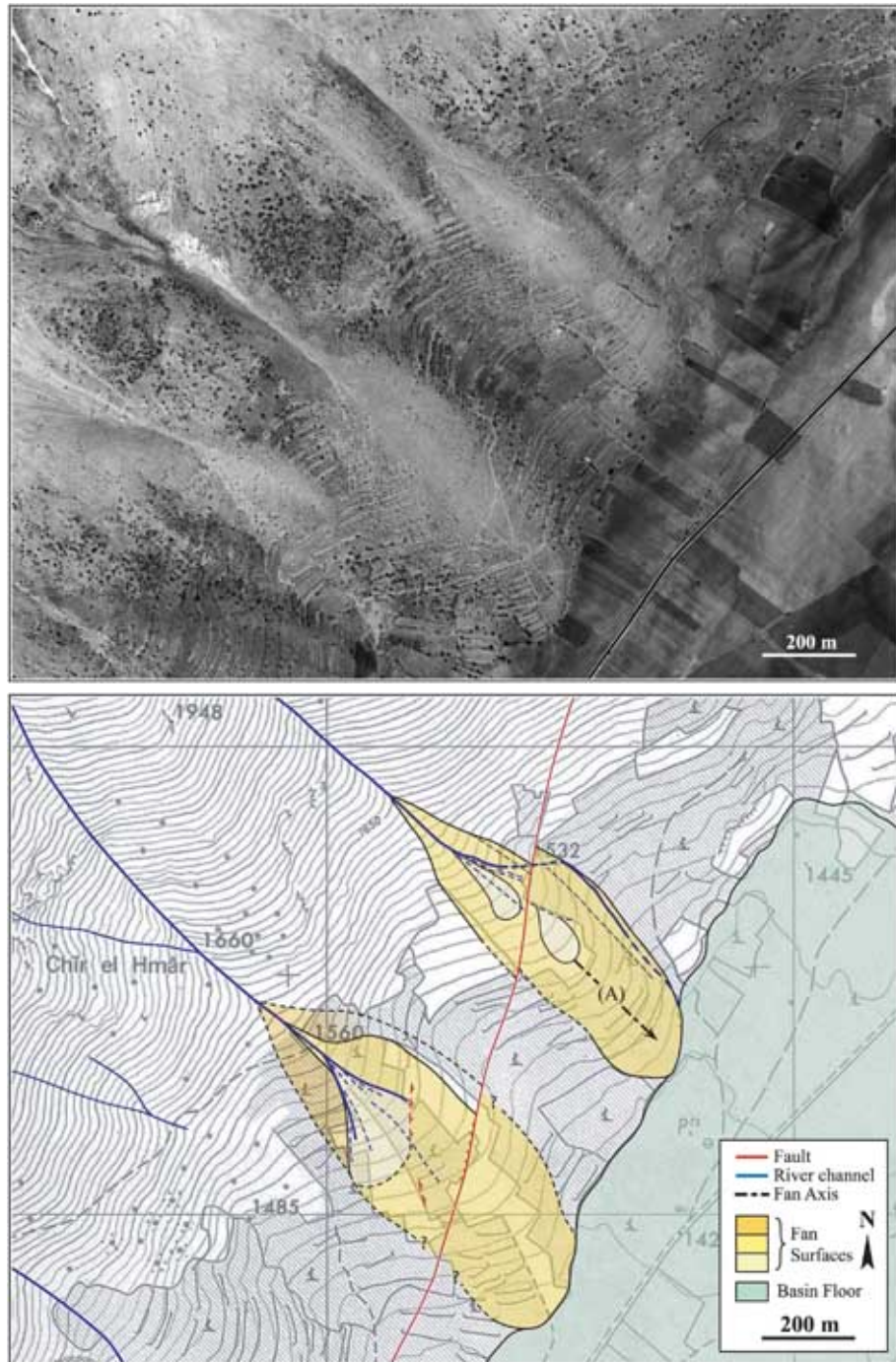


Figure 35: (Top) QuickBird satellite image of two northern fans in Yammoûneh basin. **(Bottom)** Corresponding map. Distinct surfaces of different ages are shown within each fan. Full lines limit extent of fan deposits, while dashed lines mark inflection of topography where range-front slope meets curved fan surface. Cumulative offsets are similar for both fans, although only northernmost one (Aajâqa fan) shows piercing line offsets clear enough to yield quantitative results. A is Aajâqa fan's topographic axis (see text).



Figure 36: Retro-fit of Yammoûneh fans. (Left) 24 ± 2 m of backward slip restores median incision on surface of Aajâqa fan. (Right) 40 ± 5 m of backward slip restores NE edge of Aajâqa fan. slightly smaller amount of back-slip (~ 35 m) restores alignment of Aajâqa fan's feeder channel and fan's axis.

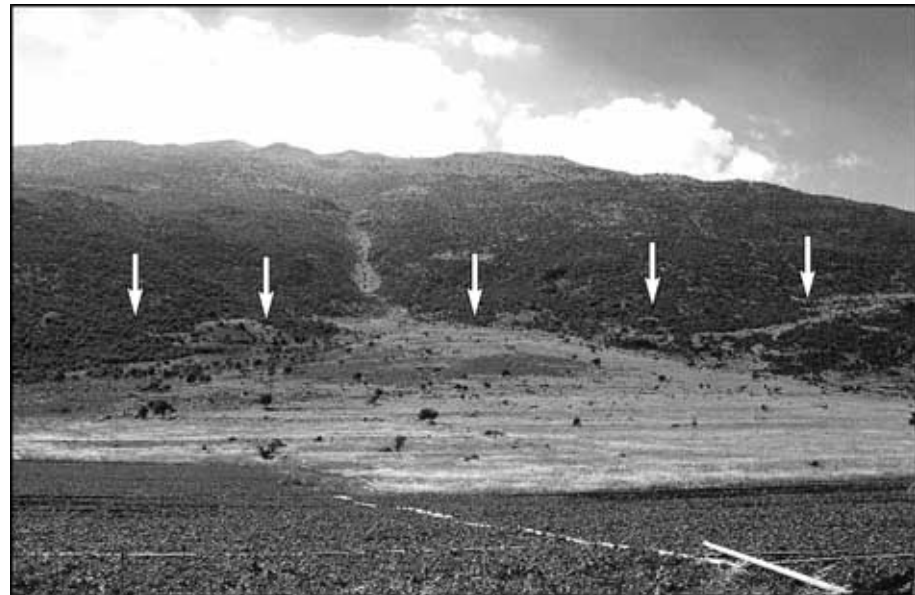


Figure 37: Field view of the Zalqa fan. Bulk of fan deposit is not aligned with main feeder channel, due to cumulative left-lateral slip on Yammoûneh fault (white vertical arrows), which cuts fan just below its apex (cf fig. 38).

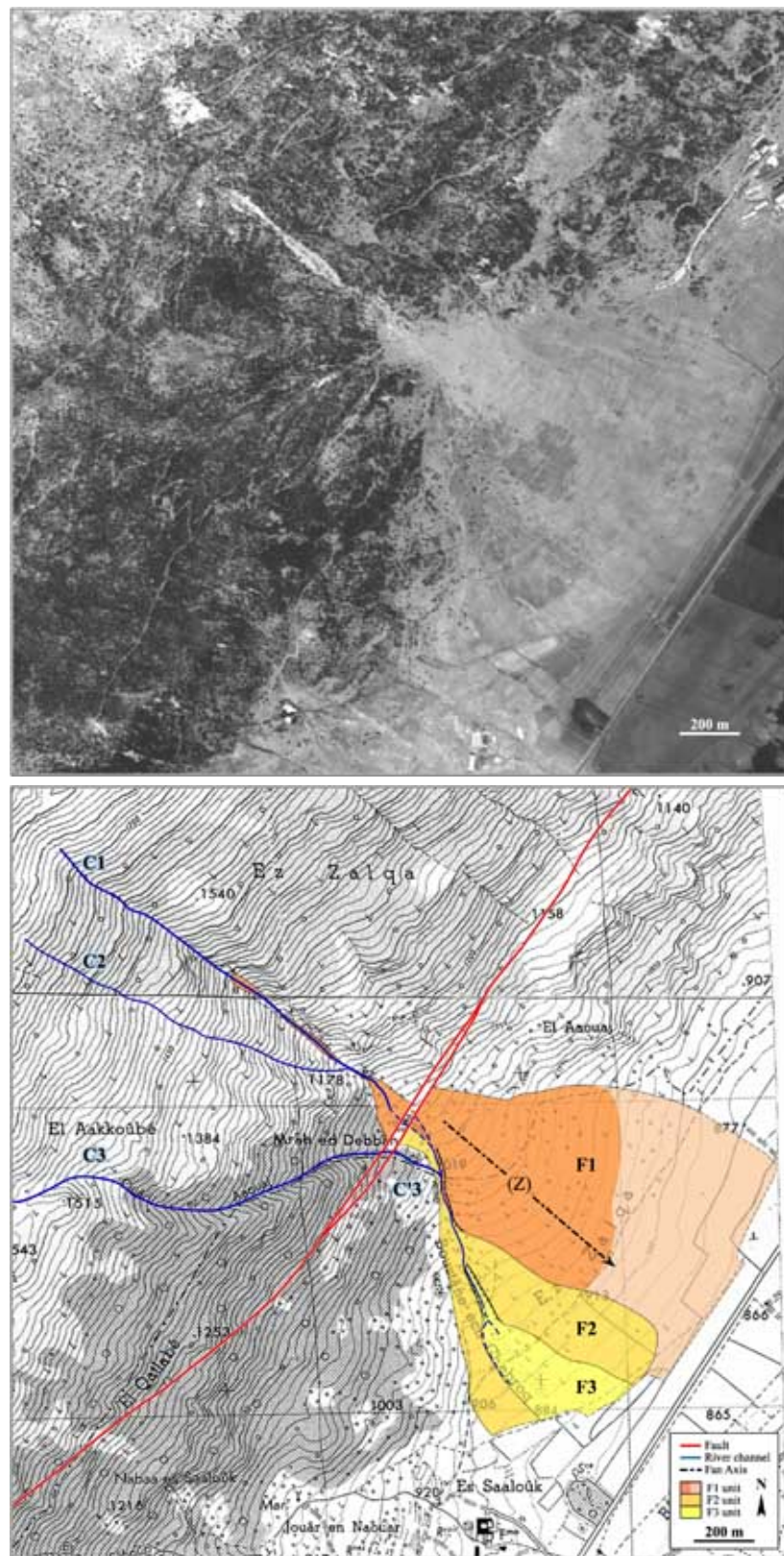


Figure 38: (Top) Spot-5 satellite image of Zalqa fan. **(Bottom)** Corresponding map. Three fan generations with different surfaces and ages (F1, F2, F3) are mapped. Oldest F1 surface is clearly offset by Yammoûneh fault. Note recent capture of channel C3. Z is topographic axis of F1 (see text).

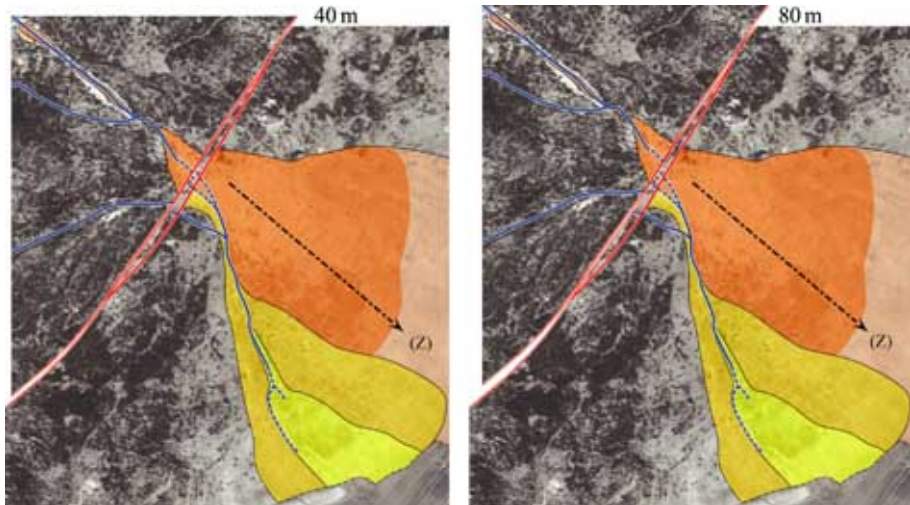


Figure 39: Retro-fit of Zalqa site. (Left) 40 ± 2 m of backward slip restores narrow channel incised in F1. **(Right)** 80 ± 8 m of backward slip restores outer edges of F1 and alignment between upstream feeder channel and topographic axis Z.

that it was recently captured by the small C'3 stream west of the fan. This inference is supported by the deepening of incision in the C3-C'3 channel downstream from the fault zone.

The Zalqa fan is composed of three sub-units (F1, F2, F3). F1 is the largest and oldest. It extends from the fan apex tip to the cultivated flats in the Beqaa. Its upper half is steeper and more cone-shaped than its distal part. A younger unit F2, inset at a lower level, was later emplaced along the SW side of F1. Later still, F2 was incised by a new channel which fed the lowest and youngest fan F3. It is unclear which feeder channel was primarily responsible for this latest aggradation event, although C3 was certainly involved.

The Yammoûneh fault's active trace cuts F1 ~ 100 m downslope from the fan apex tip. Cumulative displacement juxtaposed the top of F2 next to the apex of F1. Similarly it brought F1 into contact with the Jurassic limestone bedrock of the mountain's flank. The trace of the fault splays into two parallel strands, ~ 20 m apart, across the fan apex. Figure 39 shows retro-fitted maps of the Zalqa fan. The restorations are performed using air photographs, topographic maps (1/20,000), Spot 5 (2.5 m resolution) and Ikonos (1 m resolution) images.

As at the previous site, two different values of cumulative offset are recorded. 40 ± 2 m of back-slip are required to realign a small but well-defined channel incision on the surface of F1. Again, however, there is no reliable way to date the incision itself, except that it must postdate the emplacement of F1. 80 ± 8 m of back-slip restore the geometry of the apex of F1, as well as the alignment between C1 and the topographic axis (Z) of F1's upper conic surface (defined as at Aajâqa). The consistency between these two fits strongly suggests that ~ 80 m is the cumulative offset since the aggradation of F1.

2.2.3 Cosmogenic dating of offset alluvial fans

Chlorine-36 surface exposure dating of limestone cobbles

Cosmogenic exposure dating of alluvial fans has so far mostly been applied to surfaces bearing silicate-rich rocks [e.g. Van der Woerd et al., 1998, 2002; Ritz et al., 2003]. In Lebanon, as in much of



Figure 40: (A) Typical cobble sampled on Zalqa fan; (B) Surface and depth profile on Aajâqa fan (see text).

the Mediterranean, however, limestone rocks are ubiquitous. Here we used ^{36}Cl to determine the surface exposure age of the limestone cobbles that pave the surface of the two alluvial fans described above. In limestone, ^{36}Cl is produced primarily through interactions of cosmic ray secondary neutrons and muons with Ca in calcite (CaCO_3) [e.g. Benedetti et al., 2002; Mitchell et al., 2001]. The production rate decreases exponentially with depth and ^{36}Cl is thus mostly accumulated near the surface [Stone et al., 1996]. In general, the accumulation of cosmogenic nuclides in a rock exposed at the earth surface may be described by:

$$N(t) = N(0)e^{-\lambda t} + \frac{P}{\lambda + \epsilon\mu}(1 - e^{-(\lambda + \epsilon\mu)t}) \quad [\text{Lal, 1991}]$$

where $N(t)$ is the concentration at time t (yr), P is the surface production rate (atom/g/yr), λ is the decay constant of the radioactive nuclide ($2.303 \times 10^{-6} \text{ yr}^{-1}$ for ^{36}Cl), ϵ is the erosion rate (cm/yr), μ is the absorption coefficient (cm^{-1}), equal to ρ/L , where ρ is the density of the sampled rock (here 2.7 g/cm^3 , since our samples are nearly pure calcite according to [Ca] measurements), and L is the absorption mean free path for interacting cosmic secondary particles in the rock (160 g/cm^2). $N(0)$ is the inheritance component.

Our goal is to date geomorphic features that have been passively preserved during displacement along the fault. The geomorphic freshness of the Aajâqa and Zalqa alluvial fans suggests that they are young enough that the effects of erosion at the surface might be expected to be small. Recent studies in the Mediterranean show that hanging bedrock carbonate surfaces can be lowered by dissolution at rates of between 8 [Benedetti et al., 2003] and 29 $\mu\text{m}/\text{yr}$ [Mitchell et al., 2001]. How these estimates can be extrapolated to gently-sloping alluvial surfaces, however, remains unclear. Karstic dissolution typically increases surface relief on horizontal scales of up to several meters, and leads to consolidation by calcite cementation of the clasts. Neither of the fan surfaces we sampled shows significant relief at such scales, and the angular limestone clasts and cobbles are loose, with interstitial clay only, down to depths of at least 2 m (Aajâqa) and 70 cm (Zalqa). Moreover, on both surfaces, cobbles show little evidence of dissolution, such as micro-karst, pits, etc. (fig. 40). Finally, there is no evidence that the cobbles now at the surface might have been buried tens of centimeters deep under shallower cobbles now removed by dissolution. For instance, none of the cobbles show remnant clay-rich concretion patches typical of long

underground burial. Hence, although we cannot completely rule out that some dissolution affected the surface of the fans, we find it likely that the amount has been too small to have a significant effect.

The rather short and steep catchments of both Ouâdi Zalqa and Ouâdi Aajâqa imply short transport times and little along-stream storage. Systematic observations in similar catchments elsewhere have shown that this configuration usually yields sample populations that, despite variable inheritance, are often characterized by sample ages that show a cluster at the youngest end of the age distribution. This young cluster typically has the same age as that, independently determined by radiocarbon dating, for the abandonment of the alluvial surface [e.g. Van der Woerd et al., 1998, 2002; Mériaux et al., 2004]. In other words, most samples show negligible systematic inheritance, but a few, which have had more complex transport histories, show much older ages and can be regarded as outliers. In view of the rather steep slopes of the fans ($\sim 8\text{--}10^\circ$), however, superficial rearrangement of the cobbles after initial emplacement cannot be ruled out. Also, we cannot rule out that parts of the fan surfaces have a composite nature, resulting from somewhat diachronous periods of deposition.

Fourteen limestone cobbles were collected and dated on each fan. The altitudes and locations of the samples were measured with a hand-held GPS. We therefore estimate the uncertainty on horizontal and vertical positions to be ~ 15 m and at least 20 m, respectively. We selected cobbles of about the same size (20–30 cm diameter), well-embedded in the ground (i.e. protruding a few centimeters above the surface, cf fig. 40), to minimize the possibility of post-emplacement disturbances.

After grinding, leaching and chemical extraction of chlorine by precipitation of silver chloride, the ^{36}Cl and chloride concentration in the carbonate was determined for all samples by isotope dilution accelerator mass spectrometry at the Lawrence Livermore National Laboratory CAMS facility. Blanks were two orders of magnitude lower than the samples and replicates agreed to better than 5%.

Results

Surface exposure ages were calculated using the ^{36}Cl production rates from calcium of Stone et al. [1998] for all relevant pathways. Other published production rates — e.g. Swanson and Caffee [2001] and other references therein — are greater than Stone et al.’s value, which would lead to ages younger by about 20%. The production rates were calculated at our site latitude and altitude using Lal [1991] coefficients. The exposure ages presented in table 3 include analysis and processing errors, as well as the error on Stone et al.’s production rate. Shielding by the surrounding topography was measured in the field and found to be negligible.

At both sites, there seems to be little systematic relationship between ^{36}Cl concentration and sample position, although at Aajâqa three of the oldest samples are located in the distal part of the fan. A 2-m-deep depth profile (fig. 40) dug in the central part of the Aajâqa fan, east of the fault, yielded ^{36}Cl concentrations that did not show the expected decrease as a function of depth consistent with single-stage deposition of a homogeneous population of cobbles.

The surface ages ranges between 4.0 ± 0.3 kyr and 27.3 ± 2.1 kyr at Aajâqa, and between 7.8 ± 0.9 kyr and 66.0 ± 6.9 kyr at Zalqa (Table 3 and fig. 41–42). Even though the data shows a fair amount of scatter at both sites, groups of ages can be discerned, with clusters of young ages. At Aajâqa, 7 samples out of 14 are between 5.7 and 9.6 ka, and 5 are between 13 and 22 ka. Two samples do not belong to these two groups: Y18 (3.9 ka) and Y3 (27 ka). At Zalqa, sample ages are generally older, with 4 out of 14 between 12 and 15 ka, and 6 between 19 and 27 kyr. ZLQ-W4 (7.8 ka) is younger by 4 kyr than the

Sample	Altitude [m]	Latitude [°N]	Ca dissolved [g]	Chlorine [ppm]	^{36}Cl [atoms.(g rock) $^{-1}$]	^{36}Cl production rate [atoms.(g rock) $^{-1} \cdot \text{yr}^{-1}$]	Age [yr]
Y18	1541	34.15	4.82	10.2	187065 ± 10046	46.9	3990 ± 327
Y19	1544	34.15	9.32	38.6	264822 ± 10246	46.2	5730 ± 419
Y1	1442	34.15	9.50	7.5	261183 ± 9938	43.2	6040 ± 464
Y5	1489	34.15	12.17	28.5	332484 ± 10756	48.2	6903 ± 498
Y17	1539	34.15	6.89	7.3	371688 ± 15029	47.1	7894 ± 586
Y8	1494	34.15	6.23	22.3	378593 ± 16710	45.0	8409 ± 657
Y11	1513	34.15	8.06	10.1	428412 ± 15962	47.5	9026 ± 663
Y6	1491	34.15	10.89	23.4	438796 ± 11568	45.4	9655 ± 672
Y14	1539	34.15	11.12	23.0	674586 ± 17797	50.2	13432 ± 909
Y4	1445	34.15	11.00	29.9	686618 ± 18370	44.5	15442 ± 1106
Y2	1442	34.15	9.82	20.1	844814 ± 22629	44.1	19148 ± 1376
Y9	1503	34.15	7.70	25.5	997896 ± 29756	48.0	20783 ± 1467
Y16	1536	34.15	9.45	45.0	1095443 ± 28919	50.1	21883 ± 1484
Y3	1442	34.15	4.58	19.2	1201051 ± 41877	44.0	27323 ± 2057
ZLQ-W4	1091	33.2	14.06	28.2	319323 ± 28375	41.0	7782 ± 921
ZLQ-E12	1049	33.2	15.41	14.3	455219 ± 39863	38.6	11794 ± 1405
ZLQ-W1	1067	33.2	15.75	20.0	494880 ± 43486	39.4	12569 ± 1490
ZLQ-E7	973	33.2	15.73	14.7	469079 ± 39237	36.7	12786 ± 1527
ZLQ-E3	947	33.2	15.81	22.3	535036 ± 36105	36.0	14874 ± 1638
ZLQ-W3	1083	33.2	15.17	36.1	734847 ± 39617	39.2	18761 ± 1792
ZLQ-E11	1056	33.2	13.65	22.2	722007 ± 48401	37.9	19050 ± 1994
ZLQ-E5	961	33.2	15.27	33.0	765504 ± 48884	37.4	20491 ± 2198
ZLQ-E10	1055	33.2	16.19	17.4	843703 ± 70037	39.1	21572 ± 2493
ZLQ-E6	969	33.2	15.38	29.0	871437 ± 78153	36.4	23911 ± 2966
ZLQ-E2	941	33.2	15.71	20.8	963681 ± 66638	35.8	26914 ± 3002
ZLQ-E8	972	33.2	15.73	19.4	1309400 ± 80555	37.3	35117 ± 3705
ZLQ-E1	943	33.2	13.12	16.9	1593818 ± 119858	35.6	45192 ± 5244
ZLQ-E9	967	33.2	16.89	12.8	2376936 ± 144957	36.0	66049 ± 6947

Table 3: Sample characteristics and exposure ages. Scaling factors for ^{36}Cl production by neutrons and muons were calculated at each site [Stone et al., 1996, 1998, and references therein]. Calcium content in each sample was measured by ICP at CEREGE, with respective average Ca/(g rock) contents of $37 \pm 1\%$ at Zalqa and $35 \pm 1\%$ at Aajâqa. ^{36}Cl measurements were standardized relative to a NIST ^{36}Cl standard.

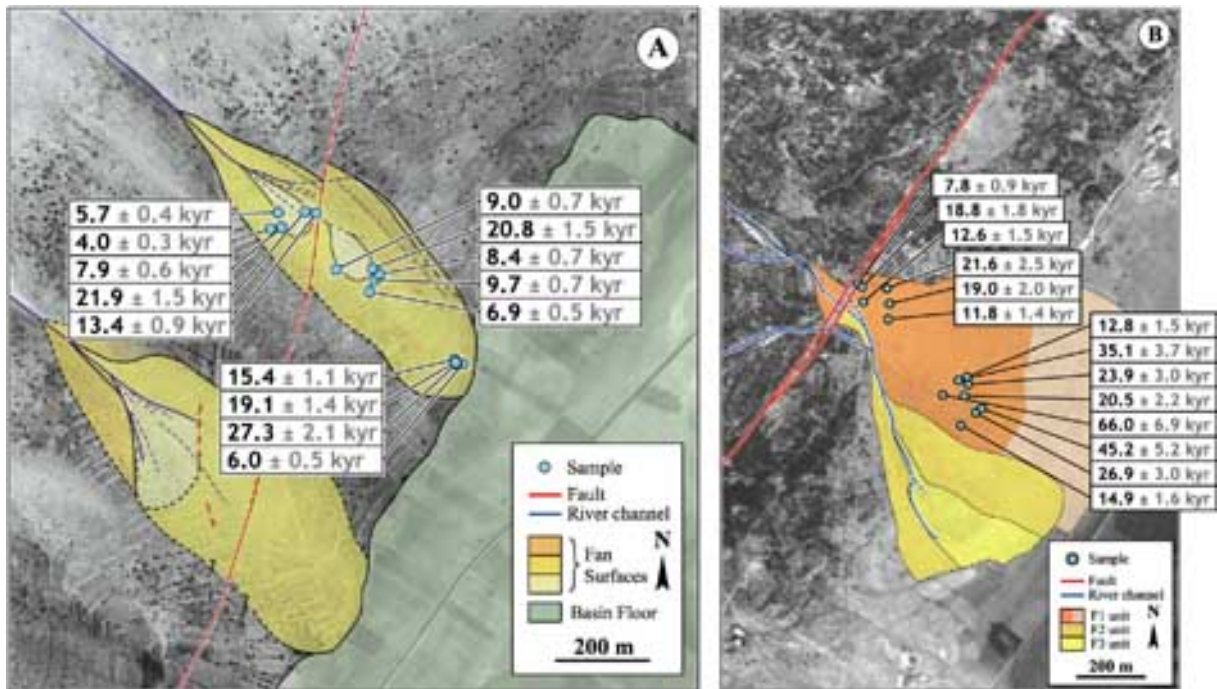


Figure 41: Position and exposure ages of dated limestone cobbles on offset Aajâqa (A) and Zalqa (B) fans. Little relationship is visible between sample position and exposure age, although old samples tend to be in distal parts of fans.

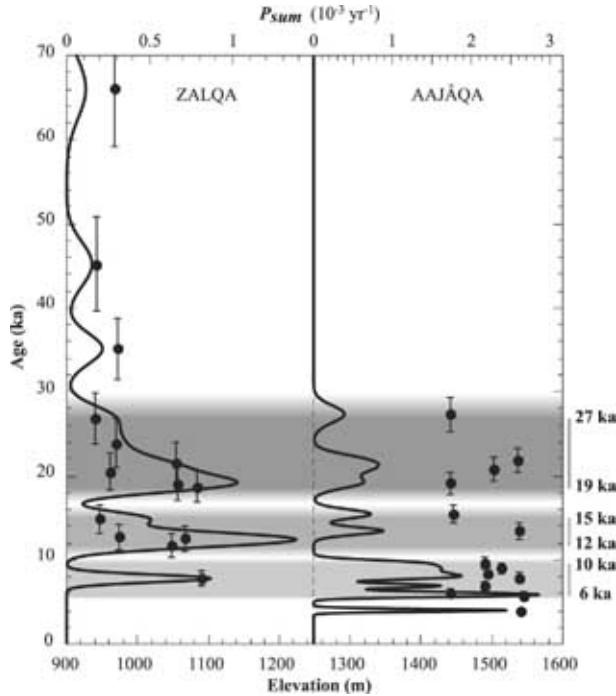


Figure 42: Exposure ages of samples, with corresponding error bars, plotted versus sample elevation (cf table 3). Curves are age probability sums (see text).

youngest sample of the first group. By comparison with other terraces and fans dated with cosmogenic isotopes elsewhere [e.g. Van der Woerd et al., 2002; Mériaux et al., 2004], we interpret ZLQ-E8 (35 ka), E1 (45 ka) and E9 (66 ka), which are much older than the oldest sample of the second group, to have experienced exposure before deposition (inheritance) and therefore consider them to be outliers.

In order to discuss this data further, we plotted on figure 42 the sum at each site of the Gaussian age probability distributions (P_{sum}) for all dated samples [Lowell, 1995], expressed as:

$$P_{sum}(t) = \sum_i e^{-(t-a_i)^2/2\sigma_i^2} / \sigma_i \sqrt{2\pi} \quad [\text{Taylor, 1997}]$$

where t is time, a_i the exposure age of sample i and $(2\sigma_i)$ the reported error. The two curves show distinct peaks that quantify the grouping of samples by age inferred from simple inspection of the data, and support our elimination of the three oldest Zalqa samples as outliers. Figure 42 demonstrates the temporal coincidence of the three main distribution peaks (~ 20 ka, ~ 14 ka and ~ 8 ka) at both sites. Such correspondence, in regions ~ 50 km apart, argues for successive emplacement episodes of distinct cobble populations. Hence, although we cannot rule out the possibility of scatter or bias due to loss of chlorine by alteration or erosion of cobbles, or by post-depositional burial or exhumation, our results are in favor of fan aggradation controlled by regional climate, leading to successive emplacement episodes of distinct cobble populations, as documented elsewhere [e.g. Van der Woerd et al., 2002; Mériaux et al., 2004]. This fan emplacement scenario is in agreement with the conclusion of Klinger et al. [2003], who relate main aggradation periods in the Dead Sea area, ~ 350 km to the south, to warm and wet pluvials before the Younger Dryas, between 15 and 13 ka (cf 15-12 ka peak at Zalqa in fig. 42), and around 7 ka (cf youngest peak at Aajâqa in fig. 42).

The observed offsets cannot predate the onset of aggradation. Alternatively, one could argue that

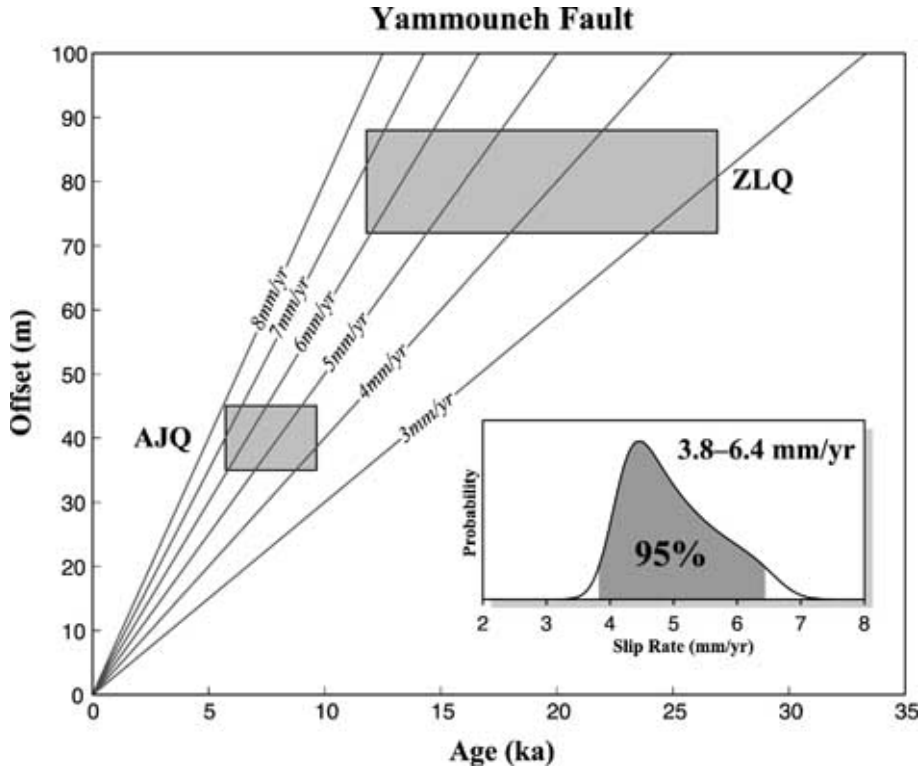


Figure 43: Constraints on slip rate of Yammoûneh fault. Plot of offsets versus ages shows consistency of results at Aajâqa (AJQ) and Zalqa (ZLQ). Inset shows corresponding probability distribution of slip rate on Yammoûneh fault (see discussion in text).

the entire offset accrued since aggradation stopped and the fan became passive. To estimate the slip rate on the Yammoûneh fault, we choose to use these guidelines to set conservative bounds, and take the recorded age of the offsets to be within the bounds of the latest major aggradation episodes, as reflected by the relative weight of age clusters on each fan (fig. 42): at Aajâqa, half of the sample ages cluster within 6–10 kyr, while at Zalqa most were emplaced between 27 and 12 ka.

Slip rate

At Aajâqa, 40 ± 5 m of slip would thus have been recorded since at most ~ 10 ka and at least ~ 6 ka, while at Zalqa 80 ± 8 m of slip would have accrued since at most ~ 27 ka and at least ~ 12 ka (fig. 43). The rates obtained are 3.5–7.5 mm/yr at Aajâqa, and 2.7–7.3 mm/yr at Zalqa.

These ranges of values are fully consistent, as they should be, given the similar orientation of the fault at both sites and its simple geometry in between. It is therefore legitimate to combine both data sets to further constrain the bounds on the slip rate, by multiplying the two rate probability distributions. At each site we take the age (a) of the offset to have a uniform probability distribution between its lower and upper bounds a_{min} and a_{max} (5.73–9.65 ka at Aajâqa and 11.8–26.9 ka at Zalqa). The value (d) of the offset has a Gaussian probability distribution whose center (d_o) and σ -value (σ_d) are such that the 95% confidence intervals are respectively 35–45 m (Aajâqa) and 72–88 m (Zalqa).

The probabilities for d and a being independent, the rate ($v = d/a$) probability distribution at each site can be written as:

$$P_v(v) = \frac{1}{\sigma_d \sqrt{2\pi} (a_{max} - a_{min})} \int_{a_{min}}^{a_{max}} \exp\left(-\frac{(vt - d_o)^2}{2\sigma_d^2}\right) t dt$$

and the combined probability distribution for v is the normalized product of the two distributions (fig. 43). The 95% confidence interval for this combined distribution argues for a slip rate within 3.8–6.4 mm/yr. In conclusion, in the Late Pleistocene-Holocene, the slip rate along the Yammoûneh fault appears to be 5.1 ± 1.3 mm/yr.

2.2.4 Summary and discussion

Quantitative geomorphic evidence at two distinct sites yields the first direct geological estimate of the Late Pleistocene-Holocene slip rate on the Yammoûneh fault, 5.1 ± 1.3 mm/yr. This estimate is derived from ^{36}Cl surface exposure ages of offset alluvial fans, assuming zero erosion of the fan surfaces, as supported by field evidence, and zero systematic inheritance, as documented in several other cosmogenic studies of similar sites [e.g. Van der Woerd et al., 1998, 2002; Mériaux, 2002; Mériaux et al., 2004]. Clearly, stronger erosion would imply older exposure ages, hence slower slip rates, while unaccounted inheritance would have the opposite effect.

Our result is consistent with Mio-Pliocene constraints. Additionally, in contrast with the claims of other authors [Butler et al., 1997; Butler and Spencer, 1999; Khair, 2001], it confirms that the Yammoûneh fault is the main strike-slip branch of the Levant Fault System in the Syro-Lebanese restraining bend.

Since the Yammoûneh fault is only one of three sub-parallel strands of the LFS in Lebanon, however, it is less straightforward to compare our recent slip rate with those proposed by previous authors to the north and south. The difference between the rate of 5.1 ± 1.3 mm/yr that we find and the rate of 6.9 ± 0.1 mm/yr inferred along the Missyaf segment of the northern LFS in Syria by Meghraoui et al. [2003] may be explained in two ways. First, the time span of our study is ~ 25 kyr, as opposed to ~ 2 kyr at Missyaf. Second, the two study areas are separated by a triple junction at the northern tip of Mount Lebanon (fig. 33), where the NE termination of the Tripoli-Roûm thrust connects back with the Yammoûneh fault. Kinematically, the slip rate on the LFS should increase north of that junction.

Comparison with the results of Klinger et al. [2000] in southern Jordan is even more delicate. Although the slip rate (4 ± 2 mm/yr) they obtain along the Araba segment of the southern LFS is, within errors, consistent with ours, at least three first-order fault junctions (with the Roûm, Râchaïya and Carmel faults) separate Mount Lebanon from the Araba valley, ~ 400 km to the south. Slip on any of these active faults should significantly change the rate on the LFS. Both the Roûm and Râchaïya faults are left-lateral, so that the slip rate south of Lake Tiberias is expected to be faster than along the Yammoûneh fault. Gomez et al. [2003], for instance, estimated a slip rate of 1.4 ± 0.2 mm/yr along the Serghaya fault, northern continuation of the Râchaïya fault. A similar kinematic effect should occur with the Carmel fault, a NW-striking normal fault. In keeping with Klinger et al.’s value, a southward-decreasing slip rate on the LFS might result from counter-clockwise rotation of the Sinai-Levant micro-plate, with a Euler pole relative to Arabia somewhere in northern Egypt or in the southern Levantine basin. This would diminish the left-slip component along the LFS in the south, and move the northern Levantine basin (west of Lebanon and SE of Cyprus) away from Arabia, consistent with the direction of subduction SE of Cyprus. Besides, this might explain why the northern LFS shows no sign of strike-perpendicular compression north of Mount Lebanon, contrary to the predictions of most Nubia-Arabia motion models [McClusky et al., 2003; Chu and Gordon, 1998].

Comparison of our results with the post-Miocene mean slip rate on the southern LFS (8–9 mm/yr), provided that it is representative of the Late Pleistocene-Holocene period, suggests that the Yammoûneh fault accounts for over one half of the north-south motion along the Levant fault in Lebanon. Clearly, better constraints on the longer-term (Pleistocene) slip rate along the Yammoûneh fault are required. Similarly, more work needs to be done on the other Lebanese faults to determine their Late-Pleistocene-Holocene rates, and to better understand the slip partitioning and crustal deformation processes at work within the restraining bend.

2.3 Jbab el-Homr

2.3.1 The Jbab el-Homr basin

The Jbab el-Homr basin (location in figure 10, p.22) is the highest (1850 m) intermontane basin along the Yammoûneh fault, at the foot of Qornet es-Saouda. Unlike the Yammoûneh basin, Jbab el-Homr shows no clear evidence of having originated as a pull-apart. There is little sign of recent faulting on the east side of the basin, where quaternary deposits simply taper out on shallow W-dipping Cenomanian limestones. On the other hand, the basin coincides with a marked 15° (W-concave) bend in the trace of the fault (figure 45). The west side of the basin is faulted, with the principal fault strand following a cumulative scarp at the foot of a ridge (Jabal el-Gharbi) that exhumes folded, W-dipping conglomerates due to transpression south of the bend. North of the bend, the fault crosses the lowest and flattest part of the basin, which is filled with clay-rich deposits. These tabular, thinly bedded deposits appear to be mostly the result of summer flooding after particularly wet winters, as is today the case, and may include lacustrine and palustrine beds from earlier, wetter climatic epochs.

Four large fan complexes are fed by catchments terminating in the basin: Ouâdi Aarîch, Ouâdi Hassân and Daoûra, Ouâdi Siyyâd and Ouâdi ed-Dichara. The fan deposits, which are mainly composed of limestone clasts, exhibit different degrees of cementation, reflecting different ages (figures 46 and 47). Three of the fan complexes (Hassân-Daoûra, Siyyâd and Dichara) are cut by the fault (figure 45). The conglomerate beds of one of them (Siyyâd) show significant deformation, with dips of up to 30°, due to small-scale folding sub-parallel to the fault. The tectonic origin of the dips is not in doubt, because near the fault most of the conglomerate dips are towards the WNW, while the depositional slopes in the fans are mostly towards the ESE (figure 48).

2.3.2 Cumulative offsets

The largest cumulative offset visible along the fault is that of the consolidated conglomerates of the fan complex fed by Ouâdi Siyyâd (figure 45). The proximal part of this complex, emplaced west of the fault where the large catchment of the river breaches the range front, is truncated by the fault. We identify the distal part (east of the fault) of the complex at the north end of the basin. It is made of gently SE- and S-dipping consolidated conglomerates that lap onto the Cenomanian basement, thinning out towards the east, suggesting that they were fed from the west. This distal fan apron is now incised by narrow canyons, and bounded along the fault by a west-facing scarp. The conglomerates, which are identical to those of Ouâdi Siyyâd, are thus completely cut off from any possible source west the fault.

Restoring the geometry of the Siyyâd fan (figure 49) yields 3.15 km of cumulative displacement

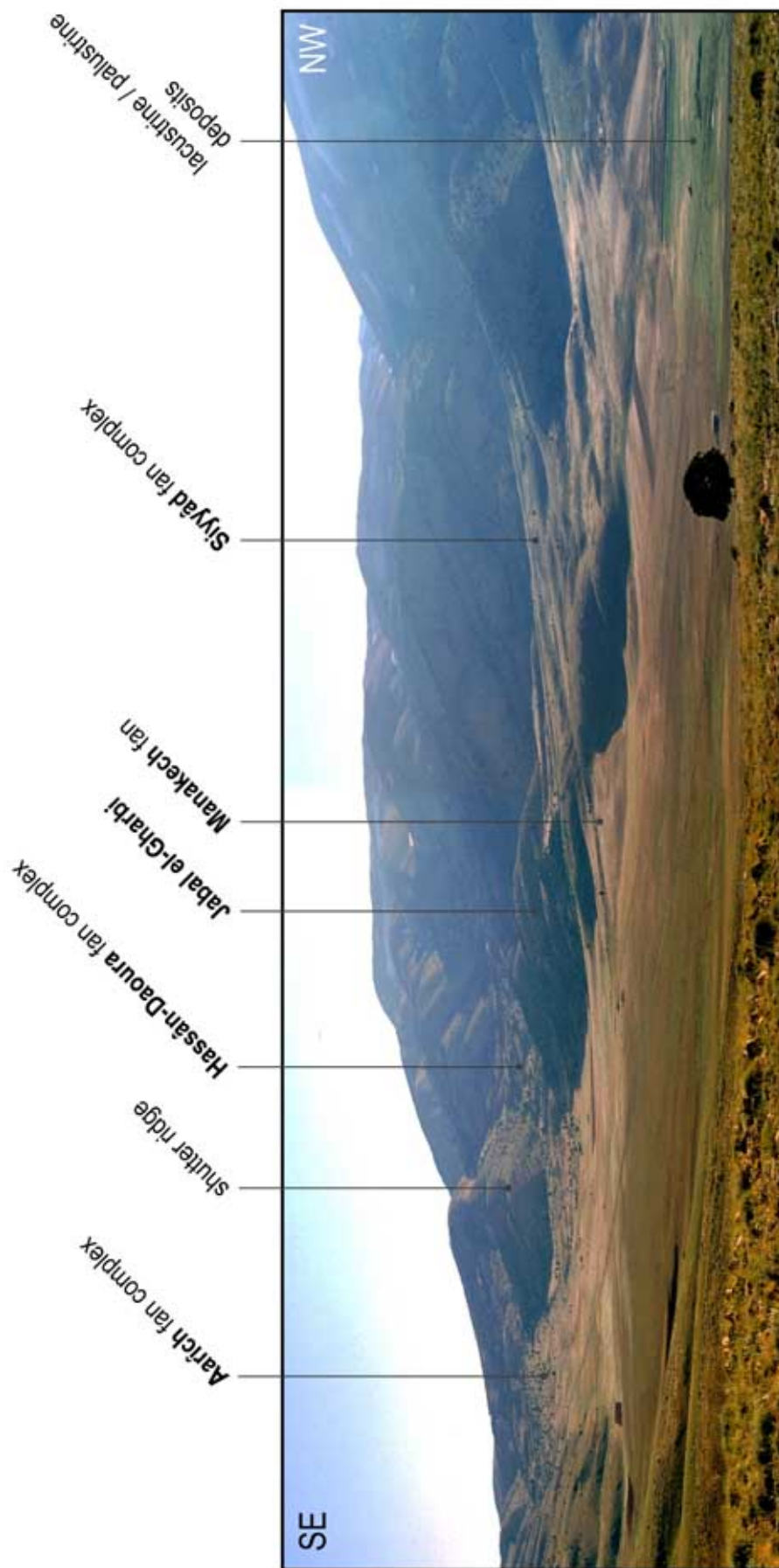


Figure 44: SW-looking panoramic view of *Jbab el-Homr*

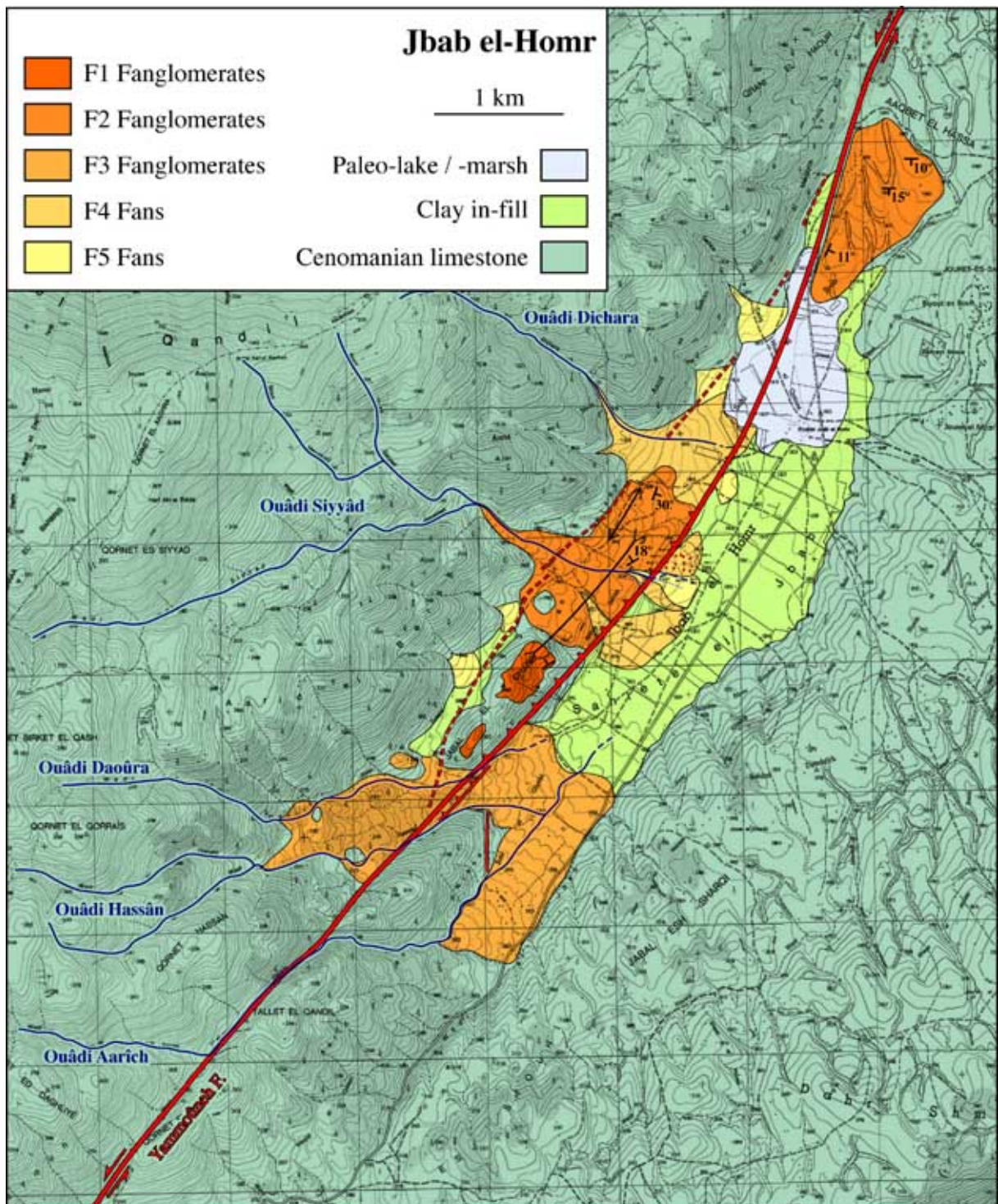


Figure 45: Active faulting in the Jbab el-Homr basin

Relative ages of the fans are inferred based on their degree of cementation and erosion.

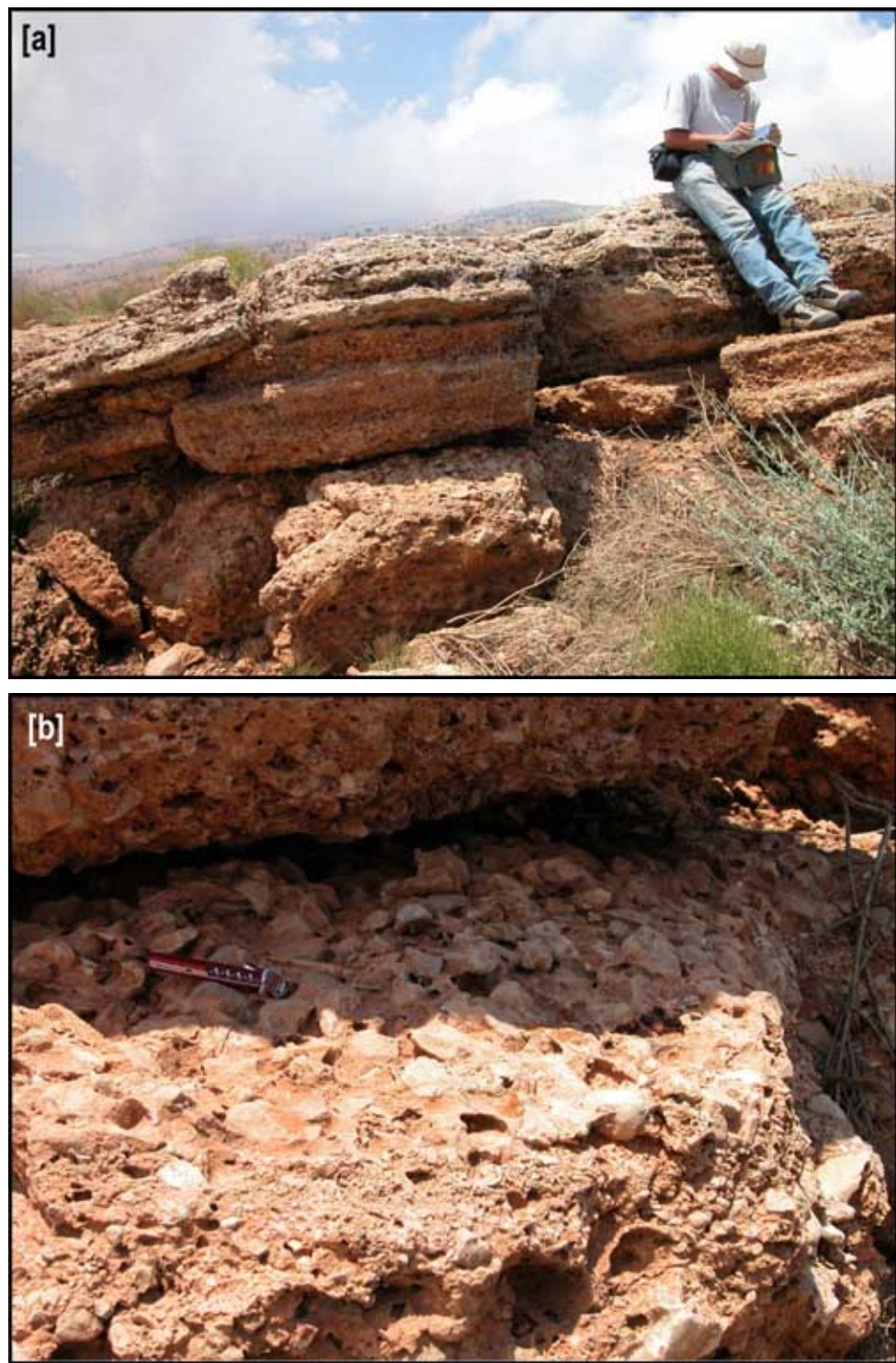


Figure 46: Field photograph of the reddish, strongly consolidated Siyyâd fan conglomerates.



Figure 47: Field photograph of the Hassân fan deposits
These fanglomerates are less consolidated than the Siyyâd conglomerates (figure 46).

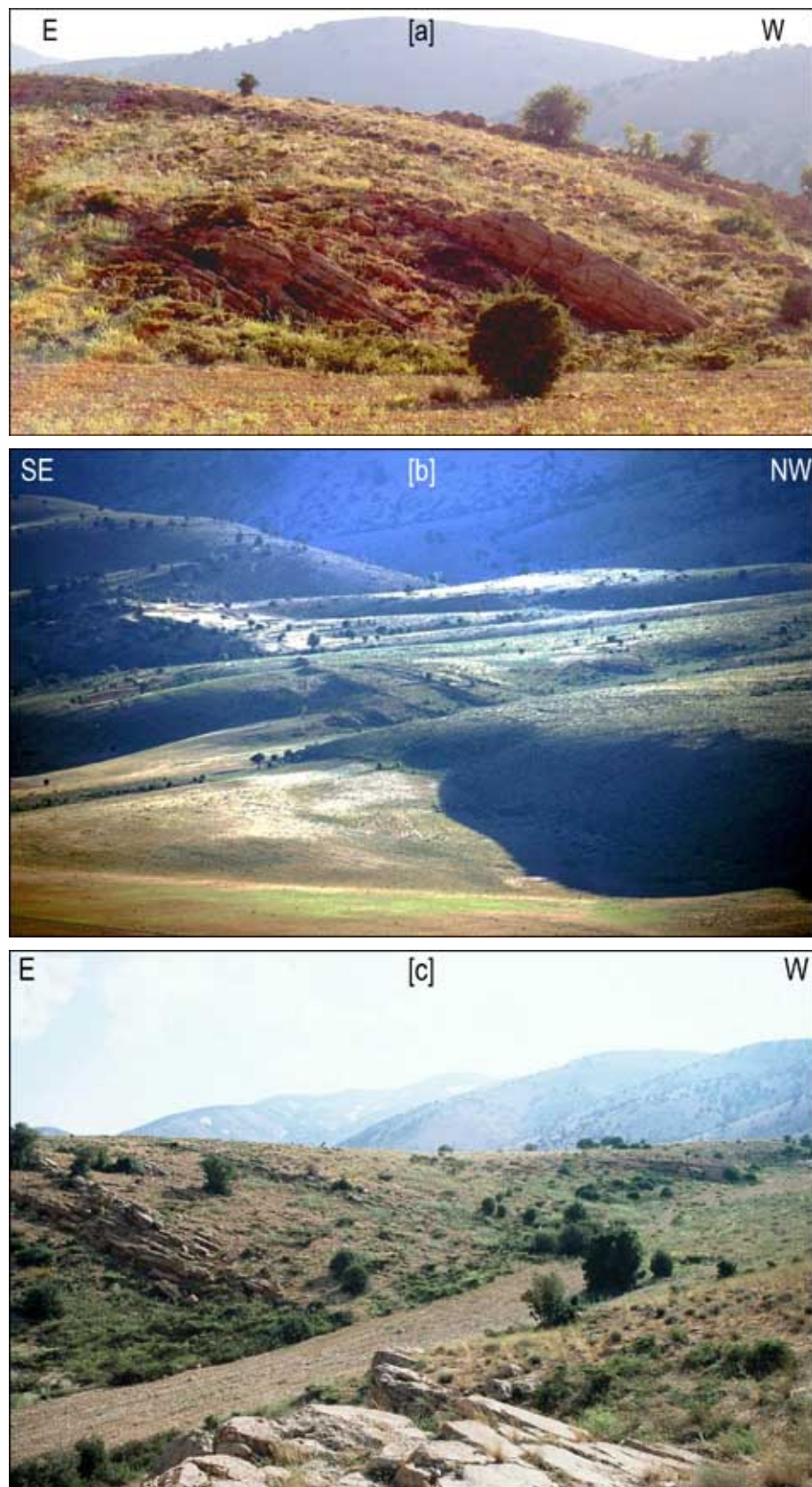


Figure 48: WNW-dipping conglomerate beds in the Siyyâd fan

These counter-slope dips are evidence of recent folding, sub-parallel to the fault. In view [c], note that the frontmost dips are steeper than the dips to the far right.

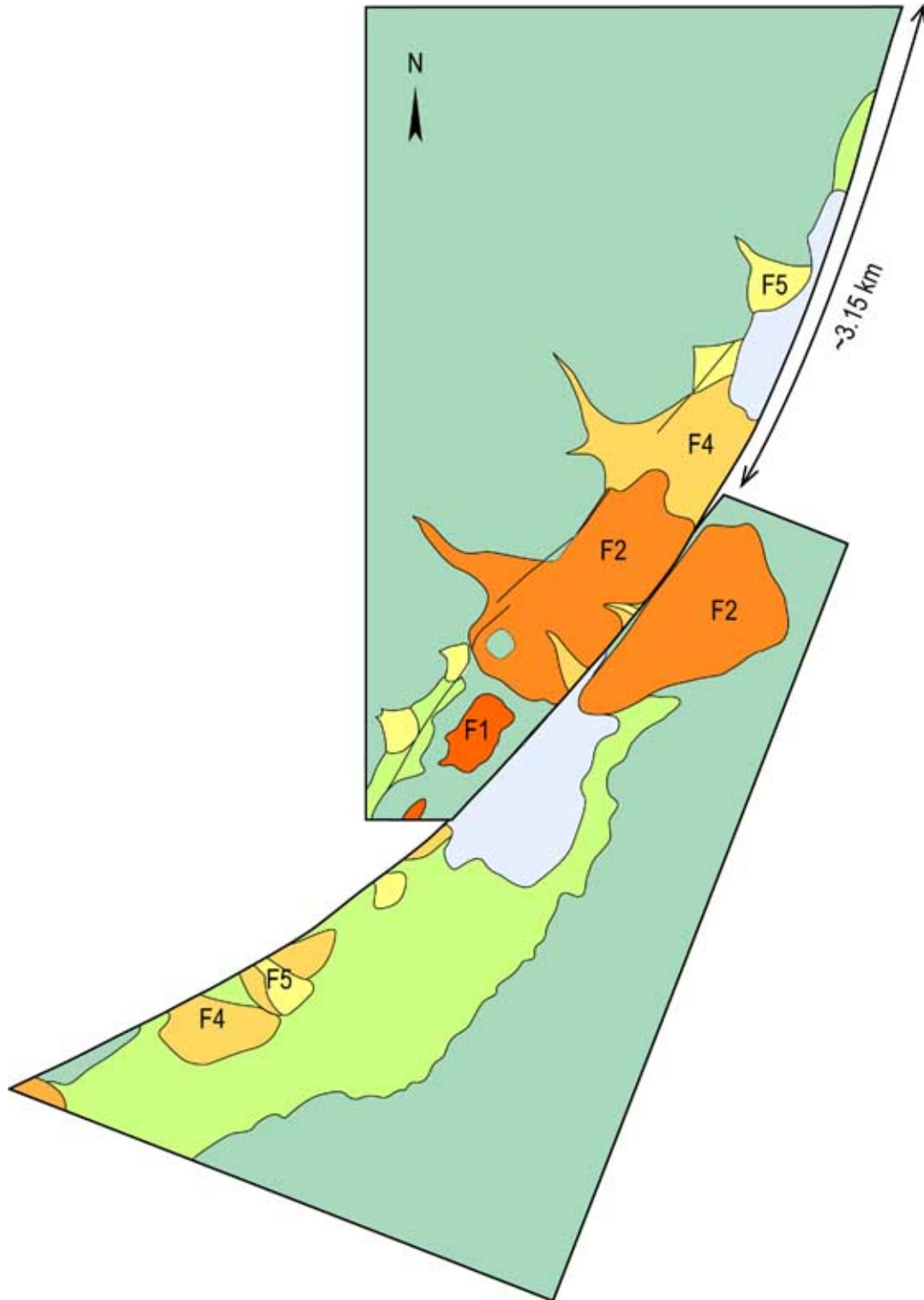


Figure 49: Restoration of the Siyyâd (F2) offset

Restoring the geometry of this fan complex requires ~ 3.15 km of back-slip, combined with a $\sim 20^\circ$ CW rotation (due to the marked bend of the fault's trace at this site).

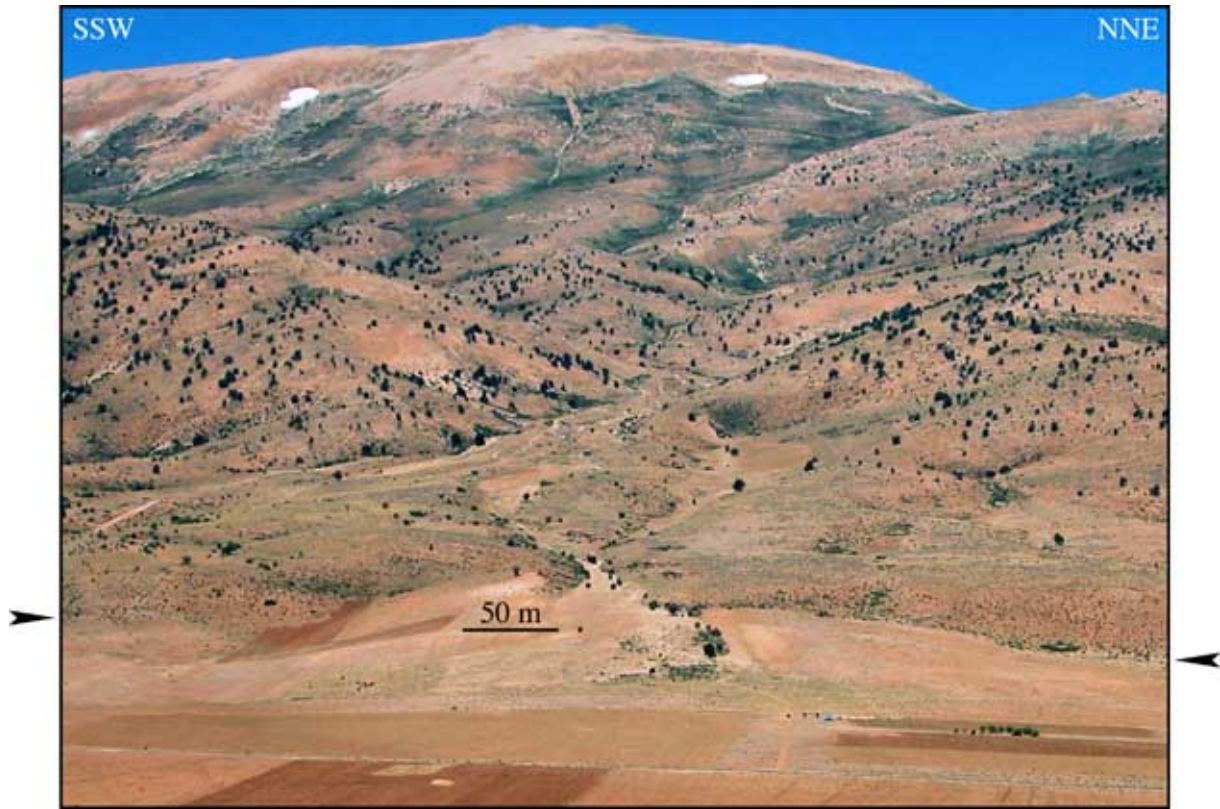


Figure 50: Field view of the Manakech fan (foreground)

In the middle: the Siyyâd fan complex. The Yammoûneh fault's active trace (black arrows) passes at the base of the frontmost scarp. Figure 51 shows an above-looking view of this fan.

along the fault. The age of the conglomerates is not well known. That they are well-consolidated, incised and folded implies that they are relatively old, the oldest in the basin. Dubertret correlates them with the well-characterized Pontian conglomerates of the Beqaa, but their local provenance and less lithified aspect suggests that they are younger, and in all likelihood Quaternary.

The next largest offset is that of Ouâdi Aarîch, which feeds the large fan at the south end of the basin. The principal, most deeply incised channel of the Aarîch catchment shows a spectacular dogleg offset, 1.2 km long, across the fault 2 km SW of the basin (figure 45).

Between Ouâdi Aarîch and Ouâdi Siyyâd, the two catchments of Ouâdi Hassân and Ouâdi Daoûra show a smaller cumulative offset. Both the channels of the rivers and the fan complexes they feed have been deviated and displaced by the fault. The fanglomerate deposits are weakly consolidated by a reddish, clay-rich cement. Their degree of cementation indicates that they are younger than the Siyyâd conglomerates. At the same time, the fact that they are cemented implies that they are older than the loose pebble/cobble deposits of the Aajâqa and Zalqa fans, which we dated at 6–10 ka and 12–27 ka respectively (cf section 2.2). The best piercing points to reconstruct the offsets are obtained with the northern lateral edge of the fan complex. Around 490 m of displacement along the fault after deposition of the fanglomerates are necessary to realign this northern edge.

The clearest smallest offset in the Jbab el-Homr section of the Yammoûneh fault is that of a 300-m-wide fan, fed by Ouâdi Manakech (the lowest reach of the Siyyâd catchment, cf figure 50). This fan, which grades into the floor of the basin just east of the Jabal el-Gharbi cumulative scarp, is among the youngest surfaces in the basin. A channel incised in this surface is offset by ~38 m. It is difficult to

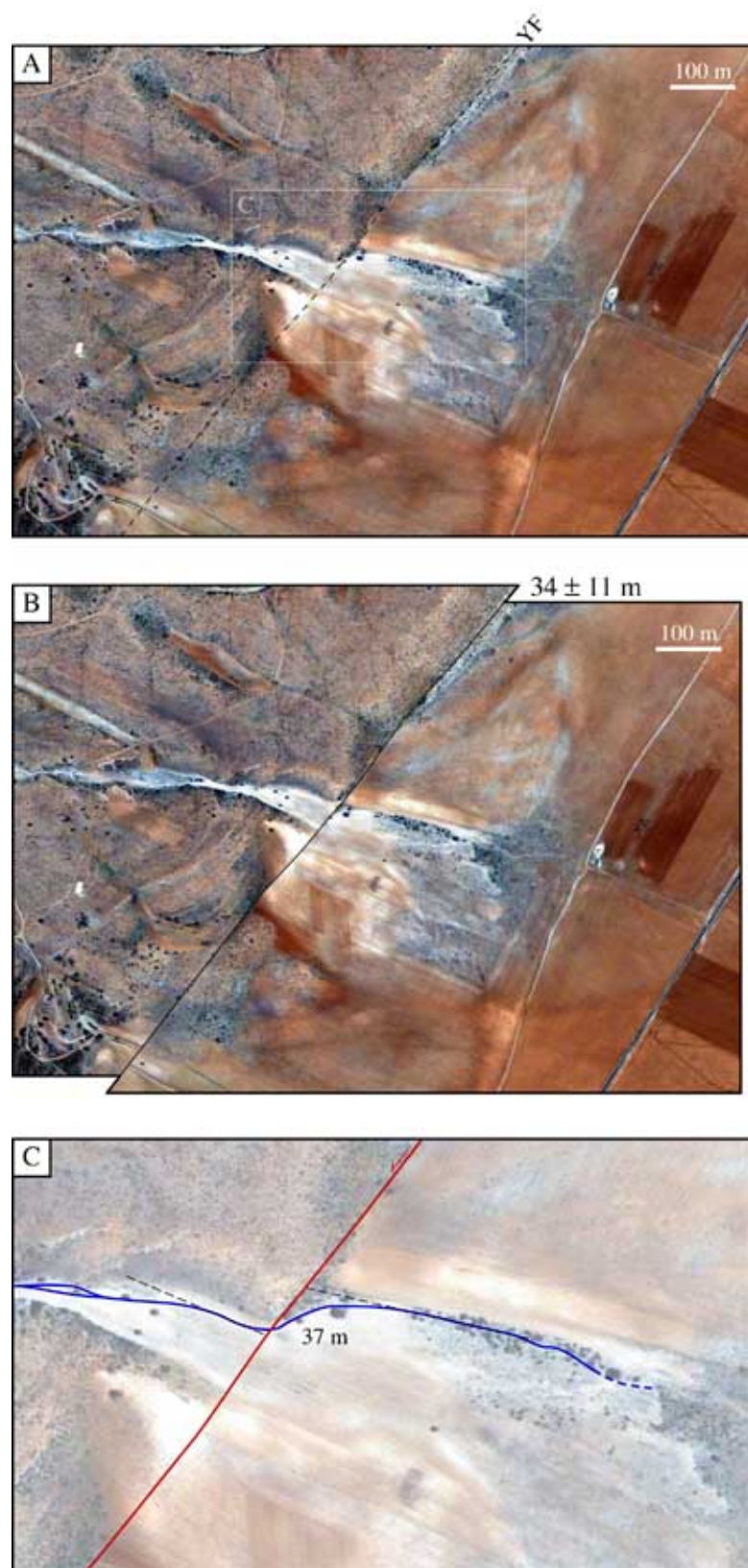


Figure 51: Restoration of the Manakech offset
23 to 45 m of back-slip provide an acceptable restoration of the young fan's geometry, and restoring the stream within this surface requires \sim 37 m of displacement.

assess bounds on this offset, because the channel's strike changes where it crosses the fault. However, it is consistent with the dogleg offset of the NE edge of the Manakech fan, whose original geometry is restored by 34 ± 11 m of back-slip (figure 51).

2.3.3 Time constraints

Following the same strategy as at the Zalqa and Aajâqa sites (cf section 2.2), we sampled the surfaces of several of the offset fans for cosmogenic exposure dating. At this time, ^{36}Cl measurements have not been completed. Hopefully, the ages of aggradation of the offset Hassân-Daoûra and Siyyâd fan complexes will yield constraints on the slip rate along the Yammoûneh fault over a much longer time period than at either Zalqa or Aajâqa.



Figure 52: W-looking view of Aarîd Mtaïyouhâne

Black arrows mark the trace of the Yammoûneh fault. The brown hills in the foreground are E-dipping Cenomanian limestones, wedged between the Nîha thrust and the Yammoûneh fault (cf section 1.2.2).

2.4 Aarîd Mtaïyouhâne

At the foot of the highest part of the Sannîne plateau (Harf Sannîne, 2678 m, figure 52), on the SE-facing slope of Aarîd Mtaïyouhâne, numerous tributaries in the upper catchment of the Nîha river show a broad range of left-lateral offsets. At this site, the elevation of the fault trace is between 2050 and 2250 m. Together with the stretch just south of Jbab el-Homr at the foot of Qornet es-Saouda, this is one of the two highest sections of the Yammoûneh fault.

The short and steep ($\sim 25^\circ$) streams incise well-bedded, nearly tabular Cenomanian limestone. The mountain flank is covered at places with patches of cemented proximal limestone breccia with angular clasts. Whether this breccia is consolidated colluvium or glacially-emplaced consolidated till is an open question. The fault trace, which follows a distinct slope break (figure 53), is marked by cumulative escarpments in between incised stream channels. Downstream from the fault, however, certain channels come to abut against the escarpments, which implies that they have been beheaded and displaced along the fault (figures 53 and 54.a).

The large number (~ 40) and broad range (from a few meters to a couple hundred meters) of the offsets imply that they have recorded fault motion over a significant time period. We systematically measured these offsets by retro-deforming an Ikonos image (1 m resolution, panchromatic). This retro-deformation was corroborated by field mapping and the interpretation of stereoscopic aerial photographs. For each offset, we estimate a minimum, maximum and best-fit value (table 4). We also divided the offsets into a “most reliable” (unambiguous tectonic offsets) and a “less reliable” categories.

In order to compare these offsets with one another, while taking into account their individual

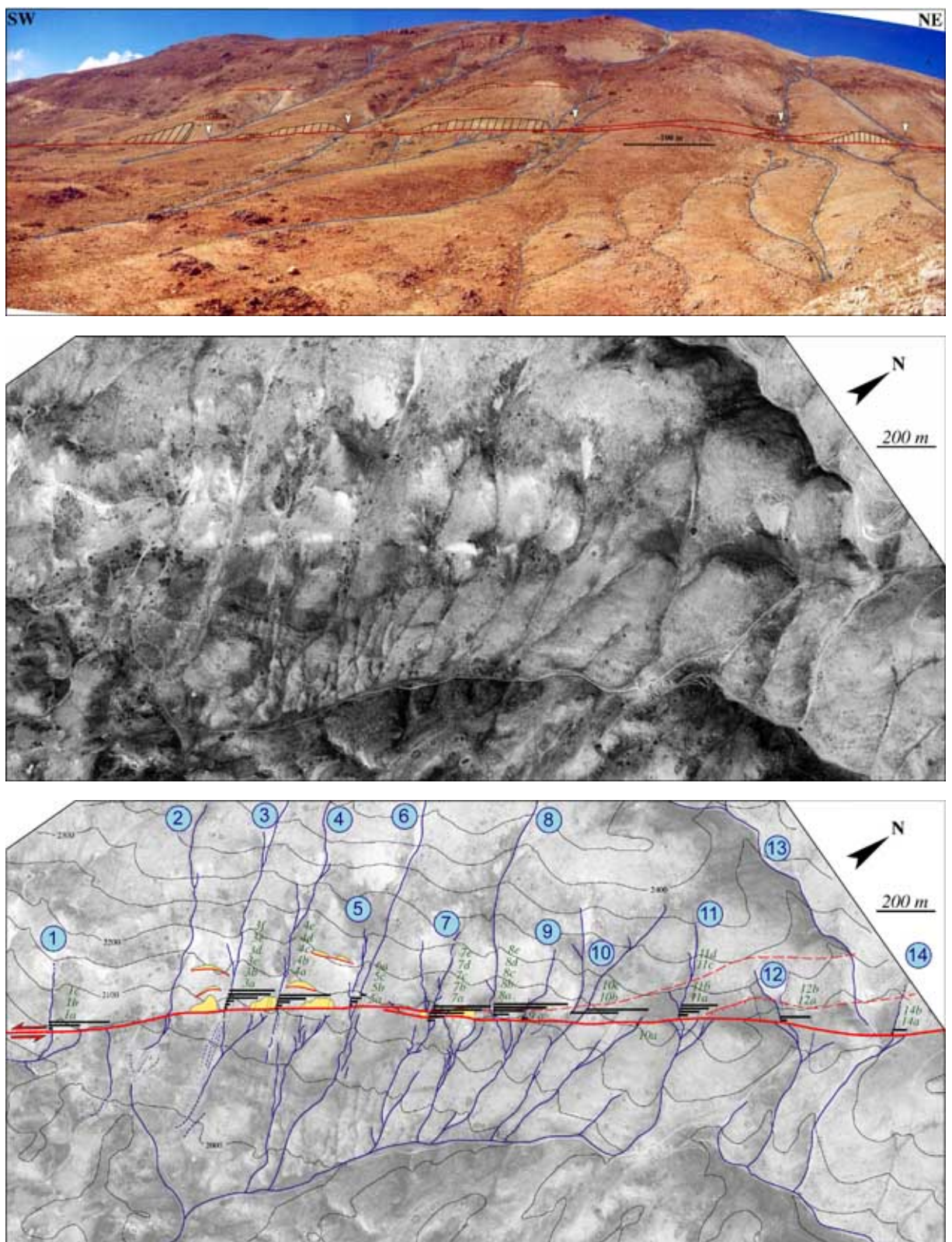


Figure 53: Panoramic view, aerial photograph and map of the Aarid Mtaïyouhâne
 In the map, the red line shows the trace of the Yammoûneh fault, yellow patches mark the location of visible, although degraded, cumulative scarps, and black bars show the measured offsets of the streams that run down from the Sannîne summiteal plateau.

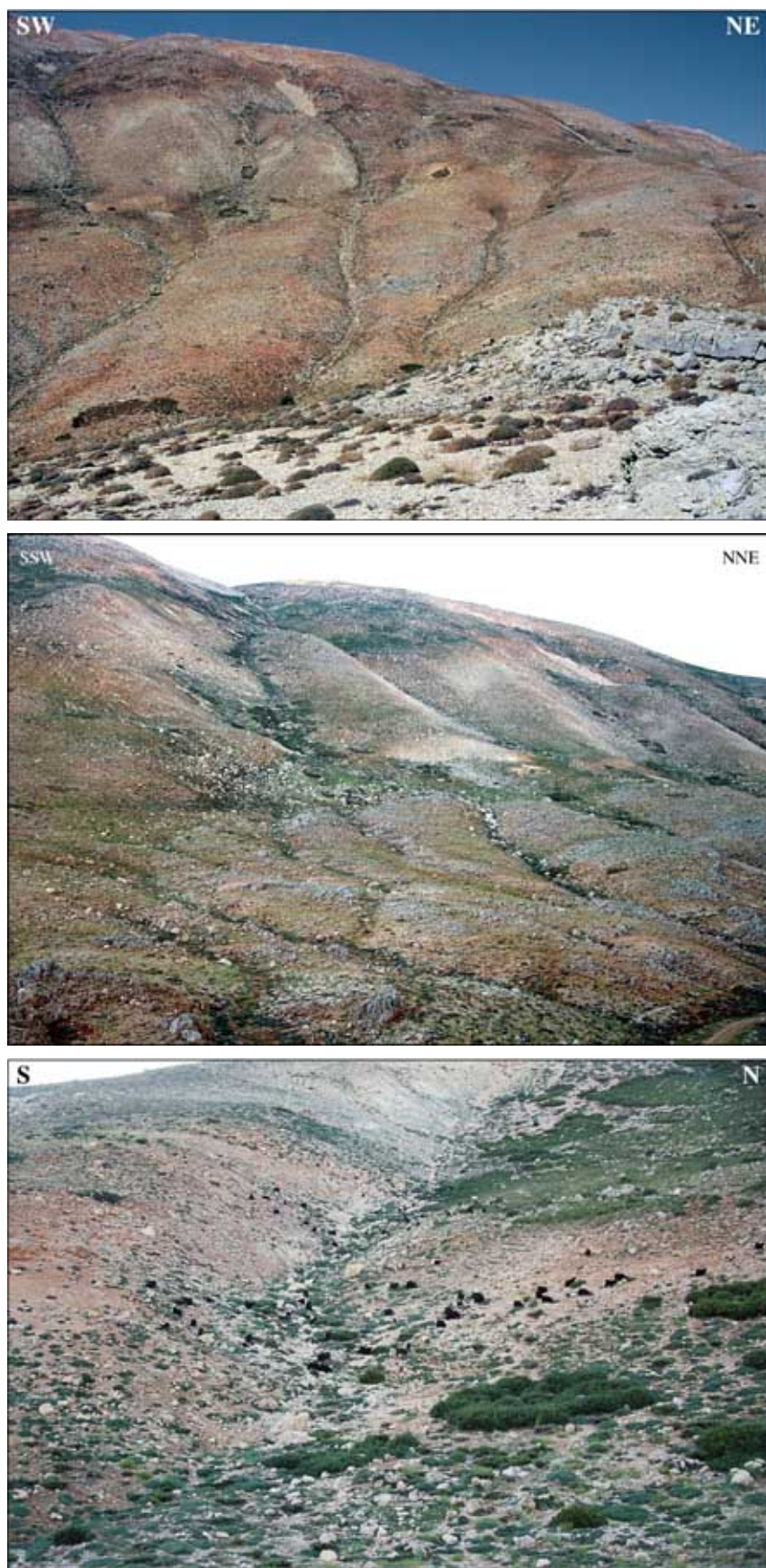


Figure 54: Field views of offset channels at Aarid Mtaïyouhâne

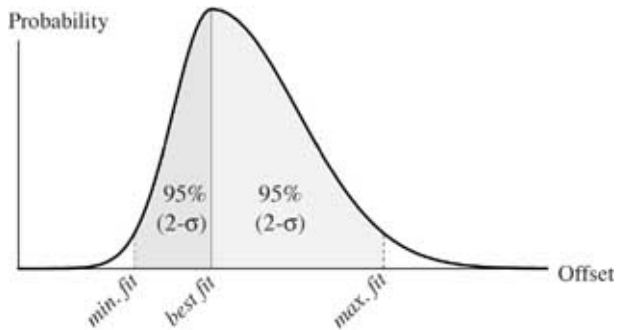


Figure 55: Assumed probability distribution of the Mtaiyouhâne offsets

Each individual probability distribution curve is built by combining two halves of a Gaussian distribution, scaled so that the minimum and maximum values of offsets correspond to 2-sigma ranges of the Gaussian half-curves.

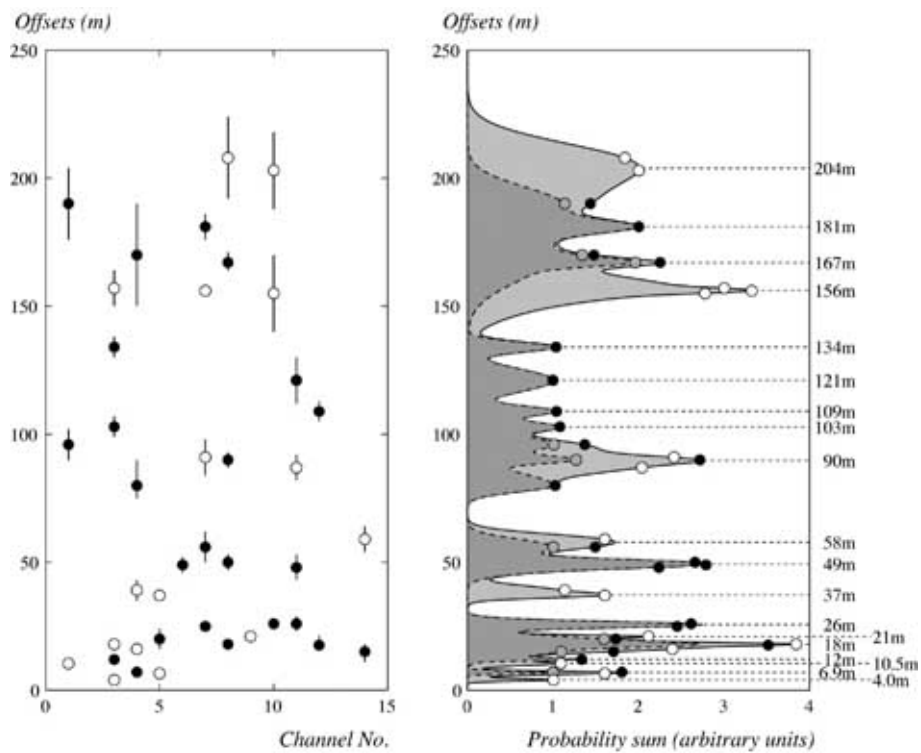


Figure 56: Probability sum of offsets at Aarid Mtaiyouhâne

[Left] Offsets plotted according to sizes and to channel numbers (cf fig. 53 for channel numbers). Full circles represent “most reliable” offsets. [Right] Plot of the sums of probability distributions for all offsets (full line) and for “most reliable” offsets only (dashed line). Dots show the positions of individual best-fit offsets.

Clusters of offsets similar within uncertainties show up as large values of the sum of probabilities.

Label	Offsets (m)			Label	Offsets (m)		
	min.	best	max.		min.	best	max.
3a	3	4	5	7b	50	56	62
5a	5	6.5	8	14b	54	59	64
4a	6	7	8	4d	75	80	90
1a	8.5	10.5	11.5	11c	82	87	92
3b	11	12	13	8c	87	90	93
14a	11	15	18	7c	84	91	98
4b	14	16	18	1b	90	96	102
12a	15.5	17.5	21.5	3d	99	103	107
3c	17	18	19	12b	105	109	113
8a	16	18	20	11d	112	121	130
5b	16	20	24	3e	130	134	138
9a	20	21	22	10b	140	155	170
7a	23	25	27	7d	154	156	158
10a	24	26	28	3f	150	157	164
11a	23	26	29	8d	164	167	171
5c	35	37	39	4e	150	170	190
4c	35	39	43	7e	176	181	186
11b	43	48	53	1c	176	190	204
6a	46	49	52	10c	188	203	218
8b	47	50	53	8e	192	208	224

Table 4: Offsets of streams measured at Aarîd Mtaïyouhâne

The labels correspond to the notations used in figure 53

Cluster	Offset channels	Offset lengths
$\sim 26 \text{ m}$	7	23–27 m
	10	24–28 m
	11	23–29 m
$\sim 37 \text{ m}$	5	35–39 m
	4	35–43 m
$\sim 49 \text{ m}$	11	43–53 m
	6	46–52 m
	8	47–53 m
$\sim 58 \text{ m}$	7	50–62 m
	14	54–64 m
$\sim 90 \text{ m}$	11	82–92 m
	8	87–93 m
	7	84–98 m
$\sim 156 \text{ m}$	10	140–170 m
	7	154–158 m
	3	150–164 m
$\sim 204 \text{ m}$	10	188–218 m
	8	192–224 m

Table 5: Clusters of offsets at Aarîd Mtaïyouhâne

Only offsets >25 m are listed here.

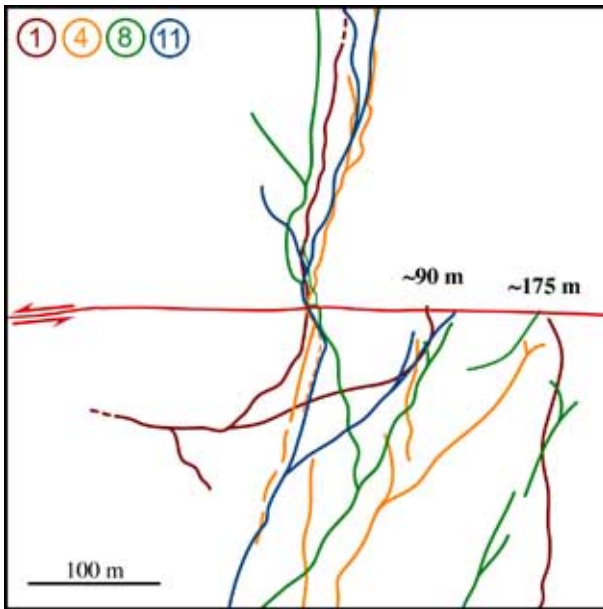


Figure 57: Similar offsets of four channels at Aarîd Mtaïyouhâne

Despite differences in strike and/or sinuosity of the channels 1, 4, 8 and 11 (cf fig. 53), several of the mapped offsets are strikingly similar, suggesting simultaneous incision episodes for all four channels.

uncertainties, each offset was assigned a asymmetrical Gaussian probability distribution (figure 55). Figure 56 shows the sum of these distributions for “most reliable” offsets (in red) and for all offsets (in gray). The smallest measured offsets (4–7 m, e.g. figure 54.b) may represent coseismic slip during the latest one or two events at this site, consistent with large, $M \sim 7.5$ historical events such as the AD 1202 or November 1759 earthquakes¹. Aarîd Mtaïyouhâne is the only site along the Yammoûneh fault where we could identify well-preserved individual (or dual?) coseismic offsets, probably owing to the high elevation of this site.

Larger cumulative offsets show clusters between 11 and 25 m, and around certain values, such as 50 m, 90 m or 155–180 m. Table 5 lists these larger clusters. The inference that such clusters are significant rather than a statistical artefact is supported by the observation that the same amount of back-slip restores the continuity of at least four catchments (figure 57). Such clusters are likely a result of short, local or regional, climate-driven episodes of rapid incision, as observed in many other sites along other active strike-slip faults in Eurasia [e.g. Van der Woerd et al., 2002; Mériaux, 2002; Mériaux et al., 2005; Gaudemer et al., 1995].

2.5 Discussion: kinematics of the LRB

2.5.1 Mid-Pleistocene to Holocene kinematics of the Yammoûneh fault

Summary of offsets along the Yammoûneh fault

Table 6 lists all the offsets described in previous sections. Some of these offsets, although measured several tens of kilometers apart, are similar. For instance, the 34 ± 11 m and 40 ± 5 m offsets of the Manakech and Aajâqa fans are comparable to each other and to the ~ 37 m Mtaïyouhâne offset cluster (comprising two offsets, at 37 ± 2 and 39 ± 4 m, respectively). Similarly, the three Mtaïyouhâne channel

¹For a detailed dicussion of the historical seismicity of the Yammoûneh fault, and particularly of the source of the AD 1202 and 1759 events, see chapter 3.

Site	Area	Offset	Ref.*
Litâni river	(N of Marjavoûn)	~26.4 km	p.28
Litâni river	(N of Marjavoûn)	~17.6 km	p.28
Litâni river	(N of Marjavoûn)	~11.6 km	p.28
Litâni river	(N of Marjavoûn)	~3.5 km	p.28
Siyyâd fan	(Jbab el-Homr)	~3.15 km	p.68
Damdoûm river	(N of Marj Hîne)	~1.9 km	p.29
Serkhâne river	(N of Marj Hîne)	~1.6 km	p.29
Aarîch river	(Jbab el-Homr)	~1.2 km	p.75
Chataouîyeh river	(S of Chtaura)	590±40 m	p.29
Saghbîne river	(N of Qaraouûn)	~540 m	p.32
Hassân-Daoûra fan	(Jbab el-Homr)	~490 m	p.75
Aarîd Mtaïyouhâne**		~204 m	p.81
Aarîd Mtaïyouhâne		~181 m	p.81
Aarîd Mtaïyouhâne		~167 m	p.81
Aarîd Mtaïyouhâne		~156 m	p.81
Aarîd Mtaïyouhâne		~134 m	p.81
Aarîd Mtaïyouhâne		~121 m	p.81
Aarîd Mtaïyouhâne		~109 m	p.81
Aarîd Mtaïyouhâne		~103 m	p.81
Aarîd Mtaïyouhâne		~90 m	p.81
Zalqa fan	(S of Chtaura)	80±8 m	p.61
Aarîd Mtaïyouhâne		~58 m	p.81
Aarîd Mtaïyouhâne		~49 m	p.81
Aajâqa fan	(Yammoûneh basin)	40±5 m	p.57
Aarîd Mtaïyouhâne		~37 m	p.81
Manakech fan	(Jbab el-Homr)	34±11 m	p.77
Aarîd Mtaïyouhâne		~26 m	p.81
Aarîd Mtaïyouhâne		~21 m	p.81
Aarîd Mtaïyouhâne		~18 m	p.81
Aarîd Mtaïyouhâne		~12 m	p.81
Aarîd Mtaïyouhâne		~10.5 m	p.81
Aarîd Mtaïyouhâne		~6.9 m	p.81
Aarîd Mtaïyouhâne		~4 m	p.81

* Refers to the page (in this memoir) where the offset is described.

** Only clusters of the offsets recorded at Aarîd Mtaïyouhâne are shown, rather than all individual values.

Table 6: Left-lateral offsets along the Yammoûneh fault

As mentioned in text, the shortest of these likely represent coseismic offset(s) of the latest few events.

offsets clustered around 90 m (87 ± 5 , 90 ± 3 and 91 ± 7 m respectively) are comparable to that (80 ± 8 m) of the Zalqa fan, 25 km to the SW. A number of larger offsets also tend to cluster around certain values (3.3 km, 1.8 km, 540 m).

Climatic origin of the offsets

All the sites listed in table 6 are located along the Yammoûneh fault. The only active faults that branch off from the Yammoûneh trace between Marjavoûn and Qoubayat are small, right-lateral faults within Mount Lebanon and the Niha thrust. The former are bookshelf faults (cf section 1.2.2) that connect with the Yammoûneh fault at high angles, and as such should have little effect on the strike-parallel component of slip on the Yammoûneh fault. The Niha thrust, that meets at a 25° angle with the Yammoûneh fault just south of Zahle, is probably too slow to have a significant effect either. Thus,

Site(s)	Offset	Projected Age	
		[3.8–6.4 mm/yr]	[5.1 mm/yr]
AJQ, AMT, MNK	35–39 m	5.5–10 ka	6.9–7.6 ka
AMT	47–52 m	7.3–14 ka	9.2–10.2 ka
AMT, ZLQ	87–88 m	14–23 ka	~17 ka
AMT	154–158 m	24–42 ka	30–31 ka
AMT	192–218 m	30–57 ka	38–43 ka
HD	~490 m	77–130 ka	~96 ka
SGB	~540 m	85–140 ka	~106 ka
CHA	~600 m	94–160 ka	~120 ka
AAR	~1200 m	190–320 ka	~240 ka
SRK	1590–1690 m	250–440 ka	310–330 ka
DMD	1825–1945 m	290–510 ka	360–380 ka
SYD	~3.15 km	490–830 ka	~620 ka
LIT	~3.5 km	540–920 ka	~690 ka

Table 7: Projected ages of the offsets recorded along the Yammoûneh fault

Each offset reported in the first column is the intersection of all similar offset ranges; the projected ages results from dividing this offset by the 5.1 ± 1.4 mm/yr slip rate derived from dating the Aajâqa (AJQ) and Zalqa (ZLQ) fans (cf section 2.2); AAR stands for Aarîch (p.75), AMT for Aarîd Mtaïyouhâne (p.81), CHA for Chataouîyeh (p.29), DMD for Damdoûm (p.29), HD for Hassân-Daoûra (p.75), MNK for Manakech (p.77), SRK for Serkhâne (p.29), SGB for Saghbîne (p.32), SYD for Siyyâd (p.68), and LIT for the smallest Litâni offset (p.28).

there is little reason for the slip rate of the Yammoûneh fault to vary much along strike.

Consequently, similar offsets at different sites along the fault imply that the landforms recording these offsets are of roughly the same age. Since all of these landforms are related either to upper-catchment channel incision or to fan aggradation, the time of their formation must correspond to regional episodes of erosion, during particularly wet periods (pluvials). Typically, in mountain regions like Lebanon, wet pluvials correspond to warm episodes (interstadials or interglacials) that separate cold and dry glacial stages.

Comparison with the regional climate record

In the absence of direct dating of many geomorphic features along the fault, we use the constraints on the slip rate of the Yammoûneh fault at Aajâqa and Zalqa (5.1 ± 1.4 mm/yr, cf section 2.2) to test the above hypothesis and to infer ages for the main values of offsets along the fault (cf table 7), which can then be compared to known regional climatic data. In the Middle East such data comes primarily from work conducted south of Lebanon, mostly in Israel. It is derived from two sets of measurements that cover different time spans: water levels in the Dead Sea and its precursor, Lake Lisan (since 70 ka), and isotopic measurements in speleothems.

During the Holocene, the Dead Sea appears to have acted as a climate gauge, with its level oscillating between high stands correlated with pluvials, and low stands testifying to dry spells [Enzel et al., 2003]. In the last 10 kyr (figure 58.a), the two highest levels of the Dead Sea (above 370 m b.s.l.) occurred around 9 ka and between 6.5 and 7.5 ka. They mark the beginning and the end of the Early Holocene Climatic Optimum (EHCO) which is well-documented as a period of generally high water levels in many other lakes in North Africa and in Central Asia [Gasse and Fontes, 1989; Audin et al., 2001],

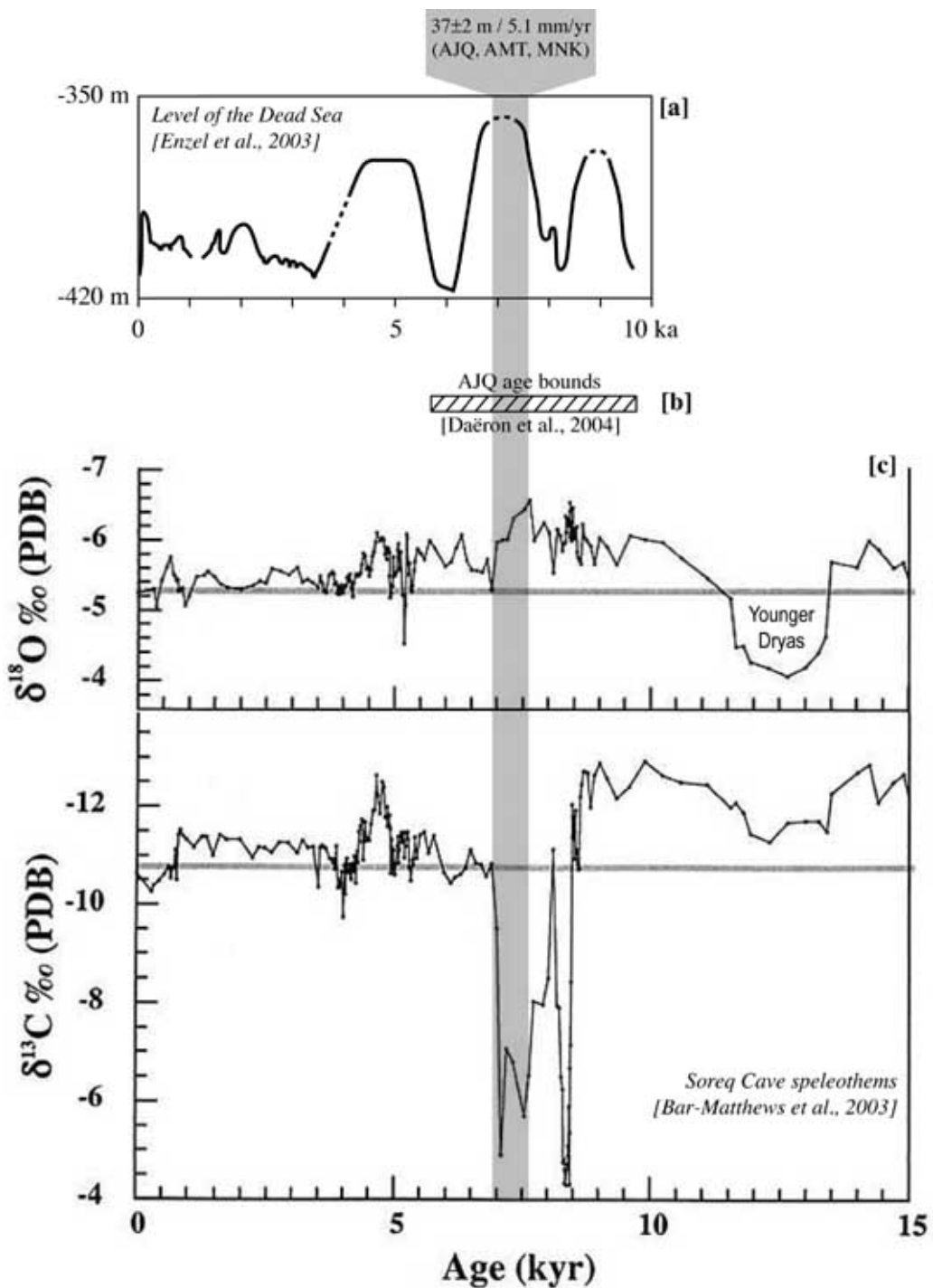


Figure 58: Regional climate variations of the past 15 kyr

The top curve shows the level of the Dead Sea since 10 ka, after Enzel et al. [2003]. The slashed bar beneath it shows the broad time constraints on the age of the Aajâqa fan, discussed in section 2.2. The two bottom curves show isotopic variations recorded in the speleothems of the Soreq cave, in Israel [Bar-Matthews et al., 2003]. The grey, vertical bar shows the age predicted by dividing the $\sim 37\text{ m}$ offset of the Aajâqa, Manakech and Aarîd Mtaïyouhâne sites by the central value of our estimate of the slip rate along the fault [section 2.2 and Daëron et al., 2004a]. Working with these narrow estimates of offset and rate suggests a possible correspondence between the establishment of the offset landforms on the Yammoûneh fault and the latest EHCO rise of the level of the Dead Sea, around 7 ka.

corresponding to a warm and wet pluvial. Prior to 10 ka, a much larger lake, the Lisan, with a level over 200 m higher than that the modern Dead Sea, occupied the rift from the Dead Sea to Lake Tiberias, yielding a record that goes back to 70 ka.

Over an even longer time scale (back to 250 ka), stable isotope compositions of calcite from speleothems in two caves in Israel yield $\delta^{18}\text{O}$ and $\delta^{13}\text{C}$ records that correlate remarkably well from one cave to the other and with the eastern Mediterranean offshore marine $\delta^{18}\text{O}$ record [Bar-Matthews et al., 2003].

In the last 15 kyr (figure 58.b), the $\delta^{13}\text{C}$ curve, which reflects mainly local changes in vegetation type, exhibits a marked double peak between 8.5 ka and 7 ka, which correlates well with the EHCO. This period, which stands out as marked pluvial in both data sets, also correlates well with the age of emplacement (5.7–9.7 ka) of the Aajâqa fan [Daëron et al., 2004a]. Although the dispersion of exposure ages at the surface of this fan leads to rather broad age bounds, the case can be made that it was emplaced during the EHCO (9 to 7 ka). This hypothesis is strengthened by the existence of at least three other offsets similar to that (40 ± 5 m) of the Aajâqa fan (37 ± 2 and 39 ± 4 m at Aarîd Mtaïyouhâne, 34 ± 11 m at Jbab el-Homr). Interestingly, if one divides the intersection of these four offset error bounds (35–39 m) by the central value of slip rate (5.1 mm/yr) measured in section 2.2 [cf also Daëron et al., 2004a], the resulting, “projected” age of this group of offsets is 6.9–7.6 ka. The beginning of this time interval coincides with the start of the second EHCO high stand of the Dead Sea, and its end with the end of the EHCO $\delta^{13}\text{C}$ peak (figure 58).

The other offset that we dated in the field is that of the Zalqa fan [cf section 2.2 and Daëron et al., 2004a]. It correlates with a cluster of at least three offsets at Aarîd Mtaïyouhâne (cf table 4, p.82, and figure 57, p.83). Surface exposure ages broadly constrain the emplacement of the Zalqa fan to have occurred between 12 and 27 ka. The most prominent climate change in this time interval is the end of the LGM. The Soreq and Peqiin speleothems [Bar-Matthews et al., 2003, and figure 60] prominently record the effects of this strong warming event around 17 ka. This is also the time of the precipitous drop of the Lake Lisan level (figure 59). Again, this date is in good agreement with the age (17 ka) “projected” by dividing the combination of the four offsets (87–88 m) by 5.1 mm/yr.

In between the two previous values, three channels at Aarîd Mtaïyouhâne are offset by 47–52 m. Using the 5.1 mm/yr slip rate mentioned above, the corresponding “projected” age is 9.2–10.2 ka. This age coincides with the earliest EHCO high stand of the Dead Sea (figure 58.a) and shortly predates the onset of the EHCO $\delta^{13}\text{C}$ peak (figure 58.b). It also corresponds roughly to the base of the calcareous marl sequence exposed in the Yammoûneh basin (Kazzâb trench, described in detail in section 3.3).

The last two offset clusters observed at Aarîd Mtaïyouhâne (~ 155 and ~ 200 m), whose error bounds are broader than those of previous clusters, yield “projected” ages of ~ 30 and ~ 40 ka, that fall in the heart of the latest glacial period, respectively at the end of and within Marine Isotope Stage 3 [Imbrie et al., 1984]. More precisely, these two “projected” dates coincide with Heinrich events H3 and H4 in the North Atlantic, which have been shown by Bartov et al. [2003] to be correlated with abrupt drops in the level of Lake Lisan, presumably due to regional arid episodes linked to the cooling of the Mediterranean Sea. That there is no obvious isotopic signal in the cave records at these dates (figure 58.b) remains to be accounted for. Since these offsets are found only at the Mtaïyouhâne site, located 2100 m a.s.l., just below the steep rim of the Sammîne plateau, they are probably related to complex, high-altitude firn or ice shifts related to moisture change.

Following the same line of reasoning, it is noteworthy that the offset of the Chataouîyeh stream,

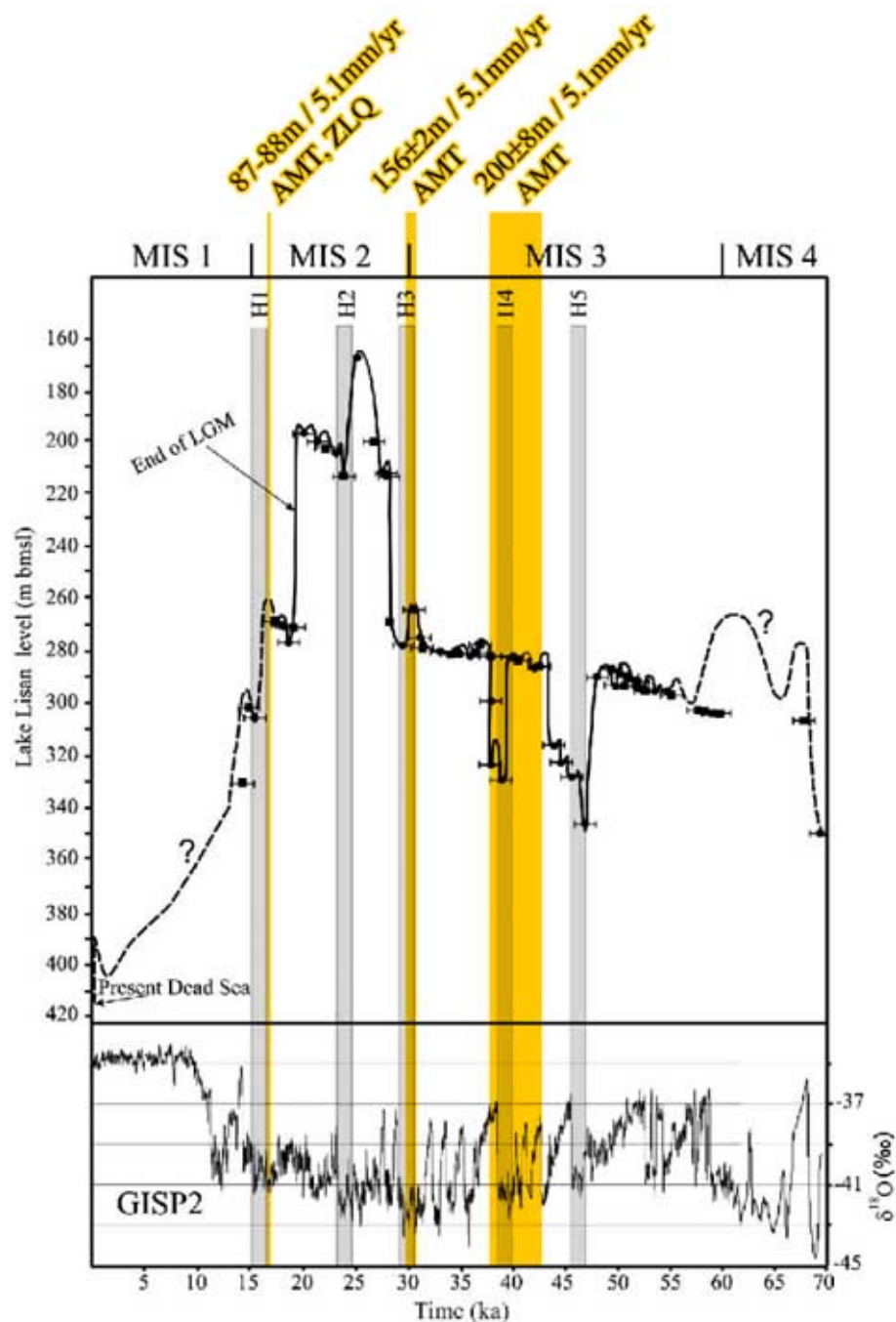


Figure 59: Comparison of “projected” ages of Yammounéh fault offsets with Lisan level variations
 Lake Lisan level variations and North Atlantic Heinrich events are from Bartov et al. [2003]. The “projected” ages, obtained by postulating a slip rate of 5.1 mm/yr on the Yammounéh fault, appear to be correlated with Heinrich events and/or with the corresponding drops in the level of the Lisan.

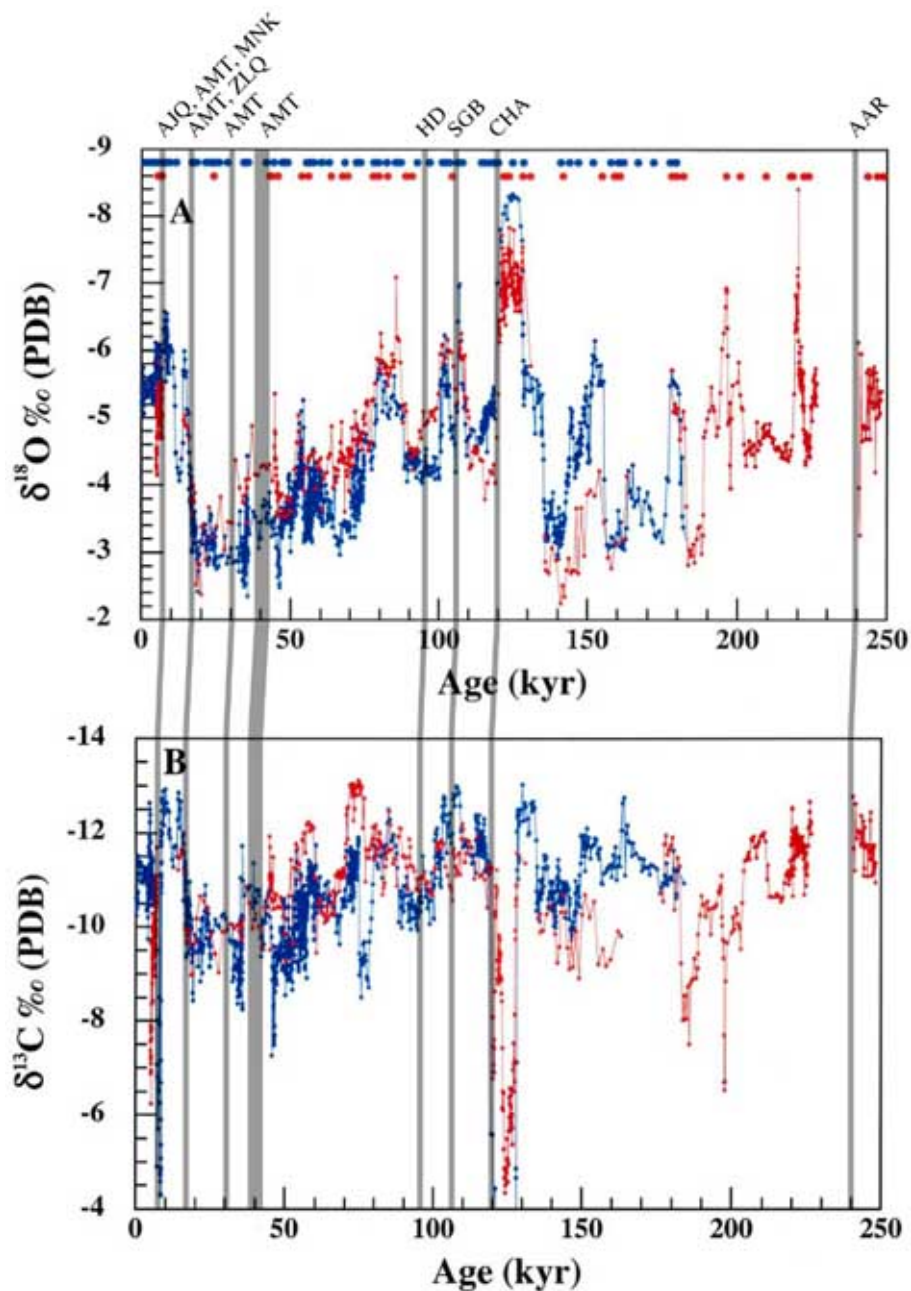


Figure 60: Comparison of “projected” ages of the Yammoûneh fault offsets with regional speleothem records

The colored curves show stable isotope variations recorded in the speleothems of the Soreq (blue) and Peqiin (red) caves [Bar-Matthews et al., 2003]. The ages proposed here for the offsets were obtained by dividing the offset amounts by 5.1 mm/yr.

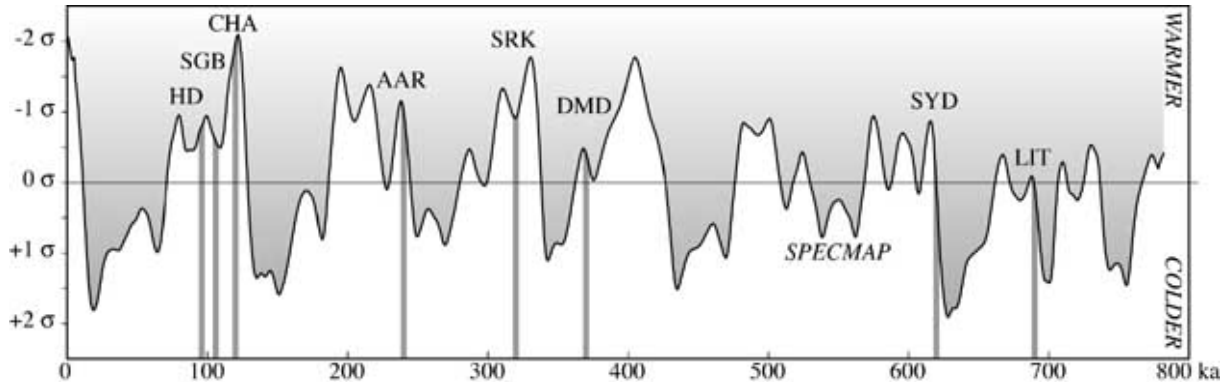


Figure 61: Comparison of “projected” ages of the Yammoûneh fault offsets with long-term global climate

The curve shows $\delta^{18}\text{O}$ variations from the SPECMAP stacked record [Imbrie et al., 1990]. The ages proposed here are obtained by dividing the cumulative offset amounts by 5.1 mm/yr.

which has fed a fan made of cemented but mildly indurated conglomerates, yields a “projected” age that corresponds roughly to the Eemian interglacial (130–120 ka, cf figures 60 and 61).

The somewhat smaller offsets of the lithologically similar Hassân-daoura fanglomerates and of the Saghbîne channel would yield younger “projected” ages. At Jbab el-Homr, this may be due either to a complicated morphology of this fan fed by two streams, or to the fact that the fault locally divides into two branches.

More generally, most offset clusters of ~ 500 m or more, appear to coincide with global warming episodes, as recorded in the SPECMAP stacked $\delta^{18}\text{O}$ record (figure 61). Although the fit between the SPECMAP record and ages “projected” using a slip rate of 5.1 mm/yr is non-unique, other rates within the range 3.8–6.4 mm/yr (cf section 2.2 and Daëron et al. [2004a]) systematically fail to provide better fits.

We conclude that the cluster of cumulative offsets at 87–88 m indeed accrued since deglaciation between 14.5 and 18.7 ka, as precisely recorded by the Soreq speleothems [Bar-Matthews et al., 2003, and figure 60] and the Lisan level drop [Bartov et al., 2003, and figure 59]. Such a revised age for this range of offsets yields a slip rate of 4.6–6.1 mm/yr along the Yammoûneh fault.

Similarly, it is possible to tie systematically the other offset clusters < 1 km listed in table 7 to the actual age constraints regionally available, to further constrain the slip rate (table 8):

- The 35–39 m cluster may thus be tied to the latest EHCO pluvial, between the rise of the Dead Sea level at 7.8 ka [Enzel et al., 2003] and the end of the $\delta^{13}\text{C}$ peak at 6.9 ka, as recorded in the Soreq cave speleothems [Bar-Matthews et al., 2003].
- The 47–52 m cluster, to the earliest EHCO pluvial, as recorded by the high stand of the Dead Sea from 9.5 to 8.4 ka.
- As mentioned above, the 87–88 m cluster is tied to the 14.5–18.7 ka deglaciation.
- The 154–158 m cluster is tied to the sharp drop in the level of Lake Lisan (28.5–31.6 ka, cf figure 59) correlated with the Heinrich event H3 cold spell.
- Similarly, the 192–218 m cluster is tied to the Lisan level drop (37.7–41 ka, cf figure 59) correlated with the Heinrich event H4 cold spell.

Site(s)	Offset	Climatic event	Age	
			min.	max.
AMT, AJQ, MNK	35–39 m	Younger EHCO Dead Sea high stand	6.9 kyr	7.8 kyr
AMT	47–52 m	Older EHCO Dead Sea high stand	8.4 kyr	9.5 kyr
AMT, ZLQ	87–88 m	Latest deglaciation	14.5 kyr	18.7 kyr
AMT	154–158 m	Heinrich event H3	28.5 kyr	31.6 kyr
AMT	192–218 m	Heinrich event H4	37.7 kyr	41 kyr
HD, SGB, CHA	490–630 m	Marine isotope stage 5	~80 kyr	~130 kyr

Table 8: Climatic interpretation of the offsets plotted in figure 62

Ages for AJQ and ZLQ were loosely constrained to 6–10 kyr and 12–27 kyr respectively, using in situ cosmogenic ^{36}Cl dating (cf section 2.2 and Daéron et al. [2004a]). Based on the $5.1 \pm 1.3 \text{ mm/yr}$ slip rate derived from these measurements, we propose most likely climatic events corresponding to each offset. Age constraints for these events are derived from regional climate records [Enzel et al., 2003; Bartov et al., 2003; Bar-Matthews et al., 2003].

- The three offsets between ~ 490 and $590 \pm 40 \text{ m}$ probably accrued since some time during the relatively warmer period from MIS 5.5 (Eemian) to 5.1 included, i.e. within 80–130 ka.

Figure 62 shows the uniform average slip rates since 100 ka compatible with all the data. The best-fitting rate is between 5.0 and 5.5 mm/yr. It is also clear that rates slower than 4.5 or faster than 6 mm/yr would fail to fit the data. Taking the best-fitting rate, and assuming that the smallest offsets measured at Aarid Mtaïyouhâne (3–8 m) bound the coseismic offset of the single, latest earthquake at this site, and that this event is typical of the longer-term behavior of the Yammoûneh fault, the corresponding bounds on the mean return time of such earthquakes would be ~ 550 and ~ 1600 years.

2.5.2 Plio-Quaternary kinematics of the Yammoûneh and Roûm faults

Plio-Quaternary slip rate along the Yammoûneh fault

Given the good fit shown in figure 62, we consider that the post-100-ka slip rate 5–5.5 mm/yr estimated on the Yammoûneh fault by combining direct surface exposure dating, geomorphic offset measurements between 20 m and 600 m, and regional climatic constraints is fairly robust. Consequently, we use this slip rate to infer the ages of the largest geomorphic offsets we have mapped along the Yammoûneh fault, assuming that this rate has been constant for longer than 100 kyr. Figure 63 and table 9 shows the corresponding predicted ages. It is possible to argue that the 17 km offset has accrued since the Zanclean-Piacenzian transition (3.6 Ma). Similarly, it is remarkable that the inferred age of the 26.4 km offset corresponds to the Pontian (5.3 Ma, the end of the Messinian).

Dubertret [1975b] and others have shown that, over much of the Upper Miocene, the Beqaa was occupied by either a large lake or a series of smaller lakes. In the Pontian, a permanent lake flooded an area over 60 km long in the Beqaa. There are no significant, younger lake deposits, which suggests that the lake vanished around that time (5.3 Ma). The Beqaa lake might have been flushed by the headward incision of the Litâni, due to the spectacular (~ 2000 m) Messinian drop of the Mediterranean Sea level. Headward incision of this age has been documented around the entire Mediterranean, and it has been suggested [e.g. Butler et al., 1998; Butler and Spencer, 1999] that most of the large canyons of the Lebanese coastal range date from that period. Although this scenario requires critical assessment

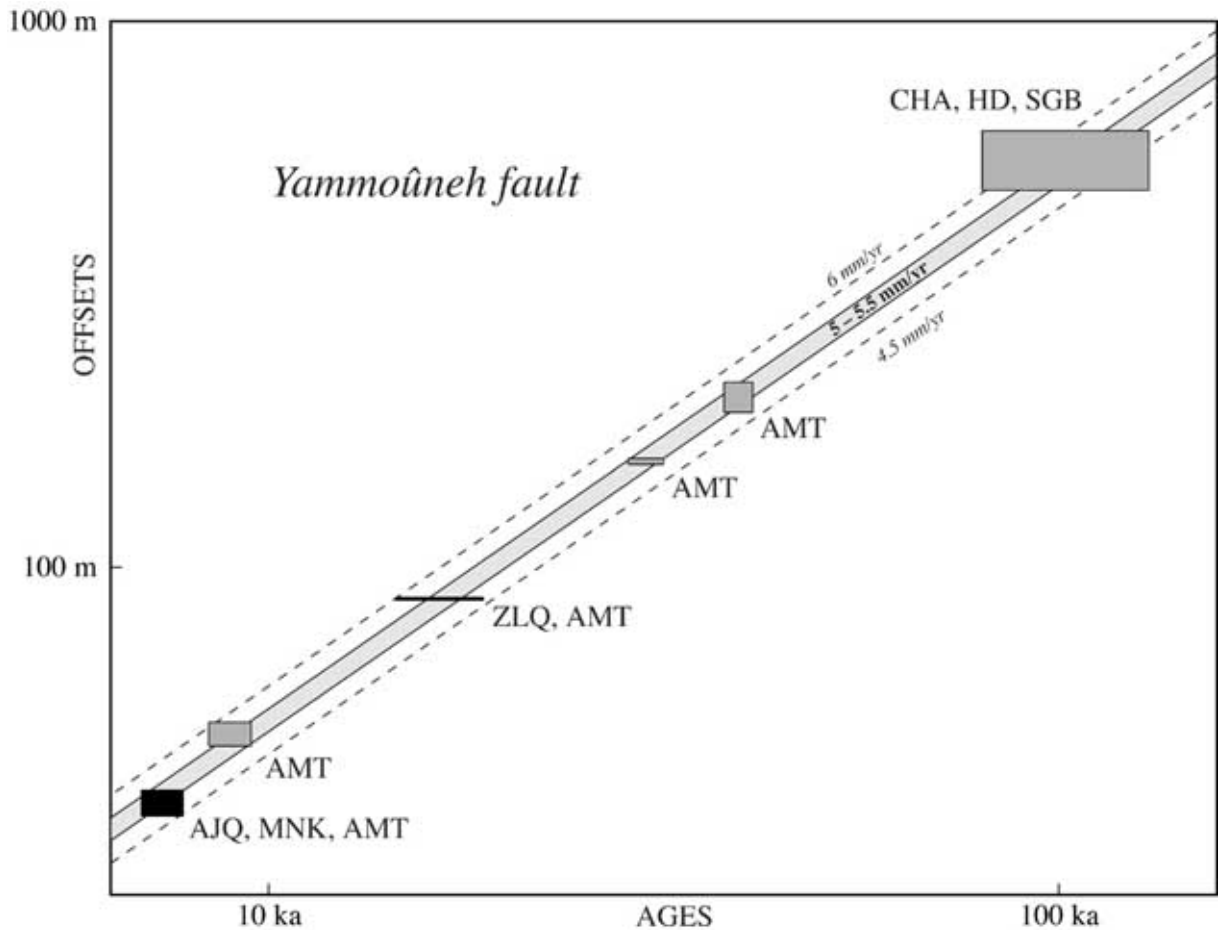


Figure 62: Plot of Yammoûneh fault offsets vs. their interpreted time constraints

Offset lengths and age values are listed in table 8. The AJQ and ZLQ fans (black boxes) were loosely dated using in situ cosmogenic ^{36}Cl measurements (cf section 2.2 and Daëron et al. [2004a]), then tied to past events of the regional climatic record. The interpreted ages of all six clusters of offsets are remarkably proportional to their lengths, implying an average slip rate of 5.0–5.5 mm/yr along the Yammoûneh fault.

Offset	Site	Inferred Age
Ouâdi Aarîch	1.2 km	220–240 ka
Ouâdi Serkhâne	1.6 km	290–320 ka
Ouâdi Damdoûm	1.9 km	350–380 ka
Siyyâd fan complex	3.15 km	570–630 ka
Litâni river	3.5 km	640–700 ka
Litâni river	11.6 km	2.1–2.3 Ma
Litâni river	17.6 km	3.2–3.5 Ma
Litâni river	26.4 km	4.8–5.3 Ma

Table 9: Estimated ages of the longest geomorphic offsets on the Yammoûneh fault, using the 5.0–5.5 mm/yr estimate derived from figure 62 (see discussion in text).

The inferred ages are plotted in figure 63.

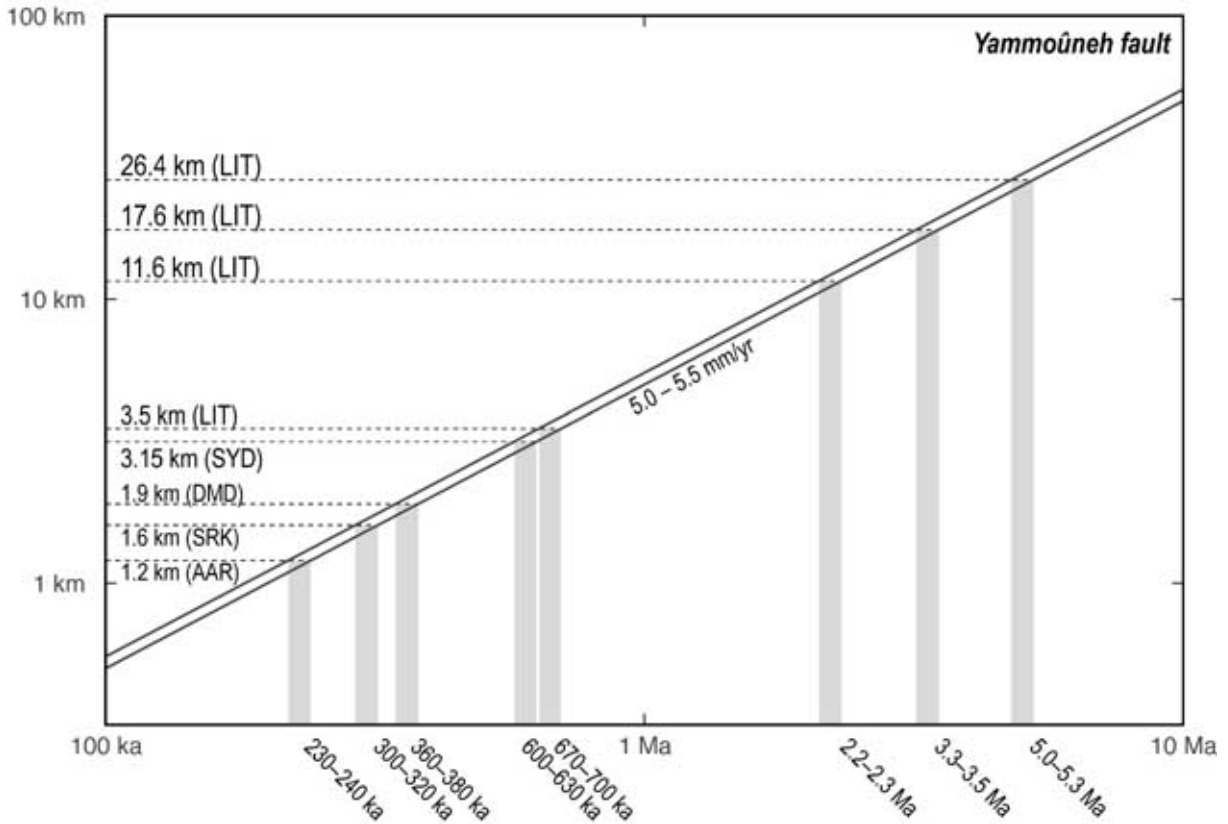


Figure 63: Estimated ages of the longest geomorphic offsets on the Yammoûneh fault, using the 5.0–5.5 mm/yr estimate derived from figure 62 (see discussion in text).

The inferred ages are listed in table 9.

and further testing, it appears to be consistent with the known paleo-climatic environment of Lebanon at the end of the Miocene.

Inferred Plio-Quaternary slip rate along the Roûm fault

Assuming the Litâni incision to be of Messinian age (5.3 Ma) and the Roûm fault to have been already in existence by that time, the largest, 9.5 ± 0.4 km offset (cf section 1.2.2) would yield a Plio-Quaternary average slip rate of 1.8 ± 0.1 mm/yr on this fault. At this rate, the smaller, 1.9 ± 0.3 km dogleg offset of the river (figure 25) would be only 1.1 ± 0.2 Myr old. One problem with this scenario is that this latter inferred age does not correspond to any of the ages inferred for the small offsets of the Litâni along the Yammoûneh fault (figure 63). One possible explanation is that offsets across the Yammoûneh fault are due to capture (upstream of the fault) as well as climate change.

Alternatively, the unique pair of Litâni offsets across the Yammoûneh fault that are in the same ratio (~ 4.9) as the two Litâni offsets across the Roûm fault are the 17.6 km and 3.5 km values (~ 5.0 ratio). This may be taken to imply that the two smaller (respectively, larger) offsets of the litani across both faults have the same age (respectively 670–700 kyr and 3.4–3.5 Myr). This would yield an average slip rate since 3.5 Ma of 2.9 ± 0.5 mm/yr on the Roûm fault.

But this interpretation would raise at least one major problem: the absence of a visible Messinian record of incision on the Litâni. Thus either the Litâni river did not cross the Roûm fault (nor, possibly,

the Yammoûneh fault) 5.3 Myr ago, or the Roûm fault did not exist as such at that time. If the Litâni did flow south, east of both faults, into the Hula depression [as inferred by Butler et al., 1998; Butler and Spencer, 1999; Horowitz, 1979], then a correspondance might be found between the upper catchment of the Zahrani and the present course of the Litâni downstream from the Roûm fault. At a constant rate of 2.9 ± 0.5 mm/yr since 5.3 Ma, the corresponding 13–18 km displacement would indeed realign both catchments across the Roûm fault. Although such a possibility cannot be ruled out, we find such a large offset, as well as even larger offsets (30 km) proposed by Butler et al. [1998], implausible. First, as stated above, the Roûm fault is clearly a lateral ramp, hence it is unlikely that its rate was constant along strike. Second, since there is almost no catchment offsets north of the Zahrani are smaller than ~ 2 km [Griffiths et al., 2000], and since there is no trough following the fault that could testify for larger offsets, 6–13 km of shortening would have had to have been absorbed in the 4-km-wide Jezzîne anticline since 5.3 Ma.

We conclude that the slower slip rate (1.8 ± 0.1 mm/yr) on the Roûm fault, and the linked hypothesis of Messinian incision of the Litâni, is preferable. Stepwise, northward decrease of this rate where the Roûm fault bypasses the western limbs of the Baroûk and Jezzîne anticlines could have accounted for the decreasing offsets of the Zahrani and Aouali rivers: it is plausible that each of the thrust ramps underlying these anticlines absorbed up to 2–3 km of shortening, corresponding to up to 4 km of Roûm-parallel strike-slip motion. It is also plausible that today the Roûm fault continues to propagate northwards.

2.5.3 Consequences on the Plio-Quaternary kinematics of the Levant fault system across the Lebanese restraining bend

Shortening across the Mount Lebanon Thrust

The map of active faulting of figure 31 suggests a large amount of slip partitioning across Mount Lebanon. A better assessment of the partitioning requires knowledge of the direction of shortening across the Mount Lebanon thrust system (MLT). Three active thrust faults may be used to constrain this direction. All three show little evidence of oblique slip, whether dextral or sinistral. Therefore, shortening is expected to be approximately perpendicular to the thrust traces. The directions of shortening thus obtained for the Tripoli, Halba and Niha thrusts are N50°W, N35°W and N40°W, respectively. We take the average direction ($N42.5 \pm 7.5^\circ$ W) to represent the direction of regional shortening.

Using this direction, the slip rate on the Yammoûneh fault, and the strikes of the Yammoûneh and Ghab faults, it is possible to estimate the rate of shortening across the MLT. A key hypothesis underlying this geometrical calculation is the assumption of pure strike-slip on the Ghab fault. Although we have not had the opportunity to test this assumption through fieldwork in Syria, as the fault resumes a northward direction at the northern tip of Mount Lebanon, geomorphic and geological evidence for transpression vanishes along the fault. The 5–6 Ma Homs basalts stand at structurally similar levels east and west of the Ghab fault, and have suffered little erosion. Although there is significant relief farther north along the west side of the Ghab basin (up to 1560 m a.s.l.), it is unclear whether the corresponding uplift is related to transtension or transpression. The structural cross-section of the Syrian coastal range shown in figure 5 of Mouty et al. [1992] would argue for large-scale block tilting due to normal faulting. The sketch of figure 64 summarizes the rigid block approximation we use, assuming pure strike-slip on the Ghab fault.

- $\alpha=28^\circ$ is the angle between the strikes of the Yammoûneh ($N30^\circ$ E) and Ghab ($N2^\circ$ E) faults;

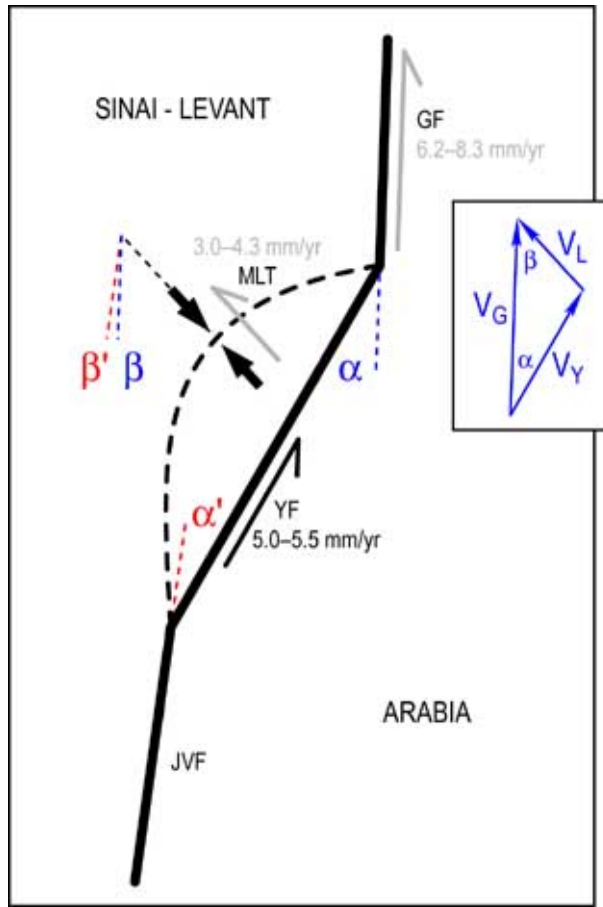


Figure 64: Sketch of the geometric model used to predict the rate of shortening across Mount Lebanon

- $\beta = 37 - 52^\circ$ is the angle between the strike of the Ghab fault ($N2^\circ E$) and the direction of shortening across the Mount Lebanon thrust system ($N35 - 50^\circ W$);
- $\vec{V}_Y = 5.0 - 5.5 \text{ mm/yr}$ is the left-lateral slip rate along the Yammoûneh fault;
- \vec{V}_G is the left-lateral slip rate along the Ghab fault;
- \vec{V}_L is the rate of shortening across the Mount Lebanon thrust system;

Since:

$$\vec{V}_Y + \vec{V}_L = \vec{V}_G \quad (1)$$

then:

$$V_Y \cdot \sin \alpha - V_L \cdot \sin \beta = 0 \quad (2)$$

$$V_Y \cdot \cos \alpha + V_L \cdot \cos \beta = V_G \quad (3)$$

it follows that:

$$V_L = V_Y \cdot \sin \alpha / \sin \beta \quad (4)$$

$$V_G = V_Y \cdot \left(\cos \alpha + \frac{\sin \alpha}{\tan \beta} \right) \quad (5)$$

With the values determined above, $V_L = 3.0 - 4.3 \text{ mm/yr}$. Such a shortening rate would imply 16 to 23 km of underthrusting since the Pontian across the entire range, including the thrusts at sea. Depending on how far the thrusts are from the coastline ($\sim 50 \text{ km?}$), this would represent 24% to 31% of crustal shortening, a value which seems appropriate for a mountain range now approximately at most 3 km above sea level, and whose inner core has undergone several kilometers of erosion: the cross-section in figure 21 (p.34) shows the 5–7-km-high structural uplift of the top of the Eocene.

Kinematic compatibility with the Ghab and Jordan valley faults

Equation (5) may be used to test whether the predicted slip rate on the Ghab fault is compatible with known kinematic constraints. It yields $V_G = 7.25 \pm 1.05 \text{ mm/yr}$, a value in good agreement with the $6.9 \pm 0.1 \text{ mm/yr}$ rate measured by Meghraoui et al. [2003] over the latest 2000 yr on the Missyaf segment of this fault, even though the error bars they propose seem unrealistic. Note that changing our initial assumption of pure strike-slip on the Ghab fault would affect this predicted Ghab rate, as well as the shortening rate across Mount Lebanon. Even a small amount of transpression along the Ghab fault would significantly increase both of these rates, which seems unrealistic given the upper bounds imposed by Arabia-Nubia motion models [Chu and Gordon, 1998; McClusky et al., 2003]. Alternatively, a small amount of transtension, compatible with normal faulting on the west side of the Ghab pull-apart, would slightly decrease both rates.

Using the MLT shortening rate and the Yammoûneh fault slip rate to extrapolate rates southwards along the Jordan Valley fault is more problematic, because of the existence of the Râchaïya-Serghaya fault system, and of likely of slip partitioning across the Anti-Lebanon and Palmyrides [Gomez et al., 2003]. Although the former has been documented by Gomez et al. [2003] at Zebadani to slip at $1.4 \pm \text{mm/yr}$ over the latest 6 kyr, the latter is poorly constrained. Since thrust orientations in the Palmyrides (figure 31) are approximately perpendicular to the regional direction of shortening we estimate in Lebanon, and since the Serghaya fault is sub-parallel to the Yammoûneh fault, we take the slip partitioning geometry west and east of the Beqaa to be similar.

To predict a rate on the Jordan valley fault, it is therefore justified to use the following equation:

$$V_J = (V_Y + V_S) \cdot (\cos \alpha' + \sin \alpha' / \tan \beta') \quad (6)$$

where V_J is the rate on the Jordan fault, $V_S = 1.4 \pm 0.2 \text{ mm/yr}$ is the rate on the Serghaya fault, $\alpha' = 22^\circ$ the angle between the strikes of the Yammoûneh (N30°E) and Jordan (N8°E) faults, and $\beta' = 43 - 58^\circ$ is the angle between the strike of the Jordan fault (N8°E) and the direction of regional shortening within the LRB (N35–50°W). The predicted Jordan valley slip rate would thus be 7.2–9.4 mm/yr, a value much higher than all those estimated until now along the southern Levant fault system. A discussion of possible reasons for this discrepancy, and of the bearing of our data on finite geological offsets on the LFS will be presented in the conclusion of this thesis.

Extrapolation to the Roûm fault

The strongest constraints that we used to assess slip partitioning come from the northern part of Mount Lebanon and from the Ghab fault. One may thus harbor doubts that extrapolating these constraints to the southern tip of Mount Lebanon, whose topography and geological structure are different, is justified. Also, the Roûm fault is not a pure strike-slip fault, but a lateral ramp with a component of thrusting. Therefore, the component of left-lateral slip on the fault, $\overrightarrow{V_{R//}}$, may be deduced from the shortening vector $\overrightarrow{V_L}$ using:

$$\overrightarrow{V_L} = \overrightarrow{V_{R//}} + \overrightarrow{V_{R\perp}} \quad (7)$$

where $\overrightarrow{V_{R\perp}}$ is the dip-slip component of motion. Equation (7) translates into:

$$V_{R//} = V_L \cdot \cos \gamma \quad (8)$$

$\gamma=23-38^\circ$ being the angle between $\overrightarrow{V_L}$ (N35–50°W) and the strike of the Roûm fault (N12°W). This yields 2.4–4.0 mm/yr of left-lateral slip along the fault. Although this value is compatible with the fastest rate we hypothesised from the Litâni offsets (2.9 ± 0.5 mm/yr, cf section 2.5.2), we find it implausible for the reasons already advocated. Moreover, the local strike of the axes of the Baroûk and Jezzîne anticlines (N22°E) is parallel to the southern stretch of the Yammoûneh fault, hinting at locally pure slip partitioning.

Another, more local estimate of the rate on the Roûm fault might thus be deduced from a model in which pure strike-slip along the average strike of the LFS north and south of Lebanon (N5°E) is purely partitioned into 5.0–5.5 mm/yr of slip along the locally, N22°E-striking Yammoûneh fault, and shortening in a direction (N68°W) perpendicular to the axes of the Baroûk and Jezzîne anticlines. According to equation (4) this would yield 1.5–1.7 mm/yr of N68°W shortening, to be taken up on the N12°W-striking Roûm fault ramp, hence a left-lateral rate of 0.85–0.94 mm/yr on this ramp. That this value is significantly smaller than the smallest rate deduced from the Litâni offsets suggests that slip partitioning in Lebanon varies from north to south in ways that remain to be understood.

– Chapitre III –

Sismicité long terme du coude transpressif libanais

The seismic behavior of the Lebanese Restraining Bend is not much better known than its tectonic features. At the scale of the whole Levant Fault System, the available instrumental data (figure 65) exhibits a rather low level of seismicity, probably representative of a longer-term quiescent period that has lasted from AD 1837 ($M \sim 7$ event near Safed) to 1995 ($M_w 7.3$ Aqaba earthquake). During this period, the largest earthquake produced by the LFS was the $M_L 6.2$ “Jericho” event, in AD 1927 [Ben-Menahem, 1991; Shapira et al., 1993]. Based on the study of historical earthquakes, several authors [e.g. Ambraseys and Barazangi, 1989; Guidoboni et al., 2004b] have stressed that this recent subdued seismic activity is not representative of the long-term behavior of the LFS. In this chapter, we try to address this issue by studying the seismicity in the area of the LRB over time scales ranging from a few centuries to several millennia.

Over the past ~ 30 centuries, the LFS has repeatedly generated large ($M > 7$) earthquakes, as documented in numerous historical sources. By combining the available historical data and our tectonic model of the LRB, we are able to re-assess the seismic history of the region of modern-day Lebanon.

Investigating the earthquake record of this area over even longer periods calls for paleoseismic trenching across the main faults of the LRB. The first results of such trenching are presented in this chapter, and shed new light on the seismic behavior of the Yammoûneh fault since at least 15 ka.

3.1 Historical earthquakes of the LRB area

As mentioned above, the 20th-century seismicity of the Levant, up to AD 1995, is rather weak, in sharp contrast with many historical descriptions, going back to Biblical times, of large, destructive earthquakes capable of killing thousands. This discrepancy makes it highly unlikely that the current instrumental record accurately reflects the seismogenic potential of the fault system. In order to study the longer-term seismic behavior of the Levant fault, one must thus rely on historical descriptions. Luckily, the rich written record of the Near East provides such data over the past three millennia. Many historical catalogues of earthquakes in this area have been compiled [e.g. Poirier and Taher, 1980; Ben-Menahem, 1979, 1991; Guidoboni et al., 1994; Ambraseys et al., 1994; Abou Karaki, 1987]. Here is an outline of the

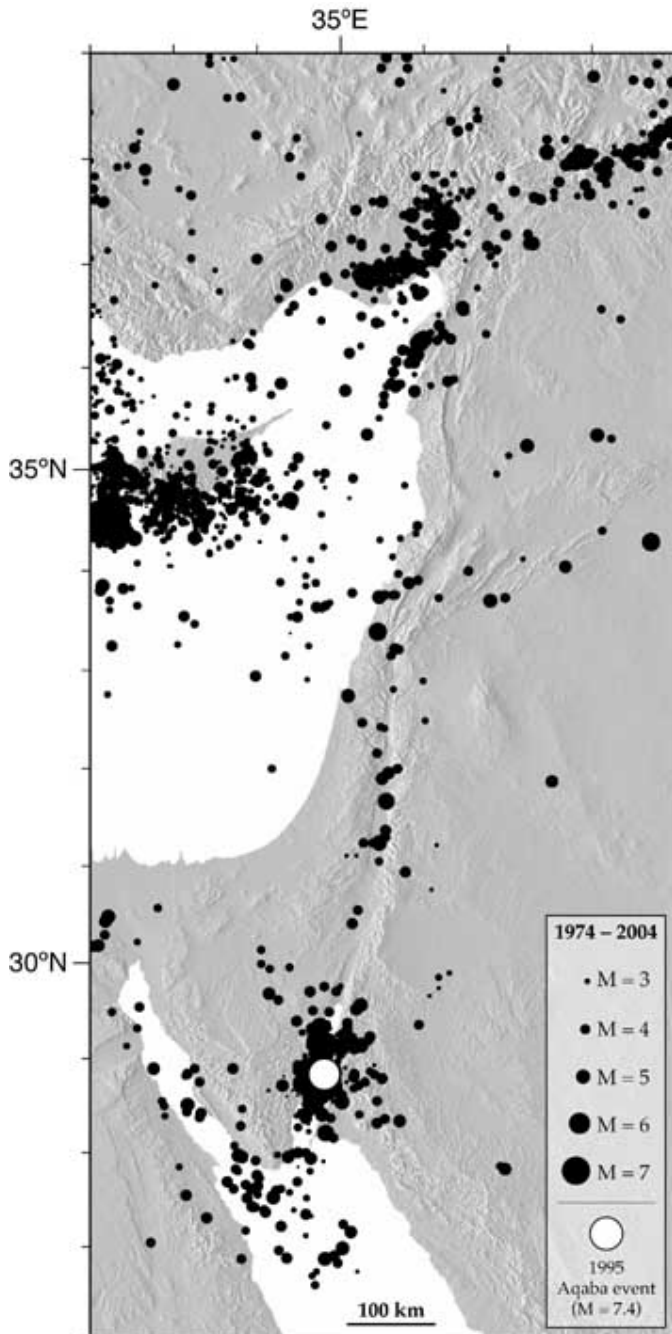


Figure 65: Instrumental seismicity of the LFS since AD 1973 (data from the National Earthquake Information Center, USGS). The cluster of epicenters in the gulf of Aqaba is due in part to the aftershocks of the November 1995 earthquake [Klinger et al., 1999; Abou Karaki et al., 1993].

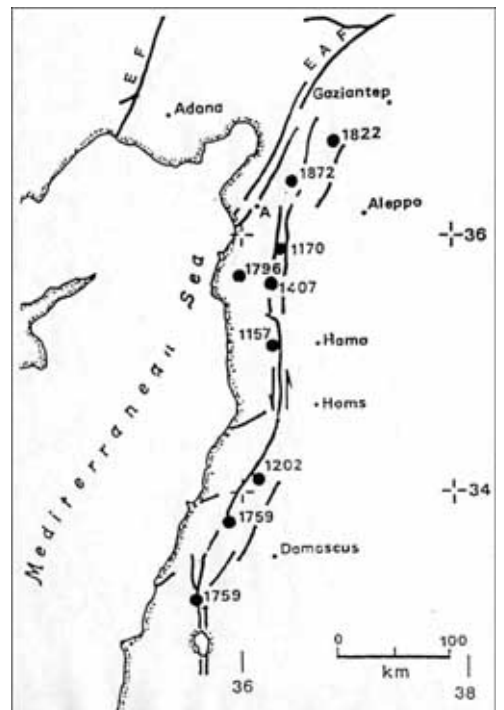


Figure 66: Epicenters proposed by Ben-Menahem [1991] for various historical earthquakes that affected the northern LFS. The latitudes of the proposed epicenters were estimated from the N-S extent of macroseismic damage, and their E-W positions were assumed to coincide with the main LFS at these latitudes. The epicenters of the AD 1202 and 1759 events, whose respective macroseismic damage zones are both centered on the Beqaa, were thus both interpreted to have been generated by the Yammoûneh fault, leading to the assumption that this fault may produce $M > 7$ earthquakes with a recurrence time of about 560 years, and that the latest such event was less than 250 years ago. As we demonstrate in section 3.2, this inference is incorrect.

steps usually followed to produce such a catalogue:

- **Historical sources relevant to the timing or the effects of earthquakes are compiled and studied critically.** Translation issues are important, particularly in culturally and linguistically heterogenous settings (e.g. the Levant states at the time of the Crusades). Ideally, contemporaneous first-hand accounts should be preferred to posterior and/or second-hand ones.
- **Timing of the earthquake:** the reported dates of seismic events often vary from source to source. Likely causes for this include (1) a mistake by the original author, because the report is second-hand, or written years after the event; (2) a mistake in the conversion from one calendar system to another, either by the author of the catalogue or by one of the intermediary copists/compilers of the original report [cf Abou Karaki, 1987, for a more thorough discussion of calendar conversion issues]; (3) a transcription mistake at any stage of the copying or cataloguing processes.
- **Intensities assessment:** For a given earthquake, all reports are compiled and compared. At each site where macroseismic effects were described, an intensity value is assessed, taking into account the inferred strength of the affected buildings.
- **Estimation of earthquake parameters:** Using the overall distribution of inferred intensities and independant calibration data, a magnitude can be proposed for each event. Some authors also propose an estimate of the epicenter or of the likely source fault.

This general methods depends strongly on the availability of relatively homogenous sets of data, and on the assessment of historical sources. Unsurprisingly, such evidence is rarely univocal, and different authors have been known to assign different magnitudes to the same event, based on the exact same sources.

3.1.1 Catalog of historical events in the LRB area

Assigning tectonic sources to historical earthquakes depends not only on assessing macroseismic effects, but also on an accurate knowledge of the active faults in the area of the event. Based on our model of the active faults of the Lebanese restraining bend (cf previous chapters, especially section 1.2) which was not available to previous authors, we propose a re-assessment of several events on the Levant fault. We compiled the macroseismic descriptions of 48 historical earthquakes in the Levant, reported by various authors (table 10)

1365 / 1356 BC [a,c]	Ghab fault? Lattakya ridge?
- earthquake followed by a seismic wave on the Syrian coast [a,c] - destruction of Ras Sharma and Ugarit [a,c]	
<p>Based on these scarce reports, we tentatively infer the source of this event to be either a segment of the northern LFS, or an offshore thrust associated with the Lattakya ridge, which trends SSW offshore from the site of Ugarit.</p>	

References for historical earthquakes

Catalogs of historical seismicity:

- a – Abou Karaki [1987]
- b – Ambraseys et al. [1994]
- c – Ben-Menahem [1979]
- d – Ben-Menahem [1991]
- e – Guidoboni et al. [1994]
- f – Taher [1979]

Reviews of individual earthquakes:

- g – Ambraseys [2004]
- h – Ambraseys and Melville [1988]
- i – Ambraseys and Barazangi [1989]
- j – Ambraseys [1997]
- k – Darawcheh et al. [2000]
- l – Guidoboni et al. [2004a]
- m – Guidoboni et al. [2004b]
- n – Marco et al. [2003]
- o – Plassard [1968]

Paleo- and archaeo-seismological studies:

- p – Ellenblum et al. [1998]
- q – Meghraoui et al. [2003]
- r – Reches and Hoexter [1981]

Table 10: References used in our catalogue of historical seismicity

~ 1250 BC [c]

Jordan Valley fault

- destruction of Jericho and other cities [c]
- archaeological evidence at Tel-Dir-Ala (Biblical Succoth, 45 km away from Jericho) [c]
- landslides of Lisan marl cut the Jordan at Damye [c]
- estimated $M_L \sim 6.5$ [c]

The area most affected by this event suggests a source along the Jordan Valley fault. Note that landslides that cut the Jordan river for days were also reported for the AD 1546 event and for the instrumental event of AD 1927 ($M \sim 7.2$).

854 BC [a,c]

area of Tiberias

- destruction of Aphek (32.8°N , 35.7°E), on the E coast of Lake Tiberias [a,c]
- estimated $M_L \sim 6.6$ [c]

759 BC (“Hazor earthquake”) [a,c,d,e]	<i>Jordan Valley fault</i>
<ul style="list-style-type: none"> - large landslide in the Kidron valley [a] - destruction of Sebastia (near Nablus) [a,c,d] - destruction of Hazor and Kinnereth (9 km N of Tiberias) [c] - destruction in Judea, Samaria and Galilee [d] - estimated I ~ VIII (MM) in Jerusalem [a] - damage to the Temple in Jerusalem, mentioned in the Bible [d,e] - felt in Israel, Egypt and Mesopotamia [a,c] - archaeological excavations at Hazor (14 km N of Lake Tiberias) revealed traces of the damage caused by this event [d,e] - additional archaeological evidence in Sebastia [c,d] - likely epicenter is NE of Hazor [c,d] - possible seismic wave in Lake Tiberias [c] - estimated $I_0 \sim XI$ [a] - estimated $M_L \sim 7.3$ [d] 	

Not only does the macroseismic damage area suggest that the source of this event is the Jordan Valley fault, but archeologic evidence of near-field seismic waves from the NE suggest that the epicenter was near the northern end of this fault, and that coseismic slip then propagated southwards.

590 BC [a,c]	<i>Tyre fault / offshore Carmel fault</i>
<ul style="list-style-type: none"> - offshore earthquake [a,c] - flooding of Tyre [a,c] - seismic wave on the Lebanese coast [a,c] - mentioned in the Bible [a] - estimated $M_L \sim 6.8$ [c] 	

In the absence of further evidence, we could infer the source to be the Tyre fault, whose geomorphic trace is clear onland (e.g. figure 25, p.39) but whose seismogenic potential is poorly known. Alternatively, mention of flooding could be interpreted as evidence of offshore faulting, either on the Tyre fault or along the offshore extension of the Carmel fault. See also the 140 BC event.

199 / 198 BC [e]	<i>area of Sidon?</i>
<ul style="list-style-type: none"> - series of shocks in the region of Sidon [e] - “a city above Sidon was swallowed up” [e] - “almost two thirds of Sidon collapsed, but the number of victims was limited, because it did not happen in a single shock” [e] - “the same disaster struck the whole of Syria, but with moderate intensity” [e] - estimated $I_0 \sim X$ [e] 	

In the absence of further evidence, one might attribute this event to a fault near Sidon (e.g. the Roûm fault or the Mount Lebanon thrust). Lack of evidence at other sites, on the other hand, might be a result of scarce historical sources rather than indicate that the area Sidon was most damaged, since it seems that the earthquake affected the rest of Syria. See also the AD 19 event.

~ 140 BC [a,c,d]	<i>Tyre fault / offshore Carmel fault</i>
<ul style="list-style-type: none"> - earthquake offshore Tyre [a] - seismic wave between Tyre and Acre [a,c,d] - partial subsidence of the island of Tyre [a,c,d] - felt strongly in Cyprus [a,c,d] - estimated $M_L \sim 7.0$ [c] - estimated $I_0 \sim X$ [d] 	

As for the 590 BC event, we infer the source to be either the Tyre fault or the Carmel fault.

65 / 64 BC [a,c,d,e]	<i>Northern Levant fault</i>
<ul style="list-style-type: none"> - earthquake near Antioch [a,c,d,e] - destruction of Antioch [d] - affects Syria [a,e] - affects Palestine [a] - in Jerusalem, Temple walls are damaged [a,c,d] - many casualties (“170,000”) and cities destroyed in Syria [e] - felt in Cyprus and Israel [a,c,d] - estimated $M_L \sim 7.5$ [d] - estimated $I_0 \sim \text{IX-XI}$ [e] 	

31 BC [a,c,d,e,r]	<i>Jordan Valley fault</i>
<ul style="list-style-type: none"> - earthquake in Judea, with many casualties (“30,000”) [c,d,e] - casualties and major destruction in southern Cisjordania, in Qumran, Jerusalem and in the Jordan valley [a,c,d] - likely one of the causes of the abandonment of Qumran [e] - destruction at Masada and Herod’s winter palace in Jericho [c,d] - archaeological evidence at Masada [d] - paleoseismic evidence of this earthquake just N of the Dead Sea [r] - likely destruction at/of Salamine, in Palestine [e] - estimated $M_L \sim 7.0$ [c] 	

AD 19 [a,c,d]	<i>area of Sidon?</i>
<ul style="list-style-type: none"> - earthquake offshore Sidon [a,c,d] - destruction at Sidon [a,d] - felt in Israel, Syria and Asia Minor [d] - estimated $M_L \sim 6.8$ [d] - estimated $I_0 \sim \text{IX-X}$ [d] <p><i>In the absence of further evidence, we tentatively attribute this event to a fault near Sidon (e.g. the Roûm fault or the Mount Lebanon thrust). See also the 199/198 BC event.</i></p>	

~ AD 112 [b]	<i>Araba fault?</i>
<ul style="list-style-type: none"> - archaeological evidence suggests destruction at Petra, Masada, Avdat and along the Petra-Gaza road [b] 	

AD 115 [a,c,d,e]	<i>Northern Levant fault</i>
<ul style="list-style-type: none"> - destruction at/of Antioch [a,c,d,e] - “many cities were badly damaged, but Antioch suffered the worst destruction” (buildings collapsed, many casualties) [e] - 260,000 casualties [a] - seismic wave on Yavne and Caesaria (coast of Israel) [c,d] - mentioned in Talmudic sources [a,c,d] - widely felt in the Near-East and Eastern Mediterranean [a,c,d] - estimated $M_L \sim 7.4$ [d] - estimated $I_0 \sim \text{X-XI}$ [a] / IX-XI [e] 	

AD 127 – 130 [c,e]	<i>area of Nicopolis / Caesaria</i>
<ul style="list-style-type: none"> - destruction of Nicopolis and Caesaria (both in Palestine) [e] - affected Damascus [c] - estimated $M_L \sim 6.1$ [c] - estimated $I_0 \sim \text{IX-X}$ [e] 	

AD 303 / 304 / 306 [a,c,d,e,o]*area of Tyre/Sidon (MLT?)*

- very destructive earthquake (offshore?) Tyre and Sidon [a,c,d,e]
- seismic wave at Caesaria (32.5°N, on the Mediterranean coast) [a,c,d,o]
- felt in Jerusalem [a,c,d]
- associated with archaeological evidence at various sites in Palestine [e]
- estimated $M_L \sim 7.1$ [d]
- estimated $I_0 \sim X$ [d] / IX-XI [e]

We tentatively infer that the source of this event is part of the Mount Lebanon thrust system.

AD 348 / 349 [a,c,d,e,o]*MLT / Yammoûneh fault*

- destructive earthquake in / offshore Beirut [a,c,d,e,o]
- affected the Syrian coast [a,c,d]
- estimated $M_L \sim 7.0$ [d]
- estimated $I_0 \sim X$ [d] / VIII-IX [e]

We interpret this event to be either a (weaker?) version of the AD 551 earthquake offshore Beirut, or caused by the Yammoûneh fault.

AD 363 [c,d,e]*Jordan Valley fault*

- earthquake in the area of Jerusalem [e] / E of the Lisan [d]
- destruction of “many cities in Palestine” [e]
- destruction of the Temple in Jerusalem [e,d]
- damage at the construction site of the emperor Julianus in Jerusalem [d]
- destruction of Sebastia, Nicopolis, Antipatris, Sepphoris [e]
- destruction of Rabbath Moab (Areaopolis) and Kir-Hareset (El-Kerak) [c,d]
- partial destruction of Beit Gubrin, Baishan, Lydda, Ascalon, Caesarea, Samaria, Paneas, Azotus, Gophna, Petra, Jerusalem, Tiberias, Areopolis [e]
- many casualties in Aina d-Gader, Haifa, Japho [e]
- seismic wave in the Dead Sea [c,d]
- estimated $M_L \sim 6.4$ [c]
- estimated $I_0 \sim X$ [e]

AD 419 [a,c,e]*area of Tiberias*

- earthquake near Safad [a]
- destruction in Khirbet Shama (32.99°N, 35.45°E) [a,c]
- destruction in Aphek (32.8°N, 35.7°E) [a,c]
- destruction of cities and villages in Palestine [a,e]
- felt in Jerusalem [c]
- estimated $M_L \sim 6.2$ [c]
- estimated $I_0 \sim$ IX-XI [e]

AD 450 – 457 [e]*area of Tripoli*

- in Tripoli, collapse of a summer bath [e]
- in Tripoli also, damage to several buildings and to the aqueduct [e]
- estimated $I_0 \sim$ VIII-X [e]

We infer the source of this event to be either the northern section of the offshore Mount Lebanon thrust system (offshore or onland), or the southern section of the Ghab fault. The former seems more likely than the latter, since Meghraoui et al. [2003] found no paleoseismic evidence of a 5th-century event on the Ghab fault [q].

AD 494 [o]

- destruction in Tripoli, Lattakiya [o]
- mild but frightening in Beirut [o]
- felt as far as Hierapolis of Syria (Membij, near the Euphrates river) [o]

Note that this event is only mentioned by Plassard [1968].



Figure 67: [a] The six remaining columns of the Jupiter Temple in Baalbek (2.2 m in diameter and 20 m high); the other 48 columns collapsed in a series of events from AD 565 to 1759. [b,c,d] The keystone of the “Bacchus” temple in Baalbek was dislodged (but did not fall) in 1759; later (1870) it was consolidated by a pillar of bricks, then (1901) uplifted back in place.

AD 502 [a,c,d,e,o]

offshore Carmel fault?

- earthquake offshore Acre [a,c,d,o]
- destruction of Akko (Acre) [c,d,e,o]
- destruction of Acre and Latrun (Nicopolis) [a]
- destruction of one half of Tyre and Sidon [c,e,o]
- in Berytus, only one synagogue collapsed [c,e,o]
- destruction in Tyre, Sidon, Beirut, Byblos (Jbeil) [a,d]
- no destruction in N Syria [o]
- estimated $M_L \sim 7.0$ [d]
- estimated $I_0 \sim X$ [d]

AD 525 [a,c]

Mount Lebanon thrust system

- earthquake offshore Sidon [a,c]
- strong in Beirut, Byblos (Jbeil), Sidon and Antioch [a]
- possible seismic wave on the Lebanese coast [a]
- estimated $M_L \sim 6.7$ [c]
- estimated $I_0 \sim IX-X$ [c]

NB: possible confusion with another event (AD 526, in Antioch); cf [a,e].

AD 551 [b,c,e,k,o]*Offshore Lebanon*

- earthquake affecting the Lebanese coast [c,e,k,o]
- destruction of Berytus, Tripolis, Sidon, Byblus, Botrys, Tyre, and 101 towns in that area, with many casualties [c,e,k,o]
- Berytus was hit the worst [o]
- seismic wave on the whole of the Phoenician coast; many ships destroyed [b,c,e,k]
- the coast north of Laodicea and south of Tyre was spared (no collapse of buildings) [e]
- in Berytus, the sea retired two miles, before returning [b,c,e,k,o]
- 30,000 known people died in Beirut, which collapsed almost completely [c,e,k,o]
- destruction of the aqueduct of Berytus [k]
- the famous school of law of Berytus could never recover [k]
- large fire in Berytus, which lasted two months [k,o]
- possible landslide near Botrys [e,k,o]
- destruction of many cities and villages in Galilee and Samaria, and possibly in present-day Jordan [k]
- collapse of many coastal cities in Galilee, Samaria, Palestine and Arabia [c,e]
- felt strongly in Antioch, Alexandria [k,o]
- felt in Phoenicia, Syria, Palestine, Arabia and Mesopotamia [b,c,e]
- estimated $M_L \sim 7.8$ [c]
- estimated $M_S \sim 7.1\text{--}7.3$ [k]
- estimated $I_0 \sim XI\text{--}XII$ [c] / X [e] / IX-X [k]

In view of the spectacular and well-documented damage to Beirut and the strong and extensive seismic wave on the Lebanese coast, we interpret this event to have been caused by slip on the Mount Lebanon thrust system, offshore Beirut [e.g. Elias et al., 2004; Daëron et al., 2004b]. The inferred trace and the SE dip of this thrust suggest that Beirut lies directly above a seismogenic part of the thrust system.

AD 565 [c,d]*area of Baalbek & Damascus*

- earthquake in Baalbek (Heliopolis) and Damascus [c]
- collapse of 2 columns (out of 54) of the Jupiter Heliopolitanus temple in Baalbek (fig. 67.b) [d]
- felt in Israel and Mesopotamia [c]
- estimated $M_L \sim 6.7$ [c]

Likely sources of this event include the Râchaïya-Serghaya fault system, or active thrusts in the Palmyrides.

AD 634 [e]*Southern Levant fault*

- earthquake in Palestine [e]
- damage in Jerusalem [e]
- tremors lasted for one month [e]
- estimated $I_0 \sim VIII\text{--}X$ [e]

AD 659 [c,e]

- earthquake in Palestine and Syria [e]
- many places collapsed, including most of Palestine [e]
- estimated $I_0 \sim VIII\text{--}X$ [e]

AD 659 / 660 [e]*Southern Levant fault*

- most of Jericho collapsed with all its churches [e]
- “many other places” were affected [e]
- estimated $I_0 \sim IX$ [e]

AD 749 (“Beit She’an earthquake”) [a,b,c,d,e,f,n,r] <i>This event was reviewed by Marco et al. [n]</i> <ul style="list-style-type: none"> - fig. 68 shows the extent of the effects of this event [n] - earthquake in Palestine, along the river Jordan and in Syria [e] - 600 settlements damaged on both sides of the Jordan, from [d] - major destruction at Tiberias, Jerusalem, Lod, Arad, Jerash (27 km E of the Jordan) and in the monasteries to the north of the Dead Sea [a,c] - the worst damage was in Jerusalem [a,e,f] - damage to the church of the Holy Sepulchre in Jerusalem [d] - collapse of churches and monasteries, especially in the desert around Jerusalem [e] - inhabitants of Jerusalem took shelter in the desert for 40 days [e] - nearly complete destruction of Tiberias, and of 30 synagogues in the area [c,d,e] - seismic wave in Lake Tiberias [d] - “countless thousands” of casualties [e] - landslide near Mt Tabor [e] - archaeological evidence at Beit She’an [e] - collapse of the temple at Mabbug [e] - destruction at Hisham’s palace (near Jericho) [a,c,d] - collapse of a fortress at Beit Qubayeh [e] - destruction at/of al-Ghouta, Darayya, Bosrah, Nawa, Dar‘at and Baalbek [e] - destruction at Gerasa (E of the Jordan) [c,d] - tremor at Damascus, which lasted for days [e] - damage at Damascus [a,f] - the sea “overflowed”) [e] - seismic wave in the Dead Sea [a,c] - a spring of water near Jericho was displaced [e] - felt in Syria, Egypt, Arabia and Mesopotamia [a,c,d] - felt on Syrian and Egyptian coasts [a] - paleoseismic evidence of this earthquake just N of the Dead Sea [r] - estimated $M_L \sim 7.3$ [d] - estimated $I_0 \sim XI$ [c] / IX-X [e] 	<i>Jordan Valley fault</i>
---	----------------------------

AD 847 [a,c,e,f] <ul style="list-style-type: none"> - earthquake in Damascus and Antioch [a,e,f] - collapse of houses and bridges at Damascus [e] - destruction of Antioch [a,e,f] - destruction and casualties at Mawsil, al-Ghouta, Darayya, al-Mazzah, Bayt Lahya and others [e] - damage extended to Al-Jazira and Mossul (many casualties) [a,f] - destruction in Lebanon (Beqaa) [a,c] - felt in the Maghreb [a,f] - estimated $M_L \sim 6.2$ [c] - estimated $I_0 \sim VIII$ [a] / IX-XI [e] 	<i>area of Damascus/Antioch</i>
--	---------------------------------

AD 853 / 854 [a,e,f] <ul style="list-style-type: none"> - earthquake and landslide in Tiberias [e] - in Tiberias, “the earth shook, the mountains [s’entrechoquèrent], a large rock fell off, killing many people” [a,f] - estimated $I_0 \sim VIII-X$ [e] / X-XI [a] 	<i>area of Tiberias</i>
---	-------------------------

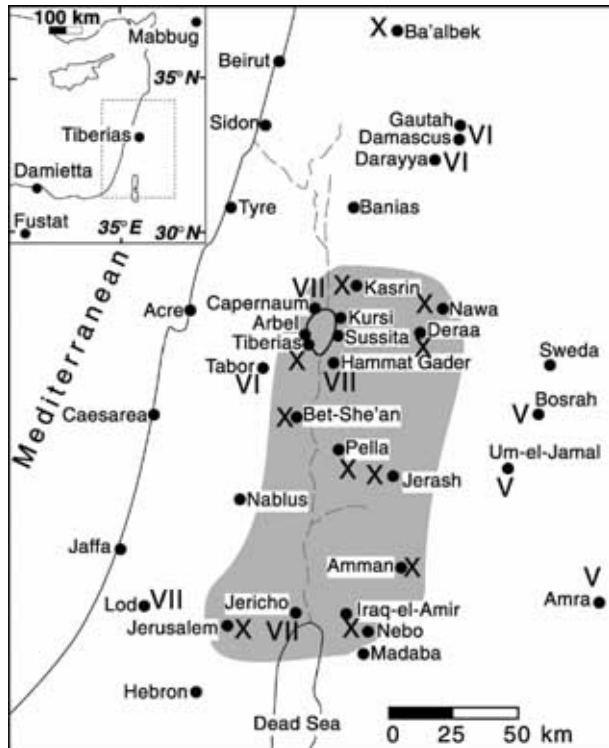


Figure 68: Effects of the 749 "Hazor" earthquake from Marco et al. [n]
Roman numbers indicate MMS intensities.

AD 859 / 860 [c,d,e]

Northern Levant fault

- earthquake affecting Antioch and many other towns along the Orontes [e]
- in Antioch, collapse of 1,500 houses and 90 towers [c,e]
- total destruction of Antioch [d]
- destruction of Laodicea and Jablah [e]
- damage in Jerusalem [c,d]
- affected Balis, Raqqa, Harran, Ras al-Ayn, Hims, Damascus, al-Ruha, Tarsus, al-Massisa, Adhana and the Syrian coast. [e]
 - landslide on Mt Casius [c,e]
 - felt in Mecca, Egypt, Turkey, Armenia, Mesopotamia [c,d]
 - estimated $M_L \sim 8.0$ [d]
 - estimated $I_0 \sim IX-X$ [e]

AD 881 [a,c]

area of Acre (offshore Carmel fault?)

- seismic wave at Acre [a,c]
- the wave was felt in Alexandria and affected the Nile [a]
- estimated $M_L \sim 6.5$ [c]

AD 972 / 974 [d,e]

area of Antioch/Damascus

- collapse of the walls and many towers of Antioch [e]
- damage in Antioch [d]
- affected Damascus and the surrounding area [e]
- estimated $M_L \sim 6.4$ [d]
- estimated $I_0 \sim VII-VIII$ [e]

AD 991 [a,c,d,e]*area of Damascus/Baalbek*

- collapse of 1,000 houses and many casualties in Damascus [a,e]
- Baalbek and the area of Damascus were ruined [a,d] / shaken [c,e]
- a village near Baalbek collapsed [a,e]
- collapse of 1 column (out of 52) of the Jupiter Heliopolitanus temple in Baalbek (fig. 67.b) [d]
- felt as far as Egypt [a,c]
- month-long period of aftershocks [a,e]
- possible seismic wave on the Syrian coast [a]
- estimated $M_L \sim 6.5$ [c]
- estimated $I_0 \sim IX-X$ [c] / IX [e]

Likely sources of this event include the Râchâïya-Serghaya fault system, or active thrusts in the Palmyrides.

AD 1033 [a,b,c,d,f]*Jordan Valley fault*

- earthquake in the Jordan valley [b]
- earthquake near Ramla “and in the entire Palestine” [a]
- one third of the houses in Ramla were destroyed [a,f]
- damage in Jericho and the areas of Jerusalem and of Nablus [a,f]
- near Nablus, a village was buried entirely [a,f]
- many houses collapsed in Acre [a,f]
- heavy damage and casualties in Tiberias [d]
- in Tiberias “mountains stirred like sheep”, “rocks exploded” and wells overflowed [a,f]
- offshore Acre [c]
- seismic wave in Acre, affected the coasts of Israel and Lebanon [a,b,c,d,f]
- “from the sea to Banias”, and “from the sea to Nablus”, “cities were leveled” [a]
- felt as far south as Jerusalem, Gaza, Ascalon, and probably in the Negev and in Egypt [b,d]
- followed by many strong aftershocks, until Feb. 17, 1034 [b]
- estimated $M_L \sim 6.7$ [d]

NB: it is possible that these effects were caused by several events; cf [a].

AD 1063 [a,f]*area of Tripoli*

- earthquake affecting Antioch, Lattakya, Tripoli, Tyre, Acre and Syria in general [a,c,f]
- the walls of Tripoli collapsed [a,f]
- estimated $M_L \sim 7.1$ [c]

Judging by the severity of the damage at Tripoli, it is possible that the source of this event is part of the northern, onland Mount Lebanon thrust system.

AD 1068 [a,b,c,d,f]*Araba fault / Gulf of Aqaba*

- earthquake in Palestine and Egypt, many casualties [a,f]
- destruction of Elat and most of its inhabitants [a,b,c,d]
- destruction of Ramla [a,b,f]
- damage in Jerusalem [a,b,c,f]
- destruction at Baniyas [b]
- wells overflowed [a,f]
- affected the S coasts of Israel [c,d]
- seismic wave at Ashdod and Yavne [c]
- the (Mediterranean?) sea retreated from the coast before returning [a,c,f]
- multiple shock [a]
- appearance of new springs in Tabuk and Taima (resp. 150 km and 350 km E of the gulf of Aqaba) [b]
- felt in Egypt and Arabia [b,c,d]
- I ~ IX in Ramla, Jerusalem, Banias, Khaybar, Tayma and Elat [a]
- I ~ VIII in Kufa [a]
- I ~ VI in Wadi as Safra [a]
- I ~ IV in Sharm Yanbu [a]
- estimated $M_L \sim 7.0$ [d]

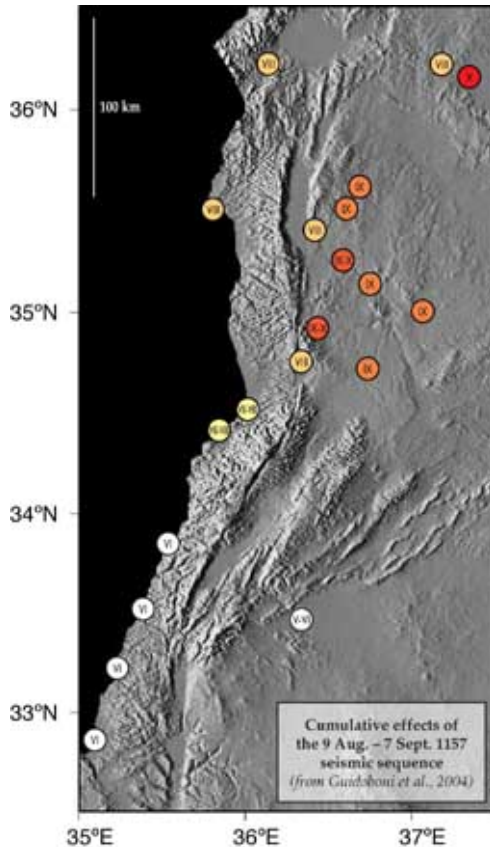


Figure 69: Cumulative effects of the main 1157 sequence, after Guidoboni et al. [2004a]

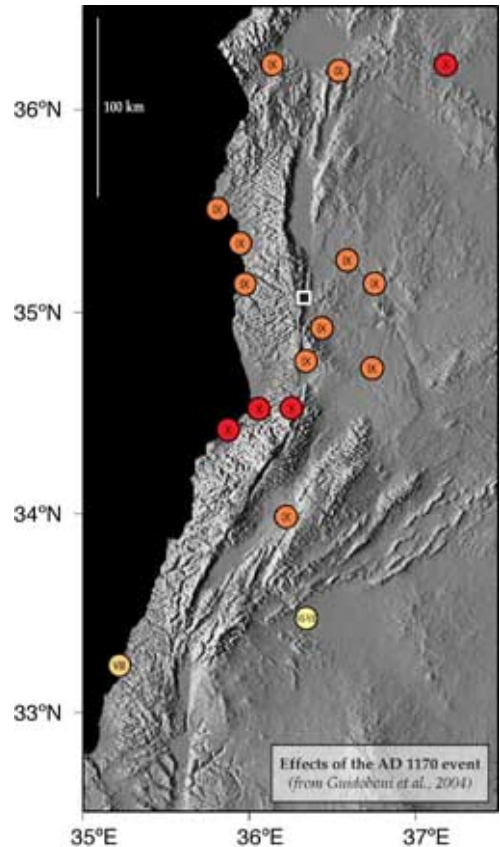


Figure 70: Effects of the 1170 earthquake, after Guidoboni et al. [2004b]. The black and white square marks the location of the study of Meghraoui et al. [q].

AD 1156–1159 sequence [d,l]

Northern Levant fault

This sequence was re-assessed thoroughly by Guidoboni et al. [l], who reviewed and re-appraised the previous catalogs. The following data is summarized from their work:

- a long and devastating series of seismic events took place from the 27th of September 1156 to the 29th of May 1159.
- various catalogs list individual episodes (e.g. July 15, 1157; Aug. 12, 1157; Aug. 15, 1157) of this long sequence.
- the most destructive shocks (fig. 69) occurred between the 9th of August and the 7th of September 1157.
- together with the 1170 event, this sequence caused the collapse of 11 columns (out of 51) of the Jupiter Heliopolitanus temple in Baalbek (fig. 67.b) [d]

Macroseismic damage areas of this sequence and of the AD 1170 event are similar, although the effects of the latter were stronger and more widespread. One could hypothesize that both “events” were generated by different segments of the northern Levant fault system.

AD 1170 [d,g,m,q]***Missyaf fault (southern Ghab fault)***

This event was reviewed by Guidoboni et al. [m]

- fig. 70 shows the extent of the effects of this strong earthquake [m]; the weighted center of the macroseismic damage zone coincided with the Missyaf segment of the Ghab fault
 - destruction of Tripoli and of the fortified settlements of Arqa and Gibelacar [m]
 - most inhabitants of Tripoli were killed [m]
 - the walls and citadel of Baalbek collapsed [m]
 - serious damage to the Crac des Chevaliers and the castle of Margat [m]
 - collapse of city walls at Barin [m]
 - damage to the citadel of Safitha [m]
 - serious damage to the walls and citadel of Homs, Hama and Shayzar [m]
 - damage at Laodicea and Gabala [m]
 - extensive destruction in Antioch (collapse of fortification walls and towers and of many buildings) and Aleppo (partial collapse of the citadel) [m]
 - damage in Damascus and Tyre [m]
 - felt as far as Iraq, [m]
 - strongly felt in Jerusalem [m]
 - paleoseismic and archaeological evidence of surface faulting associated with this event was discovered near Missyaf (cf location in fig. 70) [q]
 - it is possible that this June 1170 event was actually two distinct shocks [m]
 - estimated Mw ~ 7.7 [m, in the case of a single event]
 - estimated Mw $\sim 7.3\text{--}7.5$ [q]
 - estimated I₀ \sim IX-X [m]
 - fall of Herod's obelisk at Caesaria [d]
 - together with the 1156–1159 sequence, this event caused the collapse of 11 columns (out of 51) of the Jupiter Heliopolitanus temple in Baalbek (fig. 67.b) [d]
 - damage to the walls, citadel and town of Shaizar (35.7°N , 36.7°E), with many casualties [g]
 - damage to the walls and citadel of Hama, with many casualties [g]
 - destruction of the castle of Barin (34.95°N , 36.4°E) [g]
 - destruction of Safitha (34.8°N , 36.13°E) [g]
 - probable destruction of Hisn al Akkar (34.35°N , 36.25°E) [g]
 - heavy damage and many casualties in Homs [g]
 - Hisn al Akrad (34.8°N , 36.25°E) was seriously damaged [g]
 - probable collapse of the castle of Arqa (34.35°N , 36.1°E) [g]
 - considerable damage to houses and defenses in Baalbek, with casualties [g]
 - mention of ground fissures in the mountains overlooking Baalbek [g]
 - damage at Jabalah (25 km SE of Latakiya), Baniyas, Margat (both 50 km SSE of Latakiya), Jubail and Aleppo [g]
 - the castle and a large part of the city of Tripolis were ruined [g]
 - limited damage in Antioch (50 casualties) and in Damascus (only one casualty) [g]
 - hints of liquefaction in Aleppo and Antioch [g]
 - aftershocks were mentioned, lasting 2 weeks to 4 months [g]

AD 1202 [d,h,p]***Yammoûneh fault***

This event was reviewed by Ambraseys and Melville [h]; only the most relevant data is summarized here. Section 3.2 presents a detailed re-assessment of the source of this earthquake.

- fig. 71 shows the intensities associated with the effects of this earthquake [h]
- rockfalls in Mount Lebanon overwhelmed ~ 200 people, suggesting the possibility of large-scale landslides [h]
- collapse of 31 columns (out of 40) of the Jupiter Heliopolitanus temple in Baalbek (fig. 67.b) [d]
- in Damascus, despite the occurrence of the 1157 and 1170 earthquakes, “old men could not recall such a severe [event] having occurred before” [h]
 - felt from Lesser Armenia, Anatolia and NW Iran to Sicily, Upper Egypt and Mesopotamia [h]
 - aftershocks were reported for at least four days in Hamah, Damascus and Cairo [h]
 - possible aftershock which destroyed what was left of Nablus [h]
 - archaeological and paleoseismic evidence of a left-lateral offset of 1.6 m of the walls of the Vadum Jacob castle (location shown in fig. 71) [p]
 - estimated M_S ~ 7.6 [h]
 - estimated I₀ \sim XI [d]

See section 3.2 [Daëron et al., 2005] for a thorough discussion of the source of this event.

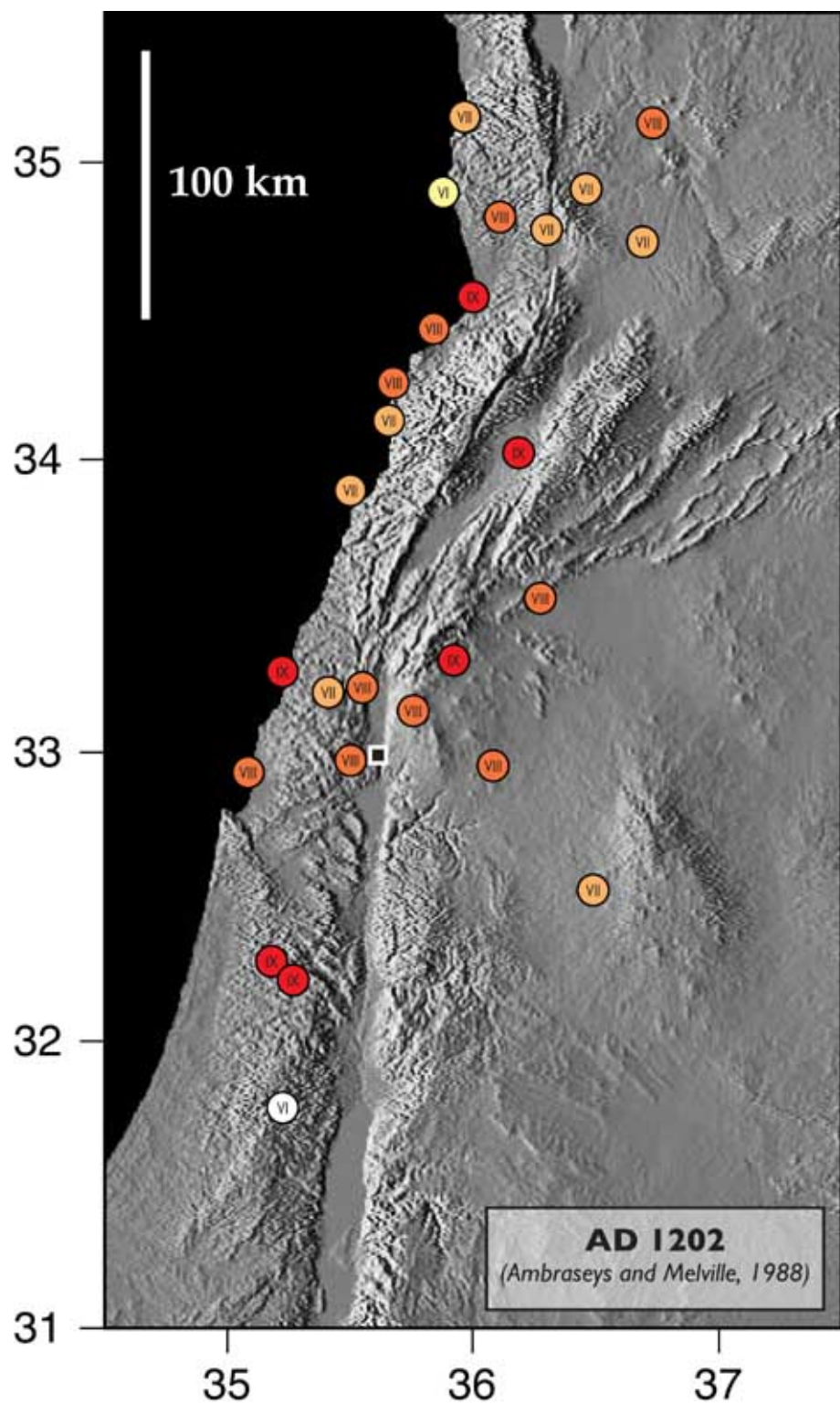


Figure 71: Effects of the 1202 earthquake, after Ambraseys and Melville [1988]. The black and white square marks the location of the study of Ellenblum et al. [p].

AD 1212 [b]*Araba fault*

- earthquake in S Palestine [b]
- strongest in Ailat [b]
- destruction of towers and houses at Kerak and Shaubak (between Kerak and Ailat), with casualties [b]
- damage to the cells and walls of the monastery of St Catherine in the Sinai [b]
- felt in Cairo and Fustat, where it destroyed a number of houses [b]

AD 1293 [b]*Southern Levant fault*

- earthquake in the region of Gaza [b]
- affected Ramla, Ludd, Qaqun (all within a Jerusalem-Gaza-Haifa triangle) and al-Karak [b]
- collapse of a minaret in Ramla [b]
- collapse of a minaret in Gaza [b]
- ruined many places in coastal Palestine [b]

AD 1458 [b]*Southern Levant fault*

- earthquake in S Palestine [b]
- destruction of parts (towers, walls) of the citadel in Kerak [b]
- destruction of many houses and of the governor's palace in Kerak [b]
- 1,000 casualties in Kerak [b]
- destruction of minarets in Ramla, Ludd and Hebron [b]
- damage in Jerusalem [b]
- felt in Cairo [b]

AD 1546 [a,b,c,d]*Jordan Valley fault*

- great damage and casualties in Nablus, Jerusalem, Tiberias, Hebron, Kerak, Es-Salt, Jaffa, Gaza and Ramle [a,b,c,d]
- most severe damage in Nablus, with hundreds of casualties [a,b,d]
- a landslide of Lisan marl cut the Jordan river for two days [a,b,c,d]
- seismic wave in the Dead Sea [a,c,d]
- seismic wave on the S Palestine coasts [b]
- felt in Damascus [a,b,c]
- estimated $M_L \sim 7.0$ [d]
- estimated $I_0 \sim IX-X$ [c] / IX [h]

Note that landslides that cut the Jordan river for days were also reported for the 1250 BC event and for the instrumental event of AD 1927 ($M \sim 7.2$).

AD 1656 [d]*area of Tripoli*

- destruction at Tripoli [d]
- felt in Israel [d]
- estimated $M_L \sim 7.0$ [d]

AD 1759 (October 30) [d,h,i]**Râchaïya Fault**

This event was reviewed by Ambraseys and Barazangi [i]; only the most relevant data is summarized here. Section 3.2 presents a detailed re-assessment of the source of this earthquake.

- strong foreshocks on the 10th of June [h]
- affected primarily the region of Safad and the mountain area to the NE of it [i]
- destruction of Safed and Qunaitra, with many casualties [i]
- widespread damage in Tiberias [i]
- collapse of the city walls of Tiberias [d]
- great damage and many casualties in Tiberias [d]
- seismic wave in Lake Tiberias [d]
- a few houses collapsed in Saida [i]
- damage to buildings in Saasaa, Nazareth and Acre [i]
- minor damage in Damascus and its area [i]
- felt in Antioch, Aleppo, Jerusalem and Gaza [i]
- a seismic wave flooded the docks of Acre and Tripoli, without apparent damage [i]
- possible surface faulting (up to 0.6 m of left-lateral offset) at the Vadum Jacob castle [p]
- followed by a series of strong aftershocks [i]
- estimated $M_S \sim 6.6$ [i]

See section 3.2 [Daëron et al., 2005] for a thorough discussion of the source of this event.

AD 1759 (November 25) [i,d]**Serghaya Fault**

This event was reviewed by Ambraseys and Barazangi [i]; only the most relevant data is summarized here. Section 3.2 presents a detailed re-assessment of the source of this earthquake.

- fig. 72 shows the intensities associated with the effects of this earthquake [i]
- almost total destruction of the villages in a 120-km-long narrow zone extending NNE from the Beqaa plain to the upper reaches of the Orontes [i]
- almost total destruction of Safed, Hasbaya, Serghaya, Baalbek [i]
- collapse of 3 columns (out of 9) of the Jupiter Heliopolitanus temple in Baalbek (fig. 67.b) [d]
- heavy damage extended to Ras Baalbek [i]
- reported ground ruptures running along the Beqaa, over 100 km long [i]
- considerable but repairable damage in Damascus [i]
- strongly felt in Antioch, Aleppo, Ladhikiya, Gaza, Al-Arish and Tarba [i]
- felt in Egypt, throughout Anatolia [i]
- seismic wave as far south as the Nile delta [i]
- in Acre, the seismic wave threw ships onto the shore [i]
- aftershocks continued up till August 1760 [i]
- estimated $M_S \sim 7.4$ [i]

See section 3.2 [Daëron et al., 2005] for a thorough discussion of the source of this event.

AD 1834 [d]**Jordan Valley fault**

- earthquake E of the Lisan [d]
- damage in Jerusalem, Bethlehem, Nablus, Gaza and Kerak [d]
- large blocks of asphalt floated in the Dead Sea [d]
- the shallow road connecting the Lisan to En-Gedi disappeared [d]
- estimated $M_L \sim 6.3$ [d]
- estimated $I_0 \sim X$ [Ben Menahem, 1981, p. 187]

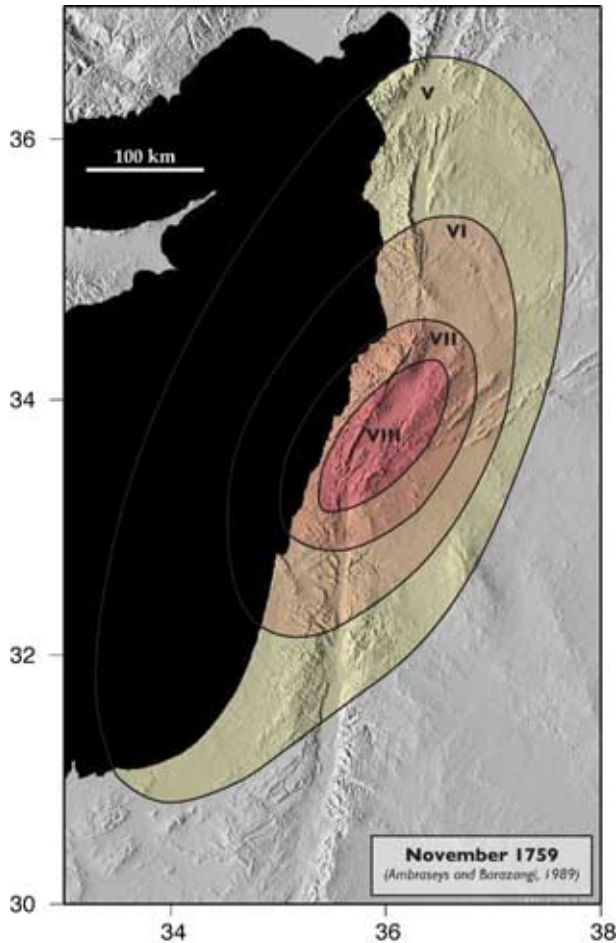


Figure 72: Effects of the Nov. 1759 earthquake, after Ambraseys and Barazangi [1989].

AD 1837 [d,j]

Roûm fault

This event was reviewed by Ambraseys [1997].

- fig. 73 shows the intensities associated with the effects of this earthquake [j]
- destruction in a narrow zone which extended from Saida to Marjayun, Bshara and Lake Tiberias, for a total length of 120 km [j]
 - destruction of Safed and Tiberias [d]
 - the destruction of Safed could be due to the instability of its site rather than to strong intensities [j]
 - 3,000 victims [d]
 - seismic wave in Lake Tiberias [d,j]
 - appearance of asphalt blocks in the Dead Sea [d]
 - three large aftershocks (Jan. 16, 22 and May 20, 1837) [j]
 - likely associated with rupture on the Roûm fault and its S continuation W of the Hule [j]
 - possible surface faulting (up to 0.6 m of left-lateral offset) at the Vadum Jacob castle [p]
 - estimated $M_s \sim 7.0\text{--}7.1$ [j]

In view of the distribution of intensities associated with this event (fig. 73), we infer that the most likely source is the Roûm fault.

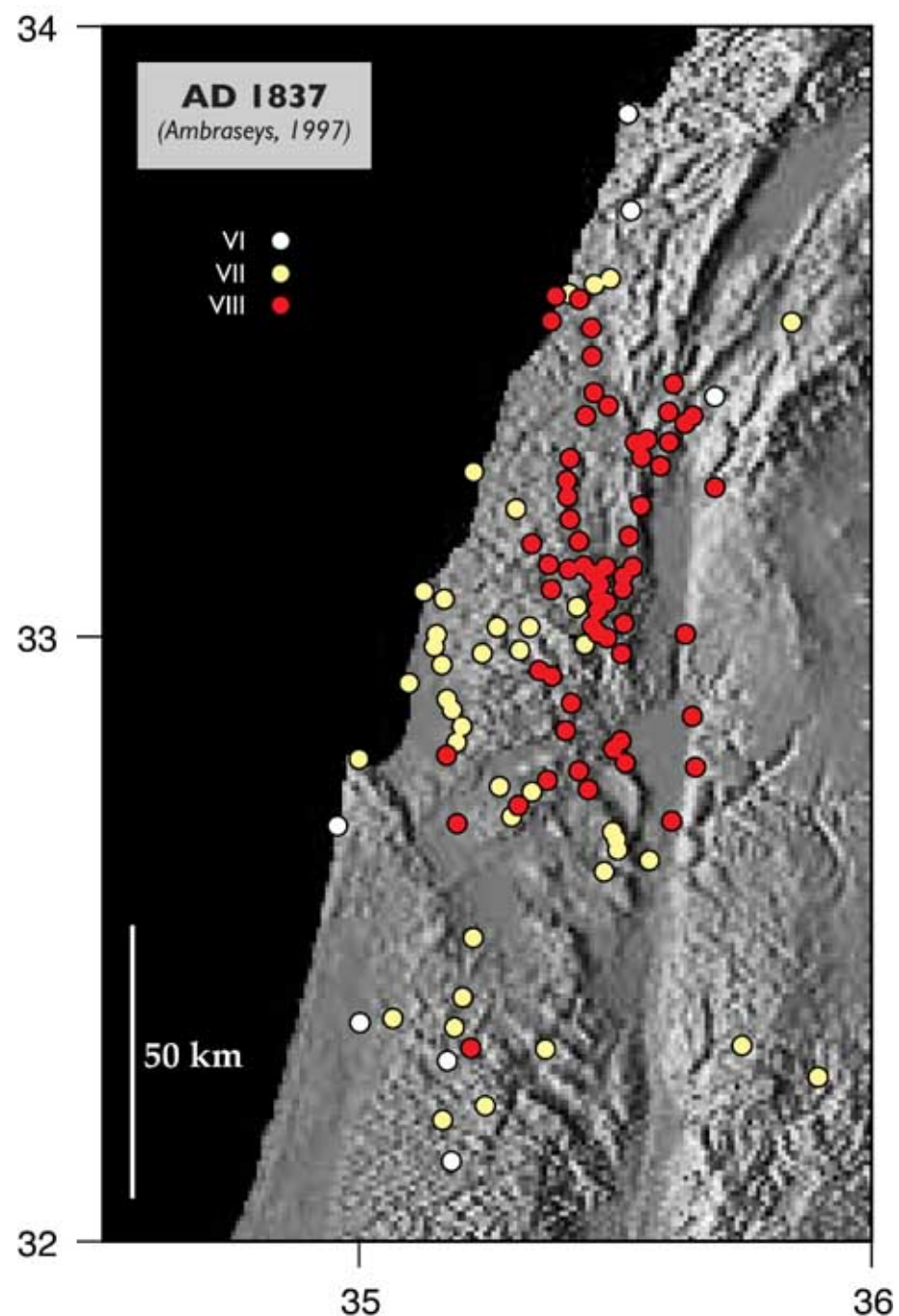


Figure 73: Effects of the 1837 earthquake, after Ambraseys [1997].

3.2 Sources of the large AD 1202 and 1759 Near East earthquakes

The contents of this section have been accepted for publication in *Geology* [Daëron et al., 2005]. We thank National Council for Scientific Research (Lebanon), *Institut National des Sciences de l'Univers (Centre National de la Recherche Scientifique, France)* and the French *Ministère des Affaires Etrangères*, for support. Without additional funding by *Coopération pour l'Evaluation et le Développement de la Recherche (Ministère des Affaires Etrangères)*, and by *Institut de Physique du Globe de Paris*, this work could not have been accomplished. We also thank G. Seitz and M. Kashgarian, from the Center for AMS (Lawrence Livermore National Laboratory, USA), for ^{14}C sample processing and AMS dating, A. Charbel and R. Jomaa for logistical help in the field, and two anonymous reviewers for constructive criticism. This is IPGP contribution no. 2030.

Abstract

The sources of the May 1202 and November 1759, M 7.5 Near East earthquakes remain controversial, because their macroseismal areas coincide, straddling subparallel active faults in the Lebanese restraining bend. Paleoseismic trenching in the Yammoûneh basin yields unambiguous evidence both for slip on the Yammoûneh fault in the twelfth-thirteenth centuries and for the lack of a posterior event. This conclusion is supported by comparing the freshest visible fault scarps, which implies more recent slip on the Râchaïya-Serghaya system than on the Yammoûneh fault. Our results suggest that the recurrence of a 1202-type earthquake might be due this century, as part of a sequence similar to that of A.D. 1033–1202, possibly heralded by the occurrence of the 1995, Mw 7.3 Aqaba earthquake. The seismic behavior of the Levant fault might thus be characterized by millennial periods of quiescence, separated by clusters of large earthquakes.

3.2.1 Introduction

The 1000-km-long, left-lateral Levant fault [e.g. Dubertret, 1932; Quennell, 1959; Freund et al., 1968; Garfunkel et al., 1981] marks the boundary between the Arabian plate and the Sinai-Levantine block [Courtillot et al., 1987; Salamon et al., 2003]. Since Biblical times, it has generated large ($M > 7$) earthquakes [e.g. Poirier and Taher, 1980; Ben-Menahem, 1991; Abou Karaki, 1987; Guidoboni et al., 2004b]. To this day, however, the sources of most historical events in the Near East remain unclear. This is particularly true between 33°N and 34.5°N , where the plate-boundary fault system is divided [Dubertret, 1955b], owing to transpression within the Lebanese restraining bend [Freund et al., 1970; Griffiths et al., 2000]. Recent results at sea [Carton et al., 2004; Elias et al., 2004], suggest that the strike-perpendicular and -parallel components of motion are accommodated by discrete features east and west of Mount Lebanon (3090 m): the offshore Tripoli-Beirut thrust [Tappognier et al., 2001], and the Yammoûneh and Râchaïya-Serghaya faults, respectively (figure 74). The latter strike-slip fault, which follows the Anti Lebanon Range (2630 m) west of the Beqaa Plain (1000 m), merges with the former at the southern tip of the Hula basin. By linking the Jordan Valley fault with the Missyaf fault, the

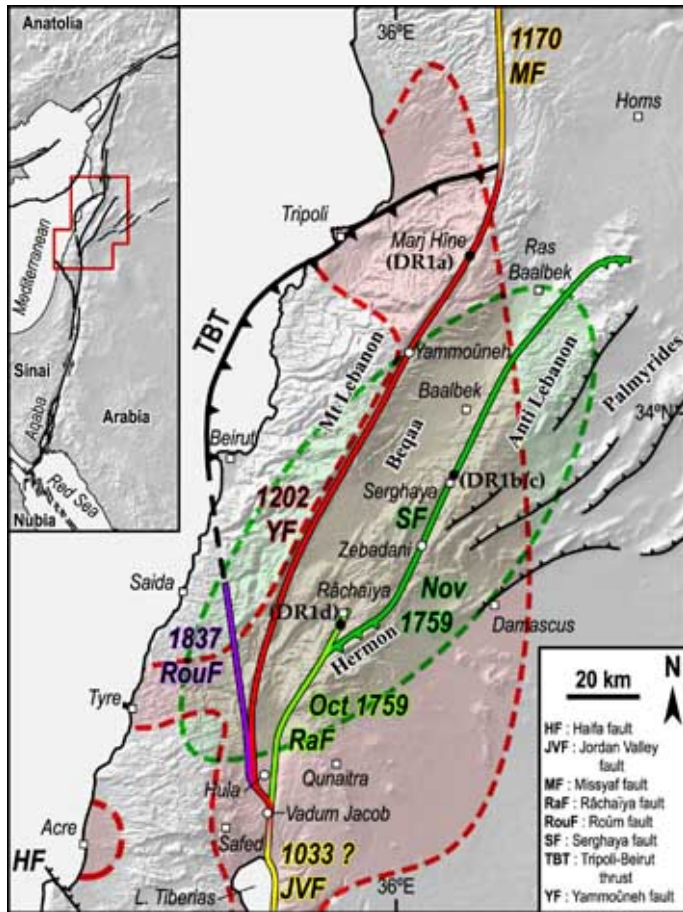


Figure 74: Schematic map of main active faults of Lebanese restraining bend: bold colored lines show maximum rupture lengths of large historical earthquakes in the past 1000 yr, deduced from this study and historical documents (see discussion in text). Bold dashed lines enclose areas where intensities \geq VIII were reported in A.D. 1202 (red) and November 1759 (green) according to Ambraseys and Melville [1988] and Ambraseys and Barazangi [1989]. Open symbols show location of cities (squares) and sites (circles) cited in text. Black dots mark location of field photographs shown in Fig. 75. (Inset: Levant transform plate boundary)

Yammoûneh fault ensures the continuity of the plate boundary across Lebanon.

Seismic hazard evaluation in this region depends critically on a better understanding of the seismic potential of the various strands and segments of the Levant fault system. On the basis of new paleoseismic data and geomorphic observations, we propose here a reassessment of the sources of arguably the two strongest historical earthquakes (A.D. 1202 and 1759), that devastated the Beqaa Plain and surrounding areas. The Yammoûneh fault has usually been held responsible for both the 1202 and November 1759 earthquakes [e.g. Ambraseys and Barazangi, 1989; Ben-Menahem, 1991]. Our results indicate instead that the paired October and November 1759 events ruptured the Râchaïya-Serghaya system, rather than the Yammoûneh fault. Although historical data alone is inconclusive, paleoseismic dating and the comparison of geomorphic observations lifts the ambiguity.

3.2.2 Macroseismic constraints on the 1202 and 1759 events

The effects of the 1202 and 1759 earthquakes were assessed by Ambraseys and Melville [1988] and Ambraseys and Barazangi [1989], respectively, using first-hand accounts. The 20 May 1202 earthquake shook western Syria and the Crusader states, toppling 31 columns of the Jupiter temple in the city of Baalbek [Ben-Menahem, 1991], which was destroyed “despite its strength and solidity”. The cities of Nablus, Acre, Safed, Tyre, Tripoli and Hamah, among others, suffered severe damage (figure 74). Rock falls in Mount Lebanon killed 200 people. Shaking was felt throughout the Mediterranean and Middle East, up to 1200 km away.

The seismic sequence of 1759 affected roughly the same region [Ambraseys and Barazangi, 1989]. The smaller, 30 October shock ruined Safed, Qunaitra, and many villages nearby, killing 2000 people and triggering a seismic wave in Lake Tiberias [Ben-Menahem, 1979]. The second, larger shock destroyed all villages in the Beqaa. Baalbek was ruined. 3 of the last 9 columns of the Jupiter temple [Ben-Menahem, 1991] and 3 columns of the Bacchus temple collapsed. Safed, Ras Baalbek and Damascus were damaged, and the earthquake was felt as far as Egypt and Anatolia, 1100 km away.

The areas of maximum destruction of the 1202 and November 1759 events overlap, covering an elongated, 150–200-km-long, south-southwest-trending zone centered on the Beqaa plain (figure 74). Historical accounts of damage thus imply that the events originated on the Yammoûneh or Serghaya fault. Macroseismic isoseismal contours tend to be biased toward populated areas: here, the fertile Beqaa Plain. It is therefore impossible to use such data alone to discriminate between the two faults.

3.2.3 Surface faulting

The identification and localization of surface faulting associated with the 1202 and 1759 events provides additional clues to determine the faults involved. Archeological and paleoseismic investigation [Ellenblum et al., 1998] showed that the 1202 earthquake caused 1.6 m of left-lateral displacement of fortification walls at Vadum Jacob (Fig. 74). A later 0.5 m offset may correspond either to the October 1759 event or to the last large regional event of 1 January 1837 [Ambraseys, 1997]. Unfortunately, the castle is located south of the junction between the Yammoûneh and Râchaïya-Serghaya faults. The question of which fault took up slip to the north during either event thus remains open. On the Serghaya fault, in the southern Zebadani valley in Syria, Gomez et al. [2001] described evidence of very recent faulting in the form of a persistent free face 0.5 m high on a scarp cutting soft lacustrine sediments. Trenching in this area, Gomez et al. [2003] exposed a colluvial wedge with modern ^{14}C ages, implying that the latest seismic event post-dates A.D. 1650. They interpreted this event to be one of two eighteenth century earthquakes (A.D. 1705 or 1759), but could not discriminate between the two.

Concerning surface disruption witnessed at the time of the earthquake, historical sources

are ambiguous. The 1202 Mount Lebanon rock falls might hint at stronger shaking on the west side of the Beqaa, hence on the Yammoûneh fault, but comparable shaking to the east might have gone unreported. Ambraseys and Barazangi [1989, p. 4010] mention 100-km-long surface ruptures in the Beqaa in November 1759, but state that “the exact location and attitude of (these ruptures) is [sic] not possible to ascertain today.” Nevertheless they infer the Yammoûneh fault to be the most likely candidate. Building on this inference, Ellenblum et al. [1998] referred to Ambraseys and Barazangi [1989] as quoting a description of ground breaks on the Yammoûneh fault by the French ambassador in Beirut. Our own investigation of the French sources cited by Ambraseys and Barazangi [1989, p. 4010] yielded only a second-hand account by the French consul in Saida, who writes: “One claims that [...] on the Baalbek side (or possibly: near Baalbek) pulling toward the plain the earth cracked open by more than [~ 6 m] and that this crack extends for over twenty leagues (~ 80 km)¹.”. The wording suggests that this rupture took place on one side of the Beqaa, and the mention of Baalbek points to the east side, thus to the Serghaya fault.

The inference that the 1759 earthquakes might be due to slip on the Râchaïya-Serghaya fault and the 1202 event on the Yammoûneh fault is qualitatively supported by comparing the preservation of scarps and mole tracks along the two faults. Figure 75 shows the freshest seismic surface breaks we studied in the field. On the east side of the Marj Hîne basin, the Yammoûneh fault juxtaposes Cretaceous limestones with Quaternary colluvial limestone fanglomerates. The surface trace of the fault is marked by a classic coseismic scarplet [“fault ribbon”: e.g. Armijo et al., 1992; Piccardi et al., 1999] that is fairly weathered (Fig. 75a). North of Serghaya, one strand of the Serghaya fault shows a scarplet of comparable origin, between limestone and limestone colluvium, but with a relatively unaltered surface and lighter color (Fig. 75b). This scarplet marks the base of a prominent slope break many kilometers long, at places only tens of meters above the valley floor, hence not due to landsliding. On the Râchaïya fault, we found fresh mole tracks in unconsolidated limestone scree (Fig. 75d), while none are preserved on the Yammoûneh fault. The fault ribbon north of Serghaya, which testifies to down to the west normal faulting, fits well the French consul’s description. Such evidence complements that of Gomez et al. [2001] at Zebadani, implying that the latest earthquakes on the Râchaïya-Serghaya fault are younger than on the Yammoûneh fault [Tapponnier et al., 2001].

3.2.4 Paleoseismic evidence

To test the inference that the 1202 earthquake is the latest event to have ruptured the Yammoûneh fault, we investigated the paleoseismic record of this fault by trenching lacustrine deposits in the Yammoûneh basin, on the eastern flank of Mount Lebanon (Figs. 74 and 76). The floor of that closed, pull-apart basin used to be flooded each year by meltwater from karstic resurgences [Besançon, 1968]. The lake was artificially dried up 70 yr ago and is now a cultivated plain. Aerial photographs and high-resolution satellite images show that the trace of the active

¹ “On prétend que [...] du côté de Balbec en tirans vers la plaine la terre s'est entrouverte de plus de trois toises et que cette ouverture dure plus de vingt lieues.” (Archives Nationales, Paris, B1/1032/1959-60)

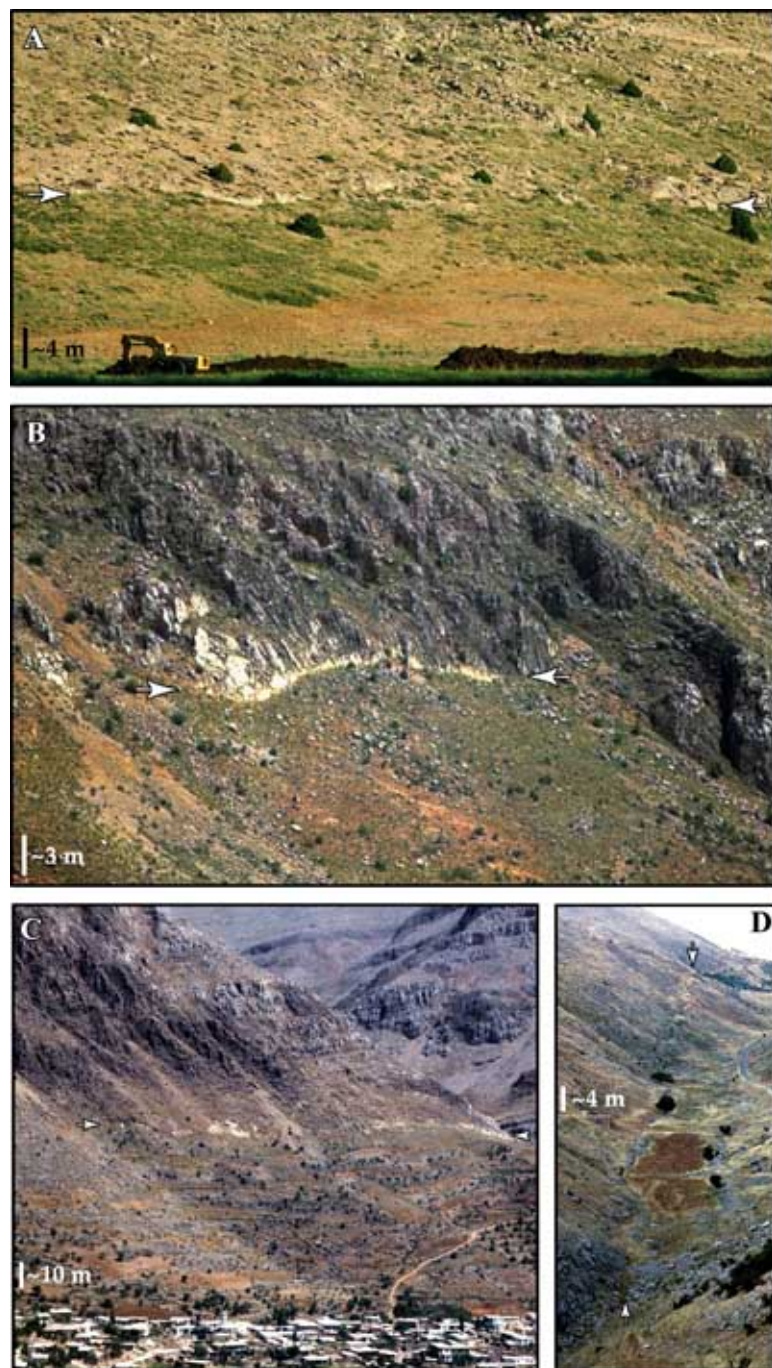


Figure 75: Comparison of weathered seismic scarplet (highlighted by white arrows) on Yammoûneh fault (A) with fresher seismic scarplet on Serghaya fault (B,C) and well-preserved mole-tracks on Râchâïya fault (D). (locations on Fig. 1)

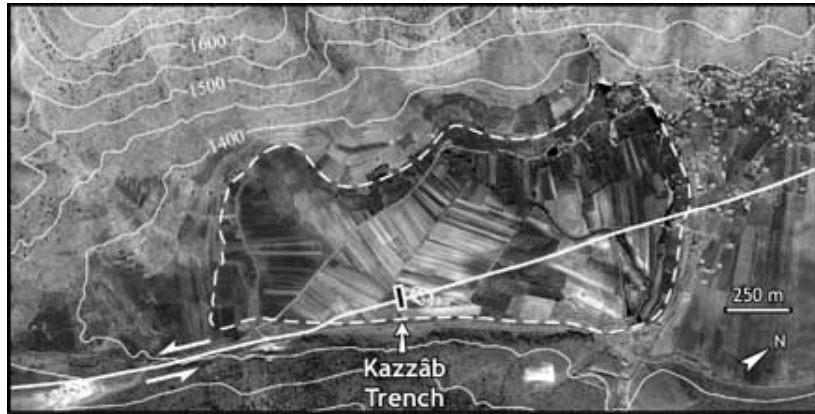


Figure 76: Satellite image of Yammoûneh paleolake (ancient shoreline dashed). Main strand of Yammoûneh fault (bold white line) cuts across lacustrine deposits. There is little evidence of current strike-slip motion on either side of the basin, where the sedimentary fill abuts the limestone edges. Resistivity measurements were previously interpreted to indicate that the Yammoûneh fault cuts across the basin, offsetting vertically the underlying bedrock [Besançon, 1968].

strike-slip fault shortcuts the pull-apart (Fig. 76). This geometry is clear from changes in soil color and vegetation, as well as inflections or offsets of gullies. Trenching on the east side of the paleolake (Fig. 76) confirmed the location of the main fault, which cuts a finely stratified, subtabular sequence of lake beds (figure 77). Here, we summarize information relevant to the 1759 and 1202 events in the shallowest part of one trench (Kazzâb trench).

Beneath the 25-cm-thick cultivated soil, the upper 2–3 m of the sequence consists mostly of compact, homogeneous, white calcareous marls, with buff to brown layers, 5–200 mm thick, richer in silts and clays. Some of the lighter-colored layers contain small (1–4 mm diameter) freshwater shells. A few of the layers are contorted and “cloudy” owing to liquefaction of probable seismic origin. Several layers contain abundant charcoal fragments (0.5–3 mm), of which 30 out of 200 have already been dated. The 75-m-long trench exposes spectacular faulting within a rather narrow (<2 m wide) zone. Figure 77 shows two north-facing trench walls, 1 m apart. Owing to minor dip-slip, the lake beds are sharply cut and vertically offset by fault splays, with local tilt and/or thickness changes. The effects of two seismic events are visible on both walls, in the uppermost 80 cm. The latest one (S1), marked by a subvertical principal splay, occurred after deposition of layer 6 and before that of layer 4. Layer 6, which is clearly visible on one wall, is preserved only east of the fault, suggesting it was eroded to the west after coseismic uplift. Unit 5, which tapers rapidly eastwards, is most likely a type of subaqueous “colluvial” wedge (redistributed lake mud) emplaced shortly after S1. The penultimate event was recorded as multiple splays (S2) cutting layers 13–16 over a width of 1 m and terminating at the base of layer 12. Layer 11 shows no disruption. Hence we interpret S2 to have occurred between the emplacement of layers 12 and 11. Older events S3, S4, etc. will be discussed elsewhere.

The timing of S1 is constrained by AMS (accelerator mass spectrometry) radiocarbon dating of samples K23, G3, G1 and K24 (Fig. 77 and Table 11). Samples K23 (A.D. 1295–1410)

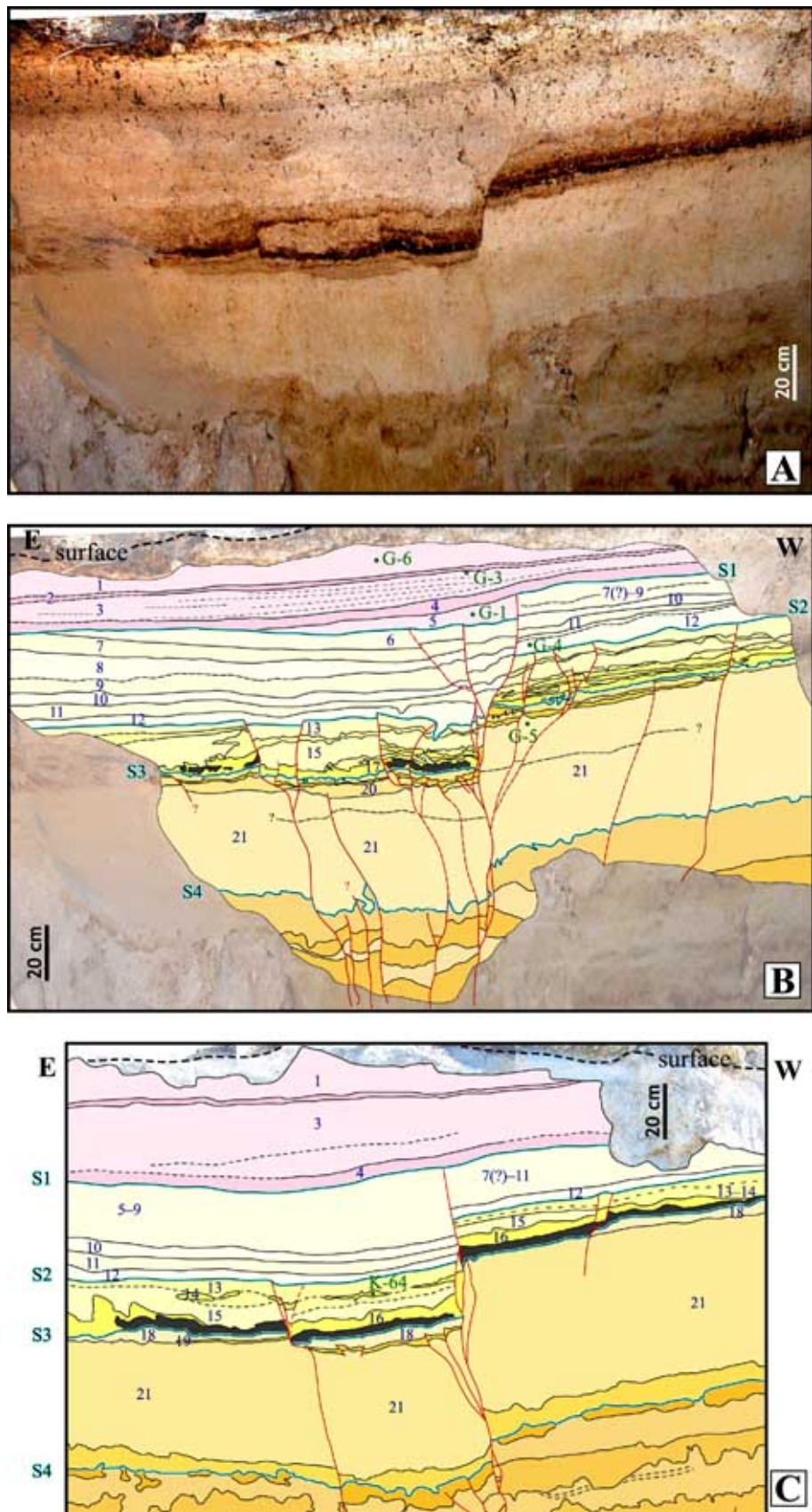


Figure 77: Photograph (A) and log (B) of wall of shallow Kazzâb-2002 trench, and log (C) of Kazzâb-2001 trench. K23, K24 and K29 were sampled on part of Kazzâb-2001 wall outside the area shown here.

and G3 (A.D. 1272–1412) clearly postdate the event. Sample K24 (A.D. 780–1001), from a paleochannel that is clearly capped by layer 4 (and likely by layer 6) to the east, predates the event. Sample G1 (A.D. 864–1002) comes from postseismic wedge 5, which likely contains samples from redistributed layers predating the event. Thus, the latest ground-breaking earthquake occurred between A.D. 864–1001 and 1295–1410. The only possible candidate for this event is the 1202 earthquake, since macroseismic damage for other large Near East events near that time was clearly located either well south (A.D. 1033) or well north (A.D. 1157 and 1170) of the Beqaa [e.g. Ben-Menahem, 1991; Meghraoui et al., 2003; Guidoboni et al., 2004a,b]. Any event postdating A.D. 1400 would have disrupted layer 2, and can be safely ruled out.

3.2.5 Summary and discussion

Our results put to rest the inference that the Yammoûneh fault might not be the main active branch of the Levant fault system in Lebanon [Butler et al., 1997]. They provide evidence of coseismic slip on the Yammoûneh fault in A.D. 1202, and show that this segment of the fault has remained locked since then. Since the size of the November 1759 event implies that it ruptured the surface, our data precludes that it took place on the Yammoûneh fault. Because the 1759 earthquake sequence comprised two large events and because of the new evidence we found—in the form of well-preserved mole tracks—of a recent, large event south of Râchaïya, the only other large fault system adjacent to the Beqaa (Râchaïya-Serghaya) is the most plausible source. We propose that the 30 October 1759 earthquake was caused by slip on the shorter (<50 km) Râchaïya fault, and the larger-magnitude November 25 event by slip on the longer (<130 km) Serghaya fault, in keeping with the evidence of recent movement on both [Tapponnier et al., 2001], and the French consul's letter. Our results thus build on those of Gomez et al. [2003] by lifting the ambiguity between the 1705 and 1759 shocks.

We interpret the occurrence of two events in 1759 and the month-long delay between them as a classic earthquake triggering example. Such triggered, delayed rupture may be due to the presence of the Mount Hermon asymmetric push-up jog, a geometrical irregularity which prevented immediate rupture propagation along the entire Râchaïya-Serghaya fault system. Though non-unique, this scenario is in keeping with scaling laws [Wells and Coppersmith, 1994; Ambraseys and Jackson, 1998], which predict (2-sigma) magnitudes of 6.4–7.3 and 7.0–8.0 respectively, compatible with those derived from historical accounts [6.6 and 7.4, Ambraseys and Barazangi, 1989] and from the ~2 m stream channel offset attributed to the last event on the Serghaya fault at Zebadani [7.0–7.2 for the November 1759 event, Gomez et al., 2003].

With its fine lacustrine sequence, midway along the Yammoûneh fault, the Yammoûneh basin has great potential for understanding the timing of ancient Lebanese earthquakes. To this day, we have investigated this sequence down to 11 m depth. 2–3 m beneath the top soil, is a major stratigraphic transition, of probable climatic origin, from the calcareous marls to a ~8-m-thick clay unit. We have already identified and mapped 10 event horizons down to this

Sample	Lab number	Material	$d^{13}\text{C}$ ‰	Radiocarbon age (BP)	Layer or unit	Calibrated age (95% probability range)
(Y-02) G1	12233	Charcoal	-25.3	1115±35	5 [r]	A.D. 864 – 1002
(Y-02) G3	12234	Charcoal	-28.5	650±60	3 (top)	A.D. 1272 – 1412
(Y-02) G4	12235	Charcoal	-21.0	1980±90	12 [r]	202 B.C. – A.D. 241
(Y-02) G5	12236	Charcoal	-32.6	2000±100	21 (top)	352 – 296 B.C. / 208 B.C. – A.D. 240
(Y-02) G6	12237	Charcoal	-29.3	718±35	1 [r]	A.D. 1222 – 1306 / A.D. 1364 – 1387
(Y-01) K23	85982	Charcoal	-25(*)	610±45	2	A.D. 1295 – 1410
(Y-01) K24	85983	Charcoal	-25(*)	1125±50	see text	A.D. 780 – 794 / A.D. 802 – 1001
(Y-01) K29	85984	Charc. & wood	-25(*)	2055±40	21	170 B.C. – A.D. 26
(Y-01) K64	86069	Charcoal	-25(*)	1640±45	14	A.D. 261 – 279 / A.D. 324 – 537

Table 11: Radiocarbon dates. Most of the catchments around the paleolake being steep and short (<4 km), it is unlikely that the dated charcoals were stored for very long before deposition. AMS measurements were made at Van de Graaff laboratory of Utrecht University ('G' samples) and at CAMS of Lawrence Livermore National Laboratory ('K' samples); ages were calibrated using OxCal 3.9 [Bronk Ramsey, 1995, 2001] and calibration curve INTCAL98 [Stuiver et al., 1998]; calibrated ages exclude ranges with probability <2%, and bold ages represent most likely range (at least 80%); (*) means $d^{13}\text{C}$ was assumed but not measured; [r] is for reworked samples.

transition, which we dated at 11 ka (onset of the Early Holocene climatic optimum).

Our results have critical implications for the assessment of seismic hazard in the area. On the Missyaf segment of the Ghab fault (figure 74), there is paleoseismological and archaeological evidence for three earthquakes since A.D. 70 [Meghraoui et al., 2003], the A.D. 1170 event, 835 yr ago, being the latest. In Lebanon, the classic inference of a ~550 yr recurrence time for large events on the Yammoûneh fault (A.D. 1202 to 1759) must be revisited. The penultimate ground-breaking event (S2) in the Kazzâb trench postdates A.D. 261–537 (Table 11), such that the quiescence interval prior to 1202 lasted 800±140 yr at most. This is to be compared with the time elapsed since then (803 yr), and with our preliminary finding of an approximate 1 kyr average recurrence time for previous events since 13 ka. The earthquake sequence of the eleventh to twelfth centuries [e.g. Poirier and Taher, 1980; Ben-Menahem, 1991; Abou Karaki, 1987; Guidoboni et al., 2004a,b; Ambraseys, 2004], which ended with the 1202 event, might thus represent a concatenation of successively triggered earthquakes, analogous to those observed on the North Anatolian and Kunlun faults in the past 100 years. Likewise, the Levant fault might exhibit millennial periods of quiescence separated by clusters of events rupturing its entire length in a couple of centuries. One might speculate that the 1995, M_w 7.3 Aqaba earthquake [Klinger et al., 1999], heralds the onset of such a clustered sequence.

Unfortunately therefore, one should be prepared for the occurrence of a large, destructive event similar to that of 1202 during the coming century in Lebanon. Given the rate of 5.1 ± 1.3 mm/yr recently derived from cosmogenic dating of offset fans along the Yammoûneh fault [Daëron et al., 2004a], such an earthquake could produce 3–5 m of coseismic slip, along with untold damage in areas vastly more populated today than in medieval times.

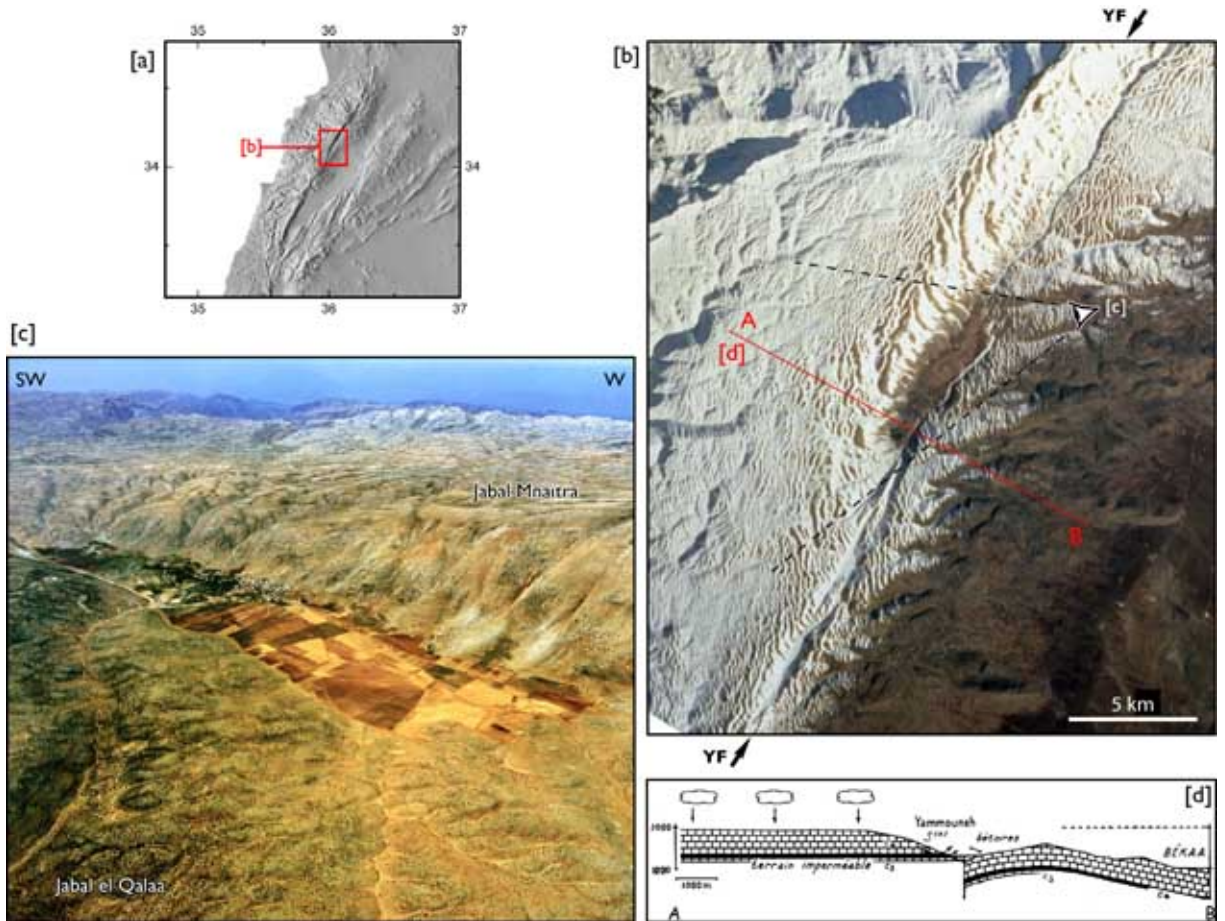


Figure 78: Overview of the Yammoûneh basin

- [a] Location of the basin within the Lebanese restraining bend;
- [b] Satellite image of the basin (in the center, surrounded by snow); black arrows labeled 'YF' point at the trace of the Yammoûneh fault;
- [c] Oblique view of the basin, looking WSW;
- [d] Simplified geological cross-section, modified from [Dubertret \[1975a, Baalbek sheet\]](#).

3.3 Paleoseismic trenching in the Yammoûneh basin

In order to investigate the seismic record of the Levant fault on time scales longer than the ~2500 years of written history in the Middle-East, we excavated and studied paleoseismologic trenches located on the central part of the Yammoûneh fault. Such a project requires a site where the fault cuts through datable Holocene sediments. The site we selected is the Yammoûneh basin, which gives its name to the fault.

3.3.1 Setting of the Yammoûneh basin

The Yammoûneh basin lies 1400 m a.s.l., on the eastern flank of Mount Lebanon (figure 78). While several other fault-controlled depressions (e.g. pull-aparts or junction basins) mark the length of the Yammoûneh fault, it is the largest (1.5×6 km) of these features.

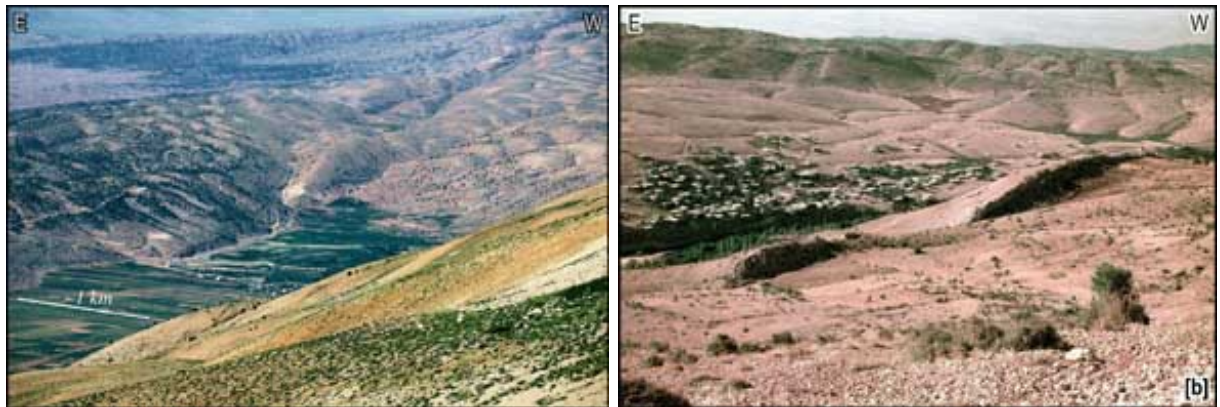


Figure 79: Evidence of the fault trace north and south of Yammoûneh basin

The basin is aligned SSW-NNE, roughly (but not exactly) parallel to the fault's trace. It is inset between thick subtabular sequences of karstified Cenomanian limestone (figure 78.d). To the west, the basin is overlooked by the Jabal Mnaïtra karstic plateau (~2100 m a.s.l.). To the east, it is separated from the Beqaa by gently sloping hills (Jabal el Qalaa), only ~100 m higher than the basin's flat floor.

The Yammoûneh fault's trace can be precisely mapped to the north and south of the basin. To the south, it follows the west-facing flank of a N-S-trending limestone ridge, and reaches the basin near its southernmost tip, connecting with its eastern rim (figure 79). To the north, Dubertret [1975a, Baalbek sheet] mapped the geological fault as following the Aïnata river. From our own observations, however, the active trace, where cumulative slip has been accumulating in geologically recent times, runs above and to the west of Aïnata (figure 79), cutting through the limestone flank of the Jabal Mnaïtra. It is thus readily apparent that the basin is associated with a left stepover in the Yammoûneh fault (figures 78 and 80). This observation, added to the basin's rhomboid shape, implies that it is a pull-apart. This had already been proposed by Garfunkel et al. [1981].

However, the study of high-resolution satellite images and 50-year-old air photographs suggests the existence of a direct connexion between the northern and southern faults, cross-cutting through the basin. Within the basin, this is supported by shallow soil color and vegetation changes, as well as by inflections or offsets of gullies. Moreover, the northern fault segment, rather than merging smoothly with the basin's western limits somewhere on the flank of the Jabal Mnaïtra, veers toward the south as it reaches it. Just before reaching the basin's floor, it offsets two alluvial fans by a few tens of meters¹. The inferred fault trace cuts through the sedimentary in-fill of the basin's southern half (figures 80 and 81). This is also supported by resistivity measurements [Besançon, 1968], which were interpreted to indicate that the Yammoûneh fault does cut across the basin, offsetting vertically the underlying bedrock (figure 82).

Thus, the available data suggests that, although fault strands originally bounded the

¹ These offsets are discussed at some length in section 2.2, and in the corresponding article [Daëron et al., 2004a].

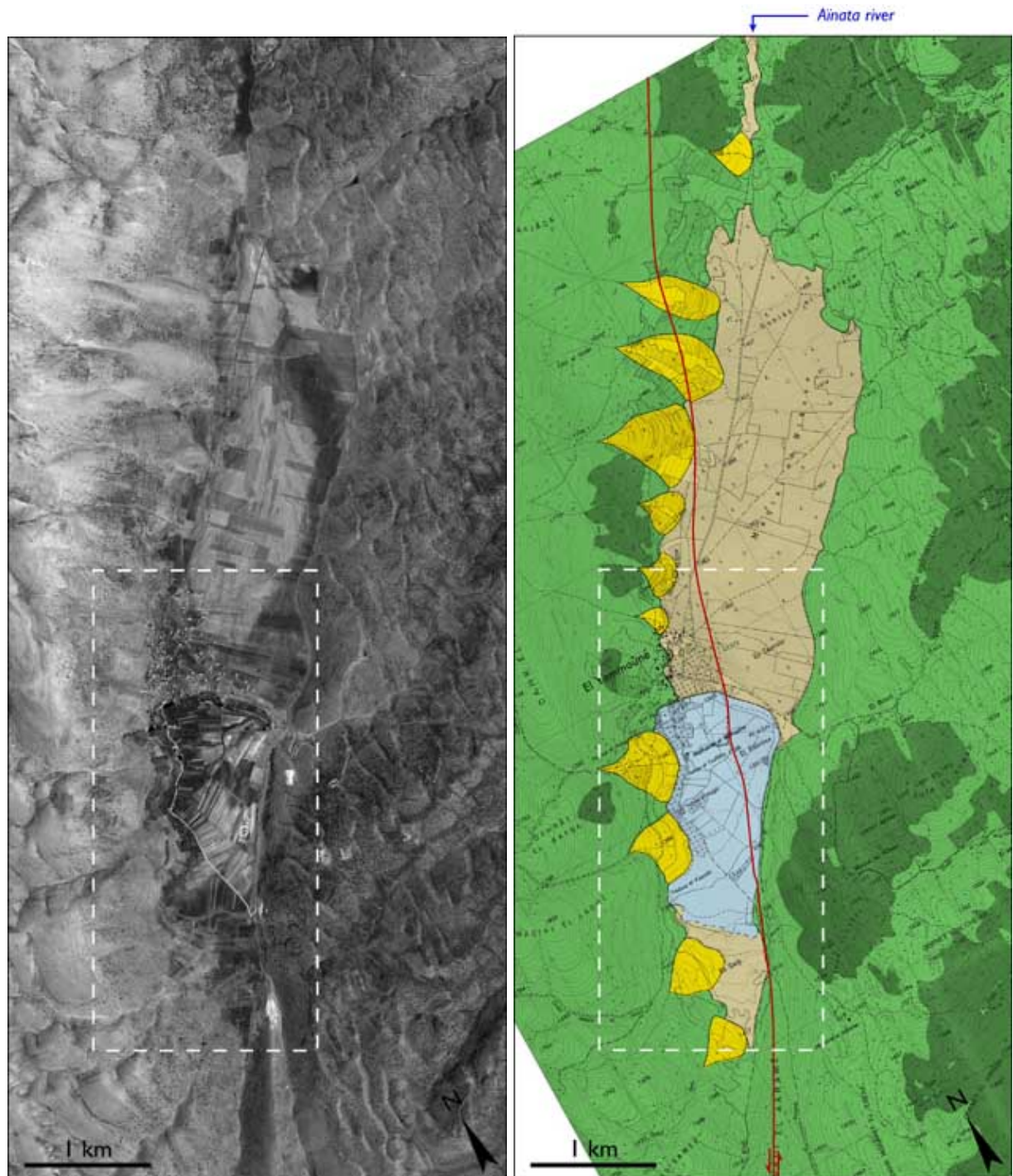


Figure 80: Surface geology and active faulting in the Yammoûneh basin
[left] Quickbird satellite image of the Yammoûneh basin. the dashed boxed area shows the outline of fig. 81.
[right] Map of the surface geology and active faults in the basin.



Figure 81: Aerial photograph of the Yammoûneh paleo-lake area (1962)
Note the trace of the active fault crossing the lake floor.

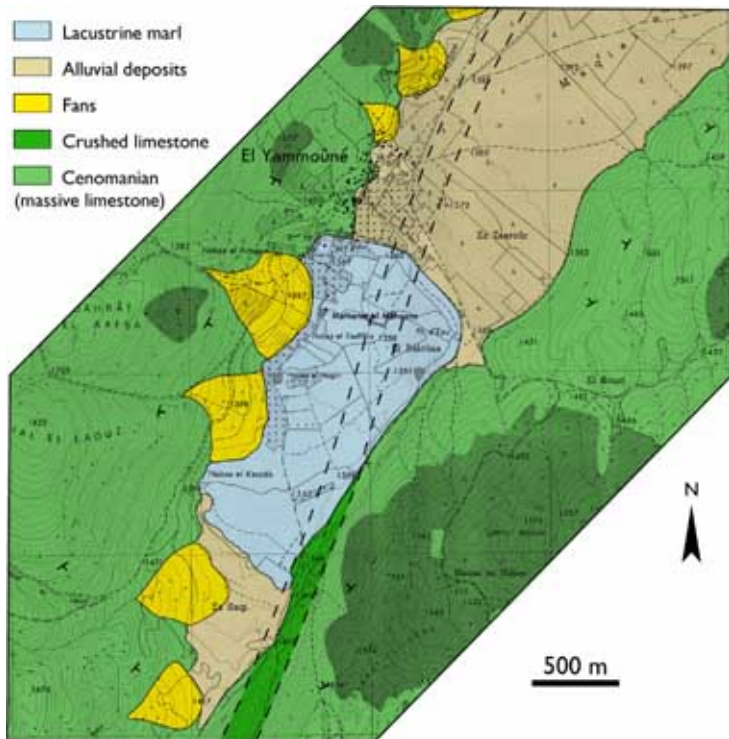
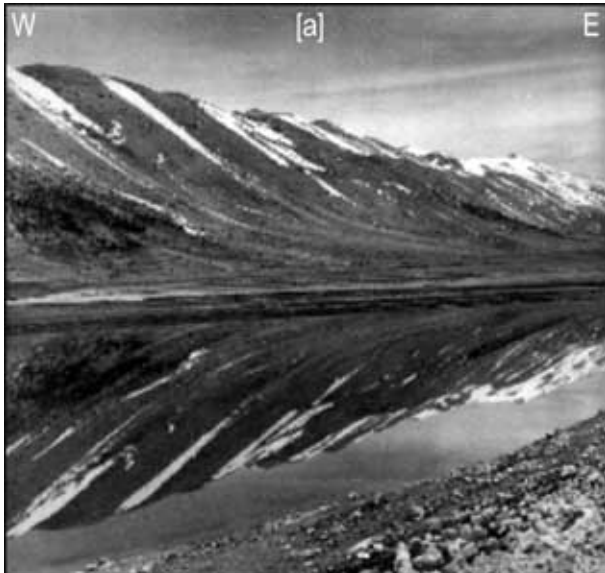


Figure 82: Results from resistivity measurements in the Yammouné basin(modified from Besançon [1968]). Besançon interpreted resistivity data as evidence of the subsurface trace of the Yammouné fault (dashed band). South of the paleo-lake, he maps the fault as coinciding with a zone of ‘crushed rock’ in the Cenomanian limestone (where, as shown in fig. 80.a, a limestone quarry has been excavated recently). The northward continuation of this ~150-m-wide band corresponds to an area of lower resistivity. Our mapping of the active fault, (based on geomorphic offsets and/or inflections, and vegetation and soil color variations) strictly fits within this band.

Yammoûneh basin, which formed as a pull-apart, the corresponding left step evolved toward a smoother, simpler geometry, with one new strand connecting the adjoining initial strands, short-cutting through the pull-apart, as observed in many pull-aparts on other strike-slip faults. On either side of the basin, where the sedimentary in-fill abuts the surrounding limestone units, there is no evidence of current strike-slip motion, which suggests that all or most of the strike-slip on the Yammoûneh fault occurs within the sediment in-fill.

The Yammoûneh basin’s floor comprises two types of Quaternary sediments. In its larger, northern part, red-brown clays and limestone fanglomerates underlie clastic limestone from the Cenomanian units that border the basin. It is likely that this material is mostly alluvium deposited by the Aïnata river (figure 80). In the southern third of the basin, a wide (700×1800 m) patch of light-colored sediment (figure 83) is inset by a few meters in the rougher alluvium. This patch is made of calcareous, powdery marls of lacustrine origin, as indicated by abundant water shells.

These white marls were deposited in the southern, lowest part of the Yammoûneh basin due to its peculiar hydrographic setting. The Jabal Mnaïtra plateau remains completely snow-covered almost 4 months a year [Atlas climatique du Liban (Service météorologique du Liban), 1971; Besançon, 1968]. Subterranean karstic networks beneath it collect meltwater, feeding a dozen springs on the western edge of the basin since at least Roman times [Besançon, 1968]. In times of slow discharge, the water followed sinuous channels in the southern portion of the basin, until it reached a series of karstic sinkholes near the opposing, eastern border. In times of stronger discharge (March to June) associated with snow melting atop the Jabal Mnaïtra, the water filled

**Figure 83: The Yammoûneh paleo-lake.**

[a] Undated field photograph of the lake.
 [b] Field photograph of the southern end of the Yammoûneh basin. Between the green orchards to the west and the white road to the east, light-colored sediments are lacustrine, calcareous marls.



a lake (figure 83), which persisted for a few months¹. This seasonal lake was artificially and permanently dried up in the early 1930's due to the construction of an underground water duct, draining the water from the sinkholes to irrigate the Beqaa plain, 500 m below. Today, the paleo-lake area has become a fertile, cultivated plain.

The peculiar tectonic and hydrographic features of the Yammoûneh basin offer some of the best *a priori* conditions for paleoseismic trenching, since the active fault trace cuts through

¹ This could explain the speculated etymology of the name ‘Yammoûneh’, which might be derived from ancient Syriac, meaning ‘little sea’.

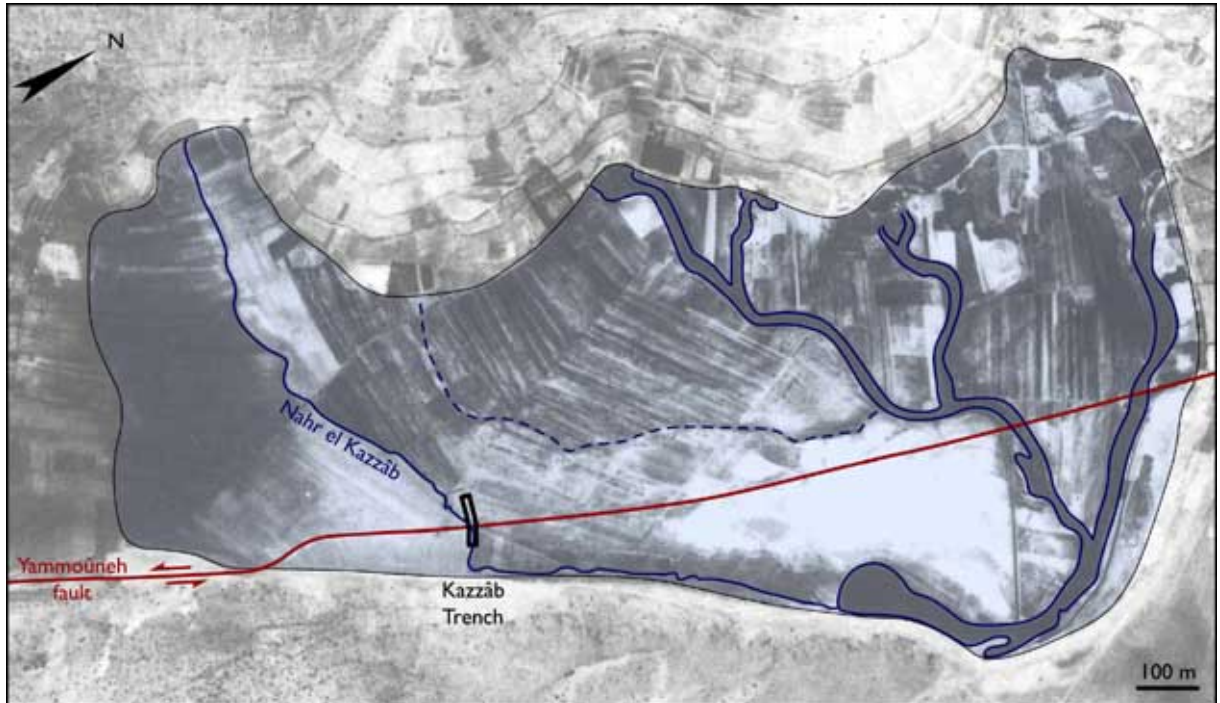


Figure 84: Location of the Kazzâb trench. The area of the former lake is in blue.

finely stratified lake beds, with hopefully a detailed stratigraphic record. Exploratory trenching of a 5-m-deep pit near the main sinkhole (el Baloua) on the eastern side of the basin revealed a rich stratigraphy of marls and clays, with peat layers exhibiting millimetric laminae (figure 86.e). Unfortunately, radiocarbon dating of these layers proved impossible, because ^{14}C content of the samples we collected proved to be below AMS sensitivity, suggesting that the peat layers are older than ~ 50 ka. Obviously, trenching in the lacustrine sediments is conceivable only because the lake has been dried up, although in — geologically — very recent times. For all these reasons, we selected this site as the focus of our efforts to decipher the millennial seismic record of the Yammoûneh fault.

3.3.2 The Kazzâb trench

Trench location

The exploratory trench we opened in the Yammoûneh basin is located in the south of the paleo-lake, on the bank of a semi-permanent stream, the Nahr el Kazzâb (figures 84 and 85). Our primary goal at the time was to verify that the trace of the active Yammoûneh fault does indeed cut through the basin, and to determine exactly where, so we started excavating well west of the expected intersection between the fault and the Kazzâb stream.

The resulting trench (thereafter referred to as ‘Kazzâb trench’) was 4 m wide, ~ 75 m long and 3–5 m deep. It exposed subhorizontal lake beds, undisturbed except in a narrow, 2-m-wide



Figure 85: Working in the Kazzâb trench

fault zone. Due to time constraints, only the central 8 m of the south wall of the Kazzâb trench were cleaned up and mapped in detail.

Exposed stratigraphy

In keeping with surface mapping of the in-fill geology of the basin, the sediments exposed in the trench were found to be divided into two distinct units: compact, calcareous marls at shallow depths, and underlying red-brown clays. The marl/clay transition is sharp and very distinctive (figure 86.c). It appears sub-horizontal across the ESE-WNW-trending trench walls, and lies 2.5–3.5 m beneath the surface.

The marls are white-gray to light beige, and become very powdery when they dry. This unit exhibits sub-horizontal layers: either distinct laminations, a few millimeters thick (figure 86.a), or more massive layers of up to 40 cm thick. Some such thick layers appear to have been disturbed in ‘cloudy’ fashion by liquefaction (figure 86.b). Small (~ 1 –4 mm) lacustrine shells can be found in many layers of the marl unit. Similar shells are observed in the active stream channels that cross the basin today, suggesting the existence, at the time of the upper marl layers’ deposition, of an ecosystem somewhat similar to the modern one.

The underlying clay series are red to brown, smoothly stratified, and display at places

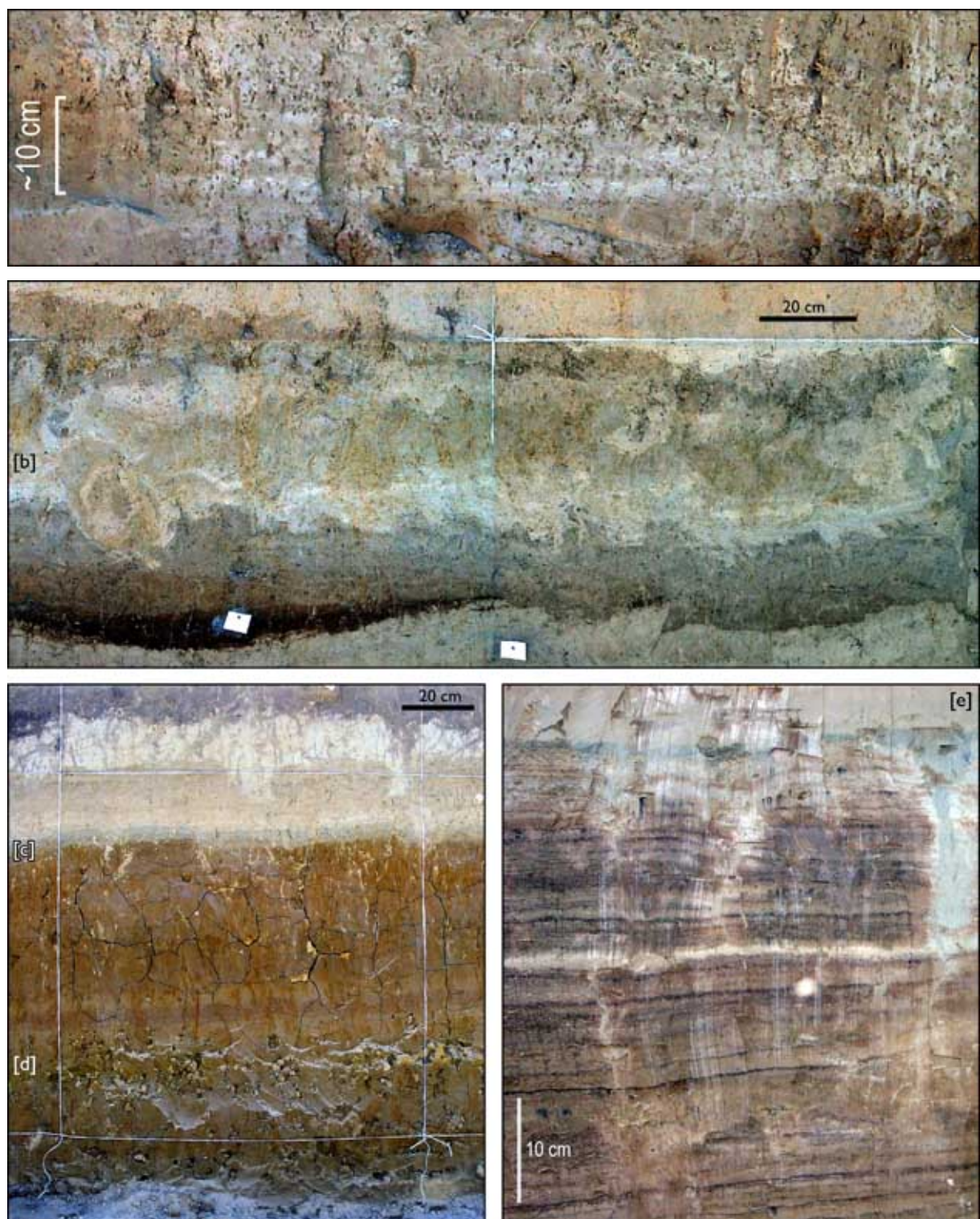


Figure 86: Views of the sediments exposed in Kazzâb trench

- [a] Fine marl layers.
- [b] 'Cloudy' deformation of thick marl layers.
- [c] The marl/clay interface.
- [d] Calcareous nodules.
- [e] peat layers in the Baloua trench

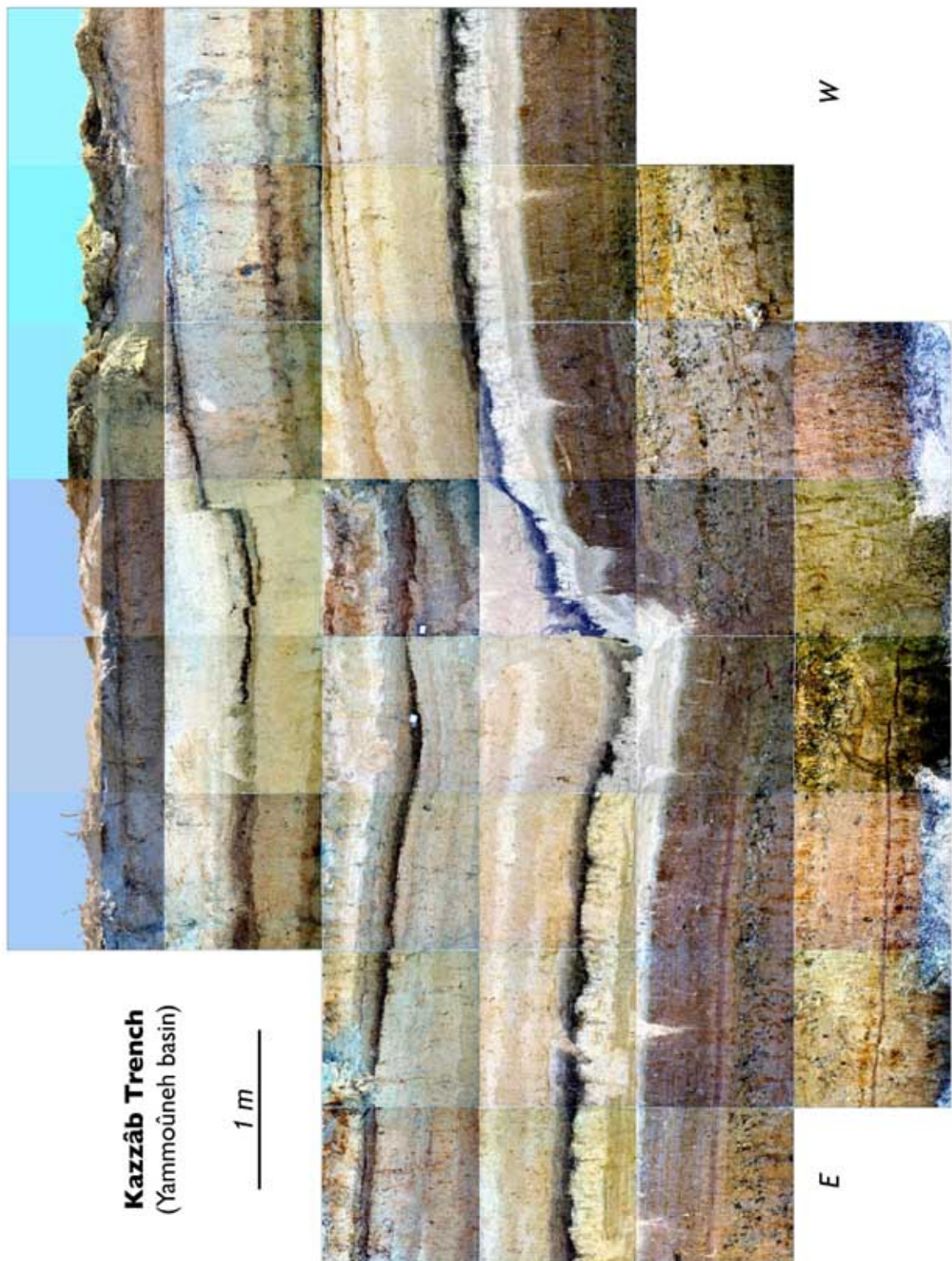


Figure 87: Photo-mosaic of the Kazzâb trench

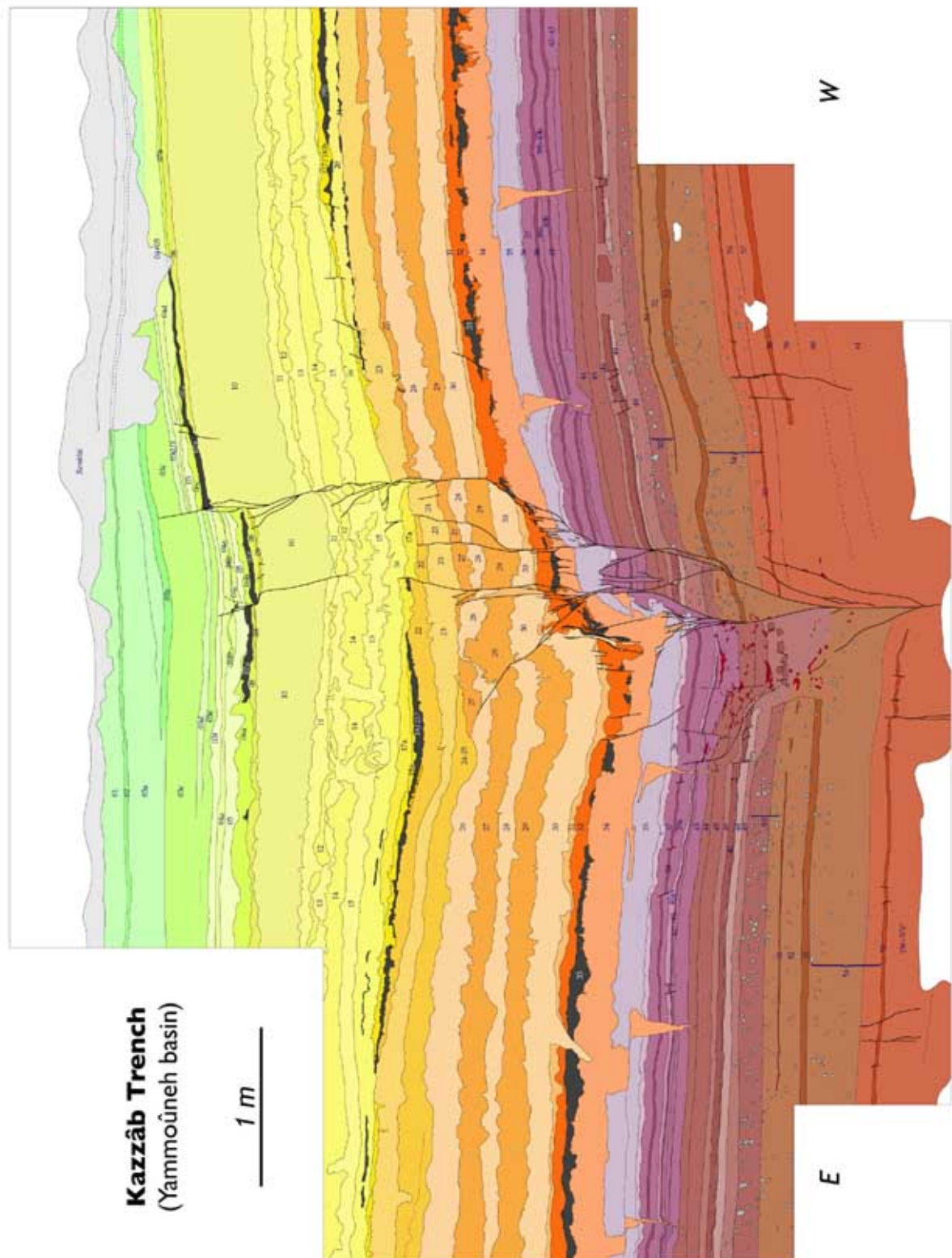


Figure 88: Log of the Kazzâb trench

fine laminations (~ 1 mm). The clay layers' thicknesses typically range from ~ 2 mm to more than 20 cm. Some of these layers contain calcareous nodules (figure 86.d). Unlike in trenches that expose alluvial/colluvial material, the granulometry and texture of the Kazzâb sediments are very homogeneous, apart from first-order variations between marls and clays. Layers are thus identified and separated based essentially on their color, thickness and on the stratigraphic sequence itself (e.g. dark-on-light or thick-above-thin pairs).

Away from the fault zone (see next section), all layers are remarkably horizontal. Although gentle dipping of the layers perpendicularly to the trench walls is possible, it is not detectable over the 4 m width of the trench. Furthermore, the trenching site is located less than 100 m west of the paleo-lake's eastern shore, so any 'natural' dipping would be expected to trend parallel to the trench, and thus to be visible on the exposed walls. This indicates that the undisturbed layers were deposited sub-horizontally, as befits deposition in a lake.

Coseismic deformations

The lake beds exposed in the Kazzâb trench are warped, disrupted and offset in a ~ 2 m-wide zone, which marks the active Yammoûneh fault in cross-section, confirming our prior mapping of the likely position of the fault trace at the surface, and consistent with the interpretation [Besançon, 1968] of resistivity measurements (figure 82). This is the only deformation zone we found along the 75 m length of the Kazzâb trench. Exploratory trenches across much of the rest of the basin showed no additional faulting. Although we cannot rule out minor active faulting elsewhere, particularly along the eastern edge of the basin, we think it likely that the Kazzâb trench fault takes up most of the strike-slip displacement.

Evidence for seismic events

Below is a detailed outline of available evidence for earthquake-induced deformation of the lake beds in the Kazzâb trench. Recall that, since throughout the following description we look at the record of motion on a strike-slip fault in a vertical cross-section, we cannot decide whether the 'vertical' offsets observed are caused by a small component of dip-slip or by slight along-strike dips of horizontally offset beds. Overall, the lake beds, which are remarkably horizontal away from the fault zone, progressively bend down in the neighboring ~ 5 m on both sides. The upper marl sequence is ~ 90 cm thicker east of the fault than west of it, implying a cumulative 'vertical' downthrow of this amount. Certain layers, often darker (e.g. 7a and 19/21), appear locally in the sag produced by flexure of the beds near the fault. The main fault zone is composed of branches that for the most part merge downwards at different depths. Certain layers (e.g. 4–10, 15–23, 34–45) away from the fault are cut and offset by smaller faults and cracks that cannot be traced down to the main fault zone.

[S1] Layer 3c (L_{3c}) is cut by a subvertical break (F_1) that uplifted vertically layer $L_{3d/f}$ by either 10 or 15 cm, depending on whether $L_{3d/f}$ is the western continuation of L_{3d} or



Figure 89: Example of the deformation of lake beds in the Kazzâb trench

The lower, dark brown unit is clay; the black layer is L₃₃, a distinctive, carbon-rich layer of probable climatic origin (see text).

L_{3f}. As a result, the thickness of L_{3c} changes drastically, from 25 cm east of the fault to 15 cm west of it. The apparent 10 cm vertical offset is consistent with the similar change in thickness of L_{3c}, suggesting that L_{3d/f} is the western continuation of L_{3d} rather than of L_{3f}. This implies that the top of the thicker, eastern L_{3c} was at the surface at the time of the corresponding event S₁, and that subsequent degradation of the resulting scarplet eroded away the top of L_{3c} west of the fault. Following this scenario, S₁ predates L_{3b} but postdates L_{3c}, and the possibility that L_{3b} might contain material re-worked from L_{3c} should be kept in mind.

[S₂] Two other faults, F₂ and F₃, about 50 cm to the east and west of F₁, cut and offset the dark layer L_{7a} by ~5 cm. These faults can be traced upwards to within the lighter layer L_{3f} (east) and to the base of L_{3d/f} (west). The corresponding event S₂ must postdate L_{4a} but predate L_{3f} and L_{3d/f}.

[S₃] In the middle of the downthrown block between F₁ and F₂, the base of L_{7a} is smooth and undisturbed, but just beneath it L₉ is disrupted by several oblique breaks with apparent thrust component. The two westernmost of these breaks merge with the downward continuation of the main, subvertical fault F₁. The corresponding event S₃ must postdate L₉ but predate L_{7a}.

[S₄] About 50 cm below the ruptures associated with S₃, a similar pair of fault splays affects



Figure 90: Photo-mosaic of the Kazzâb fault zone

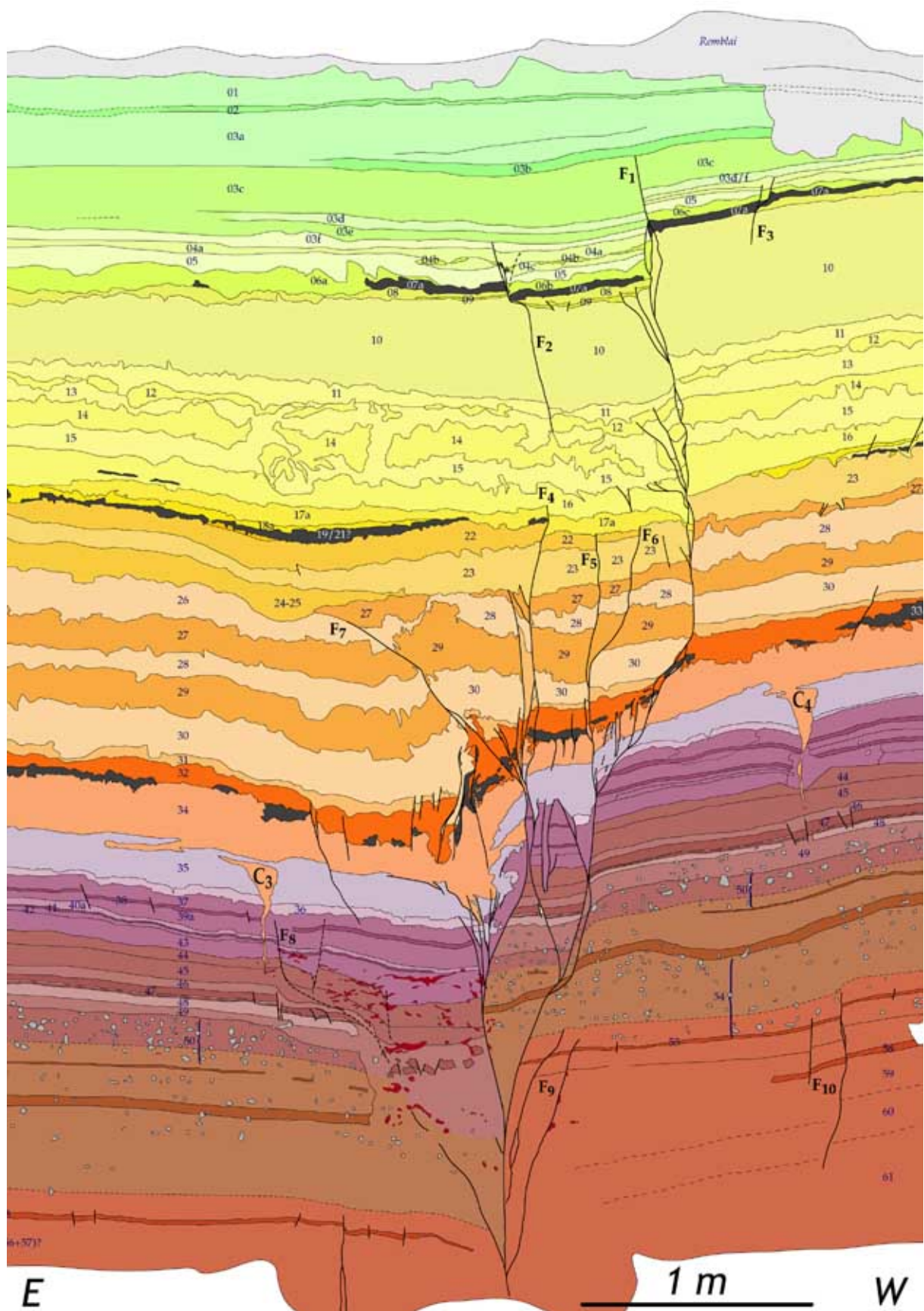


Figure 91: Log of the Kazzâb fault zone

layers L₁₂ to L₁₆. The corresponding event is labeled S₄. Even though these fault splays do not appear to reach the top of L₁₁, this latter layer is locally tilted parallel to the faulted L₁₂. Moreover, east of the fault zone, L₁₀ thins continuously eastwards. Since the lake beds exposed in this trench are generally horizontal, with no systematic thinning or thickening away from the fault zone, this suggests that the top of L₁₁, which ought to have been horizontal before S₄, was tilted downwards by this event over a width of a few meters, and warped upwards near F₁ over a few tens of centimeters. Subsequent deposition of L₁₀ over the west-dipping top of L₁₁ restored a horizontal surface, resulting in the observed gradual thickening of L₁₀ toward the fault. We thus interpret S₄ to postdate L₁₁ but to predate L₁₀.

[Liquefaction in L_{12–15}]

Layers L₁₂ to L₁₅ appear to have been disturbed in by liquefaction, forming irregular convoluted features, particularly in a ~2-m-wide zone east of F₁. It is likely that such liquefaction was the result of thixotropy due to coseismic shaking within the water-saturated, superficial lake-beds. The paleo-surface at the time of this shaking is also constrained by the presence of a sand-blow/mud fountain in layer L₁₀, about 40 m west of F₁. We attribute such liquefaction to event S₄. Although S₂ postdates the liquefaction, the contorted shapes of the sediments in L₁₂ to L₁₅ make it difficult to trace the downward continuation of F₂ (cf 3.3.2).

[S₄] From minor splays that appear to cut L₁₆ just east of F₁, terminating upwards by fissures filled with L₁₅ deposits, and small, coeval faults that offset L_{21–16} west of F₁, to the base of L₁₅, we infer the possible existence of another event S'₄. This event, which we consider more speculative than the previous ones, would therefore postdate L₁₆ and predate the end of deposition of L₁₅.

[S₅] L_{17a} is offset vertically (5 cm) by a subvertical fault F₄, which appears to be distinct from the ruptures above it. There is no evidence that this fault connects upwards with F₂, and it does not appear to reach the top of L₁₆. We interpret this break as evidence of the S₅ event, which clearly postdates L_{17a}. Note that while the available evidence suggests that it predates L₁₅, it is impossible to rule out that liquefaction might have erased an upward continuation of F₄.

[S₆] In the central part of the fault zone, the base of L₂₂ is offset vertically by a subvertical rupture F₅. About 20 cm to the west, L₂₂ disappears altogether, as L₂₃ is brought up into contact with L_{17a} by another fault, F₆. It is unclear whether or not F₆ offsets the base of L_{17a}, but there is no doubt that L_{17a} seals the top of F₅. Thus it is necessary that a previous event S₆ occurred before deposition of L_{17a}, but after that of L₂₂. Deformation associated with this event could be responsible for the sag located ~1m east of F₄, in which layers L_{18a} and L_{19/21} were deposited.

[Erosion of L_{17–23}]

At the scale of a few meters on either side of F₁, the base of L₁₆ is unconformable on

top of layers L_{17–23}. This suggests erosion of the latter layers, possibly during a period when the lake dried up. The potential existence of a gap in the corresponding stratigraphic — and thus, paleoseismic — record should be taken into account.

[S₇] L₂₃, and locally L_{24–25}, appear to have eroded layers L_{26–28} near the fault zone and west of it. This appears to be mostly due to strong warping and folding of L_{26–29}, caused by thrust motion on a 45° west-dipping fault, F₇. L₂₆ has been completely eroded above the thrust, and only part of L₂₇ remains. It is probable that two of the subvertical faults just east of F₄, that end abruptly where they reach the base of L₂₃, are associated with this same event, S₇. This event postdates L₂₆ and predates L₂₄, whose eastward thickening east of F₄, and absence west of F₁, suggest it was derived from eroded layers L_{26–27}. The shortening feature associated with F₇ is typical of the en-echelon pressure ridges of mole tracks, commonly observed along strike-slip surface breaks [e.g. Yeats et al., 1996; Armijo et al., 1989]. The graben-like sag between F₁ and F₂, apparently created by S₂ (cf 3.3.2), on the other hand, is typical of extensional features usually found within the steps separating pressure ridges.

[S₈] Numerous breaks affect layers L_{31–34}, and die out within or at the top of L₃₁. Faulting associated with this event S₈ is more broadly distributed, mostly in the couple of meters east of F₁, than that due to later earthquakes. This may be due to different surface conditions at the time: L_{32–33} is a gray and black layer pair, rich in organic matter, overlying the white marl of L₃₄. This marl layer exhibits clear evidence of bioturbation, probably by roots or by burrowing molluscs, that extend downwards from the base of L₃₃. This suggests the existence of a vegetation mat, perhaps corresponding to a dryer climatic episode during which the lake was replaced by a seasonal swamp. Immediately underneath the white, bioturbated marl layer L₃₄, the ~20-cm-thick sequence of gray-green, thinly laminated layers L₃₅ marks the bottom of the calcareous marly deposits, topping the clay series that characterize the lower part of the Kazzâb stratigraphy. The mechanical coupling between the L_{34–35} marl layers and the clay beds is expected to differ from that between the marl layers above, which conditioned the rheology of surface deposits at the time of later events S₁ to S₇. This might explain the more distributed rupture pattern of event S₈.

[S₉] Five cracks (C₁ to C₅), 40–50 cm deep and ~15 cm at their widest, are observed in the central 8 m of the trench. Their spacing (~1.5 m) is fairly regular. They start to open in the marl layer L₃₄ and taper rapidly down to disappear within the clay beds L_{44–45} (figure 92). They are filled with white marl from L₃₄, with evidence for east-directed plastic flow and associated asymmetric folding of the lower part of L₃₄ between C₂ and C₄. A few similar cracks exist farther away, but they are smaller and with wider spacing. Most of the cracks, such as C₂, exhibit a peculiar pattern of opening, with a ‘lightening bolt’ shape (figure 92) related to a bedding-parallel décollement within L₃₅. The décollement, although located at slightly different depths, always shifts the bottom part of the cracks westwards relative to the upper part, whether on the east or west side of the fault zone. The spatial distribution

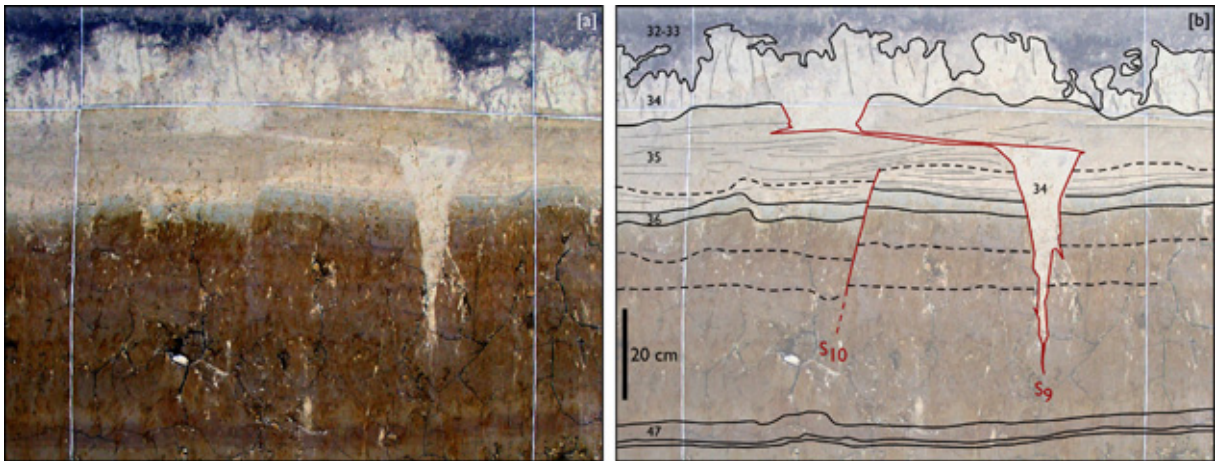


Figure 92: View of one of the cracks that affect the upper clay sequence and the base of the marls
These cracks progressively disappear away from the fault.

and ‘lightening bolt’ shape of the cracks, as well as the evidence for plastic flow, make it implausible that the cracks result from dessication. It is much more likely that they were due to coseismic deformation (more severe near the fault), and were filled by L₃₄ at the time of the corresponding event. Bending of the bioturbation marks by the plastic flow at the base of L₃₄ suggests that the vegetation mat of L₃₃ was also already in place, at least in part, at the time of the cracks’ opening. We thus attribute the formation of the cracks to an event, S₉, postdating L₃₅ and coeval with the development of L₃₃. Mechanically, the cracks could be due to inward warping, due to flexure of the clay/marl interface, a consequence of greater plasticity of the clays distributing deformation over a broader width away from the fault. The ‘lightening bolt’ pattern is more difficult to explain, since the sense of shear on the décollement is the same on both sides of the fault zone. One might speculate that the décollement attests to very shallow, pancake-thin block rotation, since the corresponding vorticity would be the same (counter-clockwise) on both sides of a left-lateral strike-slip rupture. This alone, however, cannot account for the eastward offsets of the upper parts of all the cracks.

[S₁₀] The uppermost clay layers, between F₄ and F₅, are offset by several fault splays that merge downwards with them. L₃₅ is ~8 cm thicker in a small graben adjacent to F₅. East of C₃, several small faults offset layers L_{36-39a} and appear to stop just above the top of the distinctive, thin blue clay layer L₃₆. We attribute this faulting to event S₁₀, which postdates L₃₆, and was coeval with deposition of L₃₅.

[S₁₁] Layer L₄₁ is downthrown by a west-dipping fault F₈ just west of C₃, east of the main fault zone. It is ambiguous whether L₃₈ is similarly faulted, but L₃₆ is clearly unaffected. Small offsets of layers L₃₈₋₄₁, west of C₂, may have been contemporaneous. Although the evidence is less definite than for most of the shallower events, we infer such faulting to reflect another event, S₁₁, clearly postdating L₄₁ and strictly predating L₃₆.

[S₁₂] Layer L₄₇ is strongly disrupted and downthrown between F₁ and F₈. Only remnant

fragments of this layer are recognizable between the downward continuations of F₇ and F₉, which bound a 90-cm-wide, ~25-cm-deep half-graben. Recognition of L₄₇ in this half-graben is only possible because of its distinctive appearance (~5-mm-thick layer overlain by a ~35-mm-thick one, both of a dark chocolate-brown color). The layers above are difficult to recognize, although clear thickening is evident within the half-graben, below L₄₁ which appears to be unaffected, smoothly overlying the corresponding trough. Clay lenses with a distinctive, brick-red color, not found elsewhere, are interstratified in the half-graben fill, mostly between L₄₁ and L₄₇. This is suggestive of local collapse, accounting for the poor state of preservation of layers L_{42–47} within the half-graben. The corresponding event, S₁₂, unambiguously predates L₄₁ and postdates L₄₇. That the western half of the graben is missing is likely due to left-lateral offset (i.e. toward the south) by posterior events, particularly on F₄ and F₇. It is arguable that more than one event caused the 25-cm-deep sag of the half-graben. Unfortunately, the degraded stratigraphic sequence within this graben precludes a more precise assessment.

[S₁₃] L₅₀ is the thick unit, filled with numerous calcareous concretions, that lies between the distinctive layers L₄₉ and L₅₁. East of the fault zone, its thickness is 21–25 cm; to the west, this number is reduced to 12–15 cm. In keeping with the assumption that the lake beds were deposited horizontally, this implies the existence of an event, S₁₃, postdating L₅₁ but predating L₄₉, that offset the lake floor vertically by ~10 cm (west up). Additional evidence of S₁₃ in terms of faulting is lacking. If the surface expression of this earthquake was localized rather than laterally distributed, it is likely that such evidence lies within the disrupted, undecipherable fault zone between F₄ and F₈, or has been displaced (north or south) by posterior events.

[S₁₄] L₅₅, a thin, continuous dark layer, is offset by numerous small faults on both sides of the main fault zone. Some, such as F₉ or F₁₀, extend down to L_{58–60} at least. Besides, as in the situation described above, the thickness of L₅₄ changes abruptly across the main fault zone from 30–36 cm (west) to 42–46 cm (east). This is evidence for event S₁₄, which also uplifted the western lake floor by ~10 cm. S₁₄ must postdate L₅₅ and predate L₅₃.

It is clear from the above description that while the evidence for many events is unambiguous, it remains more tentative for others. Furthermore, it is possible that we have overlooked some events, or that their stratigraphic record is missing altogether. Nevertheless, the analysis of the Kazzâb trench reveals, overall, a succession of ~15 seismic events over a stratigraphic depth of ~5 m.

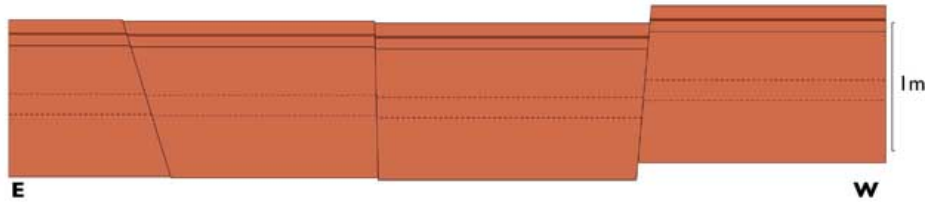
Tentative restoration of the disrupted layers

In order to summarize the events recorded in the Kazzâb trench, here is a series of sketches outlining the succession of sedimentation and coseismic deformation that we propose.

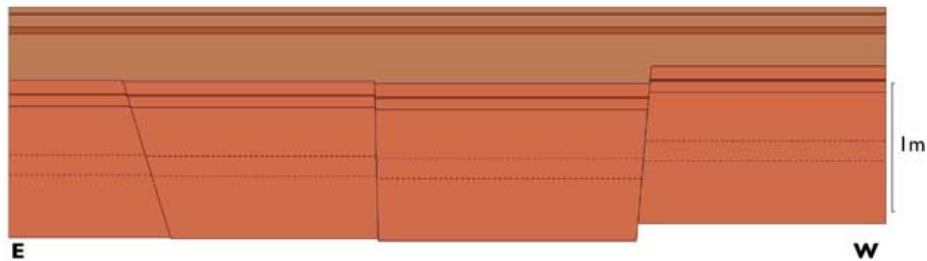
Shortly before S₁₄: deposition of the layers L₆₁ to L₅₅, as well as the base of layer L₅₄.



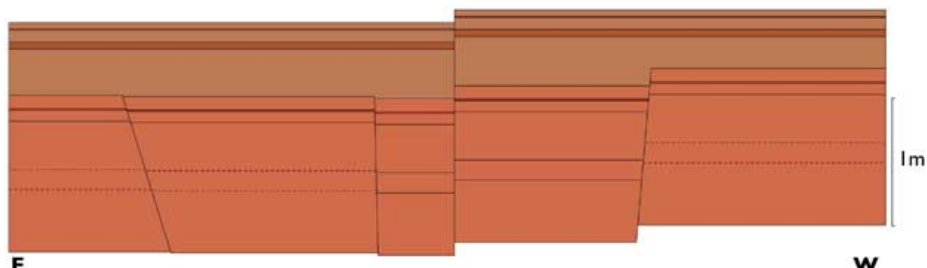
Immediately after S₁₄: several faults offset the pre-existing sequence.



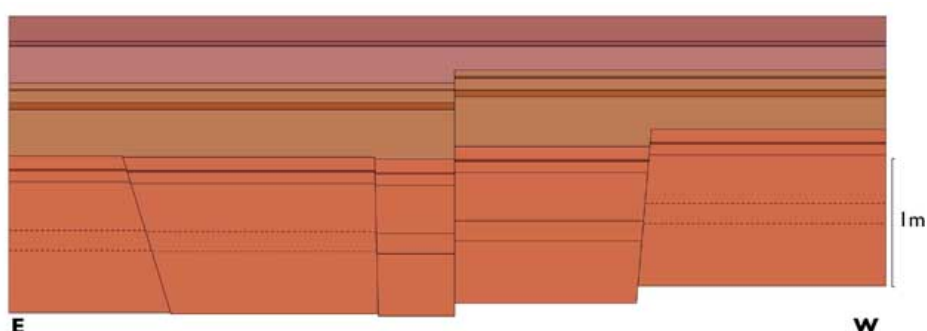
Shortly before S₁₃: deposition of the top of L₅₄, of layers L₅₃ to L₅₁ and of the base of L₅₀.



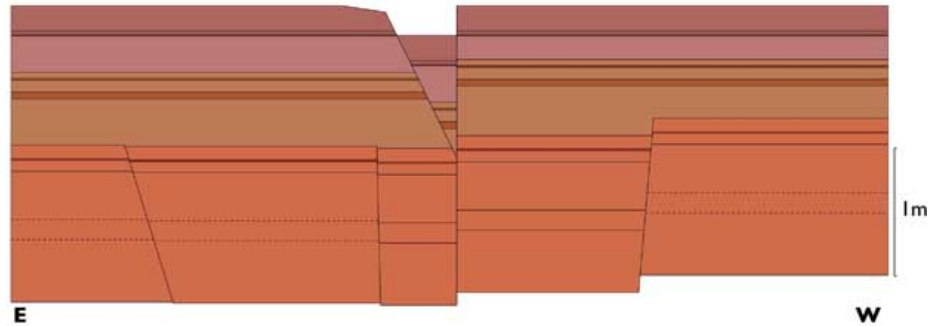
Immediately after S₁₃: this event is evidenced by vertical separation only (discussed p. 144). The sketch below depicts only a simplified, vertical break to account for this vertical separation.



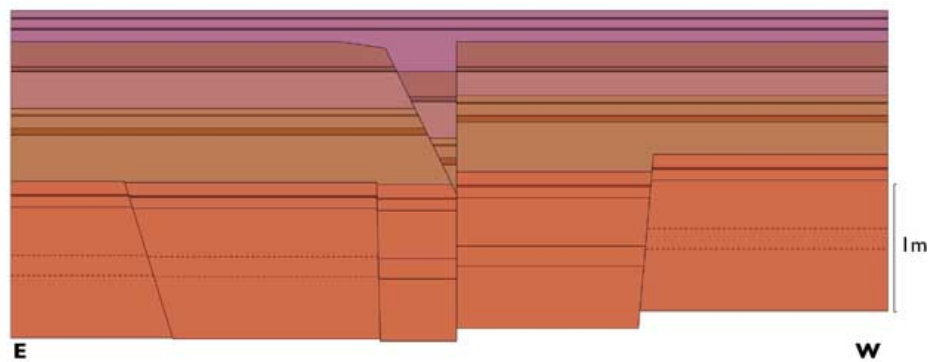
Shortly before S₁₂: deposition of the top of L₅₀ and of layers L₄₉ to L₄₇ (at least) or L₄₃ (at most).



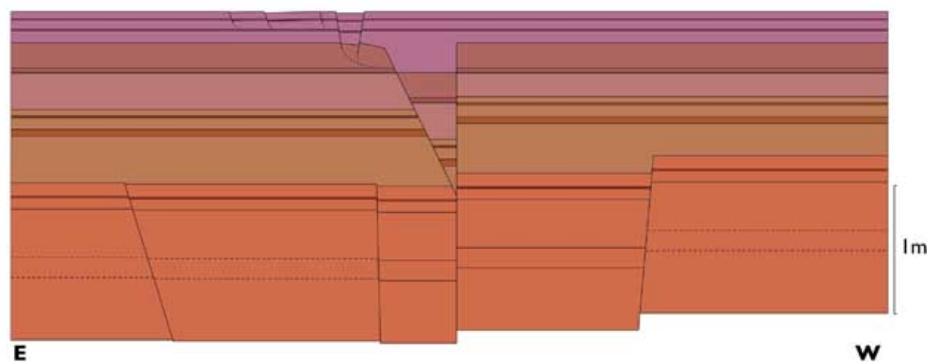
Immediately after S₁₂: downthrowing and fragmentation of the distinctive layer L₄₇. The corresponding graben-like depression probably did not end abruptly to the west at this time, but subsequent faulting by later events must have displaced the western part of the graben toward the south.



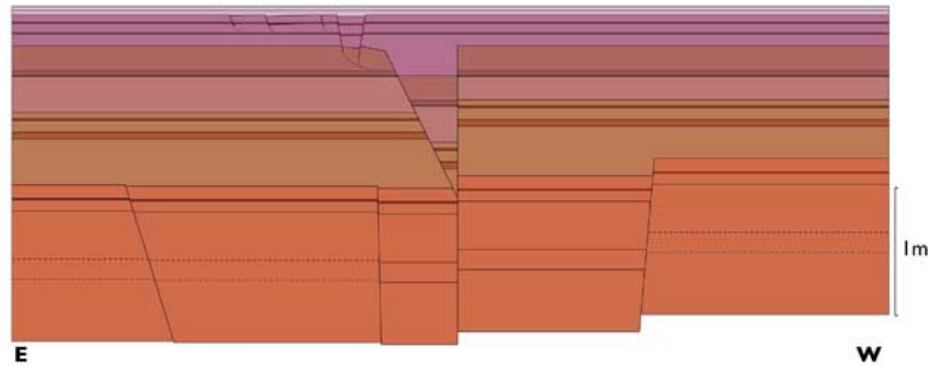
Shortly before S₁₁: deposition of the subsequent layers, up to L₃₇.



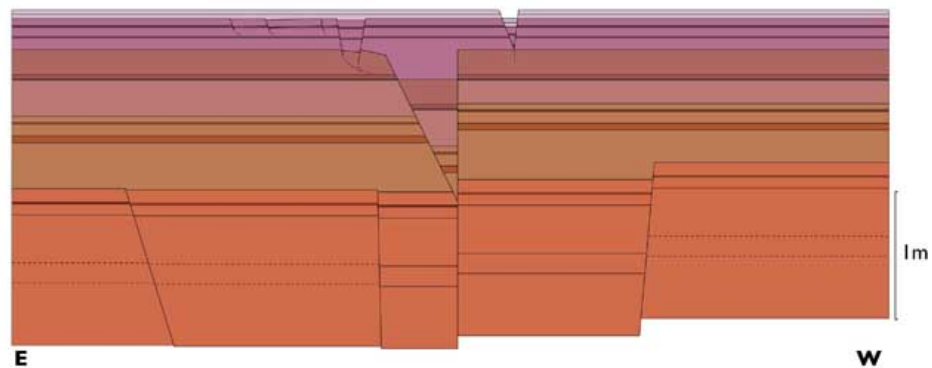
Immediately after S₁₁:



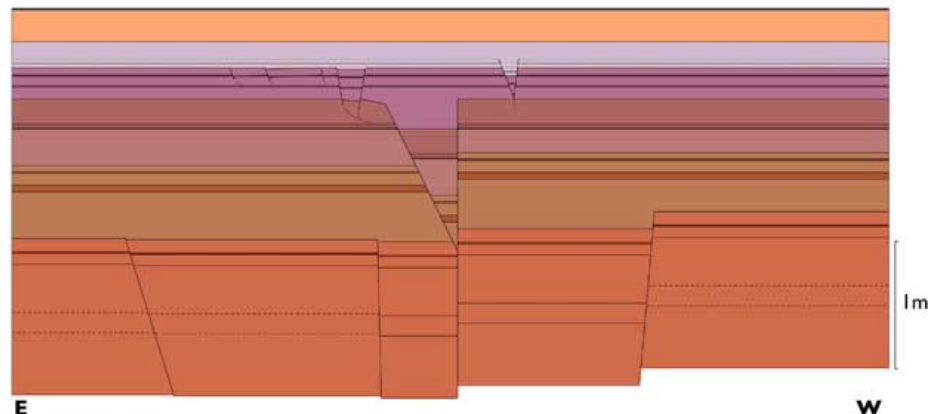
Shortly before S₁₀: deposition of layers L₃₆ and possibly of the base of L₃₅.



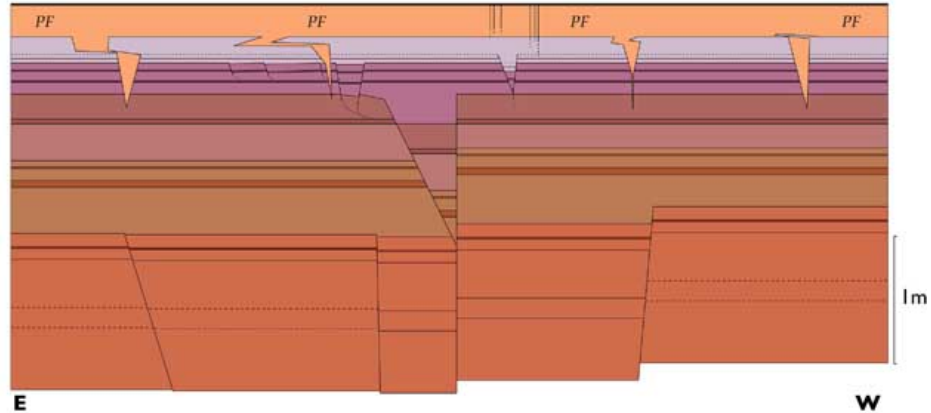
Immediately after S₁₀:



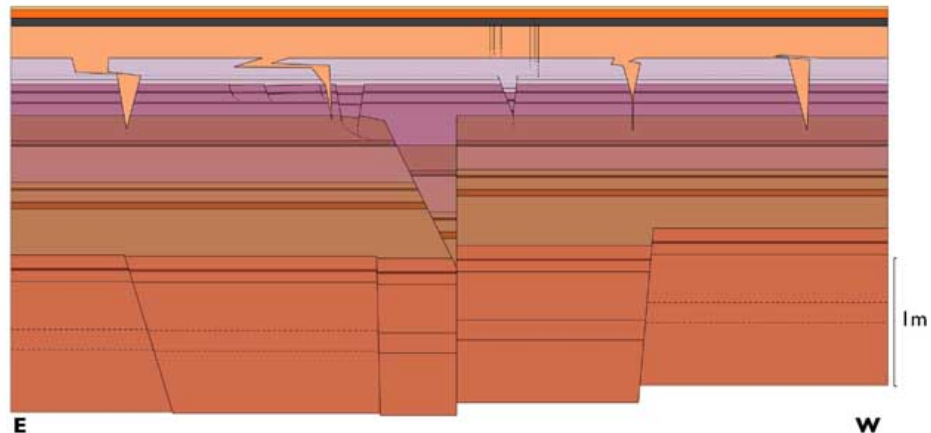
Shortly before S₉: deposition of L₃₅ and L₃₄, and possibly of the base of L₃₃.



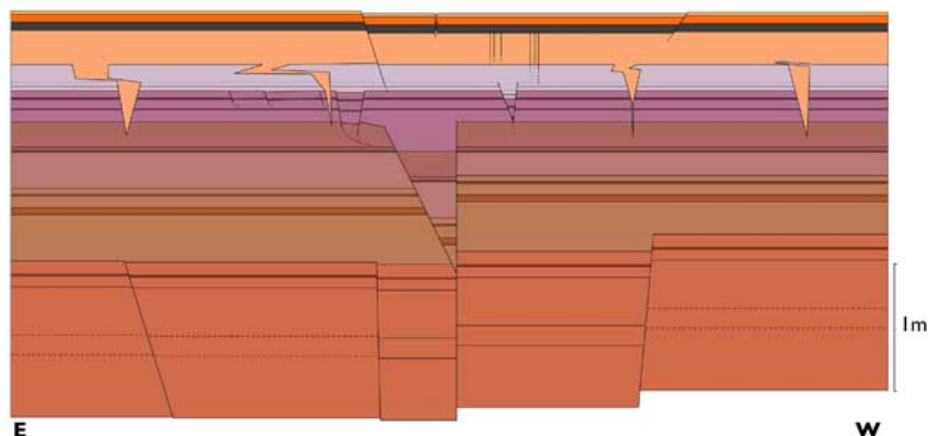
Immediately after S₉: opening of cracks, that do not propagate to the surface because of liquefaction of L₃₄, which flows into the cracks.



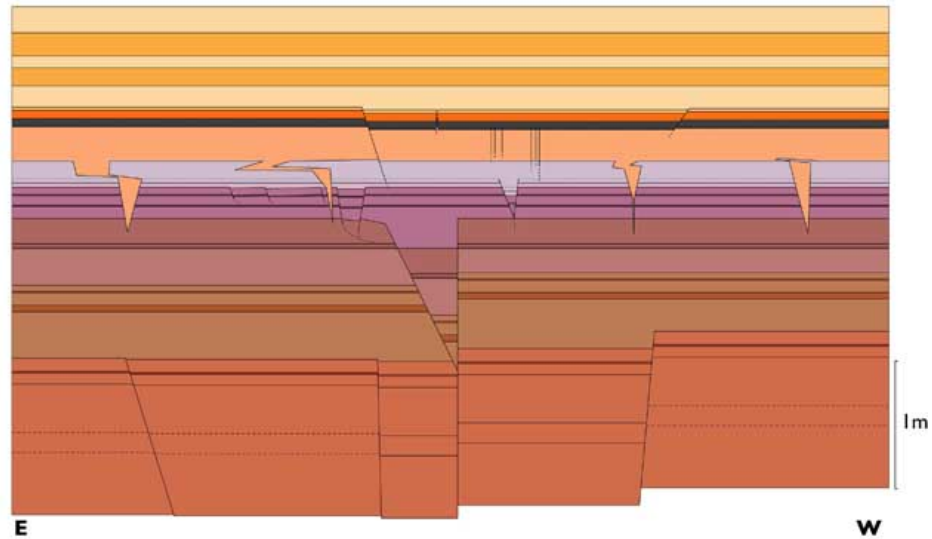
Shortly before S₈: desposition of layers L₃₃ to L₃₁.



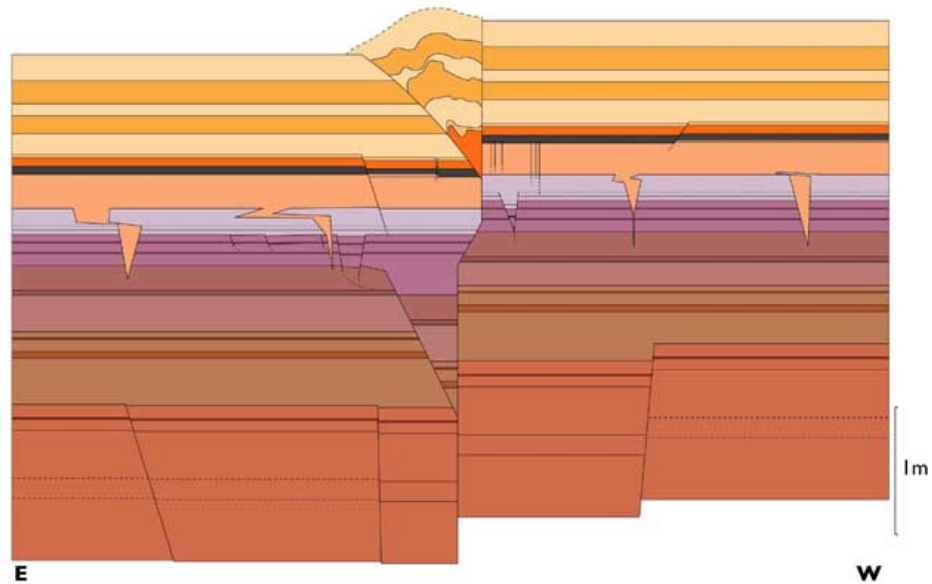
Immediately after S₈:



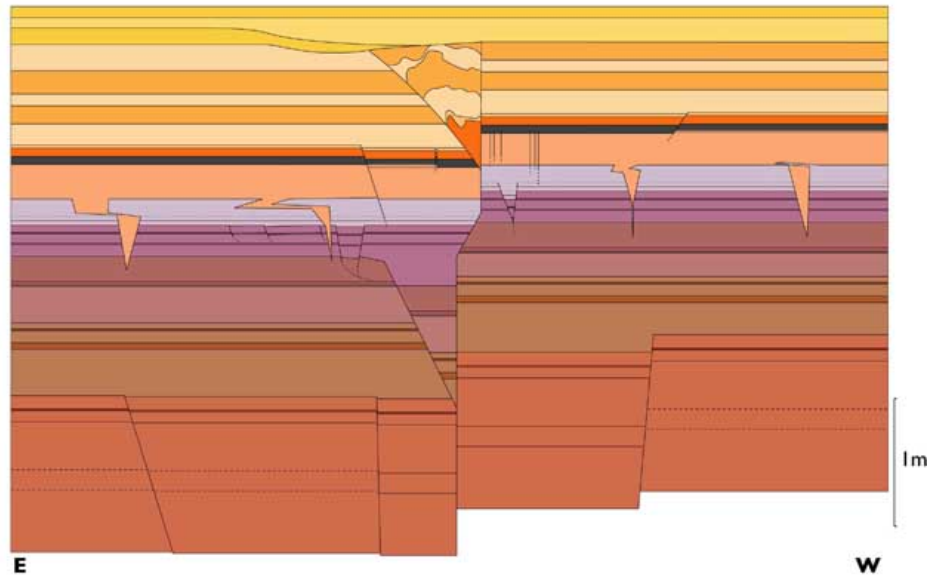
Shortly before S₇: deposition of layers L₃₀ to L₂₆.



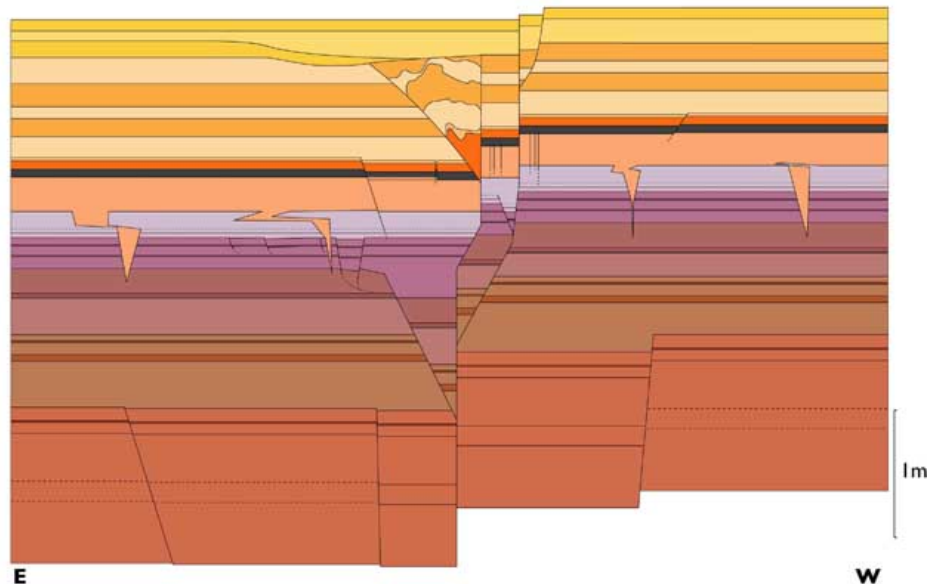
Immediately after S₇: Strong warping of the marl layers, and upthrow of the block W of the fault.



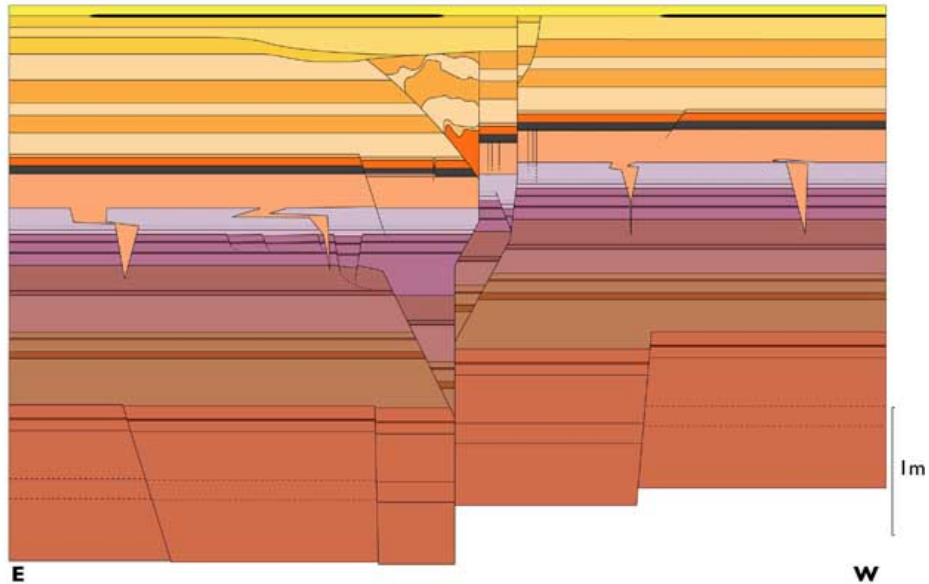
Shortly before S₆: deposition of layers L₂₅ to L₂₂.



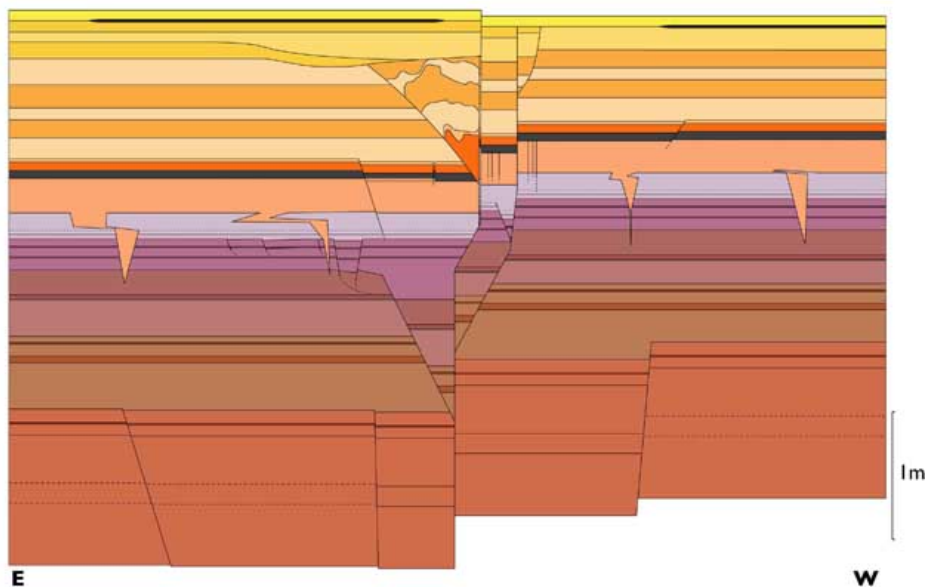
Immediately after S₆:



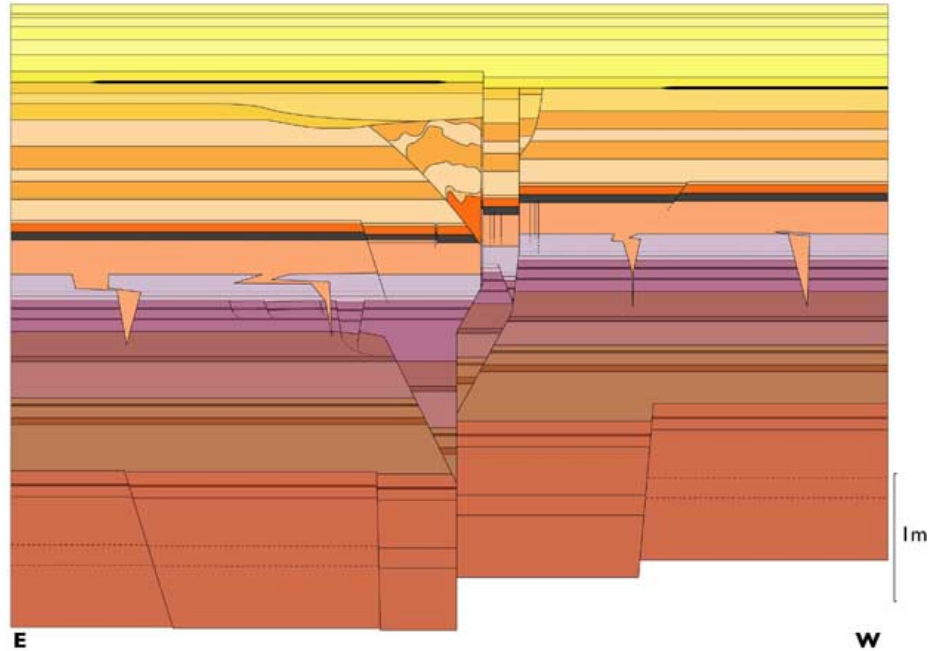
Shortly before S₅: After erosion of L₂₂ in the block uplifted by the previous event, deposition of L_{19/21} to L₁₇.



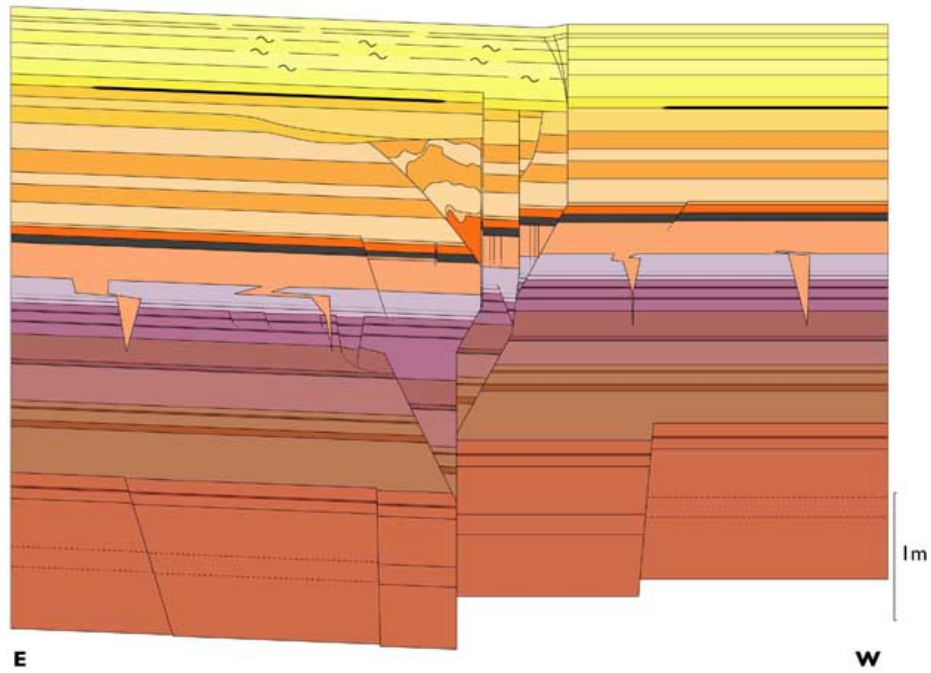
Immediately after S₅:



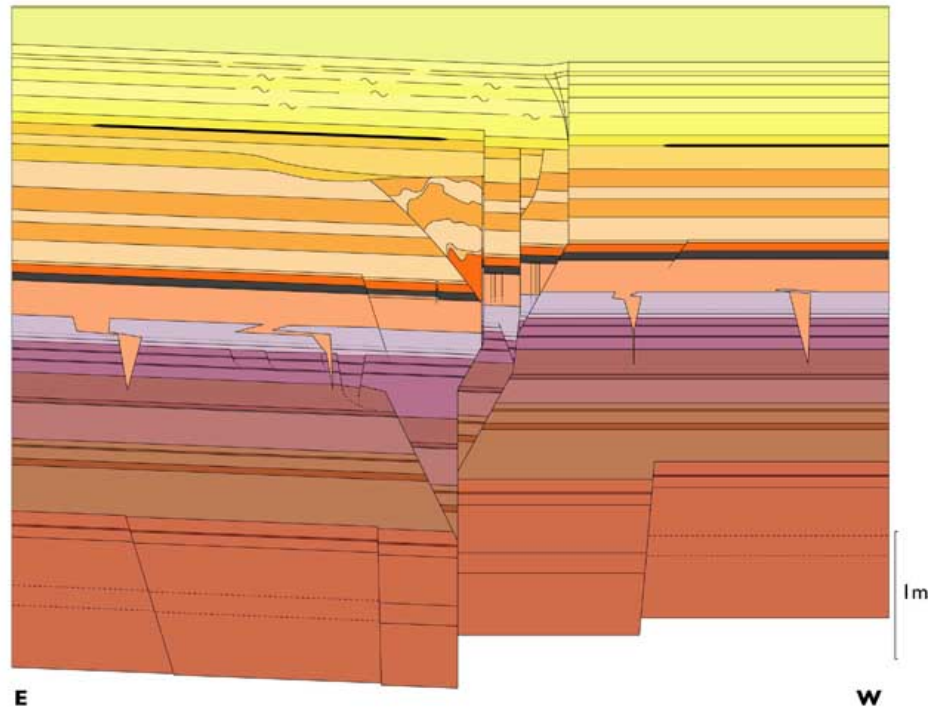
Shortly before S₄: deposition of layers L₁₆ to L₁₁, after a probable erosional episode affecting layers L_{17–23}.



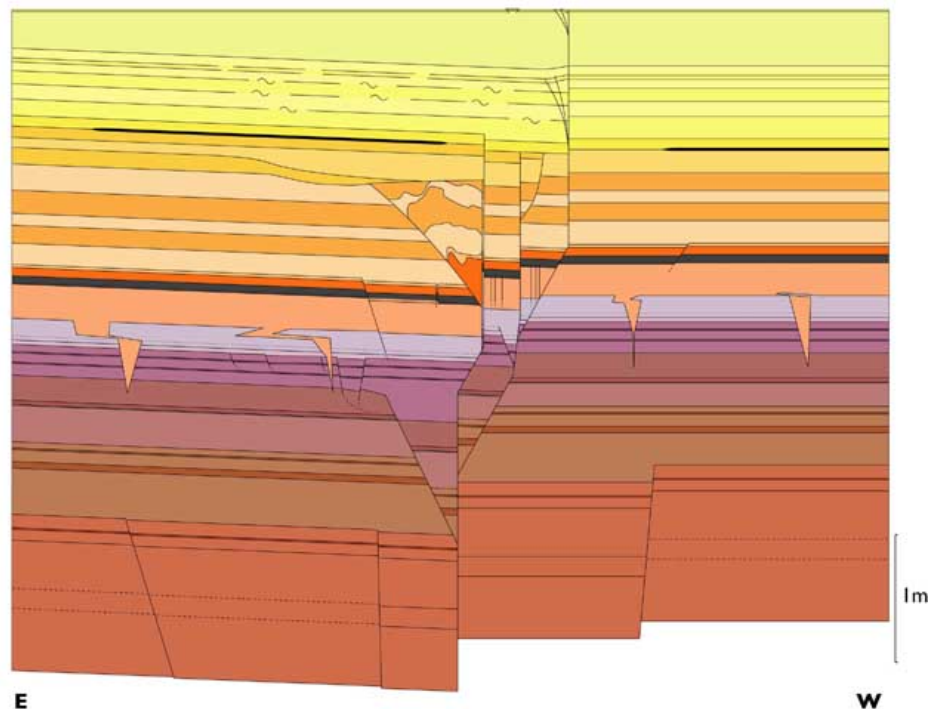
Immediately after S₄: during S₄, subsurface liquefaction within layers L_{12–15} and tilting of the surface to the E of the fault.



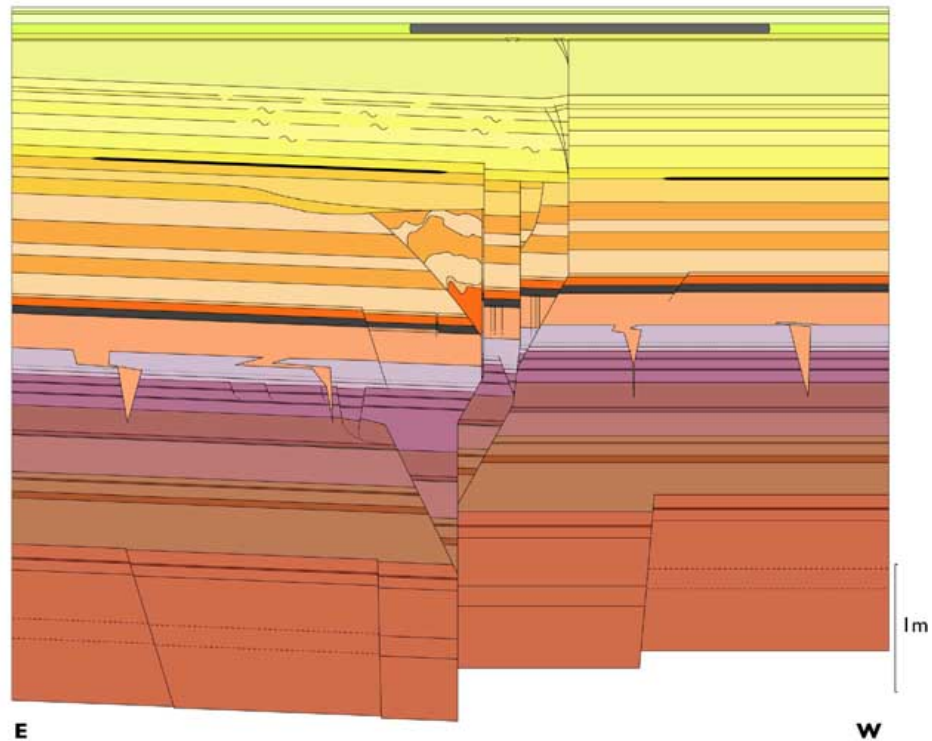
Shortly before S₃: deposition of layers L₁₀ and L₉.



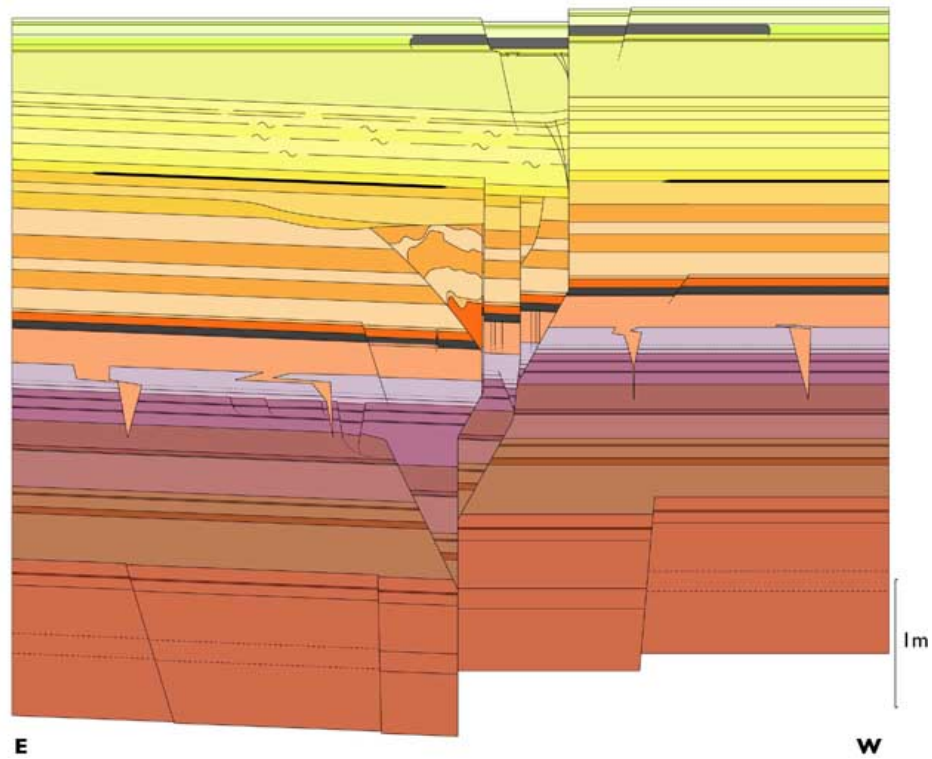
Immediately after S₃:



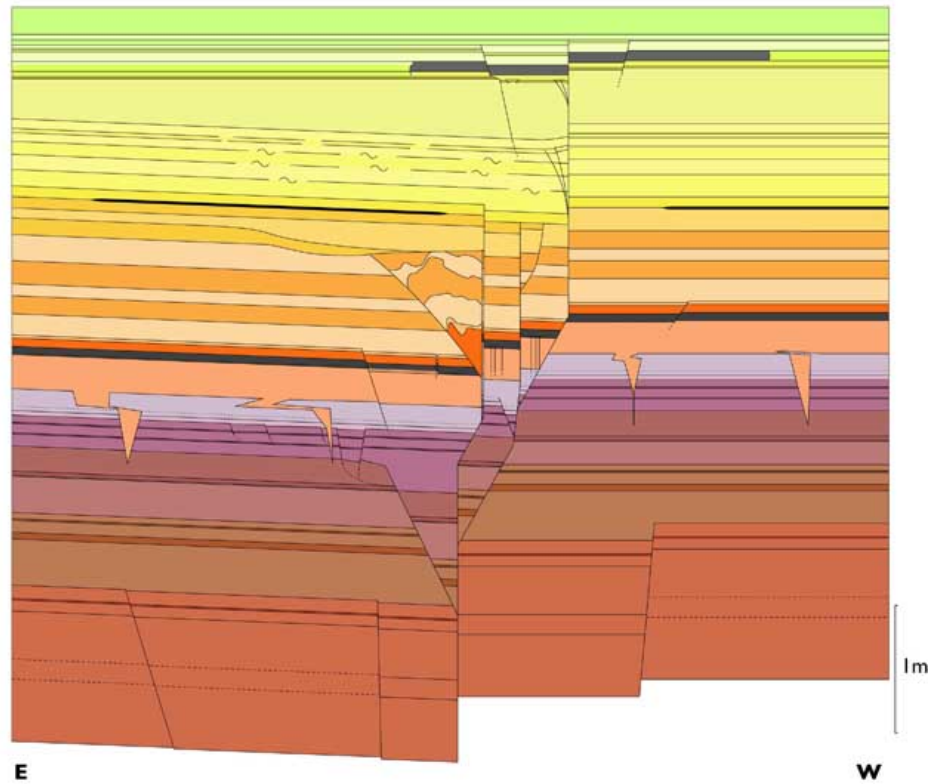
Shortly before S₂: deposition of layers L₈ to L₄.



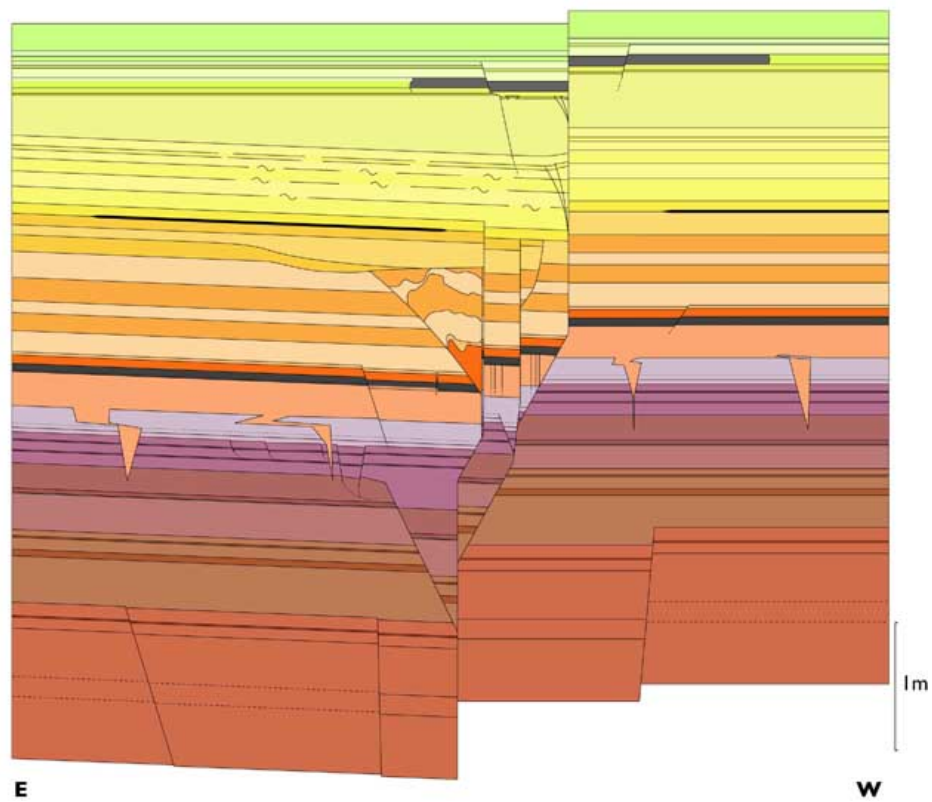
Immediately after S₂:



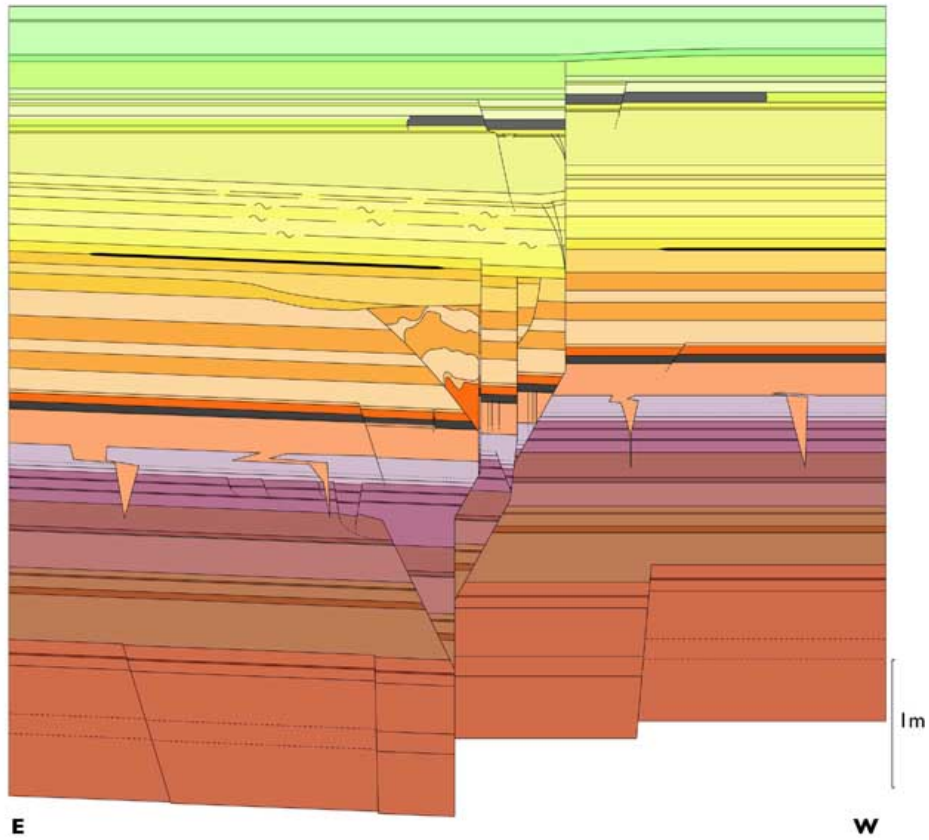
Shortly before S₁: deposition of layers L_{3f} to L_{3c}.



Immediately after S₁:



Modern-day situation: After erosion of layer L_{3c} W of the fault, deposition of layers L_{3c} to modern.



Dating

In order to date the lake beds exposed in the Kazzâb trench, we collected charcoal and organic samples, as well as small lake shells. All the samples were dated at the Center for AMS of the Lawrence Livermore National Laboratory (USA). Radiocarbon dating of the shells systematically yielded old ages (>8 ka), even in the shallowest sampled layers, which we infer to be due to a reservoir effect in the paleo-lake waters. Since the resurgent springs feeding this lake drain water from a vast subterranean karstic network, it is unlikely that all of the carbon in it comes from the atmosphere. Dating the shells thus proved unreliable, and too difficult to attempt without independant time constraints from other methods.

The positions of the charcoal fragments and organic matter samples that we could date are shown in figure 93. As mentioned before, the Kazzâb trench was excavated and studied within tight time constraints (~ 5 days). Making case of the remarkably uniform stratigraphy, we sought to maximize the efficiency of dating of several marker horizons by collecting samples from trench walls more than 4 m away from the fault zone, i.e. outside of the section logged in figure 88. For this reason, and because the layers can be followed without ambiguity away from the fault, we depict the positions of the dated samples in figure 93, relative to the layer in which they were sampled.

Unfortunately, a radiocarbon contamination problem occurred at the AMS dating labora-

Figure 93: (caption on next page)

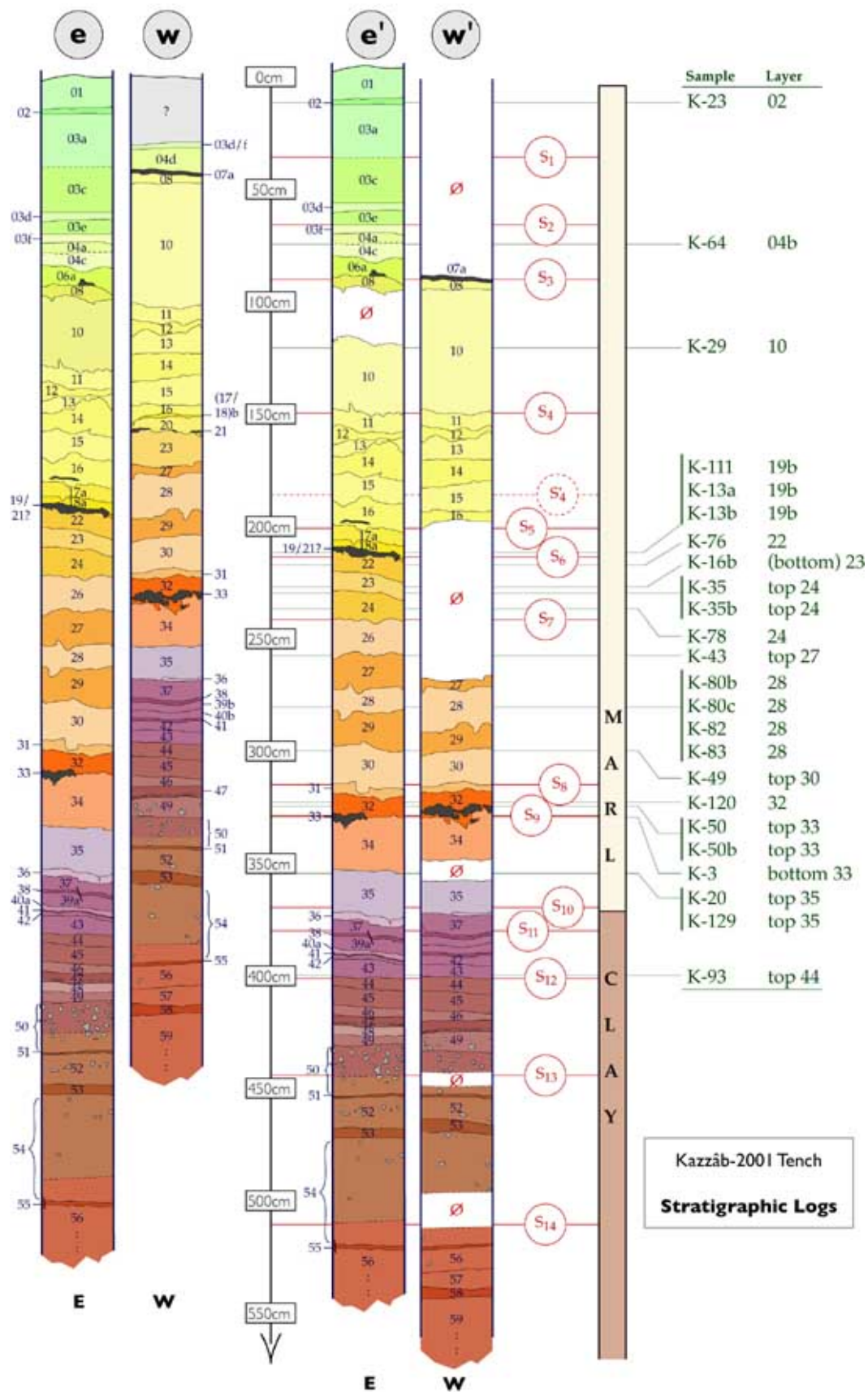


Figure 93: Stratigraphic log of the sediments exposed in the Kazzâb trench: [e] east of the fault zone; [w] west of the fault zone. Logs [e'] and [w'] are combined to produce a composite log, representing the sediments on both sides of the fault zone. Positions of dated samples and event horizons are also plotted.

Sample	Layer	Depth (cm)	$d^{13}\text{C}^*$ (‰)	Fraction Modern (‰)	$d^{14}\text{C}$ (‰)	^{14}C Age (yr BP)	Calibrated Age Range (95%, yr BP)
K-23	02	12	-25	927.1 ± 5.1	-72.9 ± 5.1	610 ± 45	540–655
K-64	04b	74	-25	815.5 ± 4.3	-184.5 ± 4.3	1640 ± 45	1413–1689
K-29	10	121	-25	774.1 ± 3.5	-225.9 ± 3.5	2055 ± 40	1901–2120
K-111	19b	212	-25	497.3 ± 3.7	-502.7 ± 3.7	5610 ± 70	6281–6554
K-13a	19b	212	-25	495.6 ± 2.8	-504.4 ± 2.8	5640 ± 50	6302–6534
K-13b	19b	212	-25	486.3 ± 2.5	-513.7 ± 2.5	5790 ± 45	6474–6722
K-76	22	217	-25	488.8 ± 2.3	-511.2 ± 2.3	5750 ± 40	6446–6660
K-16b	(bottom) 23	227	-25	482.5 ± 2.2	-517.5 ± 2.2	5855 ± 40	6549–6782
K-35	top 24	230	-25	487.6 ± 2.3	-512.4 ± 2.3	5770 ± 40	6451–6717
K-35b	top 24	230	-25	472.4 ± 2.1	-527.6 ± 2.1	6025 ± 40	6746–6984
K-78	24	237	-25	467.5 ± 2.1	-532.5 ± 2.1	6105 ± 40	6802–7158
K-43	top 27	258	-25	480.1 ± 2.1	-519.9 ± 2.1	5895 ± 40	6638–6850
K-80b	28	281	-25	401.2 ± 2.0	-598.8 ± 2.0	7335 ± 45	8011–8284
K-80c	28	281	-25	406.7 ± 2.1	-593.3 ± 2.1	7230 ± 45	7956–8163
K-82	28	281	-25	397.0 ± 4.5	-603.0 ± 4.5	7420 ± 100	8018–8392
K-83	28	281	-25	406.8 ± 2.0	-593.2 ± 2.0	7225 ± 40	7944–8157
K-49	top 30	300	-25	386.0 ± 8.6	-614.0 ± 8.6	7650 ± 180	8054–8987
K-120	32	323	-25	351.3 ± 1.4	-648.7 ± 1.4	8405 ± 35	9300–9525
K-50	top 33	325	-25	358.0 ± 1.6	-642.0 ± 1.6	8250 ± 40	9032–9402
K-50b	top 33	325	-25	367.2 ± 1.9	-632.8 ± 1.9	8045 ± 45	8720–9088
K-3	bottom 33	330	-25	348.6 ± 1.6	-651.4 ± 1.6	8465 ± 40	9331–9534
K-20	top 35	355	-25	312.8 ± 1.6	-687.2 ± 1.6	9335 ± 45	10399–10689
K-129	top 35	355	-25	306.3 ± 2.5	-693.7 ± 2.5	9510 ± 70	10579–11110
K-93	top 44	400	-25	277.9 ± 6.2	-722.1 ± 6.2	10290 ± 190	11338–12810

Table 12: Radiocarbon dates from the Kazzâb trench. AMS measurements were made at the CAMS of Lawrence Livermore National Laboratory. [*] $d^{13}\text{C}$ was assumed but not measured.

tory at the time when the first batch of our samples arrived there. As a result, several samples were lost, including some from the upper part of the Kazzâb sequence, where time constraints are now scarce. The ages of the 24 samples we could date are reported in table 12.

The calibrated ages are plotted in figure 94. There is good agreement between the ages and stratigraphic depths of most samples, suggesting sedimentation rates of ~ 0.76 mm/yr near the surface (L_{2-10}) and ~ 0.34 mm/yr in the lower marl and upper clay units (L_{19b-44}). The transition between these two regimes may occur somewhere between layers L_{10} (sample K₂₉) and L_{19b} (samples K₁₁₁, K_{13a} and K_{13b}). In that time interval, either sedimentation slowed down considerably (~ 0.18 mm/yr), or there is a hiatus in the sedimentary record. Such a hiatus could be the result of a ‘dry’ climatic episode during which the lake would have dried up, or it could be due to the erosion of part of the stratigraphic record, or both. Within the relevant stratigraphic frame, layers $L_{(17/18)b}$ to L_{21} appear angularly truncated and capped, west of the fault zone, by layer L_{16} (as mentioned above, cf p.141). The most likely hypothesis is that the sedimentary hiatus was caused by subaerial erosion by L_{16} of lake beds previously deposited over $L_{(17/18)}$. We

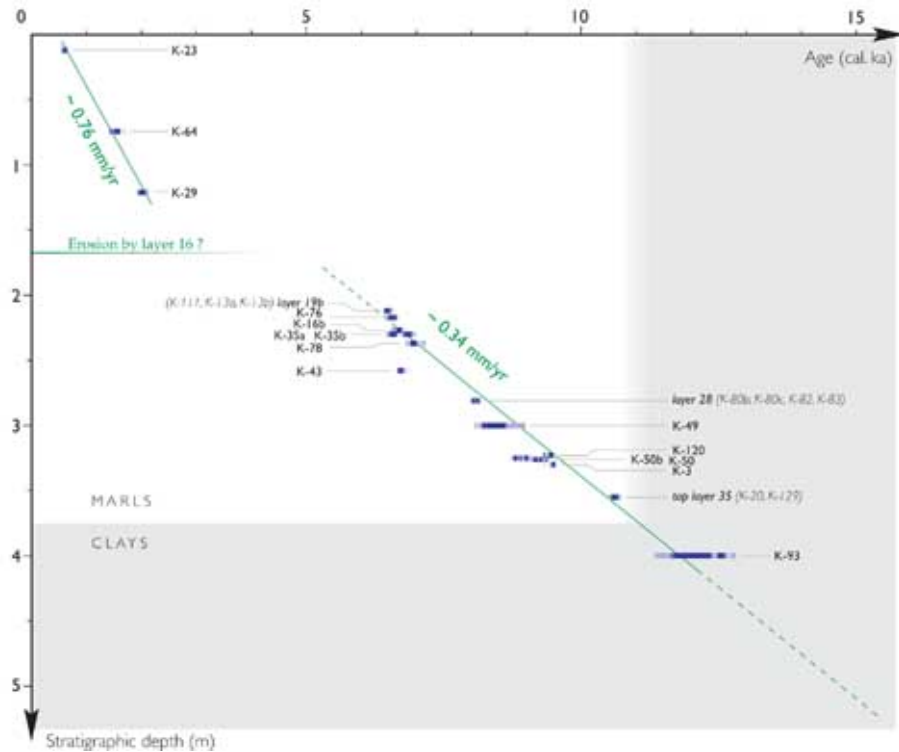


Figure 94: Age vs. depth in the Kazzâb trench. Radiocarbon ages were calibrated using OxCal 3.9 [Bronk Ramsey, 1995, 2001] and calibration curve INTCAL98 [Stuiver et al., 1998].

will show below that this period roughly corresponds to the end of the warm and humid Early Holocene Optimum (EHO), after which dryer climatic conditions became established Gasse and Fontes [1989]; Gasse et al. [1991, 1990].

Discussion

Time constraints on the Kazzâb events

Figure 95 summarizes the time constraints on the 14 events identified in the Kazzâb trench. Those concerning S_1 are thoroughly discussed in section 3.2. This event could only be one of two great historical earthquakes, in May 1202 or November 1759 (AD), which caused widespread destruction in and around the Beqaa plain. Since it clearly predates sample K₂₃, whose calibrated age is AD 1295–1410 (95% confidence interval), it cannot be the second of these events. Radiocarbon dating of supplementary samples (detailed in section 3.2) confirms that S_1 is the May 20th, AD 1202 earthquake [Ambraseys and Melville, 1988; Ellenblum et al., 1998].

Lower events S_4 to S_{11} are bracketed by various samples. S_4 and S_5 , as well as the hypothetical event S'_4 , predate sample K₂₉ and postdate the sampled layer L_{19b}. The age of this layer was constrained by combining the uncalibrated radiocarbon ages of K₁₁₁, K_{13a} and K_{13b}, and by then calibrating the result, since the three ^{14}C ages are in good agreement (table 12). It must be noted that these constraints on the timing of S_5 are valid even if a former upwards

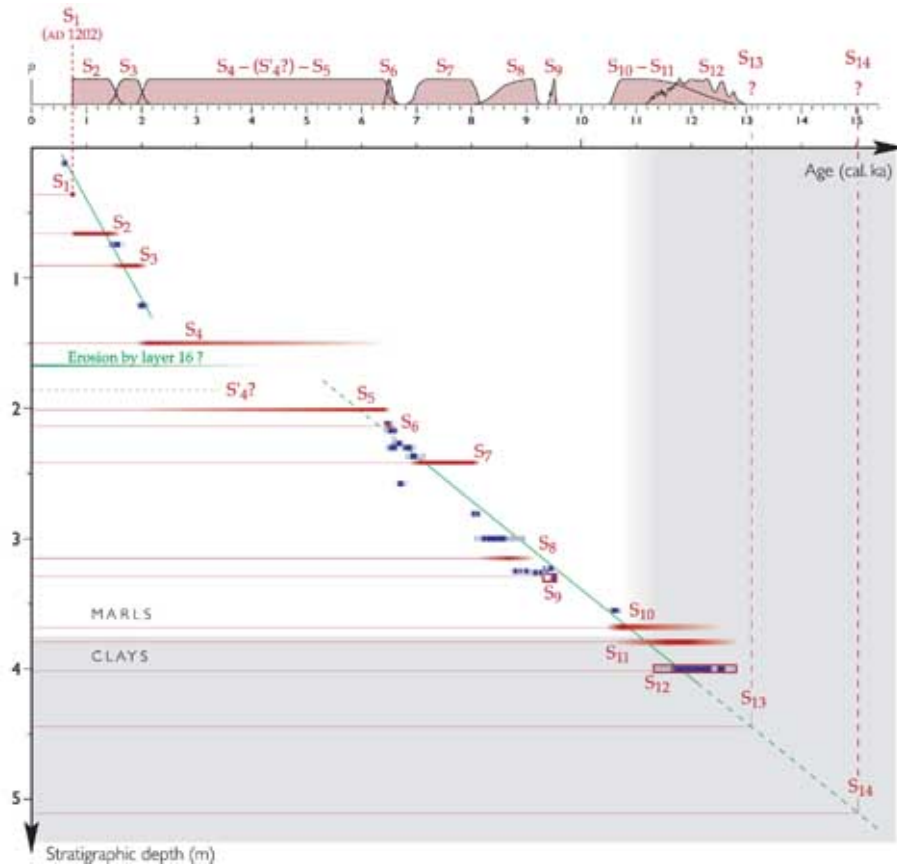


Figure 95: Time constraints on the events in the Kazzâb trench.

continuation of F₄ was subsequently erased by liquefaction, as discussed page 141.

The age of S₆ is tightly bracketed by that of layer L_{19b}, discussed above, and that of sample K₇₆.

S₇ predates sample K₇₈, and postdates layer L₂₈. Sample K₄₃ lies at a lower stratigraphic level than this event, but is significantly younger than K_{35b} and K₇₈ above it, suggesting that it does not reflect the true age of L₂₇ where it was collected.

The seismic horizon of S₈ lies below sample K₄₉, and above a cluster of samples corresponding to K₁₂₀, K₅₀, K_{50b} and K₃. The ages of these latter samples constrain the deposition period of layers L₃₂₋₃₃, that was already in place at the time of S₈. We therefore infer that this event is younger than the youngest of the samples within L₃₂₋₃₃, i.e. than K_{50b}.

As described on page 142, the crack opening and plastic flow associated with S₉ affected the bioturbation marks in L₃₄, that were likely related to the vegetation mat in L₃₃. As mentioned above, three samples (K₅₀, K_{50b} and K₃) were collected in L₃₃. We inferred their age spread to represent the period of active deposition in layer L₃₃. The age of S₉ is thus bracketed between that of the youngest (K_{50b}) and oldest (K₃) of these samples.

Both S₁₀ and S₁₁ are younger than K₉₃, and older than the group of samples collected at

Event(s)	Stratigraphic constraints	Time constraints	
		[cal. yr BP]	[AD / BC]
S ₁	(cf section 3.2)	748	AD 1202
S ₂	K ₆₄ – S ₁	748–1502	AD 448–AD 1202
S ₃	K ₂₉ – K ₆₄	1500–2050	100 BC–AD 450
S ₄ -(S' ₄)-S ₅	L _{19b} – K ₂₉	2128–6429	.
S ₆	K ₇₆ – L _{19b}	6422–6628	.
S ₇	L ₂₈ – K ₇₈	6960–8059	.
S ₈	K _{50b} – K ₄₉	8278–9009	.
S ₉	K ₃ – K _{50b}	8885–9506	.
S ₁₀ -S ₁₁	K ₉₃ – L ₃₅	10564–12292	.
S ₁₂	[K ₉₃]	11338–12810	.
S ₁₃	? – K ₉₃	?	.
S ₁₄	? – S ₁₃	?	.

Table 13: Timing of the Kazzâb events.

the top of layer L₃₅. This latter group is composed of samples K₂₀ and K₁₂₉, whose uncalibrated age distributions overlap (table 12), allowing us to combine them before calibration, in order to better constrain the age of L₃₅.

Sample K₉₃ was collected at the top of L₄₄, that coincides with the seismic horizon of S₁₂. In the absence of stratigraphically close samples above or below K₉₃, we considered that the age of S₁₂ is best represented by that of K₉₃.

Events S₁₃ and S₁₄ are older than the oldest dated samples, so their age was estimated by extrapolating the best-fitting sedimentation rate down to the corresponding event horizons. The estimated ages are \sim 13 ka and \sim 15 ka respectively. This estimate is inherently imprecise, since the sedimentation rate is loosely constrained, and approximated as constant, when it may in fact exhibit centennial or millennial variations. Moreover, the fitting of this rate applies to samples K₁₁₁ to K₉₃, i.e. to layers L_{19b} to L₄₄, corresponding to the lower marl series, with only K₉₃ collected in the clay beds. One would expect the sedimentation rates in the clay beds to be different from that in the marls. For these reasons, the ages of S₁₃ and S₁₄ remain poorly constrained.

Earthquake recurrence on the Yammoûneh fault

Overall, the 11 inter-seismic time intervals between S₁ and S₁₂ span a total duration of 10.6–12.1 kyr. At face value, the mean recurrence time (MRT) of earthquakes at the Kazzâb site over this period was thus 963–1097 yr. This number is reduced to 882–1005 yr if the hypothetical event S'₄ is taken into account as well. However, as mentioned above, it is possible that we failed to recognize evidence for one or more earthquakes, and/or that the probable hiatus in the sedimentary record corresponds to one or more ‘missing’ events. Both of these possibilities would cause us to over-estimate the MRT, but not by much if the number of ‘missing’ events is

no more than 2 or 3.

This overall estimation can be refined for the period from S_1 to S_3 , which covers the two latest inter-seismic intervals at this site. This period spans 752–1302 yr, which yields a MRT of 376–651 yr. The overall MRT (\sim 1000 yr) cannot be reconciled with this ‘later’ one using the ‘missing’ earthquakes hypothesis alone: the number of events needed to bring it down to \sim 650 yr exceeds 6, which is unrealistic considering the 4.3 kyr maximum duration of the inferred hiatus and the time distribution of events in the rest of the record.

The pre-hiatus event recurrence times can be constrained using the 6 inter-seismic intervals from S_6 to S_{12} , which span 4.7–6.4 kyr. The resulting, ‘earlier’ MRT is 785–1065 yr, which is similar to the overall MRT. Two different hypothesis may explain this. First, one could propose that earthquake occurrence slowed down at this site during the time period between S_3 and S_6 , encompassing the potential hiatus in the Kazzâb record. If this reduced frequency of events (1093–1709 yr) did not correspond to significantly greater left-lateral coseismic slip for each event, and if elastic loading of the Yammoûneh fault continued at a rate similar to that before S_6 , then a ‘slip deficit’ should have accumulated. This could explain the significantly shorter MRT of the post- S_3 period. The similarity between the overall MRT and the pre- S_6 one would then suggest that the fault has now roughly caught up with this slip deficit, perhaps explaining the relatively long¹ duration since the latest event. It should be noted that this hypothesis relies on the absence of more ‘missing’ events.

An alternative hypothesis would be that the typical frequency of event occurrence changed over time, accelerating from a ‘infrequent’ pre- S_6 behaviour (785–1065 yr MRT) to a ‘frequent’ post- S_3 one (376–651 yr MRT). According to this explanation, the timing of the transition would be obscured by one or more missing events between S_6 and S_3 . This hypothesis assumes that the frequency of events on a fault can change significantly over a few thousand years [Weldon et al., 2004; Bennett et al., 2004]. Such a change might possibly mark the end of episodic activity on the eastern and western bounding faults of the pull-apart, in favor of the central fault strand that shortcuts through the lake beds. The Kazzâb record would then include, before the change, only part of the earthquakes occurring on the Yammoûneh fault. To this day, no observation supports this ‘shortcut pull-apart’ activity migration: as mentioned above, there is no evidence of recent strike-slip motion on the eastern and western bounding faults. This, however, does not preclude the more general hypothesis of a change in the frequency of events, that might also be related, perhaps more plausibly, to a change in slip rate and corresponding pattern of earthquake strain release [Weldon et al., 2004].

Finally, if the modern behaviour of the Yammoûneh fault is similar to that of the past two millennia, it must be stressed that the \sim 800 years now elapsed since S_1 exceed significantly the 376–651 yr mean recurrence time of events over the latest two inter-seismic intervals. This would suggest that the likelihood of an earthquake occurring in the next decades or century on the Yammoûneh fault is high.

¹ Eight centuries, versus the 376–651 years MRT from S_3 to S_1

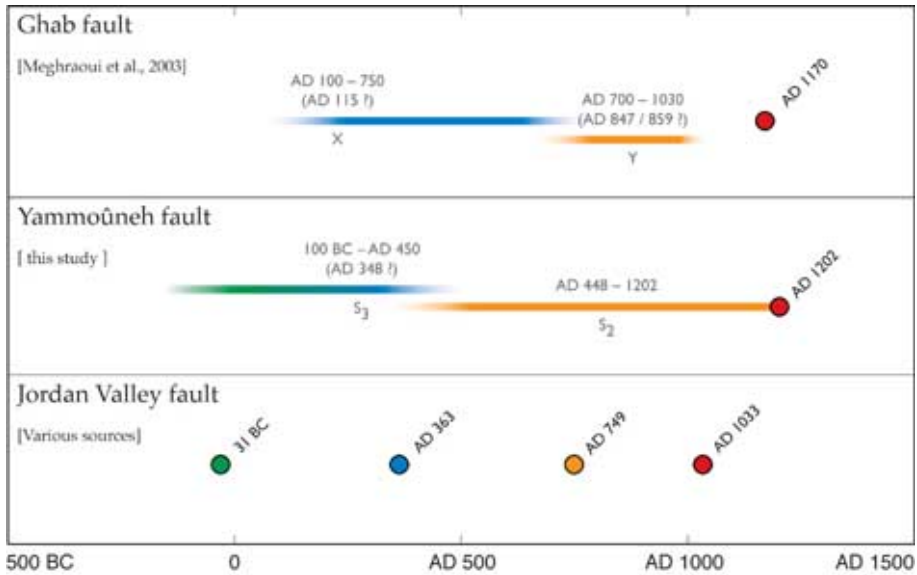


Figure 96: Comparison with the segments of the DSF adjacent to the Yammoûneh fault [Meghraoui et al., 2003; Reches and Hoexter, 1981; Marco et al., 2003]

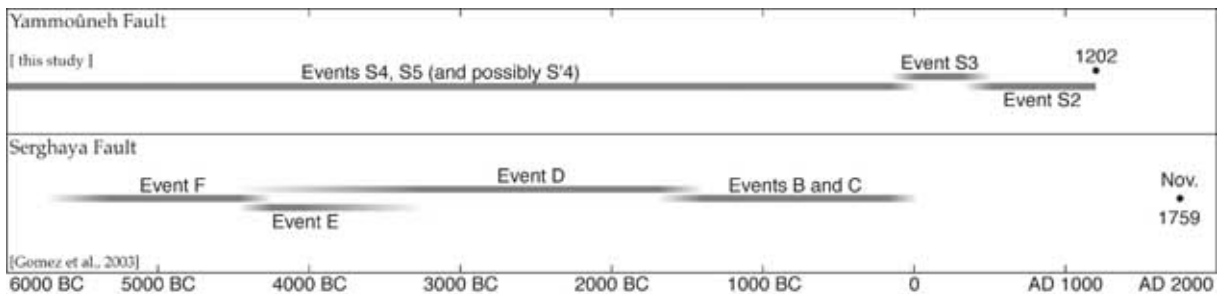


Figure 97: Comparison with the Serghaya fault [Gomez et al., 2003]

Comparison of the Kazzâb record with regional historical seismicity and paleoseismicity

Historical, archeological and paleoseismic results from the sections of the Dead Sea fault located directly north and south of the Yammoûneh fault can be compared with the Kazzâb record. To the north, Meghraoui et al. [2003] have described evidence for the three latest events on the Ghab fault, in western Syria. The youngest of these is the AD 1170 historical earthquake. The two preceding ones are constrained to AD 100–450 (event X) and AD 700–1030 (event Y).

The three latest events from the Kazzâb trench, the three events documented by Meghraoui et al. [2003] on the Ghab fault, and the three latest large historical earthquakes on the Jordan Valley fault are all plotted in figure 96. In spite of the loose time constraints on 4 of these events, it is tempting to infer a correlation between the timing of events on these three adjoining faults, with three seismic ‘episodes’, each one affecting all three faults. This does not mean, however, that giant earthquakes ruptured several of these faults at once: this is not what happened in the latest sequence, composed of the AD 1033, 1170 and 1202 events. Rather, it is likely that the two earlier ‘episodes’ resembled the latest sequence, with triggered earthquakes separated by several decades.

Gomez et al. [2003] has investigated the paleoseismic record of the Serghaya fault in the Zebadani valley, in Syria. They identified the six latest events at this site, the youngest of which occurred in the 18th century AD. As discussed in section 3.2, the combination of historical sources, geomorphic observations and paleoseismology provides evidence that this latter event is the November 1759, $M_s \sim 7.4$ historical earthquake. Figure 97 shows these results, plotted with relevant events from the Kazzâb record. All the Zebadani events, except for the AD 1759 earthquake, occurred within our poorly constrained interval between S_6 and S_3 . It is thus difficult to compare the two records, particularly concerning the Zebadani sequence B to F. Nevertheless, over the past 2 millennia, seismic activity on the Yammoûneh fault, in terms of event occurrence, appears to be anti-correlated with that on the Serghaya fault. If this is the case, the occurrence of the AD 1759 event on Serghaya would be consistent with the observation, mentioned above, that 8 centuries elapsed since the latest event on Yammoûneh significantly exceeds the ‘recent’, 376–651 yr MRT. Slip in AD 1759 is expected to have unloaded shear stresses along the plate boundary, delaying the occurrence of a 1202-type event on the Yammoûneh fault.

Climatic record of the Kazzâb trench

Some of the main stratigraphic divisions in the lacustrine sequence of the Kazzâb trench probably reflect climatic changes. The interpretation of other horizons (dark) that stand out in the uppermost light-colored marls is less straightforward. Some of these horizons may be localized near the fault zone, due to ponding because of seismic warping of the underlying layers, and therefore unrelated to the regional climate. This may be the case of layer L_{7a}, deposited right after event S_3 , and which thins and vanishes away from the fault. The same may apply to layer L_{19/21}, deposited after S_6 , although this layer thins away from the fault but does not vanish.

On the other hand, it seems likely that the clay/marl transition and the thick grey layers L₃₂₋₃₃, which are uniform across the entire 70 m length of the Kazzâb trench, and ubiquitous in the rest of the paleo-lake, are linked with climatic change. The age constraints we have on these layers may be compared to the regional paleoclimatic record (figures 58 and 59, pp.86–88). The clay/marl transition’s age bounds (10.4–12.8 ka, cf figure 95), seems to be correlated with the Younger Dryas (11.5–13.5), more specifically with the end of the Younger Dryas. Layers L₃₂₋₃₃, dated at 8.7–9.5 ka, appear to correspond to the rise of the level of the Dead Sea at the beginning of the Early Holocene climatic optimum (EHCO). The uniform stack of beige and white marl layers L₂₂₋₃₁ above L₃₂₋₃₃ would then represent sedimentation during the entire span of the EHCO, ending with layer L_{19/21} mentioned above, dated at 6.3–6.7 ka. At a more speculative level, the color alternance within this EHCO sequence may reflect pluricentennial cycles due to solar forcing on the climate [e.g. as documented in the Lisan by Prasad et al., 2004].

Conclusion

The Yammoûneh fault and the Mount Lebanon thrust, main active faults of the LRB

Although the hypothesis that the Yammoûneh fault is the main active fault of the Lebanese restraining bend was proposed early on in the original works of Quennell [1958], Freund et al. [1970] and Garfunkel et al. [1981], and although the large-scale geomorphic signature of the Yammoûneh fault is fully consistent with this hypothesis, doubt on the present-day activity of the fault has been strongly voiced in recent years by a number of authors, based on regional kinematics [Girdler, 1990] or on the basis of field geological observations [Butler et al., 1997]. The new quantitative geomorphic evidence, time constraints and paleoseismologic data we present in this work make it clear that such doubts are not warranted. The Yammoûneh fault is indeed a very active feature, that has consistently offset geomorphic markers of climatic origin, from the scale of meters to kilometers, due to the cumulative effect of recurrent, if infrequent, large earthquakes.

Lifting this doubt was only possible by integrating small-scale quantitative geomorphic observations in the field with surface and subsurface geological data. In particular, it is essential to date landforms, whether directly or relative to past climate events that have left an imprint in the landscape. In this respect, the mountainous Lebanese landscape displays a rich record. As other authors have proposed [e.g. Butler et al., 1998], and as is widely observed around the Mediterranean, deep fluvial incisions probably date back to the Messinian crisis. Closer to modern times, the strong Quaternary fluctuations of the global climate appear to have played a major role in shaping Mount Lebanon. Although most authors prior to 1975 [e.g. Besancon et al., 1973] had dismissed the possibility of strong glacial action on Mount Lebanon, we argue, in view of field observations and of the general acceptance of global climate change, that during glacial maxima, the summits plateaus of the Lebanon range, as well as the top of Mount Hermon, were covered with an ice cap. The proximity of the Yammoûneh fault to these ice capped summits may explain, in part, the sensitive response to climate of the hydrological systems that cross the fault.

In the Tripoli-Halba piedmont, combining a structural study of the folding of young (Pontian to Piacenzian) beds with geomorphic evidence of active thrust faulting, implies that SE-dipping thrust ramps govern the growth of anticlines in the foreland of Mount Lebanon, accounting for most the transpression related to the bend of the Levant fault. These active thrusts

appear to continue offshore, as least as far south as Beirut and probably Saida, accounting for the ongoing uplift of the coast between the Akkar plain and the Saida-Tyre coastal strip. In this new model, the Roûm fault is simply interpreted as one of the lateral ramps transferring slip from the Jordan Valley fault to these thrusts, and Mount Lebanon is a thrust wedge completely surrounded by active faults.

Plio-Quaternary slip rates and comparison with regional kinematics

Not only is the Yammoûneh fault still active, but we have shown quantitatively that it is the fastest-slipping fault of the LRB. Cosmogenic surface exposure dating of two post-glacial alluvial fans broadly constrains the slip rate to be 3.8–6.4 mm/yr. Using these bounds, we estimate the ages of the other measured offsets along this fault, which are found to be strongly correlated with either warm pluvials during interglacials, or with dry/cold spells during the latest glacial. Taking in turn the regionally well-determined ages of these climatic events in the last 120 kyr makes it possible to narrow the bounds on the late Pleistocene slip rate of the Yammoûneh fault to 5.0–5.5 mm/yr.

This rate is greater than that [1.4 ± 0.2 mm/yr, Gomez et al., 2003] of the Serghaya fault, which we connect to the Râchâïya fault through the active Mount Hermon push-up. It is also greater than the $\sim N45^\circ W$ shortening rate across the Mount Lebanon thrust system, geometrically constrained between 3.0 and 4.3 mm/yr by the Yammoûneh fault's slip vector and the strike of the southern Ghab fault. Using similar constraints to assess the left-lateral component of slip on the Roûm fault is less straightforward, probably because the geometry of transpression varies from north to south.

The kinematic model quantitatively consistent with our Yammoûneh fault slip vector and the derived Mount Lebanon shortening vector predicts a left-lateral slip rate of 6.3–8.4 mm/yr along the Ghab fault, fully compatible with the ~ 7 mm/yr measured by Meghraoui et al. [2003]. Using our data to predict a slip rate on the Jordan Valley fault requires the addition of the Serghaya slip rate and the associated transpression. The value thus estimated (7.2–9.4 mm/yr) south of the LRB is less well-constrained than that to the north, principally because our constraints on the Mount Lebanon shortening vector come from the north of the range, and because active transpression across the Râchâïya-Serghaya fault system remains to be quantified.

This value is large. It is fully compatible with the ~ 8 mm/yr rate deduced from Pliocene geological constraints and topographic restoration of the Gulf of Aqaba pull-aparts. It is also compatible with the upper bound on LFS-parallel motion found for the last 3 Myr by Chu and Gordon [1998] assuming that the rotation of the Sinai-Levant micro-plate, required by the opening of the Gulf of Suez, generates little strike-parallel motion relative to Arabia on the northern Levant fault. On the other hand, the upper bound of short-term Arabia/Nubia motion found by McClusky et al. [2003] barely coincides with the lower bound of our prediction. One cannot rule out that this incompatibility is due to a flaw in our prediction, or that it might reflect a recent decrease of slip rate along the Levant fault. But it must be noted that the GPS model

constrains the motion of Arabia using only four stations, three of which are survey stations that might be influenced by plate boundary effects [McClusky et al., 2003, bottom of p.128].

Finally, there are two slip rate estimates on the southern LFS, one geomorphic [Klinger et al., 2000, 4 ± 2 mm/yr], the other geodetic [Wdowinski et al., 2004, 3.3 ± 0.4 mm/yr], that cannot be reconciled with our data. Although a N-S variation of rate is expected along the Levant fault, all the intervening faults between the Araba valley and the Yammoûneh fault (Carmel fault, Râchaïya-Serghaya system) imply a northward rather than southward decrease of the left-lateral component of slip. Thus we argue that the results of both studies are flawed. The GPS network used by Wdowinski et al. [2004] comprises many stations that are close (≤ 20 km) to active faults (Carmel fault, Jericho fault, Damascus thrust) other than the Dead Sea fault. Moreover, the network crucially lacks stations east of the Levant fault, especially far-field ones. Thus, at this stage, little can be deduced from this data set about the Dead Sea fault's rate.

The 4 ± 2 mm/yr rate determined by Klinger et al. [2000] just south of the Dead Sea, rests on geomorphic offsets dated in reference to climate change Klinger et al. [2003], with subsurface ^{14}C , U/Th and cosmogenic surface exposure. The largest offset they use, loosely constrained to 300–900 m, is that of the Dahal alluvial fan. The fan was broadly emplaced between 140 and 32 ka, based on 5 cosmogenic ^{10}Be samples and 2 U/Th ages. The authors choose the lower half of this age span, inferring that the fan strictly predates the establishment of Lake Lisan, around 70 ka, even though the Dahal fanglomerates show distal interfingering with the Lisan beds. Their choice is thus debatable, and it can be argued that the offset and age ranges of the Dahal fan in fact allow for rates between 2 and 30 mm/yr (!). A different type of problem may bias the rate deduced from the El Ghor terraces. Here, the ages of the terrace deposits, since then confirmed by Niemi et al. [2001] are not in doubt. It is the ages of the rills which incise the terraces that are ambiguous. Since the rate is deduced from the rill offsets, dating the incised terraces can only yield lower bounds. Assuming terraces/rills to be emplaced/incised during pluvials, it is tempting to interpret rill incision episodes to coincide with pluvials corresponding to deposition of the terraces younger than those in which the rills are incised. This line of interpretation would yield higher rate ranges (4.9–6.1 and 3.6–10.5 mm/yr based on Klinger et al.'s data, 4.4–10 mm/yr based on that of Niemi et al.). Clearly, solving this issue will require further dating of other offset landforms in the Wadi Araba. Field work on this problem has already been engaged, in close association with Yann Klinger.

Total offset on the Yammoûneh fault

Our data provides only marginal insight into the long-debated problem of the finite offset on the Yammoûneh fault and on the northern Levant fault in general. Extrapolation, however, of the 5–5.5 mm/yr slip rate on the Yammoûneh fault to the Messinian yields a displacement compatible with the largest offset (26.4 km) inferred for the Litâni river, consistent with the idea that its incision across the Baroûk anticline was driven by the drastic Messinian drop in

Mediterranean sea level. Adding this value to the 9.5 ± 0.4 km offset of the same river across the Roûm fault suggests that ~ 36 km of left-lateral displacement have accrued across the northern Levant fault since the beginning of the Pliocene. This is to be compared to the 40 ± 5 km of Plio-Quaternary motion along the Dead Sea fault [Freund et al., 1968, 1970; Garfunkel, 1981], suggesting that the Râchaïya-Serghaya fault system and the Palmyrides thrusts might have absorbed up to ~ 10 km. Note that the ratio between the Plio-Quaternary finite offsets on the Yammoûneh and Serghaya faults would then be comparable to the ratio of their Holocene rates.

By contrast, a Plio-Quaternary finite offset on the northern Levant fault consistent with all the above would be in blatant contradiction with the inference that the apparent ~ 10 km offset of the 5–6-Myr-old Homs basalts provides a valid constraint on motion along the Ghab or Yammoûneh faults since that time. The fact that these basalts are deformed along the Halba-Qoubayat thrust, contrary to the claims of Butler et al. [1998], suggests that they may have been eroded west of the Yammoûneh fault due to the recent uplift of northern Mount Lebanon.

Seismic behavior of the Yammoûneh fault and earthquake triggering on the LFS

The results of trenching in the Yammoûneh basin’s lake beds provide a ~ 15 -millennia-long paleoseismic record, the longest obtained thus far in Middle East trenches. Although longer records exist [Migowski et al., 2004], they are based on far-field seismites in the Lisan beds, not on cross-fault logs, and cannot discriminate between source faults. Despite its fine stratigraphy, which makes it possible to identify 14 or 15 earthquakes, the Kazzâb trench record appears to be interrupted by a hiatus between 6 ka and 2 ka, either due to lack of deposition or to erosion. Whether this record can be improved and correlated with that of other trenches in the same basin, or elsewhere along the Yammoûneh fault, is under investigation.

On the Yammoûneh segment of the Levant fault, it appears that earthquakes occur infrequently, every ~ 1000 yr on average. Since we can demonstrate that the latest event in the Yammoûneh basin is the devastating AD 1202 earthquake, the issue of the occurrence of a large earthquake in Lebanon within the next few centuries should readily be taken into account by risk management planners. Furthermore, because the latest three earthquakes on the Yammoûneh fault took place between ~ 50 BC and 1202, one might argue for a “modern” mean recurrence time of about six centuries, thus that the next event on the Yammoûneh fault is overdue.

Combining the bounds on the mean recurrence times of events and on the average slip rate on the Yammoûneh fault implies that slip amounts per event are large, comprised between 3.2 and 5.5 m, which is not inconsistent with the smallest stream offsets preserved at Aarîd Mtaïyouhâne (4–7 m). Using earthquake scaling laws such as Wells and Coppersmith [1994]’s, such coseismic slip amounts are also compatible with rupture lengths on par with the total length of the Yammoûneh fault (~ 160 km), and with the estimated 7.6 magnitude of the 1202 event [Ambraseys and Melville, 1988].

Aside from the long-term record they provide, the paleoseismic results of the Kazzâb

trench, combined with a critical re-assessment of historical seismicity based on our new map of the active faults of the LRB, shed new light on the most destructive earthquakes in Lebanon since the 6th century AD. The most significant result is that none of the two AD 1759 shocks ruptured the Yammoûneh fault, implying that this sequence was due to slip on the Râchaïya-Serghaya fault system. This new scenario, along with the presence of the active, offshore Mount Lebanon thrust, which likely produced the AD 551 earthquake and tsunami¹ that ruined Beirut and the Phoenician coast, calls for a complete re-assessment of seismic hazard in and around the Lebanese restraining bend.

A particularly ominous possibility is that of large earthquakes triggering one another from one fault to the other. For instance, a large thrust event offshore Lebanon could trigger a second earthquake on the Yammoûneh fault due to Coulomb stress release. By contrast, elastic strain release due to coseismic slip on the Serghaya fault is expected to lower the probability, hence delay, the occurrence of events on the Yammoûneh fault, and vice versa. Tentative support for this comes from the comparison of the Kazzâb and Zebadani [Gomez et al., 2003] paleoseismic records, respectively on the Yammoûneh and Serghaya faults, which appear to display anti-correlated event frequencies over the past few millennia. Conversely, the 1202 event concluded a 200-yr-long sequence that ruptured the entire Levant fault from Aqaba to Antioch, starting in AD 1033. The duration of this sequence is sufficiently short, relative to the mean event return time on the Yammoûneh fault, that earthquake triggering is plausible. The seismic record of the Yammoûneh, Ghab and Jordan Valley faults prior to AD 1033 does not contradict this inference. In keeping with this idea, we speculate that the November 1995 event in the Gulf of Aqaba might mark the beginning of another such sequence. It would not be surprising if such a large-scale behavior which is typical of other large strike-slip faults such as the North Anatolian or Kunlun faults, characterized the Levant fault as well. Confirming or disproving this hypothesis calls for targeted, combined paleoseismic and archeologic investigation of events S₂ and S₃ in the Yammoûneh record. Lebanon, with its wealth of archeological remains, its relatively humid climate and the tectonically controlled sediment traps all along the Yammoûneh fault, is an ideal place for such an endeavor.

¹evidence for the AD 551 earthquake on the MLT from coastal uplift data and marine geophysics, will be discussed fully in the PhD thesis of Ata Elias [Elias, 2003; Elias et al., 2004]

Références

- ABOU KARAKI, N., 1987. *Synthèse et carte sismotectonique des pays de la bordure orientale de la Méditerranée : sismicité du système de failles du Jourdain - Mer Morte.* Ph.D. thesis, Université Louis Pasteur de Strasbourg
- ABOU KARAKI, N., DORBATH, L. and HAESSLER, H., 1993. *La crise sismique du golfe d'Aqaba de 1983 : implication tectonique.* Comptes-Rendus de l'Académie des Sciences de Paris, vol. 317, pp. 1411–1416
- ALLEN, C.R., 1981. *The modern San Andreas fault.* In *The geotectonic development of California*, edited by ERNST, W.G. Prentice Hall
- AMBRASEYS, N.N., 1997. *The earthquake of 1 January 1837 in southern Lebanon and northern Israel.* Annali di Geofisica, vol. XL, n. 4, pp. 923–935
- AMBRASEYS, N.N., 2004. *The 12th century seismic paroxysm in the Middle East: a historical perspective.* Annals of Geophysics, vol. 47, n. 2/3, pp. 733–758
- AMBRASEYS, N.N. and BARAZANGI, M., 1989. *The 1759 earthquake in the Bekaa valley: implications for earthquake hazard assessment in the Eastern Mediterranean region.* Journal of Geophysical Research, vol. 94, n. B4, pp. 4007–4013
- AMBRASEYS, N.N. and JACKSON, J.A., 1998. *Faulting associated with historical and recent earthquakes in the Eastern Mediterranean region.* Geophysical Journal International, vol. 133, pp. 390–406
- AMBRASEYS, N.N. and MELVILLE, C.P., 1988. *An analysis of the eastern Mediterranean earthquake of 20 May 1202.* In *History of Seismography and Earthquakes of the World*, edited by LEE, W.K.H., MEYERS, H. and SHIMAZAKI, K., pp. 181–200. Academic Press, San Diego, CA
- AMBRASEYS, N.N., MELVILLE, C.P. and ADAMS, R.D., 1994. *The Seismicity of Egypt, Arabia and the Red Sea - a historical review.* Cambridge University Press
- ARMIJO, R., LYON-CAEN, H. and PAPANASTASSIOU, D., 1992. *East-west extension and Holocene normal-fault scarps in the Hellenic arc.* Geology, vol. 20, pp. 491–494
- ARMIJO, R., TAPPONNIER, P. and TONGLIN, H., 1989. *Late cenozoic right-lateral strike-slip faulting in southern Tibet.* Journal of Geophysical Research, vol. 94, n. B3, pp. 2787–2838
- AUDIN, L., MANIGHETTI, I., TAPPONNIER, P., MÉTIVIER, F., JACQUES, E. and HUCHON, P., 2001. *Fault propagation and climatic control of sedimentation on the Ghoubet Rift Floor: insights from the Tadjouraden cruise in the western Gulf of Aden.* Geophysical Journal International, vol. 144, pp. 391–413
- AVOUAC, J.P., TAPPONNIER, P., BAI, M., YOU, H. and WANG, G., 1993. *Active thrusting and folding along the northern Tien Shan and late Cenozoic rotation of the Tarim relative to Dzungaria and Kazakhstan.* Journal of Geophysical Research, vol. 98, n. B4, pp. 6755–6804. doi:10.1029/92JB01963

- BAR-MATTHEWS, M., AYALON, A., GILMOUR, M., MATTHEWS, A. and HAWKESWORTH, C.J., 2003. *Sea-land oxygen isotopic relationships from planktonic foraminifera and speleothems in the Eastern Mediterranean region and their implication for paleorainfall during interglacial intervals.* Geochimica et Cosmochimica Acta, vol. 67, n. 17, pp. 3181–3199
- BARTOV, Y., GOLDSTEIN, S.L., STEIN, M. and ENZEL, Y., 2003. *Catastrophic arid episodes in the Eastern Mediterranean linked with the North Atlantic Heinrich events.* Geology, vol. 31, n. 5, pp. 439–442
- BEN-MENAHEM, A., 1979. *Earthquake catalogue for the Middle East (92 B.C.-1980 A.D.).* Boll. Geofis. Teor. Appl., vol. 21, pp. 245–310
- BEN MENAHEM, A., 1981. *Variation of slip and creep along the Levant rift over the past 4500 years.* Tectonophysics, vol. 80, pp. 183–197
- BEN-MENAHEM, A., 1991. *Four thousand years of seismicity along the Dead Sea rift.* Journal of Geophysical Research, vol. 96, n. B12, pp. 20 195–20 216
- BENEDETTI, L., FINKEL, R., KING, G., ARMJO, R., PAPANASTASSIOU, D., RYERSON, F.J., FLÉRIT, F., FARBER, D. and STAVRAKAKIS, G., 2003. *Motion on the Kaparelli fault (Greece) prior to the 1981 earthquake sequence determined from ^{36}Cl cosmogenic dating.* Terra Nova, vol. 15, pp. 118–124
- BENEDETTI, L., FINKEL, R., PAPANASTASSIOU, D., KING, G., ARMJO, R., RYERSON, F., FARBER, D. and FLÉRIT, F., 2002. *Post-glacial slip history of the Sparta fault (Greece) determined by ^{36}Cl cosmogenic dating: evidence for non-periodic earthquakes.* Geophysical Research Letters, vol. 29, n. 8, p. 1246
- BENEDETTI, L., TAPPONNIER, P., KING, G., MEYER, B. and MANIGHETTI, I., 2000. *Growth folding and active thrusting in the Montello region, Veneto, northern Italy.* Journal of Geophysical Research, vol. 105, n. B1, pp. 739–766
- BENNETT, R.A., FRIEDRICH, A.M. and FURLONG, K.P., 2004. *Codependent histories of the San Andreas and San Jacinto fault zones from inversion of fault displacement rates.* Geology, vol. 32, n. 11, pp. 961–964. doi:10.1130/G20806.1
- BESANÇON, J., 1968. *Le poljé de Yammoûné.* Hannon, vol. 3, pp. 3–62
- BESANCON, J., DRESCH, J. and TRICART, J., 1973. *Observations sur les processus morphogénétiques “froids” au Liban.* Revue de Géographie Physique et de Géologie Dynamique, vol. 15, n. 3, pp. 231–270
- BEYDOUN, Z.R., 1977. *The Levantine countries: the geology of Syria and Lebanon (maritime regions).* In *The ocean basins and margins Vol. 4a, The Eastern Mediterranean*, edited by NAIRN, A.E.M., KANES, W.H. and STEHLI, F.G., pp. 319–353. Plenum Press, New York, NY
- BLANCHE, C.I., 1847. *Lettre du Liban.* Bulletin de la Société Géologique de France, vol. 2, n. 5, pp. 12–17
- BOWMAN, D., KING, G. and TAPPONNIER, P., 2003. *Slip partitioning by elasto-plastic propagation of oblique slip at depth.* Science, vol. 300, pp. 1121–1123
- BRIAIS, A., SINGH, S.C., TAPPONNIER, P., ELIAS, A., SURSOCK, A., JOMAA, R., CARTON, H., DAËRON, M., KING, G. and JACQUES, E., 2004. *Neogene and active shortening offshore the reactivated Levant margin in Lebanon: results of the SHALIMAR cruise.* In *Eos (Transactions, American Geophysical Union)*, vol. 85. Abstract T53B-0490
- BRONK RAMSEY, C., 1995. *Radiocarbon calibration and analysis of stratigraphy: the OxCal program.* Radiocarbon, vol. 37, n. 2, pp. 425–430

- BRONK RAMSEY, C., 2001. *Development of the radiocarbon program OxCal*. Radiocarbon, vol. 43, n. 2A, pp. 355–363
- BUTLER, R.W.H. and SPENCER, S., 1999. *Landscape evolution and the preservation of tectonic landforms along the northern Yammounéh Fault, Lebanon*. In *Uplift, erosion and stability: geological and geomorphological perspectives on landscape evolution*, edited by SMITH, B.J., WHALLEY, W.B. and WARKE, P.A., vol. 162, pp. 143–156. Spec. Publ. Geol. Soc. Lond.
- BUTLER, R.W.H., SPENCER, S. and GRIFFITHS, H.M., 1997. *Transcurrent fault activity on the Dead Sea Transform in Lebanon and its implications for plate tectonics and seismic hazard*. Journal of the Geological Society, London, vol. 154, pp. 757–760
- BUTLER, R.W.H., SPENCER, S. and GRIFFITHS, H.M., 1998. *The structural response to evolving plate kinematics during transpression: evolution of the Lebanese restraining bend of the Dead Sea transform*. In *Continental, transpressional and transtensional tectonics*, edited by OLDSWORTH, R.E., STRACHAN, R.A. and DEWEY, J.F., pp. 81–106. Geological Society, London, Special Publication, 135
- CARTON, H., SINGH, S.C., ELIAS, A., TAPPONNIER, P., BRIAIS, A., SURSOCK, A., JOMAA, R., DAËRON, M., KING, G. and JACQUES, E., 2004. *Miocene to Quaternary folding and thrusting offshore Lebanon from SHALIMAR seismic profiles*. In *Eos (Transactions, American Geophysical Union)*, vol. 85. Abstract T53B-0488
- CHU, D. and GORDON, R.G., 1998. *Current plate motions across the Red Sea*. Geophysical Journal International, vol. 135, pp. 313–328
- COURTILLOT, V., ARMEDO, R. and TAPPONNIER, P., 1987. *The Sinai triple junction revisited*. Tectonophysics, vol. 141, pp. 181–190
- DAËRON, M., BENEDETTI, L., TAPPONNIER, P., SURSOCK, A. and FINKEL, R.C., 2004a. *Constraints on the post ~25-ka slip rate of the Yammounéh fault (Lebanon) using in situ cosmogenic ^{36}Cl dating of offset limestone-clast fans*. Earth and Planetary Science Letters, vol. 227, pp. 105–119
- DAËRON, M., ELIAS, A., KLINGER, Y., TAPPONNIER, P., JACQUES, E. and SURSOCK, A., 2004b. *Sources of the AD 551, 1202 and 1759 earthquakes (Lebanon and Syria)*. In *Eos (Transactions, American Geophysical Union)*, vol. 85. Abstract T41F-1294
- DAËRON, M., KLINGER, Y., TAPPONNIER, P., ELIAS, A., JACQUES, E. and SURSOCK, A., 2005. *Sources of the large A.D. 1202 and 1759 Near East earthquakes*. Geology. In press
- DAËRON, M., TAPPONNIER, P., JACQUES, E., ELIAS, A., KING, G., SURSOCK, A., GÈZE, R. and CHARBEL, A., 2001. *Evidence for Holocene slip and large earthquakes on the Yammounéh fault (Lebanon)*. In *Eos (Transactions, American Geophysical Union)*, vol. 82. Abstract S52D-0666
- DARAWCHEH, R., SBEINATI, M.R., MARGOTTINI, C. and PAOLINI, S., 2000. *The 9 July 551 AD Beirut earthquake, Eastern Mediterranean region*. Journal of Earthquake Engineering, vol. 4, n. 4, pp. 403–414
- DE VAUMAS, E., 1948. *Sur la structure du Liban*. Comptes Rendus de l'Académie des Sciences, vol. 226, n. 25, p. 2086
- DE VAUMAS, E., 1954. *Le Liban*. Firmin Didot, Paris
- DEMETS, C., GORDON, R.G., ARGUS, D.F. and STEIN, S., 1994. *Effects of recent revisions to the geomagnetic reversal time scale on estimates of current plate motions*. Geophysical Research Letters, vol. 21, n. 20, pp. 2191–2194
- DUBERTRET, L., 1932. *Les formes structurales de la Syrie et de la Palestine*. Comptes Rendus de l'Académie des Sciences, Paris, vol. 195

- DUBERTRET, L., 1955a. *Carte géologique du Liban au 1/200 000*
- DUBERTRET, L., 1955b. *Note explicative de la carte géologique du Liban au 1/200 000*
- DUBERTRET, L., 1975a. *Carte géologique du Liban au 1/50 000*
- DUBERTRET, L., 1975b. *Introduction à la carte géologique à 1/50 000 du Liban.* Notes et Mémoires du Moyen-Orient, vol. 13, pp. 345–403
- ELIAS, A., TAPPONNIER, P., KING, G., SINGH, S.C., SURSOCK, A., BRIAIS, A., CARTON, H., JACQUES, E., DAËRON, M. and JOMAA, R., 2004. *Fresh submarine seismic breaks due to historical thrust earthquakes offshore Lebanon.* In *Eos (Transactions, American Geophysical Union)*, vol. 85. Abstract T13C-1382
- ELIAS, A. ET AL., 2003. *Quaternary deformations associated with the Tripoli-Roum thrust, and the rise of the Lebanese coast.* Geophysical Research Abstracts, vol. 5. Abstract no. 10137
- ELLENBLUM, R., MARCO, S., AGNON, A., ROCKWELL, T. and BOAS, A., 1998. *Crusader castle torn apart by earthquake at dawn, 20 May 1202.* Geology, vol. 26, pp. 303–306
- ENZEL, Y., BOOKMAN (KEN TOR), R., SHARON, D., Gvirtzman, H., DAYAN, U., ZIV, B. and STEIN, M., 2003. *Late Holocene climates of the Near East deduced from Dead Sea level variations and modern regional winter rainfall.* Quaternary Research, vol. 60, pp. 263–273. doi:10.1016/j.yqres.2003.07.011
- FREUND, R., 1965. *A model of the structural development of Israel and adjacent areas since Upper Cretaceous times.* Geological Magazine, vol. 102, pp. 189–205
- FREUND, R., GARFUNKEL, Z., ZAK, I., GOLDBERG, I., WEISBROD, T. and DERIN, B., 1970. *The shear along the Dead Sea rift.* Philos. Transactions of the Royal Society of London, vol. 267, pp. 107–130
- FREUND, R., ZAK, I. and GARFUNKEL, Z., 1968. *Age and rate of the sinistral movement along the Dead Sea rift.* Nature, vol. 220, pp. 253–255
- GARFUNKEL, Z., 1981. *Internal structure of the Dead Sea leaky transform (rift) in relation to plate kinematics.* Tectonophysics, vol. 80, pp. 81–108
- GARFUNKEL, Z., 1998. *Constraints on the origin and history of the Eastern Mediterranean basin.* Tectonophysics, vol. 298, pp. 5–35
- GARFUNKEL, Z. and BEN-AVRAHAM, Z., 1996. *The structure of the Dead Sea basin.* Tectonophysics, vol. 266, pp. 155–176
- GARFUNKEL, Z., ZAK, I. and FREUND, R., 1981. *Active faulting in the Dead Sea rift.* Tectonophysics, vol. 80, pp. 1–26
- GASSE, F., ARNOLD, M., FONTES, J.-C., FORT, M., GIBERT, E., HUC, A., BINGYAN, L., YUANFANG, L., QING, L., MELIERES, F., VAN CAMPO, E., FUBAO, W. and QINGSONG, Z., 1991. *A 13,000-year climate record from western Tibet.* Nature, vol. 353, n. 742–745
- GASSE, F. and FONTES, J.C., 1989. *Paloenvironments and paleohydrology of a tropical closed lake (Lake Asal, Djibouti) since 10000 yr B.P.* Palaeogeography, Palaeoclimatology and Palaeoecology, vol. 69, pp. 67–102
- GASSE, F., TEHET, R., DURAND, A., GIBERT, E. and FONTES, J.-C., 1990. *The arid-humid transition in the Sahara and the Sahel during the last deglaciation.* Nature, vol. 346, pp. 141–146
- GAUDEMÉR, Y., TAPPONNIER, P., and TURCOTTE, D.L., 1989. *River offsets across active strike-slip faults.* Annales Tectonicae, vol. 3, pp. 55–76

- GAUDEMÉR, Y., TAPPONNIER, P., MEYER, B., PELETZER, G., GUO, S.M., CHEN, Z.T., DAI, H.G. and CIFUENTES, I., 1995. *Partitioning of crustal slip between linked, active faults in the Eastern Qilian Shan, and evidence for a major seismic gap, the Tianzhu gap, on the Western Haiyuan fault, Gansu (China)*. Geophysical Journal International, vol. 120, n. 3, pp. 599–645
- GINAT, H., ENZERL, Y. and AVNI, Y., 1998. *Translocated Plio-Pleistocene drainage systems along the Arava fault of the Dead Sea transform*. Tectonophysics, vol. 284, pp. 151–160
- GIRDLER, R.W., 1990. *The Dead Sea transform fault system*. Tectonophysics, vol. 180, pp. 1–13
- GOMEZ, F., MEGHRAOUI, M., DARKAL, A.N., HIJAZI, F., MOUTY, M., SOULEIMAN, Y., SBEINATI, R., DARAWCHEH, R., AL-GHAZZI, R. and BARAZANGI, M., 2003. *Holocene faulting and earthquake recurrence along the Serghaya branch of the Dead Sea fault system in Syria and Lebanon*. Geophysical Journal International, vol. 153, pp. 658–674
- GOMEZ, F., MEGHRAOUI, M., DARKAL, A.N., SBEINATI, R., DARAWCHEH, R., TABET, C., KHAWLIE, M., CHARABE, M., KHAIR, K. and BARAZANGI, M., 2001. *Coseismic displacements along the Serghaya Fault: an active branch of the Dead Sea Fault System in Syria and Lebanon*. Journal of the Geological Society, London, vol. 158, pp. 405–408
- GREGOR, C.B., MERTZMAN, S., NAIRN, A.E.M. and NEGENDANK, J., 1974. *The paleomagnetism of some Mesozoic and Cenozoic volcanic rocks from the Lebanon*. Tectonophysics, vol. 21, pp. 375–395
- GRIFFITHS, H.M., CLARK, R.A., THORP, K.M. and SPENCER, S., 2000. *Strain accommodation at the lateral margin of an active transpressive zone: geological and seismological evidence from the Lebanese restraining bend*. Journal of the Geological Society, London, vol. 157, pp. 289–302
- GUIDOBONI, E., BERNARDINI, F. and COMASTRI, A., 2004a. *The 1138–1139 and 1156–1159 destructive seismic crises in Syria, south-eastern Turkey and northern Lebanon*. Journal of Seismology, vol. 8, pp. 105–127
- GUIDOBONI, E., BERNARDINI, F., COMASTRI, A. and BOSCHI, E., 2004b. *The large earthquake on 29 June 1170 (Syria, Lebanon, and central southern Turkey)*. Journal of Geophysical Research, vol. 109, n. B07304
- GUIDOBONI, E., COMASTRI, A. and TRAINA, G., 1994. *Catalogue of ancient earthquakes in the Mediterranean area up to the 10th century*. Instituto Nazionale di Geofisica
- HOROWITZ, A., 1979. *The Quaternary of Israel*. Academic Press, New York
- IMBRIE, J., HAYS, J.D., MARTINSON, D.G., MCINTYRE, A., MIX, A.C., MORLEY, J.J., PISIAS, N.G., PRELL, W.L. and SHACKLETON, N.J., 1984. *The orbital theory of Pleistocene climate: support from a revised chronology of the marine $\delta^{18}\text{O}$ record*. In *Milankovitch and Climate (Part I)*, edited by BERGER, A.L., IMBRIE, J., HAYS, J.D., KUKLA, G. and SALTZMAN, B., pp. 269–305. Dordrecht (Reidel)
- IMBRIE, J., MCINTYRE, A. and MIX, A.C., 1990. *Oceanic response to orbital forcing in the Late Quaternary: observational and experimental strategies*. In *Climate and geosciences, a challenge for science and society in the 21st century*, edited by BERGER, A., SCHNEIDER, S.H. and DUPLESSY, J.-C. D. Reidel Publishing Company. Data from SPECMAP Archive #1 (<http://www.ngdc.noaa.gov/mgg/geology/specmap.html>)
- KHAIR, K., 2001. *Geomorphology and seismicity of the Roum fault as one of the active branches of the Dead Sea fault system in Lebanon*. Journal of Geophysical Research, vol. 106, n. B3, pp. 4233–4246
- KLINGER, Y., AVOUAC, J.-P., ABOU KARAKI, N., DORBATH, L., BOURLÈS, D. and REYSS, J.-L., 2000. *Slip rate on the Dead Sea transform fault in northern Araba valley Jordan*. Geophysical Journal International, vol. 142, pp. 755–768

- KLINGER, Y., AVOUAC, J.-P., BOURLES, D. and TISNERAT, N., 2003. *Alluvial deposition and lake-level fluctuations forced by Quaternary climate change: the Dead Sea case example*. Sedimentary Geology, vol. 162, pp. 119–139
- KLINGER, Y., RIVERA, L., HAESSLER, H. and MAURIN, J.-C., 1999. *Active Faulting in the Gulf of Aqaba: New Knowledge from the Mw 7.3 Earthquake of 22 November 1995*. Bulletin of the Seismological Society of America, vol. 89, n. 4
- LAL, D., 1991. *Cosmic ray labelling of erosion surfaces: in situ nuclide production rates and erosion models*. Earth and Planetary Science Letters, vol. 104, pp. 424–439
- LARTET, L., 1869. *La géologie de la Palestine*. Paris
- LAWS, E.D. and WILSON, M., 1997. *Tectonics and magmatism associated with Mesozoic passive continental margin development in the Middle East*. Journal of the Geological Society, London, vol. 154, pp. 459–464
- LOWELL, T.V., 1995. *The application of radiocarbon age estimates to the dating of glacial sequences: an example from the Miami sublobe, Ohio, USA*. Quaternary Science Reviews, vol. 14, pp. 85–99
- MANIGHETTI, I., TAPPONNIER, P., COURTILLOT, V., GRUSZOW, S. and GILLOT, P.-Y., 1997. *Propagation of rifting along the Arabia-Somalia plate boundary: the Gulfs of Aden and Tadjoura*. Journal of Geophysical Research, vol. 102, pp. 2681–2710
- MANIGHETTI, I., TAPPONNIER, P., GILLOT, P.-Y., JACQUES, E., COURTILLOT, V., ARMIJO, R., RUEGG, J.-C. and KING, G., 1998. *Propagation of rifting along the Arabia-Somalia plate boundary: Into Afar*. Journal of Geophysical Research, vol. 103, n. B3, pp. 4947–4974
- MARCO, S., HARTAL, M., HAZAN, N., LEV, L. and STEIN, M., 2003. *Archaeology, history and geology of the A.D. 749 earthquake, Dead Sea transform*. Geology, vol. 31, pp. 665–668
- MASCLE, J., BENKHELIL, J., BELLAICHE, G., ZITTER, T., WOODSIDE, J. and LONCKE, L., 2000. *Marine geologic evidence for a Levantine-Sinai plate, a new piece of the Mediterranean puzzle*. Geology, vol. 28, pp. 779–782
- MCCLUSKY, S., REILINGER, R., MAHMOUD, S., BEN SARI, D. and TEALEB, A., 2003. *GPS constraints on Africa (Nubia) and Arabia plate motions*. Geophysical Journal International, vol. 155, pp. 126–138
- MCKENZIE, D.P., 1978. *Some remarks on the development of sedimentary basins*. Earth and Planetary Science Letters, vol. 40, pp. 25–32
- MEGHRAOUI, M., GOMEZ, F., SBEINATI, R., VAN DER WOERD, J., MOUTY, M., DARKAL, A.N., RADWAN, Y., LAYYOUS, I., AL NAJJAR, H., DARAWCHEH, R., HIJAZI, F., AL-GHAZZI, R. and BARAZANGI, M., 2003. *Evidence for 830 years of seismic quiescence from palaeoseismology, archaeology and historical seismicity along the Dead Sea fault in Syria*. Earth and Planetary Science Letters, vol. 210, pp. 35–52
- MÉRIAUX, A.-S., 2002. *Détermination par datation cosmogénique des variations de la vitesse de glissement sur la faille de l'Atlyn Tagh depuis 100 ka*. Ph.D. thesis, Université de Paris VII
- MÉRIAUX, A.-S., RYERSON, F.J., TAPPONNIER, P., VAN DER WOERD, J., FINKEL, R.C., XU, X., XU, Z. and CAFFEE, M.W., 2004. *Rapid slip along the central Altyn Tagh fault: morphochronologic evidence from Cherchen He and Sulamu Tagh*. Journal of Geophysical Research, vol. 109, n. B6
- MÉRIAUX, A.-S., TAPPONNIER, P., RYERSON, F.J., XU, X.W., KING, G., VAN DER WOERD, J., FINKEL, R.C., LI, H.B., CAFFEE, M.W., XU, Z.Q. and CHEN, W.B., 2005. *The Aksay segment of the northern Altyn Tagh fault: tectonic geomorphology, landscape evolution and Holocene slip-rate*. Journal of Geophysical Research. In press

- MEYER, B., TAPPONNIER, P., BOURJOT, L., METIVIER, F., GAUDEMER, Y., PELETZER, G., SHUNMIN, GUO and ZHITAI, CHEN, 1998. *Crustal thickening in Gansu-Qinghai, lithospheric mantle subduction, and oblique, strike-slip controlled growth of the Tibet plateau.* Geophysical Journal International, vol. 135, n. 1–47
- MIGOWSKI, C., AGNON, A., BOOKMAN, R., NEGENDANK, J.F.W. and STEIN, M., 2004. *Recurrence pattern of Holocene earthquakes along the Dead Sea transform revealed by varve-counting and radiocarbon dating of lacustrine sediments.* Earth and Planetary Science Letters, vol. 222, pp. 301–314
- MITCHELL, S.G., MATMON, A., BIERMAN, P.R., ENZEL, Y., CAFEE, M. and RIZZO, D., 2001. *Displacement history of a limestone normal fault scarp, northern Israel, from cosmogenic ^{36}Cl .* Journal of Geophysical Research, vol. 106, n. B3, pp. 4247–4264
- MOUTY, M., DELALOYE, M., FONTIGNIE, D., PISKIN, O. and WAGNER, J.-J., 1992. *The volcanic activity in Syria and Lebanon between Jurassic and Actual.* Schweiz. Mineral. Petrogr. Mitt., vol. 72, pp. 91–105
- NIEMI, T.M., ZHANG, H.W., ATALLAH, M. and HARRISON, J.B.J., 2001. *Late Pleistocene and Holocene slip rate of the Northern Wadi Araba fault, Dead Sea Transform, Jordan.* Journal of Seismology, vol. 5, n. 3, pp. 449–474
- PHILIP, H. and MEGHRAOUI, M., 1983. *Structural analysis and interpretation of the surface deformation of the El Asnam earthquake of October 1980.* Tectonics, vol. 2, pp. 17–49
- PICCARDI, L., GAUDEMER, Y., TAPPONNIER, P. and BOCCALETTI, M., 1999. *Active oblique extension in the central Apennines (Italy): evidence from the Fucino region.* Geophysical Journal International, vol. 139, pp. 499–530
- PLASSARD, J., 1968. *Crise séismique au Liban du IVe au VIe siècle.* Mélanges de l'Université Saint-Joseph, vol. XLIV, n. 2, pp. 9–20
- POIRIER, J.P. and TAHER, M.A., 1980. *Historical seismicity in the Near and Middle East, North Africa, and Spain from Arabic documents (VIIth-XVIIIth century).* Bulletin of the Seismological Society of America, vol. 70, n. 6, pp. 2185–2201
- PRASAD, S., VOS, H., NEGENDANK, J.F.W., WALDMANN, N., GOLDSTEIN, S.L. and STEIN, M., 2004. *Evidence from Lake Lisan of solar influence on decadal- to centennial-scale climate variability during marine oxygen isotope stage 2.* Geology, vol. 32, n. 7, pp. 581–584. doi: 10.1130/G20553.1
- QUENNELL, A.M., 1958. *The structural and geomorphic evolution of the Dead Sea rift.* Quarterly Journal of the Geological Society of London, vol. 114, pp. 2–24
- QUENNELL, A.M., 1959. *Tectonics of the Dead Sea rift.* In *Proceedings of the 20th International Geological Congress, Mexico*, pp. 385–403
- RECHES, Z. and HOEXTER, D.F., 1981. *Holocene seismic and tectonic activity in the Dead Sea area.* Tectonophysics, vol. 80, pp. 235–254
- REPLUMAZ, A., LACASSIN, R., TAPPONNIER, P. and LELOUP, P.H., 2001. *Large river offsets and Plio-Quaternary dextral slip rate on the Red River fault (Yunnan, China).* Journal of Geophysical Research, vol. 106, n. B1, pp. 819–836
- RICOU, L.-E., 1995. *The plate tectonics history of the past Thetys Ocean.* In *The oceans basins and margins 8: the Thetys Ocean*, edited by NAIRN, A.E.M., RICOU, L.-E., VRIELYNCK, B. and DERCIORT, J., pp. 3–70. Plenum Press, New York, NY

- RITZ, J.F., BOURLÈS, D., BROWN, E.T., CARRETIER, S., CHERY, J., ENHTUVSHIN, B., GALSAN, P., FINKEL, R.C., HANKS, T.C., KENDRICK, K.J., PHILIP, H., RAISBECK, G., SCHLUSSP, A., SCHWARZ, D.P. and YIOU, F., 2003. *Late Pleistocene to Holocene slip rates for the Gurvan Bulag thrust fault (Gobi-Altay, Mongolia) estimated with ^{10}Be dates*. Journal of Geophysical Research, vol. 108, n. B3
- RON, H. and EYAL, Y., 1985. *Intraplate deformation by block rotation and mesostructures along the Dead Sea transform, Northern Israel*. Tectonics, vol. 4, pp. 85–105
- RON, H., NUR, A. and EYAL, Y., 1990. *Multiple strike-slip fault sets: a case study from the Dead Sea Transform*. Tectonics, vol. 9, pp. 1421–1431
- SALAMON, A., HOFSTETTER, A., GARFUNKEL, Z. and RON, H., 1996. *Seismicity of the eastern Mediterranean region: perspective from the Sinai subplate*. Tectonophysics, vol. 263, pp. 293–305
- SALAMON, A., HOFSTETTER, A., GARFUNKEL, Z. and RON, H., 2003. *Seismotectonics of the Sinai subplate — the eastern Mediterranean region*. Geophysical Journal International, vol. 155, pp. 149–173
- SANLAVILLE, P., 1977. *Etude géomorphologique de la région littorale du Liban*. Publications de l'Université Libanaise (section des études géographiques)
- SELLA, G.F., DIXON, T.H. and MAO, A., 2002. *REVEL: a model for recent plate velocities from space geodesy*. Journal of Geophysical Research, vol. 107, n. B4. doi:10.1029/2000JB000033
- SHAPIRA, A., AVNI, R. and NUR, A., 1993. *A new estimate for the epicenter of the Jericho earthquake of 11 July 1927*. Israel Journal of Earth Sciences, vol. 42, pp. 93–96
- STONE, J.O.H., ALLAN, G.L., FIFIELD, L.K. and CRESSWELL, R.G., 1996. *Cosmogenic chlorine-36 from calcium spallation*. Geochimica et Cosmochimica Acta, vol. 60, n. 4, pp. 679–692
- STONE, J.O.H., EVANS, J.M., FIFIELD, L.K., ALLAN, G.L. and CRESSWELL, R.G., 1998. *Cosmogenic chlorine-36 production in calcite by muons*. Geochimica et Cosmochimica Acta, vol. 63, n. 3, pp. 433–454
- STUIVER, M., REIMER, P.J., BARD, E., BECK, J.W., BURR, G.S., HUGHEN, K.A., KROMER, B., MCCORMAC, G., VAN DER PLICHT, J. and SPURK, M., 1998. *INTCAL98 radiocarbon age calibration, 24000–0 cal BP*. Radiocarbon, vol. 40, n. 3, pp. 1041–1083
- SWANSON, T.W. and CAFFEE, M.L., 2001. *Determination of ^{36}Cl production rates derived from the well-dated deglaciation surfaces of Whidbey and Fidalgo Islands, Washington*. Quaternary Research, vol. 56, pp. 366–382
- TAHER, M.A., 1979. *Corpus des textes arabes relatifs aux tremblements de terre et autres catastrophes naturelles de la conquête arabe au XII H./XVIII J.C.* Ph.D. thesis, Université de Paris I
- TAPPONNIER, P., DAËRON, M., KING, G., JACQUES, E., SURSOCK, A. and ELIAS, A., 2001. *Active faulting and seismic hazard in Lebanon*. Journal of Conference Abstracts, vol. 6 (EUG XI)
- TAPPONNIER, P., DAËRON, M., SURSOCK, A., JOMAA, R., BRIAIS, A., CARTON, H., SINGH, S.C., ELIAS, A., KING, G. and JACQUES, E., 2004. *Passive-active margin inversion along the Levant plate boundary: subduction birth and growth of Mt Lebanon*. In *Eos (Transactions, American Geophysical Union)*, vol. 85. Abstract T52B-05
- TAYLOR, J.R., 1997. *An introduction to error analysis, the study of uncertainties in physical measurements*. University Science Books, Sausalito, CA, second edn.
- VAN DER WOERD, J., RYERSON, F.J., TAPPONNIER, P., GAUDEMUS, Y., FINKEL, R., CAFFEE, M., GUOGUANG, ZHAO and QUNLU, HE, 1998. *Holocene left slip-rate determined by cosmogenic surface dating on the Xidatan segment of the Kunlun Fault (Qinghai, China)*. Geology, vol. 26, pp. 695–698

- VAN DER WOERD, J., TAPPONNIER, P., RYERSON, F.J., MÉRIAUX, A.-S., MEYER, B., GAUDEMÉR, Y., FINKEL, R.C., CAFTEE, M.W., GUOGUANG, ZHAO and ZHIQIN, XU, 2002. *Uniform postglacial slip-rate along the central 600 km of the Kunlun Fault (Tibet), from ^{26}Al , ^{10}Be , and ^{14}C dating of riser offsets, and climatic origin of the regional morphology*. Geophysical Journal International, vol. 148, pp. 356–388
- VAN DER WOERD, J., XU, X.W., LI, H.B., TAPPONNIER, P., MEYER, B., RYERSON, F.J., MÉRIAUX, A.-S. and XU, Z.Q., 2001. *Rapid active thrusting along the northwestern range front of the Tanghe Nan Shan (western Gansu, China)*. Journal of Geophysical Research, vol. 106, n. B12, pp. 30 475–30 504
- WALLEY, C.D., 1988. *A braided strike-slip model for the northern continuation of the Dead Sea Fault and its implication for Levantine tectonics*. Tectonophysics, vol. 145, pp. 63–72
- WALLEY, C.D., 1998. *Some outstanding issues in the geology of Lebanon and their importance of the tectonic evolution of the Levantine region*. Tectonophysics, vol. 298, pp. 37–62
- WDOWINSKI, S., BOCK, Y., BAER, G., PRAWIRODIRDJO, L., BECHOR, S., NAAMAN, S., KNAFO, R., FORRAI, Y. and MELZER, Y., 2004. *GPS measurements of current crustal movements along the Dead Sea Fault*. Journal of Geophysical Research, vol. 109, p. B05 403
- WELDON, R., FUMAL, T. and BIASI, G., 2004. *Wrightwood and the earthquake cycle: what a long recurrence record tells us about how faults work*. Geological Society of America Today, vol. 14, n. 9, pp. 4–10
- WELDON, R.J., MEISLING, K.E. and ALEXANDRE, J., 1993. *A speculative history of the San Andreas fault in southern California, a reconstruction based on new cross-fault correlation*. In *The San Andreas fault system: displacement, palinspastic reconstruction and geologic evolution*, edited by POWELL, R.E., WELDON, R.J. and MATTI, J.C., vol. 178, pp. 161–198. Geol. Soc. Mem.
- WELLS, D.L. and COPPERSMITH, K.J., 1994. *New Empirical Relationships among Magnitude, Rupture Length, Rupture Width, Rupture Area, and Surface Displacement*. Bulletin of the Seismological Society of America, vol. 84, pp. 974–1002
- YEATS, R.S., SIEH, K.E. and ALLEN, C.R., 1996. *The geology of earthquakes*. Oxford University Press
- ZUMOFFEN, G., 1926. *Géologie du Liban*. Barrère, Paris

Abstract:

The left-lateral Levant transform system ("Levant fault") displays a conspicuous, 160-km-long restraining bend whose location coincides with modern-day Lebanon. The Yammounéh strike-slip fault, whose surface trace bisects Lebanon, has usually been considered the main active strand of the Lebanese restraining bend, although several authors have recently voiced doubt on its present-day activity.

By combining geological observations, quantitative geomorphology and in situ cosmogenic surface exposure dating, we are able to lift this doubt and demonstrate that the Yammounéh fault is quite active, that it consistently offsets geomorphic markers of climatic origin, from the scale of meters to kilometers, due to the cumulative effect of recurrent, if infrequent, large earthquakes. Its Late Pleistocene to Holocene slip rate, constrained by surface exposure ages of offset limestone-clast fans, is 3.8 to 6.4 mm/yr.

Structural and geomorphic observations from the Lebanese coast and the foreland of Mount Lebanon provide evidence of active thrust faulting and folding, implying that SE-dipping thrust ramps govern the growth of anticlines in the foreland of Mount Lebanon, accounting for most the transgression related to the bend of the Levant fault. These active thrusts appear to continue offshore, as far south as Beirut and probably Saida. In this new model, the Roûm fault is simply interpreted as one of the lateral ramps transferring slip from the Jordan Valley fault to these thrusts, and Mount Lebanon is a thrust wedge completely surrounded by active faults.

This new model of the main active faults of the Lebanese restraining bend calls for a critical reassessment of historical earthquakes. We propose that the source of the M>7 earthquake and tsunami that destroyed Beirut in A.D. 551 was the offshore Mount Lebanon thrust rather than the Yammounéh fault. Furthermore, we demonstrate, by combining historical sources, qualitative geomorphic evidence and paleoseismology, that the latest event along the Yammounéh fault was the great (M~7.5) A.D. 1202 earthquake, and that the two A.D. 1759 events (M~6.6 and 7.4) were generated by the Râchaïya-Serghaya fault system.

Paleoseismic trenching of a paleo-lake in the Yammounéh basin yield further information on the earthquake record of this fault over about 15 kyr (~14 events). The average recurrence time of earthquakes at this site is ~1000 yr.

Based on the re-assessment of the three largest historical earthquakes of the restraining bend, on the long-term mean return time of events along the Yammounéh fault, and on its ~5mm/yr slip rate, we conclude that the next large earthquake on this fault is probably due earlier than previously thought. Seismic hazard in this densely populated region should be re-assessed accordingly.

